Impact of aging of dehydrated plant-based biopolymers on their functionality

Gisella de Oliveira Coelho

THÈSE DE DOCTORAT DE L'ÉTABLISSEMENT UNIVERSITÉ BOURGOGNE FRANCHE-COMTE

préparée à L'Institut Agro Dijon (UMR PAM)

Ecole doctorale n°554

ED ES : Environnements santé

Doctorat de Biotechnologies Agro-Alimentaires

par

Madame COELHO Gisella

Impact of aging of dehydrated plant-based biopolymers on their functionality

Thèse présentée et soutenue à Dijon, le 15/11/2024

Composition du Jury :

M. Rouilly, Antoine	Maître de Conférences, Toulouse INP	Rapporteur
M. Gouanvé, Fabrice	Maître de Conférences, Univ. Claude Bernard Lyon 1	Rapporteur
M. Assifaoui, Ali	Professeur, Université de Bourgogne (UFR)	Examinateur
Mme. Vittadini, Elena	Professeur, Université de Camerino	Examinatrice
Mme. Roudaut, Gaëlle	Maître de Conférences, L'Institut Agro Dijon	Directrice de thèse
Mme. Champion, Dominique	Professeur, L'Institut Agro Dijon	Codirectrice de thèse
M. Wallecan, Joël	Leader Science des Matériaux, Cargill	Invité
Mme. Déleris, Isabelle	Chercheur scientifique senior, Cargill	Invité

“I realized that – in spite of all the risks involved – a thing in motion will always be better than a thing at rest; that change will always be a nobler thing than permanence.”

Olga Tokarczuk

ÉCOLE DOCTORALE
Environnements - Santé
Bourgogne | Franche-Comté

Titre : Impact du vieillissement des biopolymères végétaux déshydratés sur leur fonctionnalité

Mots clés : Fibres d'agrumes ; biopolymères ; propriétés fonctionnelles ; stockage ; mobilité moléculaire.

Résumé : Les agrumes sont la culture la plus importante dans la production mondiale de fruits, avec une production mondiale d'environ 104 millions de tonnes en 2022. La plupart des fruits produits sont utilisés pour la production de jus, ce qui entraîne une quantité de sous-produits correspondant à 50 à 60% du poids initial du fruit entier. Les biopolymères sont les principaux constituants de ces déchets agro-industriels et présentent de nombreuses propriétés qui les rendent intéressants pour des applications, telles que la durabilité, le faible coût, la biodégradabilité, l'écologie et la recyclabilité. Les poudres de fibres d'agrumes (CF), fabriquées à partir de l'extraction de pectine des sous-produits de l'industrie des jus de citron, se caractérisent par leur capacité à retenir l'eau et à stabiliser les émulsions, et pourraient avoir de nombreuses applications alimentaires dans les produits de boulangerie, les viandes, les produits laitiers, les sauces et les assaisonnements. Les fibres sont séchées pour faciliter leur distribution et commercialisation en tant qu'ingrédient alimentaire. La qualité de la poudre déshydratée est influencée par les conditions de traitement et de stockage. Cette étude visait à investiguer les mécanismes responsables de l'instabilité des CF observée pendant le stockage et dont l'origine est jusque-là mal comprise. Des échantillons ont été stockés dans différentes conditions de température et d'humidité pendant 12 mois. La fermeté du gel (suivie au travers du module de rigidité G'), la capacité de rétention d'eau et la capacité de gonflement lors de l'hydratation ont été utilisées pour évaluer l'effet du stockage sur les propriétés fonctionnelles. De plus, la composition de surface de la poudre, les propriétés chimiques, la répartition de l'eau à l'échelle moléculaire et l'impact de l'humidité et de la température sur la mobilité moléculaire des fibres d'agrumes, ont été étudiées pour comprendre la modification des propriétés physico-chimiques pendant le stockage. Les résultats ont mis en évidence que la capacité de rétention d'eau, la fermeté du gel et la capacité à absorber de la vapeur d'eau diminuaient avec le temps de vieillissement. La perte de fonctionnalité a été accélérée à 40 °C et 75% HR par rapport à 25 °C et 30% HR. Ces modifications pourraient être liées à plus d'un mécanisme opérant au sein des fibres d'agrumes : la réorganisation et l'agrégation de molécules semblent être affectées par l'humidité, et la réticulation entre les molécules et les cations au sein des fibres d'agrumes montrant une indépendance par rapport aux conditions de température et d'humidité testées.

UBFC
UNIVERSITE
BOURGOGNE FRANCHE-COMTE

Université Bourgogne Franche-Comté
32, avenue de l'Observatoire
25000 Besançon

ÉCOLE DOCTORALE
Environnements - Santé
Bourgogne | Franche-Comté

Title: Impact of aging of dehydrated plant-based biopolymers on their functionality

Keywords: Citrus fibers; biopolymers; functional properties; storage; molecular mobility.

Abstract: Citrus is the most important crop in global fruit production, with worldwide production of around 104 million tons in 2022. Most of the fruits produced are used for juice production, which results in a huge quantity of by-products corresponding to 50-60% of the original whole fruit weight. Biopolymers are the main constituents of these agro-industrial wastes and present many properties that make them interesting for applications such as sustainability, inexpensive, biodegradability, friendly to the environment, and recyclability. Citrus fiber (CF) powders, manufactured from pectin extraction of lemon juice industry by-products, are characterized by an ability to retain moisture and to stabilize emulsion, and could have many food applications in baked products, meats, dairy products, sauces, and dressings. The fibers are dried to facilitate distribution and commercialization as a food ingredient. The quality of the dehydrated powder is influenced by the processing and storage conditions. However, the mechanism of the storage induced modifications of the powder's functional properties (especially rehydration properties) were not fully understood. This study aimed at investigating the mechanisms responsible for CF evolution upon storage. Samples were stored in different conditions of temperature and humidity for 12 months. Gelation, water holding capacity, and swelling capacity were used to evaluate the effect of storage on functional properties. In addition, powder surface composition, chemical properties, the moisture distribution in the matrix and the impact of humidity and temperature on the molecular mobility of citrus fibers were studied to understand the modification of physicochemical properties during storage. The results highlighted the properties related to moisture retention, emulsifying stability, and rehydration decreased with increasing aging time. The loss in functionality was accelerated at 40 °C and 75% RH compared to 25 °C and 30% RH. These modifications might be linked to more than one mechanism operating within the citrus fibers: reorganization and aggregation of molecules within the citrus fibers which seems to be appears to be affected by water and/or temperature, and crosslinking between molecules and cations within the citrus fibers showing independence from the tested temperature and humidity conditions.

UBFC
UNIVERSITÉ BOURGOGNE FRANCHE-COMTÉ

Université Bourgogne Franche-Comté
32, avenue de l'Observatoire
25000 Besançon

Acknowledgments

This thesis was carried out in L'Institut Agro Dijon, within the PCAV team (physico chemistry of food and wine) belonging to the UMR PAM (joint research unit for food and microbiological processes) in collaboration with Cargill R&D Europe Center.

First of all, I would like to sincerely thank **Dr. Antoine ROUILLY**, **Dr. Fabrice GOUANVE**, **Dr. Elena VITTADINI** and **Dr. Ali ASSIFAOUI** to have kindly accepted to evaluate my work and to be part of the jury of my Ph.D. defense. I would like also to thank the members of thesis committee **Dr Vincent PLACET** (Université de Franche-Comté) and **Dr Pierre-Yves PONTALIER** (Toulouse INP) for all their contributions during this thesis.

I would like to thank my supervisor **Gaëlle ROUDAUT** for the opportunity to do this thesis, for believing in my potential, for all the exchanges and learnings, and for having welcomed me so well in the middle of the pandemic period. I would also like to thank my co-supervisor, **Dominique CHAMPION**, for all great ideas, exchanges, and follow-up over the three years.

I would like to thank Cargill for the financial support of my thesis and thank all the people I had the opportunity to meet there, work with and have moments of leisure, even if it was brief! A special thank you to **Isabelle DÉLERIS** for always being a great support, being available and for all the learning! **Stephane DEBON** for his lightness and tranquility, and all the suggestions during the thesis! To **Joël WALLECAN** for being an example of a leader for me and always motivating me! To **Maxime TOUFFET** for all the help and availability!

To the team PCAV, a huge thank you to **Bernadette ROLLIN** and **Adrien LEBRET** for always helping me with the experiments and teaching me so much! To **Alexandra DA SILVA** for helping me solve all the problems and for the relaxing conversations! A big thank you to my colleagues and friends for all the exchanges and for making this journey much lighter and more fun, in especially **Syuzanna, Truc, Maria, Taisiia, Gayane, Tiffany, Mélissa, Leo, Laura, Julie, Max, Pierre and Mersha**! To my interns **Ana** and **Adrià** who contributed to research and became good friends!

I also wish to acknowledge all those who supported us by contributing to some analytical approaches. This includes **Jean-Marc DACHICOURT** (ESIREM), **Marie-Laure LEONARD** (ESIREM), **Dr. Olivier HEINTZ** (ICB) and **Anna KRYSTIANIAK** (ICB).

At least but not less important, I am so grateful to have my husband and partner, **Marcus**, in this journey, who believed in me, gave me the necessary support, accepted to always be between Brazil and France for three years and be my home. I also want to thank

you my family for the love and care even miles away and my friends in Brazil to understand my absence and always be my safe harbor! It's my honor to have all of you in my life!

List of publications and communications

Published papers

Coelho, G. O., Deleris, I., Champion, D., Wallecan, J., Debon, S., & Roudaut, G. (2024). Multiscale dynamics and molecular mobility in cellulose-rich materials. *Carbohydrate Polymers*, *344*, 122490. https://doi.org/https://doi.org/10.1016/j.carbpol.2024.122490

Submitted

G. O. Coelho, D. Champion, O. Heintz, A. Krystianiak, S. Debon, I. Deleris, J. Wallecan, G. Roudaut. Impact of processing and storage on citrus fiber functionality: insights from spectroscopic techniques.
Submitted to International Journal of Biological Macromolecules (IF 7.7) 28/06/2024

Prepared to be submitted

Coelho, G. O., Champion, D., Deleris, I., Wallecan, J., Debon, S., & Roudaut, G. Investigation of water distribution and dynamics in citrus fiber matrix in the glassy state: DSC and NMR studies.

Poster communication

G. O. Coelho, M. Touffet, D. Champion, I. Deleris, J. Wallecan, S.Debon, G. Roudaut. Can storage stability of citrus fiber powder be explained by modifications of their physicochemical properties? FJL 2023, 28e Forum des Jeunes Chercheurs, Besançon, France, 6-7 June 2023.

G. O. Coelho, M. Touffet, D. Champion, I. Deleris, J. Wallecan, S.Debon, G. Roudaut. Can storage stability of citrus fiber powder be explained by modifications of their physicochemical properties? ICEF14, International Congress on Engineering and Food, Nantes, France, 20-23 June 2023.

Table of contents

List of figures

List of tables

List of abbreviations

ACS	Apparent crystal sizes
AFM	Atomic Force Microscopy
AHP	Alkaline hydrogen peroxide
ANOVA	Analysis of variance
AOAC	Association of Official Analytical Chemists
ACP	Analyse en composantes principales
ATR	Attenuated total reflection
BmimCl	1-Butyl-3-methylimidazolium chloride
b.s.	Base sèche
CPMG	Carr-Purcell-Meiboom-Gill
CWM	Cell wall material
CEM	Teneur en eau d'équilibre
CF	Citrus fiber (spent peels processed and dry in pilot scale)
CF_A	Citrus fiber stored at accelerated conditions (40 °C and 75% RH)
CF_R	Citrus fiber stored at room conditions (20 °C, 30% RH)
CFV	Spent peels that were processed and stored in 40-45% isopropanol/water and dry in lab scale
CI	Crystallinity index
d.b.	Dry basis
DESs	Deep eutectic solvents
DF	Dietary fiber
DM	Degree of methyl esterification
DMA	Dynamic mechanical analysis
D_2O	Deuterium oxide
DRS	Dielectric relaxation spectroscopy
DRX	Diffraction des rayons X
DSC	Differential scanning calorimetry
Ea	Activation energy
EMC	Equilibrium moisture content
FTIR	Fourier Transform Infrared Spectroscopy
FAAS	Free amino acids
FID	Free Induction Decay
FWHM	Full width at half maximum
GAB	Guggenheim-Anderson-de Boer
HEC	Hydroxyethyl cellulose
HG	Homogalacturonan
HHP	High hydrostatic pressure
HM	High methoxyl
HMF	5-hydroxymethylfurfural
HPH	High pressure homogenization
HPMC	Hydroxypropyl methylcellulose

HR	Humidité relative
IR	Infrared spectroscopy
K_2CO_3	Potassium carbonate
KCH_3CO_2	Potassium acetate
KWW	Kohlrausch-Williams-Watts function
LM	Low methoxyl
LVR	Linear viscoelastic region
MCC	Microcrystalline cellulose
$MgCl_2.6H_2O$	Magnesium dichloride hexahydrate
MW	Molecular weight
NaBr	Sodium bromide
NaCl	Sodium chloride
NMR	Nuclear magnetic resonance
OHC	Oil-holding capacity
P_2O_5	Phosphorus oxide
PCA	Principal component analysis
RG-I	Rhamnogalacturonan I
RG-II	Rhamnogalacturonan II
RH	Relative humidity
RMN	Résonance magnétique nucléaire
SANS	Small-angle neutron scattering
SAXS	Small-angle X-ray Scattering
SNV	Standard normal variate
Tg	Glass transition temperature
TMCT-DMA	Thermal Mechanical Compression
TSC	Thermally stimulated currents
TD-NMR	Time domain NMR
TD-RMN	RMN pulsée
TEC	Triethyl citrate
WAXS	Wide-Angle X-ray Scattering
WBC	Water binding capacity
WSC	Water swelling capacity
WHC	Water-holding capacity
w.b.	Wet basis
XRD	X-ray diffractrometry
XPS	X-ray Photoelectron Spectroscopy
μGISAXS	Micro-focusing grazing-incidence small-angle X-ray scattering

List of symbols

A:	Pre-exponential factor from activation energy equation
A_{1610} :	Area of the band around 1610 cm^{-1}
A_{1730} :	Area of the band around 1730 cm^{-1}
a_w :	Water activity
β :	Constant representing the distribution of relaxation times from Kohlrausch-Williams-Watts function
C and K	GAB model constants
G' or E' :	Storage modulus (Pa)
G" or E":	Loss modulus (Pa)
I_{002} :	Crystalline material from crystalline index equation
I_{am}:	Amorphous material from crystalline index equation
K_1 and K_2:	Inverse of t_1 and t_2 from double exponential model (h^{-1})
k_s :	Constant proportional to the plasticizing effect of water from Gordon-Taylor equation
M (t):	NMR signal intensity
M :	More mobile protons determined by FID sequence (NMR)
m_0 :	Weight of empty centrifuge tube from WHC equation (g)
m_1 :	Weight of the centrifuge tube with sample prior to hydration from WHC equation (g)
m_2 :	Weight of centrifuge tube with centrifuged hydrated fiber from WHC equation (g)
M_1 and M_2 :	More mobile protons determined by CPMG sequence (CPMG)
M_1' and M_2' :	M_1 and M_2 calculated in relation to the total proton content (%)
M_D :	The amplitude of deuterium in the mobile fraction
M_{1D} :	The amplitude of deuterium in the less mobile fraction
M_{2D} :	The amplitude of deuterium in the more mobile fraction
M_W :	The amplitude of water in the mobile fraction
M_{1W} :	The amplitude of water in the less mobile fraction
M_{2W} :	The amplitude of water in the more mobile fraction
n :	The number of experimental data points from percentage error modulus equation
p:	The mean absolute percentage error modules
P_M :	The water contribution in the mobile fraction

P_{M1} :	The contribution of water in each fraction M_1
P_{M2} :	The contribution of water in each fraction M_2
P_{M1}' :	The corrected PM_1 relative value to the total water contribution in the matrix
P_{M2}' :	The corrected PM_2 relative value to the total water contribution in the matrix
P_S :	The water contribution in the solid fraction
P_w :	Total of water proton in the matrix
P_{WM} :	The total of water protons in the mobile fraction (determined by CPMG sequence)
R :	Gas constant (8.314 J / mol·K)
S :	Rigid protons determined by FID sequence (NMR)
S_D :	The amplitude of deuterium in the solid fraction
T_a :	Aging temperature from Tool-Narayanaswamy-Moynihan expression
t_1 and t_2 :	Time constant of a fast and slow process from double exponential model (h)
T_1 :	Proton-spin relaxation time
T_{11}, T_{12}, T_{21}, T_{22}:	Relaxation times measured in the time ranges window 1 and 2 (ms) for T_1 and T_2, respectively
T_2 :	Spin-spin relaxation time
tan δ:	Loss factor
T_f :	Fictive temperature for a material at the actual temperature T (structural state) from Tool-Narayanaswamy-Moynihan (TNM) expression
Tg :	Glass transition temperature (°C)
Tg_1 and Tg_2:	Reference temperature with the inflection points from deconvolution of Tg (°C)
Tg_i	Glass transition temperature for different phases (i)
Tg_m, Tg_s, Tg_w:	Glass transition temperature of mixture, solids and water from Gordon-Taylor equation (°C)
T_m :	Melting temperature (°C)
T_{max} :	Temperature maximum from tan δ curve (°C)
TNM :	Tool-Narayanaswamy-Moynihan expression
T_α :	α-relaxation temperature (°C)
T_β :	β-relaxation temperature (°C)
T_γ :	γ-relaxation temperature (°C)
τ :	Molecular relaxation time from Kohlrausch-Williams-Watts function
τ_0 :	Relaxation time in equilibrium at an infinitely high temperature from Tool-Narayanaswamy-Moynihan (TNM) expression
V_1:	Content of esterified carboxyl groups in the sample from DM titration equation (mL)

V_2:	Content of carboxyl without esterification from DM titration equation (mL)
X_0 :	Moisture content of the sample at time zero from double exponential model
X_1 and X_2 :	Moisture contents at infinite time associated with the fast and slow process from double exponential model
X_{cal} :	Predicted values from percentage error modulus equation
X_{eq}:	Equilibrium moisture content from GAB model and from double exponential model
X_{exp}:	Experimental values from percentage error modulus equation
X_m :	Monolayer from GAB model (g H_2O/g d.b.)
x_s:	Mass fraction of solids Gordon-Taylor equation
x_w:	Mass fraction of water Gordon-Taylor equation
ΔCp :	Specific heat (J/g)
Δh :	Apparent activation energy in the equilibrium state above Tg from Tool-Narayanaswamy-Moynihan (TNM) expression
Φ :	Property of concern from Kohlrausch-Williams-Watts function

General Introduction

General Introduction

Citrus is the most important crop in global fruit production with a production of around 104 million tons in 2022, over half of the production is destined to citrus juice production (USDA, 2024). Consequently, an enormous quantity of by-products is generated including peels and leaves which can be a potential source of pectin and essential oils (Bejar *et al*., 2012). The peels by-product originating from pectin extraction has an interesting composition (80% carbohydrate, 8% of protein and small quantity of ash and lipids) which may be a key factor for potential physicochemical properties such as water holding, swelling capacity and oil holding capacity (He *et al.*, 2023; Jiang *et al.*, 2022; Lundberg *et al.*, 2014).

Due to their functional properties, citrus fibers, used in powder form, can be used as fat and egg replacers, water retention agents, controlled flavor release agents, thickeners, gelling agents, stabilizers, and even material for food packaging (Kristensen *et al.*, 2022; Su *et al.,* 2020). A major challenge in the food powders industry is the loss of the functional properties upon water reconstitution. Several studies have suggested that irreversible structural changes occurring during drying, such as the cross-linking between cellulose microfibrils could be the most plausible reason for the reduction of these properties (Agoda-Tandjawa *et al.*, 2010; Déléris & Wallecan, 2017).

However, the modifications of the functional properties induced by storage time have been poorly investigated. Many studies are related to the modifications of dairy powders rehydration properties induced by storage (Fyfe *et al*., 2011; Gaiani *et al.,* 2007; Masum *et al.,* 2020), others works studied the impact of storage on vegetable and fruit powders focusing on the effect of water activity and the glass transition temperature on the product stability (Liu *et al.,* 2010; Staniszewska *et al.,* 2021). Fernández-López *et al.* (2009) studied the changes in the chemical, microbiological, and physicochemical characteristics of high dietary fiber powder from oranges, during storage exploring different packaging and storage conditions. Nevertheless, to our knowledge only one very recent study to date has addressed the relation between molecular mobility and storage stability on citrus fiber matrices (Putri *et al*., 2024). Consequently, the mechanism underlying the loss of functional properties of citrus fiber during storage remains unclear.

Thus, the current work aims to investigate i) the physical state and dynamics of citrus fiber at different scales (from molecular to macromolecular), ii) the ability of functional properties of citrus fiber to evolve upon storage and the mechanism responsible for

functionality loss of citrus fiber upon storage considering the impact of temperature and humidity.

This thesis manuscript consists of **seven chapters (**Figure 0-1**).** It begins with a state of the art (**first chapter**) describing the matrix of interest, citrus fiber, as well as its origin, composition, and functional properties. Afterwards, the functional properties are more deeply explored, studying the factors that influence these properties such as composition and physical properties. As the main objective of this thesis is to study the stability of the cell wall materials powders over time, this literature study focuses on the shelf-life of complex cell wall materials comprising factors that impact the stability of powders during storage, and the studies found in the literature for similar matrices. The last part consists of the study of molecular dynamics of cellulose-rich cell wall materials and the experimental approaches for a multiscale exploration as well as the contribution of the plant components to the dynamics. To close this chapter, the main and specific objectives of this research work are presented, as the assumptions which shaped this research.

The **second chapter** is dedicated to the materials and methods section which describes the sample preparation and storage, and methods to the determination of their functional properties and their physicochemical characterization in the initial time and after storage.

The results and discussion are presented in chapters 3 to 5. The **third chapter** is devoted to the physicochemical characterization of citrus fiber at the initial time and different processing are compared. For this, the water sorption isotherm was determined, and the molecular mobility was investigated at different scales considering the impact of temperature and water content. Additionally, the chemical composition and the chemical surface composition were investigated.

The **fourth chapter** presents the functional properties of citrus fiber and their survey during storage. The functionality (water holding capacity, water swelling capacity, and gel rigidity) and pH of dried citrus fiber were determined during 360 days of storage in two different conditions: accelerated aging conditions (40 °C, 75% RH) and room aging conditions (20 °C, 30% RH).

The **fifth chapter** describes the impact of storage time on the physicochemical properties of citrus fibers comprising the evolution of moisture distribution on the matrix and the effect of moisture and temperature on molecular mobility of citrus fiber upon storage. Additionally, the effect of long-term storage on chemical structures and surface composition of citrus fiber was determined by comparing the samples stored in both storage conditions.

This manuscript will be concluded, with an overall view of the work and a discussion of the gaps and perspectives that stem from this study (**sixth chapter**), followed by a synthesis in French highlighting the main points of this research (**seventh chapter**).

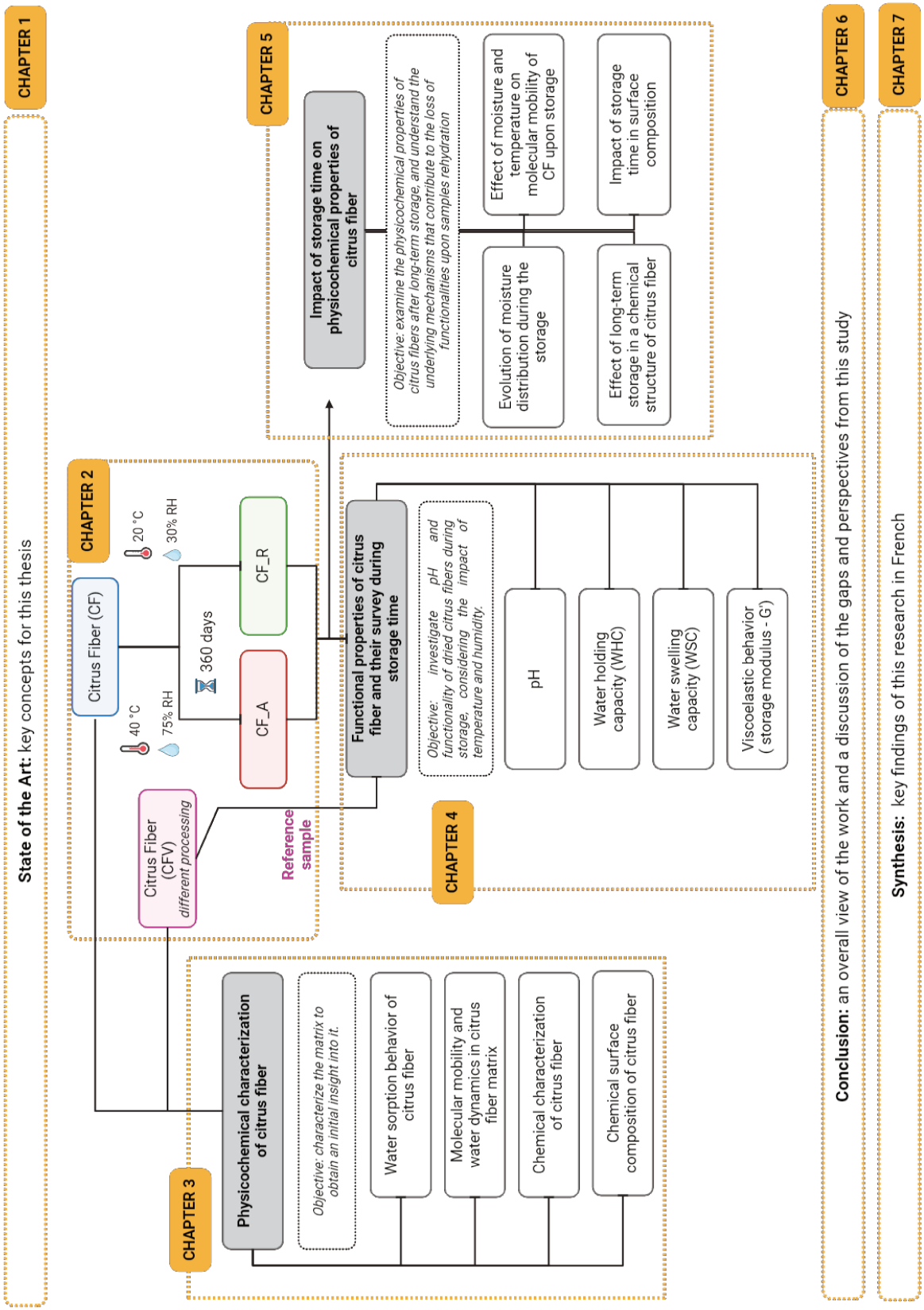

Figure 0-1. Thesis division schema.

Chapter 1. Literature Review

Chapter 1. Literature Review

1.1. Citrus fiber

Citrus (*i.e.* orange, lemon, pomelo) are the most important crops in the world, with an annual production of around 104 million tons (USDA, 2024). An important part of this production is processed in juice, jams, jellies, marmalades, essential oil, and pectin (Andrade *et al*., 2023; Suri *et al.,* 2022). However, this enormous range of applications results in a huge quantity of by-products which corresponds to 40-60% of total fruit mass which includes peels, seeds, and pomace (Jiang *et al.*, 2022). Food waste is a growing problem that has an impact on waste management in its entirety, especially due to the large quantity and high-water content (Maqbool *et al.,* 2023; Suri *et al*., 2022). For this reason, many researchers are looking to maximize the utilization of citrus waste to reduce environmental damage.

Citrus by-products are potential biosource since they may contain proteins, lipids (linolenic, oleic, palmitic, stearic acids), sugars (glucose, fructose, sucrose), carbohydrates (cellulose, pectin, hemicellulose, dietary fibers), pigments/carotenoids (carotene, lutein), vitamins (vitamins C and B complexes), and polyphenols (flavonoids, phenolic acids) (Panwar *et al.,* 2019). Therefore, they can be used in various food and non-food applications as: animal feed, additives (candies preparation, confectionary/bakery), source of bioactive compounds (pectin, essential oil, colorant and flavoring substances), to produce bio-adsorbent, biofuel, biofertilizer, packaging material and activate carbon (Andrade *et al.,* 2023; Panwar *et al*., 2019; Suri *et al.*, 2022).

Citrus fiber is a by-product of citrus processing, especially following the extraction of pectin from citrus peels. It has superior physicochemical qualities including water-holding capacity (WHC), water swelling capacity (WSC), oil-holding capacity (OHC), and rheological properties. The elementary composition of citrus fiber are carbohydrates, protein, ash and lipids which depend on the source and extraction method (Figure 1-1) (Jiang *et al.*, 2022). Carbohydrates are the most abundant components of citrus fiber (around 80%) comprising cellulose, hemicellulose, and pectin. In plant cell wall material, they are organized as a cellulose-hemicellulose network embedded in pectin with 5-8% of proteins contributing to the organization (Cosgrove, 1997; Zhang *et al.,* 2021). The protein fraction is mainly composed of extensins and glycoproteins that have an independent structure (Wallecan *et al.*, 2015). There is only a small contribution of lipids and ash (<5%). The composition depends on the raw material source and the conditions of the processing.

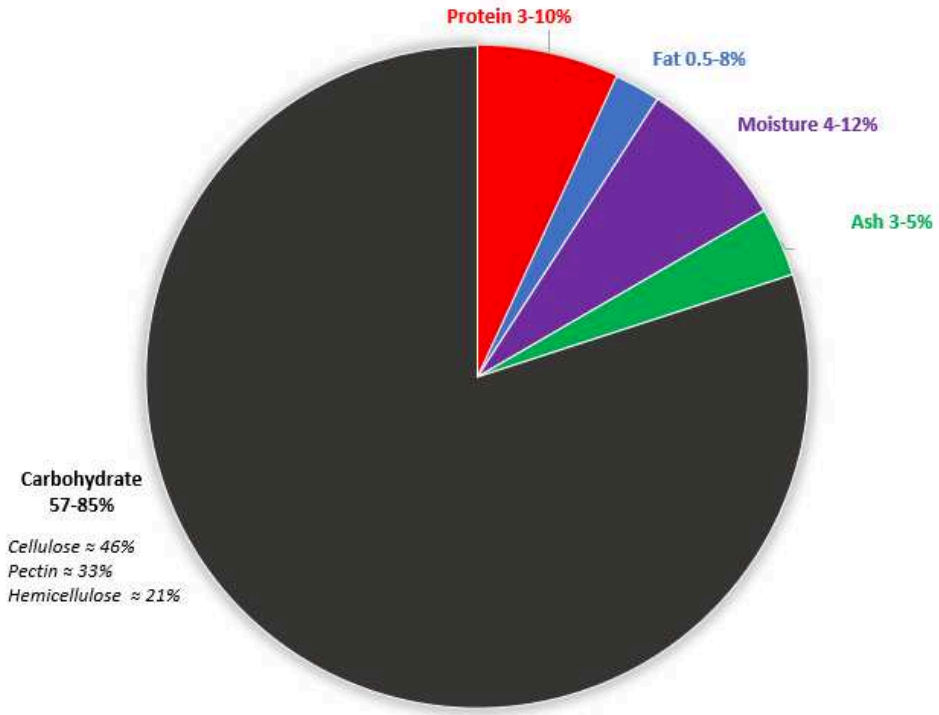

Figure 1-1. Citrus fiber average composition after Aravantinos-Zafiris *et al.*, (1994); Grigelmo-Miguel & Martín-Belloso, (1998); Huang *et al*., (2021); Jiang *et al*., (2022); Kohajdová *et al.,* (2011); Lundberg *et al.*, (2014) and Noguerol *et al.*, (2021).

Cellulose is formed by a linear chain of glucose units (1,4-β-D-glucopyranose) linked via hydrogen bonds and van der Waals forces, forming a long thread-like crystalline structure, microfibril (Figure 1-2a) (Cosgrove, 1997; Rongpipi *et al.,* 2019). This structure results in an insoluble, dense, and enzyme-resistant material (Kalla-Bertholdt *et al.,* 2023), it is responsible for the mechanical strength of the plant cell wall and determines cell growth through the microfibril's distribution and orientation (Cosgrove, 1997; Rongpipi *et al.,* 2019).

Hemicelluloses are composed by β-1,4- glycosidic bonds linked monosaccharides as glucose, xylose, galactose, and arabinose (Figure 1-2b) (Kalla-Bertholdt *et al.,* 2023). The monosaccharide and the combination, depends on the genre of the plant (Cosgrove, 1997). The predominant hemicellulose in the primary cell wall of dicotyledon (some fruits and vegetables) is xyloglucan. It is characterized by a β-1,4-linked glucan backbone, accompanied by side chains composed of xylose, galactose, and fucose residues, the specific composition of which varies depending on the plant species (Anderson & Kieber, 2020; Liu *et al.,* 2020; Zhang *et al*., 2021). Hemicelluloses are interacting with cellulose through hydrogen bonds (Anderson & Kieber, 2020; Liu *et al.*, 2020).

Pectin is one of the principal components of primary plant cell wall (20 to 35% d.b.) and the most structurally complex plant cell wall polysaccharide. It is also considered to be the

most soluble polysaccharide present in the plant cell wall (Cosgrove, 1997). In the plant, this polysaccharide plays an important role in the structure, contributing to intercellular adhesion, to rigidity and integrity of the cell wall. Its structure depends on the source and the method used to extract it (Cui *et al*., 2021). Pectin is a heterogeneous polysaccharide composed of different acidic sugars (glucuronic acid and galacturonic acid) (Figure 1-2c) (Cosgrove, 1997). This heterogeneous polysaccharide is classified into three types or domains: unbranched homogalacturonan (HG) which is mainly composed of galacturonic acid (monosaccharide partially methyl esterified, negatively charged, depending on the pH), rhamnose-alternated rhamnogalacturonan I (RG-I) which is the main hairy region of pectin (neutral sugars: galactose, rhamnose and arabinose), and complex branched rhamnogalacturonan II (RG-II) (Zhang *et al*., 2021). In addition, pectin can be classified according to degree of methyl esterification (DM) in high methoxyl (HM) pectin with DM>50% and low methoxyl (LM) pectin with DM< 50% (Agoda-Tandjawa *et al*., 2012).

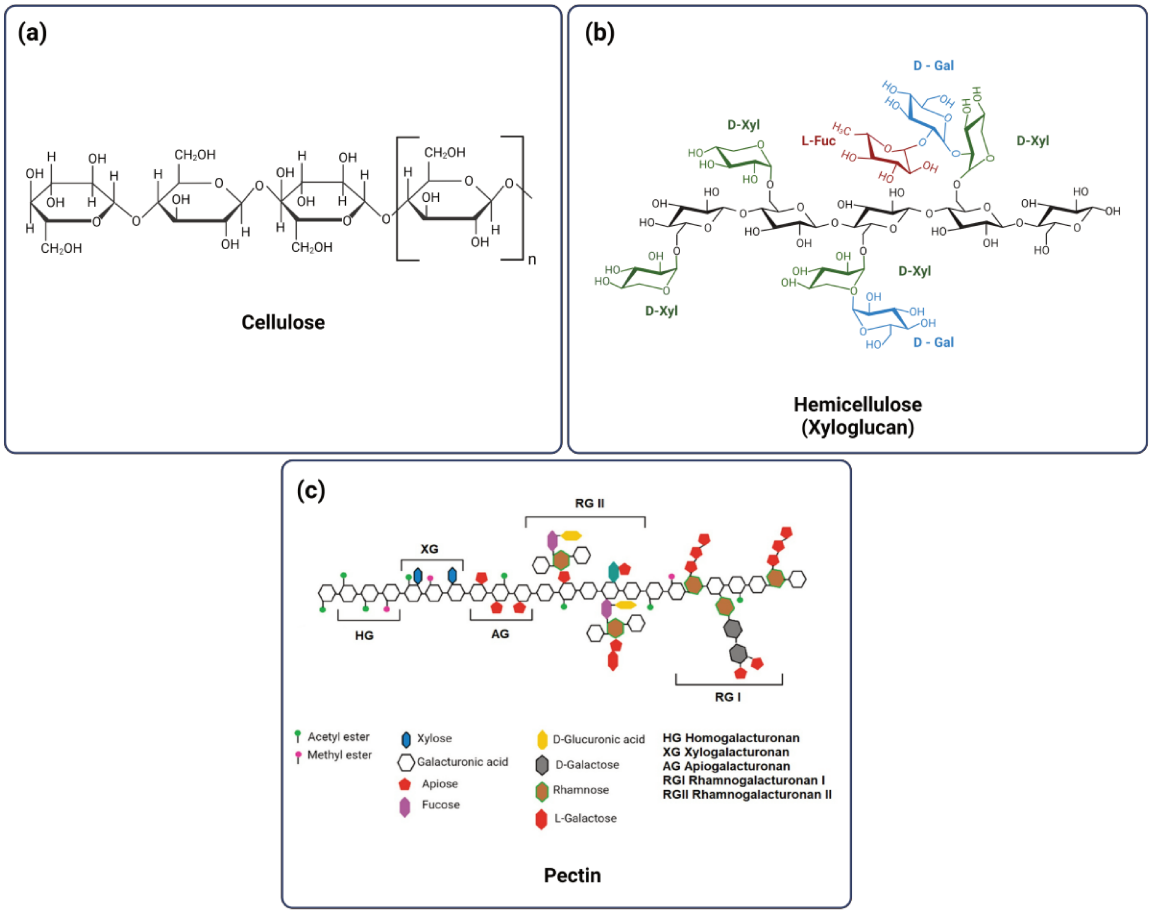

Figure 1-2. Cellulose, hemicellulose, and pectin chemical structure.

Although citrus fibers show interesting functional properties, they may be improved to be even more useful (Jiang *et al*., 2022; Lundberg *et al*., 2014; Zhang, *et al.,* 2020a). With

increasing industry demand for more sustainable alternatives to food hydrocolloids and novel texturizers, there are several studies concerning fiber modification focusing on improving hydration and rheological properties. Most common techniques explored in literature are chemical methods (alkaline and alkaline hydrogen peroxide (AHP) methods), mechanical (homogenization, high pressure homogenization (HPH), ball milling, high hydrostatic pressure (HHP)) and chemical-mechanical treatment (ultrasound-assisted alkali method or combination of AHP and HPH) (Bi *et al*., 2020; Chau *et al.,* 2007; Wallecan *et al.,* 2015; *Ye et al.,* 2016; Zhang *et al.,* 2020a; Zhang *et al.,* 2020b).

High-pressure homogenization stands out as a prominent treatment for citrus fiber, aiming to enhance its functional properties. This process disrupts the cell wall material, leading to a decrease in particle size and the formation of a porous structure within the cellulose-hemicellulose network. Additionally, it induces a transformation in the structure of citrus fibers, shifting from spherical particles to a sheet-like, multi-branched configuration (Bi *et al.,* 2020; Willemsen *et al.,* 2017). Therefore, HPH treatment produces a more homogeneous suspension with smoother appearance, increases the apparent viscosity, significantly improves the emulsifying property of citrus fibers (with finer oil droplets) as well as their stability, increase the WHC, WSC and storage modulus (G') (Bi *et al.*, 2020; Van Buggenhout *et al.,* 2015; Wallecan *et al.,* 2015).

Because of the enhanced functional characteristics of citrus fiber, it can improve the viscosity and the ability to form gels notably for ice cream to improve their sensory properties and non-fusibility (de Moraes Crizel *et al.,* 2013). In the bakery sector, citrus fiber can be incorporated in breads to reduce the firmness of gluten free bread through its great water holding capacity (Bosmans *et al*., 2013; Bugarín & Gómez, 2023; Korus *et al.,* 2020). Due to their excellent oil holding capacity, citrus fiber can be added into pancakes, doughnuts, and muffins dough (Kohajdová *et al.,* 2011). The emulsifying property of citrus fiber allows its use in meat-based items, replacing saturated fatty acids content in meat products and the nitrite levels in sausage (Bi *et al.,* 2020; Fernández-López *et al.,* 2004; Howard *et al.,* 2024; Powell *et al.,* 2019; Zhu *et al.*, 2023).

Understanding the functional properties and impact on their performance in different uses as well as their stability upon storage, is essential to expand the citrus fiber valorization.

1.2. Functional properties

The functional properties of citrus fiber (Table 1-1) associated with their neutral color, taste, and odor make it suitable for many applications in which other fibers are not considered

(an ingredient in formulated food and pharmaceutical supplements) (Garau *et al*., 2007; Grigelmo-Miguel & Martín-Belloso, 1998).

Solubility in food systems consists in the capacity of substances to dissolve in solvents. It is influenced by chemical and physical properties, as well as environmental factors like pressure, pH, temperature, and other solution components (Awuchi *et al.*, 2019). Citrus fiber is considered partially water soluble (Lundberg *et al*., 2014) with cellulose being insoluble and pectin and hemicellulose partly soluble. Willemsen *et al.* (2017) observed that the concentration of water-soluble pectin is low in the insoluble acid residue from pectin extraction. Therefore, the concentration of water soluble and insoluble polysaccharides in citrus fiber may be related to their processing. The insoluble fraction of fruits and legumes pulp and pomace are correlated with the functional properties such as WHC, WSC, OHC (Bengtsson & Tornberg, 2011; Chau et al., 2007).

WHC is the ability to absorb and retain water molecules (Awuchi *et al.,* 2019). The water is held via hydrophilic groups of fibers or entrapment in porous areas within the molecular structure (Kalla-Bertholdt *et al*., 2023), it corresponds to the retained water by an amount of dried material when submitted to an external force (g force - centrifugation) (Ramasamy, 2014). Besides, the WSC is another functional property that defines the ability of biopolymers to absorb and retain water, leading to an increase in volume (Kalla-Bertholdt *et al*., 2023). In both cases, the water is not only merely bound on the surface of fibers, but also absorbed inside. Consequently, water forms a “gel-like” network (Lundberg *et al.*, 2014).

This “gel-like” network is another fundamental property that enhances the versatility of biopolymers in industries of foods and cosmetics, for example. The gel structure consists of a formation of stable intermolecular “junction zones" between chain sequences through electrostatic, hydrogen bonding, hydrophobic or van der Waals interactions, or a combination of them. In addition, crosslinking in food gels can happen by chemical interaction, *e.g.* intermolecular disulfide bonds (Cao & Mezzenga, 2020). There are different mechanisms to form a gel which depends on the polymer structure:

(a) ion-induced gelation mechanism which consists in the formation of junction zones by ion-polymer interactions, for example, multivalent cations such as Ca^{2+} interact with alginate or pectin forming “egg-box structure”;

(b) another mechanism involves the conformation transition from disordered coil geometry to double helix, forming aggregations of double helices into supercoiled (tertiary structure) or coiled-coil helices (quaternary structure) such as agarose, carrageenan and gellan;

(c) when submitted to treatments involving variation of temperature (freeze-thaw cycles or heating), polysaccharides can form a gel via hydrogen bonds resulting in microcrystalline zones due to great amount of hydroxyl and carboxyl groups in polysaccharide backbone, or via the formation of hydrophobic micellar aggregates acting as intermolecular crosslink sites and thus creating a gel network like hydroxypropyl methylcellulose (HPMC).

The gel formation will be controlled by the stability of intermolecular associative structures (ordered) and adequate gelation conditions (temperature, polymer concentration, and ionic environment) (Yang *et al.,* 2020).

Different from other functional properties that are related to interaction with water, the oil holding capacity (OHC) is the ability of fiber to absorb fat or oil. This property is related to the hydrophobic groups and porous structure of fibers (Jiang *et al.*, 2022). Fibers OHC prevent fat loss during the cooking of fiber-containing foods. This property enables the fibers to absorb lipids in the intestinal lumen lowering cholesterol. Finally, OHC offers the possibility to use fibers as a stabilizer of emulsion and can favor the retention of food flavor (Noguerol *et al.*, 2021; Rivas *et al.*, 2021).

In conclusion, the functional properties of fruit fibers, particularly those of citrus fiber, play a pivotal role in shaping the characteristics of food products.

Table 1-1. Citrus fiber from different sources and their functional properties.

Source	**Pretreatment**	**WHC** (g of water/g of dry sample)	**WSC** (mL of water/ g of dry sample)	**OHC** (g of oil/g of dry sample)	**Reference**
CF (Orange pomace)	none	7.30	-	1.3	Grigelmo-Miguel & Martín-Belloso (1998)
CF (orange - pomace)	none	6.40	7.85	0.1	Kohajdová *et al*. (2011)
CF (lemon - pomace)		3.23	9.25	0.1	
CF (orange - pomace)	none	8.5	12	-	Lundberg *et al.* (2014).
CF (orange pomace)	Ordinarily ground powder	7.33	7.14	1.3	Ye *et al.* (2016)
	Mechanically ground powder	6.44	7.12	1.3	

	Jet ground powder	5.74	6.17	1.3	
CF (orange pulp)	none	15.2	-	5.6	Wallecan *et al*. (2015)
	HPH (6000 psi)	17.0	-	4.8	
CF (orange peel)	none	8.64	7.32	2.7	Zhang *et al.* (2020b)
	HPH (30Mpa)	14.97	15.15	3.5	
	AHP	13.25	11.63	2.6	
CF (lemon peel)	none	8.24	4.86	3.8	Zhang *et al.* (2020a)
	Alkaline treatment	20.18	17.84	4.6	
	Homogeneization	25.52	35.56	5.0	
CF - Fiberstar	Commercial	8.32	8.08	2.1	
CF (orange peel)	AHP	21.32	32.70	2.1	Huang *et al*. (2021)
CF (orange peel)	Homogenization	18.26	27.90	2.2	
CF - Fiberstar	Commercial	15.21	13	1.3	Jiang *et al*., (2022)
CF - Laimeng		9.88	29	1.5	
CF - Jinkangjun		13.33	22.5	2.0	

1.2.1. Factors influencing functional properties

A wide range of factors influences the functional properties of fibers, which play an important role in establishing the material's overall performance and features (Figure 1-3). These characteristics are diverse, ranging from the fibers' inherent features, such as composition, structure, and morphology, to extrinsic conditions and treatment techniques used during processing. These factors highlight the complexity of optimizing fiber functionality and the importance of a comprehensive approach to fiber processing and application.

The WHC, one of the most important properties of citrus fiber, is influenced by factors such as the type of raw material, processing conditions, structural parameters (particle size), molecular parameters (monosaccharide composition), and the ratio of soluble and insoluble

fractions (Kristensen *et al*., 2022; Schalow *et al.,* 2018). The water swelling capacity in these fibers relies on water interacting with available hydroxyl groups, breaking secondary interactions between macromolecules, with the degree of crystallinity affecting this interaction (Kristensen *et al.,* 2022; Mihranyan *et al.,* 2004). Additionally, the ability of citrus fibers to form gels is attributed to their highly entangled fiber network, providing ample space for water uptake and retention, particularly favored by longer and thinner fibers (Kristensen *et al.*, 2022).

1.2.1.1. Composition

The composition of citrus fibers, primarily cellulose, hemicellulose, and pectin, contributes significantly to their functional properties. High molecular weight, charge, and polysaccharide conformation play crucial roles, with linear polysaccharides favoring gelation and ribbon-like conformations influencing solubility (Goff & Guo, 2019). Chemical, mechanical, and physical treatments, such as HPH, are commonly applied to improve properties by reducing particle size, enhancing water entrapment (Jiang *et al.*, 2022; Wallecan *et al.,* 2015).

The amount and ratio of the constituents in fibers can influence moisture uptake as well as the interlocking of these constituents (Khodayari *et al.,* 2021; Tang & Huang, 2022; Wang *et al.*, 2024).

When cellulosic fibers are dispersed in water, the microfibrils build a strong network between them, resulting in a gel-like structure in aqueous medium (Agoda-Tandjawa *et al*., 2012). The network formed by microfibrils can trap water molecules in a void space between fibrils as “free” water and can form hydrogen bonds due to greater number of hydroxyl groups of glucose. However, compared to other polysaccharides such as pectin with a WHC of 37.8 g of water/g of dry sample according to Boulos *et al.* (2000) and locust bean gum with a WHC of 5.7 g of water/g of dry sample, cellulose presents a low water uptake (WHC = 0.32 g of water/ g of dry sample) under external force of 3000x g due to its linear structure: a branched configuration creates a capillary space in which water is absorbed by surface tension, and holds a great quantity of hydrophilic groups allowing the occlusion of water within the structure, and increasing the WHC of a compound (Boulos *et al.*, 2000).

Besides cellulose, pectin is another important polysaccharide of primary cell wall which has been considered as the main responsible for functional properties of fruits and vegetables (Agoda-Tandjawa *et al.*, 2012; Holloway & Greig, 1984; Khodayari *et al*., 2021). The functionality of pectin includes rheological capacity, since it can increase the viscosity of

several products, and emulsifying capacity which is associated to the hydrophobic groups coming from protein residues in the case of sugar beet pectin, and methyl ester in citrus pectin. In this case, these hydrophobic groups can absorb and attach on the O/W interface to reduce interfacial tension, subsequently, the carbohydrate chains found in pectin form a protective film around oil droplets, preventing their coalescence (Cui *et al.*, 2021; Zhao *et al.*, 2020). The pectin rheological and emulsifying properties strongly depend on its structure: composition, degree of methyl esterification (DM), ionic state (charges), molecular weight (MW), RG I/HG ratio and spatial conformation (Cui *et al.*, 2021).

The DM of HG fraction can govern the formation of junction zones and calcium cross linking, which are favored with low esterification degree (Lundberg *et al.*, 2014). The high DM requires both an acidic environment (pH<3.5) and a presence of cosolute (sugar>60%) to form a gel (Agoda-Tandjawa *et al.*, 2012). RG-I domain plays an important role in the rheological properties: the extent of branching affects the degree of inter-chain entanglement and the number of network junctions between independent pectin molecules in concentrated solutions. Then, de-branched pectin results in lower viscosity compared to branched one (Cui *et al.*, 2021; Wang *et al*., 2021). The highly branched pectin with long side chains favors a rapid hydration (Lundberg *et al.,* 2014).

The MW of pectin depends on the source and the method of extraction, for instance, MW of orange peel pectin extracted under alkaline conditions is 51 kDa while under acid conditions MW is 139 kDa (Cui *et al.*, 2021). MW affects the emulsifying capacity of pectin: higher molecular weight increases the steric hindrance of polysaccharide, preventing both aggregation and flocculation, forming solutions with higher viscosity, and improving the stabilization (Cui *et al.*, 2021; Tang & Huang, 2022). In addition, MW determines pectin conformation in solution and ability to form protective layers around oil droplets for a stable emulsion. Oppositely, low MW pectins are unable to stabilize an emulsion producing very thin adsorbed layers within the water/oil system and lower number of intermolecular interactions (Cui *et al*., 2021).

Another factor that can affect the gelling process and thus rheological properties is the ionic state of pectin. For instance, an anionic polysaccharide only undergoes gelation in the presence of certain cations. The extent of interactions between cations and anionic polysaccharide depends on factors such as ionic radius, ionic strengths, hydration number of the cation, as well as charge density and distribution, and polysaccharide structure. Based on these properties, the cation can effectively mitigate intermolecular electrostatic repulsion,

facilitating the association of polysaccharide chains through intermolecular H-bonding, ultimately resulting in gel formation (Wang *et al.*, 2024).

Hemicellulose can also contribute to the functional properties of fibers. Holloway & Greig (1984) observed that the chemical composition of hemicellulose has a stronger influence than morphological structure on WHC. The content in arabinose and xylose especially contributes positively to WHC. The degree of substitution and its pattern play an important role on functional properties of hemicellulose (Khodayari *et al.,* 2021).

The functional properties of citrus fiber may be correlated to the interactions between pectin and cellulose/hemicellulose network. In the primary cell wall, glucose units are linked by H-bonds forming cellulose microfibrils. Xyloglucans interact with cellulose by hydrogen bonds (Huang *et al.*, 2021). Regarding pectin, some studies suggested that pectin interacts with cellulose through neutral sugar sides chains (arabinan and galactan side chains) (Zykwinska *et al.,* 2005), while others mentioned that most pectin has limited molecular association with cellulose microfibrils (Lopez-Sanchez *et al*., 2016). Despite the opposite conclusions found in literature, Agoda-Tandjawa *et al.* (2012) who studied the properties of cellulose/pectin composites, observed that part of pectin backbones can strongly associate with cellulose providing negative surface charges to cellulose fibers. However, they found that the presence of pectin within cellulose does not impact the viscoelastic properties of the cellulose network. The gelation of a system containing cellulose, and pectin is mainly governed by cellulose as well as the mechanical properties of the plant cell wall.

To study the impact of polysaccharides on cellulose structure as well as on its properties, Szymańska-Chargot *et al.* (2017) used a system based on bacterial cellulose. They observed that pectin and hemicellulose may impact cellulose microfibrils diameter and crystallinity as well as the strength of the system. However, recent studies showed that hemicellulose slightly affects the viscoelasticity of the cell wall. Besides these contributions of hemicellulose and pectin to cellulose arrangement, Cybulska *et al*. (2023) showed that the interactions of hemicellulose and pectin with cellulose can also impact both the amount and in the rate of water absorption. The interaction of hemicellulose with cellulose fibrils may reduce the height of fibrils and surface roughness, increasing the water absorption capacity. Pectin does not change the number of hydrophilic sites but enhances their availability, improving the rate of water absorption.

In addition to polysaccharide interactions, they could combine with proteins via hydrophobic interactions and hydrogen bonds to form complexes, especially in acidic medium (pH 2.5). The drying process can contribute to the formation of polysaccharide-protein

complexes (Yi *et al*., 2020). In this synergy, proteins manifest as hydrophobic structures, while the polysaccharide chains exhibit hydrophilic characteristics. Then, the emulsifying capacity of polysaccharides arises from the intricate interaction between these compounds and their associated proteins, since a limited amount of polysaccharides have surface activity at the oil–water interface, which are required to be used as emulsifiers (Tang & Huang, 2022). Besides, protein affects the texture, stability, functional properties, and economic value of food products (Panwar *et al.*, 2023).

1.2.2. Physical properties

The intrinsic properties of the material, such as its structure, composition, and surface characteristics, play a pivotal role in the functional properties that define its performance in different applications (Garau *et al.*, 2007; Rivas *et al.,* 2021).

The porosity and surface area contribute to WHC, WSC and OHC: a great surface area contribute to the exposition of components (Kalla-Bertholdt *et al*., 2023), whereas a higher porosity favors the absorption and holding of larger amount of water or oil depending on the hydrophobicity of the material (Jiang *et al.,* 2022). The presence of hydrophilic or hydrophobic functional groups on the material's surface also affects its interaction with water or oil (Noguerol *et al.*, 2021).

Additionally, the structure of fibers is considerably important for water interaction since water interacts better with layer-like networks than with the spider-web-like structure (Kalla-Bertholdt *et al*., 2023)**.**

Divergent discussions regarding the impact of particle size in functional properties are found in the literature. On one hand, the hydration properties (WHC and WSC) and OHC decrease with decreasing particle size, due to the reduction of void space between two particles and the increase of packing density (Boulos *et al.,* 2000; Noguerol *et al.*, 2021). On the other hand, the ability of the fiber to entrap water and oil within the structure is further improved by the reduction in particle size due to greater number of potential water-binding sites and polar groups as well as the enhancement of molecular interactions and van der Waals forces between oil particles and non-polar groups (Bruno *et al*., 2021; He *et al*., 2023; Jiang, Zhang *et al.*, 2022; Su *et al*., 2019). As discussed by Lundberg *et al.* (2014), the competing forces of setting one another may be considered.

The rheological properties are influenced by both the degree of cross-linking and the MW, determining the material's ability to form stable gels under specific conditions (Yi *et al.*, 2020). Besides, the charges also contribute to apparent viscosity and gelling properties

(Lundberg *et al.*, 2014). The presence of charges, for example from carboxyl groups, can promote repulsion, facilitating interaction with water (Ramasamy, 2014).

Regarding extrinsic attributes, temperature and pH conditions during processing or use further modulate these properties. Especially for rheological properties, these extrinsic parameters can control the gelling process (Fatimi *et al.*, 2009).

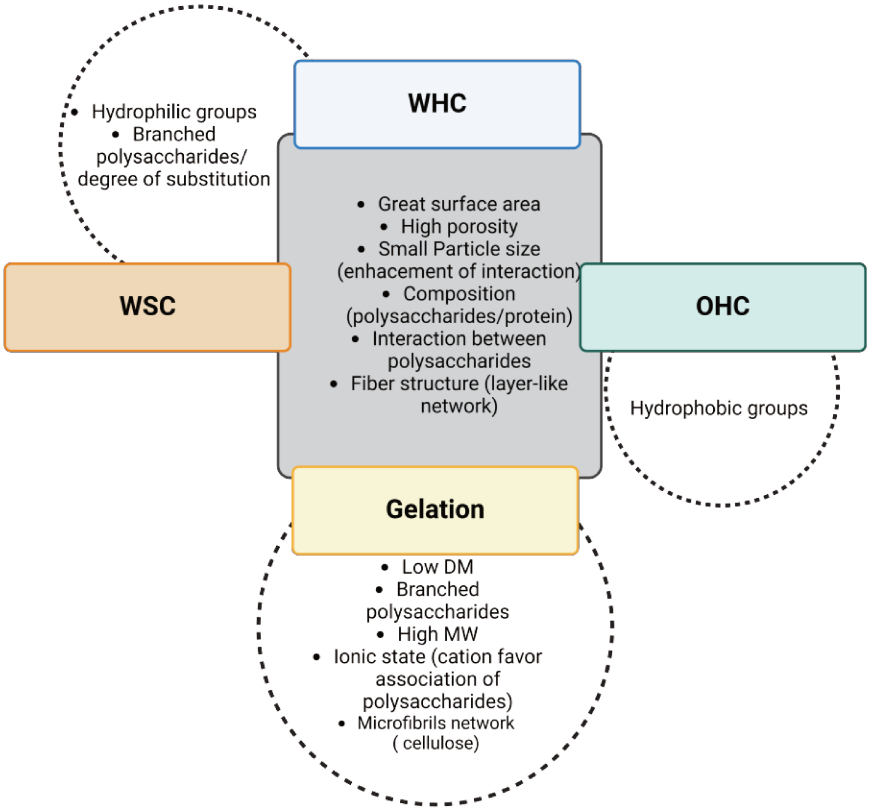

Figure 1-3. Factors that positively affect the functional properties of fibers.

1.3. Shelf-life of complex cell wall materials

Understanding the evolution of functional properties over time is crucial for ensuring the stability of food products. Although these products, especially originating from fruits, are relatively stable due to their low intrinsic pH and low water activity, they are sensitive to moisture, temperature, light, and oxygen which are critical factors for storage (Hedegaard & Skibsted, 2013; Korese *et al.,* 2022). While existing literature has extensively explored the influence of storage conditions, type of packaging, processing parameters, additives of food powders, a nuanced investigation of the mechanisms controlling the stability of functional properties remains a relatively underexplored terrain.

Studies to date have delved into the effects of time on food powders, revealing insights into physical and chemical alterations resulting in changes in functional properties, and deterioration of sensory or nutritive quality (Hedegaard & Skibsted, 2013).

One of the products that impose significant challenges to shelf life are milk powder and derivatives (infant milk formula, micellar casein powder) (Fyfe *et al.*, 2011; Gaiani *et al.*, 2007; Masum *et al.*, 2020a; Nasser *et al.*, 2017; Thomas *et al*., 2004). These products undergo various physical and chemical changes during storage, such as alterations in wettability, solubility, flowability, lactose crystallization, and surface composition (surface hydrophobicity) (Fyfe *et al*., 2011; Thomas *e*t *al*., 2004).

Similar to other food powders, the powders derived from natural sources pose challenges in preserving their functionalities and nutritional integrity. In addition, with the increasing reuse of agro-industrial waste, the studies seeking to understand the functionalities demand greater knowledge of the stability of these powders. The storage of fruit powders, depending on the storage conditions (temperature and/or humidity), causes the decrease of pH, free amino acids (FAAS), total soluble solid, phenolic content, vitamins, antioxidants, and total sugar. Besides, the color usually changes during the storage accompanied by the formation of 5-hydroxymethylfurfural (HMF) and increase of browning degree and titratable acid (Korese *et al.*, 2022; Liu *et al.*, 2010; Pacheco *et al.,* 2020). These changes may be associated with chemical reactions such as Maillard, oxidation, and isomerization (Harnkarnsujarit & Charoenrein, 2011). Additionally, other reactions can occur *e.g.* hydrolysis since hydrogen ions from carboxyl groups of polysaccharides can have an auto hydrolysis, demethoxylation or depolymerization (β-elimination) in pectic polysaccharides (Lewin, 1997; Morris *et al.*, 2010).

The loss of functionality (WHC, WSC and OHC) upon storage can be associated to physical modifications in fiber matrix, pores collapse, crystallization as well as to chemical reactions. Fernández-López *et al*. (2009) investigated the impact of 11 months of storage in different conditions (vacuum or air exposure and under dark or light exposure at 23 °C) on citrus rich in dietary fiber (DF). After 6 months, significant changes in color, moisture content, and physicochemical properties occurred, but microbiological content remained stable. WHC and WSC decreased with storage time, attributed to fiber matrix modifications. Conversely, OHC increased. The study also highlighted the influence of oxygen and light on citrus fiber quality during storage mainly on degradation of pigments (carotenoids) by oxidation reactions.

The most important factors that impact food stability are water, temperature, and time. Understanding the interplay between water activity of food powders and temperature, it is crucial to avert undesirable physical and chemical occurrences like caking or clumping, lipid oxidation, enzymatic activities, and microorganism growth. Thus, the water sorption isotherm,

a tool revealing the relation between water activity and water content of a material, as well as the glass transition temperature (Tg) serve as fundamental parameters in assessing the stability of food products (Sablani *et al.*, 2007; Staniszewska *et al*., 2021).

The diagram that relates the equilibrium water content and Tg as a function of water activity can be used to determine the critical values of a_w (Figure 1-4). Above these values, the stability at ambient temperature is likely to decrease because Tg is reduced below that temperature (Karel *et al*., 1994). Staniszewska *et al.* (2021) used this correlation to determine the optimal storage conditions of dried powdered coriander, parsley, and celery. To be shelf stable a product may be stored below its Tg to avoid deterioration due to microbial growth, chemical reactions and reduce the molecular mobility. While the monolayer moisture content contributes to microbial development, the molecular mobility can explain deteriorative transformations such as stickiness, crispness, collapse, crystallization, non-enzymatic browning. In addition, water can be also indirectly related to these physical and chemical changes since it can act as a plasticizer decreasing the Tg and increasing the mobility of reactants (Hankarnsujarit & Charoenrein, 2011; Sablani *et al.*, 2007).

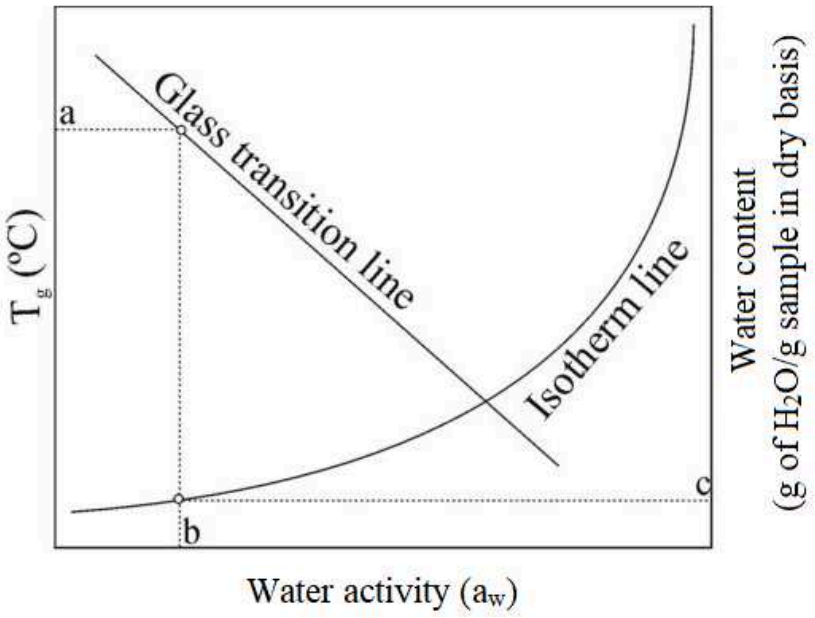

Figure 1-4 Schematic plot of glass transition temperature (Tg) and equilibrium water content as a function of water activity: a is the critical storage temperature in certain water activity (a_w) b and water content of a sample c. After Santivarangkna *et al.* (2011).

Furthermore, it was observed that stability-related phenomena, such as the diffusion of water and food components, as well as chemical reactions, including non-enzymatic browning, were notably influenced by the Tg, particularly under conditions of elevated humidity and temperature *(*Karel *et al.,* 1994).

Although the glass transition temperature has been shown as an indicator for food quality during storage, emerging evidence suggests that physicochemical changes occur even below this critical temperature. Below Tg, amorphous or semi-crystalline materials may have a residual mobility allowing slow movements within the material during storage, and thus, inducing structural modifications in the material such as densification at a molecular level associated with a reduction of free volume concomitant to an enthalpy reduction. This structural relaxation of glassy material can be measured by differential scanning calorimetry (DSC), evidenced by an endothermic peak which represents the recovery of the energy named enthalpy relaxation (Ho & Vu-Khanh, 2003; Hodge, 1994) prior to the glass transition. Amorphous biopolymers and polymers usually exhibit an endotherm peak over a broad range between 40 and 80 °C upon a first heating as amorphous starch (Anzai *et al*., 2011; Chung & Lim, 2004; Kim *et al*., 2003; Monnier *et al*., 2017; Rolandelli *et al.*, 2022; Tananuwong & Reid, 2004), breakfast cereal (Masavang *et al.*, 2019), amylopectin (Borde *et al.*, 2002) and poly(latic) acid (Lee *et al.,* 2020).

Based on relaxation phenomena, Putri *et al*. (2024) evaluated the storage stability of lemon peel cell wall material's (CWM) rheological properties (G', the storage modulus of the reconstituted material in water) over 14 weeks. At 25 and 40 °C, G' significantly declined, with the 40 °C samples experiencing a rapid decrease after 5 weeks, while the 25 °C samples reached a similar G' value after 14 weeks. The observed loss of functionality was attributed to the collapse of CWM structure, influenced by temperature-induced molecular mobility and interactions between biopolymers chains, such as cellulose microfibrils. Consequently, it restrains the formation of an open network that would entrap water during rehydration. On the other hand, moisture content upon storage did not impact G', suggesting a restricted water plasticizing effect on the matrix. The material was primarily composed of cellulose, a rigid polymer with crystalline regions in its native form. These crystalline regions can impede water migration into the amorphous region. The study highlighted the importance of understanding structural relaxation phenomena for preserving the functionality of fiber powder materials under specific storage conditions.

Investigating the alterations occurring upon storage, particularly in relation to water content and molecular mobility, can offer valuable insights into the mechanisms responsible for functionality loss.

1.4. Molecular dynamics of cellulose-rich cell wall materials and experimental approaches

To progress in the understanding of the behavior of biosystems during processing and shelf life, investigation of transitions at the molecular and supramolecular scales is of importance (Al-Khalili *et al*. 2023a; Paes *et al.*, 2010; Rolandelli *et al*., 2022). This investigation scans different kinds of motion such as rotation of atoms groups and/or polymeric segments linked by covalent bonds, molecular displacement/deformation due to solvent migration, molecular diffusion (Brownian movements) resulting from chemical potential gradient or electric field (Roudaut *et al.*, 2004).

The properties of polymers may change gradually with temperature until achieving the critical temperature(s) at which an abrupt alteration of various characteristics is observed due to an associated molecular mobility increase. This phase transition is commonly known as glass transition or α-relaxation when related to mobility change inducing the flow and/or a rubbery behavior. This transition is associated with the large-scale mobility of polymer chains.

In addition to the glass transition, polymers exhibit secondary relaxations, known as β and γ relaxations, which occur at temperatures below the glass transition temperature and are associated with localized mobility within the polymer structure. β-relaxation involves the motion of segments of the polymer backbone, providing insight into the flexibility and interaction of these segments. On the other hand, γ-relaxation involves even more localized motions of atomic groups or side chains, reflecting the mesoscopic-level dynamics of the polymer (Ioelovich, 2016).

The phase transition can be measured by different ways such as calorimetric (differential scanning calorimetry (DSC)), mechanical (dynamic mechanical analysis (DMA)) or dielectric (dielectric relaxation spectroscopy (DRS)) spectroscopies, and even methods including measurements of volume expansion coefficient (Blanshard, 1995; Perdomo *et al*., 2009). These methods provide insight into dynamics at macro and mesoscopic scales.

1.4.1. Macroscale: glass transition temperature of cellulose-rich material

The determination with DSC of the glass transition temperature (Tg) of cellulose-based systems is challenging for multiple reasons:

- the semi-crystalline nature of these materials makes it difficult to characterize the transitions due to the weak fraction of amorphous phase (Roig *et al*., 2011). Indeed, cellulose has a crystallinity ranging from 25% to 80% (Dassanayake *et al.*, 2019; Ioelovich, 2021) depending on its botanical origin (Table 1-2).

Table 1-2. Crystallinity index of different plant fibers.

	Crystallinity Index (%)	Cellulose content (%)	Method	Reference
Corn stover	47	33	X-ray diffraction (Segal method)	Thygesen *et al.* (2005)
Norway spruce	47	49		
Hemp fibers	77	63		
Citrus Pomelo fiber	25	21	X-ray diffraction (Segal method)	Zain (2014)
Jute fiber	34	45-71	X-ray diffraction (Segal method)	Poletto *et al.* (2014)
Kenaf	35	31-72		
Ramie	35	69-91		
Sisal	57	65-67		
Citrus Fiber	33	40	X-ray diffraction (Segal method)	Zhang *et al.* (2020b)
Pineapple crown fiber	62	17	X-ray diffraction (Segal method)	Pereira *et al.* (2021)
Pure cotton cellulose	70	100	X-ray diffraction (ratio of intensities of crystalline regions and the whole sample)	Ioelovich (2021)
Flax fiber	67	64-85	X-ray diffraction (peak deconvolution)	Simon *et al.* (2022)

A semi-crystalline structure is defined as comprising a highly ordered fraction, a disordered amorphous domain exhibiting almost isotropic chain alignment and significant chain mobility (Molnár *et al*., 2021; Schäler, 2012; Termonia, 1995). The interphase between crystalline and amorphous regions, named paracrystalline fraction, is considered partially ordered and with a mobility even more restricted than the amorphous phase (Walczak, 2012). These three fractions have very different organization characteristics (Mazeau & Heux, 2003).

- the Tg of cellulose (Table 1-3) may be close (above 200 °C) to its degradation temperature (Al-Khalili *et al.*, 2023a; Paes *et al.*, 2010).

- this kind of material may have a complex glass transition, due to multi-domain phases, with a small change in heat capacity compared to conventional polymers, especially in the dry state (Al-Khalili *et al.,* 2023a; Liu *et al*., 2009; Paes *et al.*, 2010).

Moreover, in many studies, on plant cell wall extracts, cellulose is not pure and even if it is the main component, some residues of pectin or hemicellulose may impact the glass transition temperature determination.

Consequently, the DSC determination of the Tg for cellulose shows a wide range of data attributed to the Tg of cellulose (Table 1-3).

Table 1-3. Literature values for Tg or Tα for cellulosic materials with the respective methods used and their references.

	Tg (°C)	Water content (% w/w)	Method		Reference
Cellulose	220	~Dry	Experimental	DSC	Kargin *et al.* (1960)
Avicel	253	~Dry	Experimental	DSC	Goring (1963)
Cellophane	244				
Bleached spruce sulphite pulp	231				
Unbleached spruce kraft pulp	245				
Hollow filament rayon	237				
Cellulose	230	~Dry	Experimental	DSC	Back & Didriksson (1969)
Microcrystalline cellulose (MCC)	-34	~15 (w.b.)	Experimental	DSC	Szcześniak *et al.* (2008)
Cotton fiber	151	~2-3 (d.b.)	Experimental	DSC	Denham (2016)
Viscose fiber	145				
MCC	145				
Cotton cellulose	160-180	~4 (w.b.)	Experimental	DSC	Nam *et al.* (2020)
Cellulose (defatted date-pits)	136	3 (w.b.)	Experimental	DSC	Al-Khalili *et al.* (2023a)
Hydroxypropyl methylcellulose (HPMC)	161	1 (w.b.)	Experimental	DSC modulated	McPhillips *et al*. (1999)
MCC	160	~Dry	Experimental	DSC modulated	Picker & Hoag (2002)
HPMC film	160-175	~Dry	Experimental	DMA	Kararli *et al.* (1990)
Cellulose film	300	~Dry	Experimental	DSC | DMA	Kim *et al.* (2013)
Ball milled cellulose	117	0-19 (d.b.)	Experimental	DMA	Paes *et al*. (2010)
	205	~Dry	Couchman–Karasz	-	
Cellulose	-33	~11 (n.i.)	Theoretical - Kaelbe's approach	-	Salmen & Back (1977)

Cellulose rich material (from lemon peels)	43	Dry	Gordon-Taylor	-	Putri *et al.* (2024)
Cellulose	220	~Dry	Gordon-Taylor	-	Batzer & Kreibich (1981)
Cellulose	183	~Dry	Gordon-Taylor (ionic liquid)	-	Wu *et al.* (2015)
Cellulose	377	~Dry	Molecular modelling	-	Mazeau & Heux (2003)
Amorphous cellulose	227	~Dry	Molecular modelling	-	Chen *et al.* (2004)
Cellulose	63	-	Molecular modelling	-	Zhang *et al.* (2012)
Cellulose	357	~Dry	Molecular modelling	-	Mazeau (2015)
	247	5 (d.b.)			
Cellulose (cotton linters)	128	~ 4.5 (n.i.)	Experimental	Thermally stimulated currents (TSC)	Jafarpour *et al.* (2007)

n.i.: no information provided in the article, d.b.: dry basis, and w.b.: wet basis.

Denham (2016) determined the Tg of cellulose-rich materials with varying degrees of crystallinity, including cotton fiber, viscose fiber, and MCC. Cotton fiber possesses the highest crystalline index (CI) and exhibited the highest Tg among the materials studied. In addition, although viscose fiber (CI 65%) has a crystallinity index similar to the cellulose-rich material derived from defatted date pits (CI 63%) studied by Al-Khalili *et al.* (2023a), the latter demonstrated a lower Tg. This discrepancy can be attributed to the complex composition of the cellulose-rich material from defatted date pits, which also contains soluble fibers, hemicellulose and lignin. Some of these additional components (soluble fibers and hemicellulose) likely contribute to increase the molecular mobility within the sample, resulting in a reduced Tg.

Goring (1963) determined a phase transition between 231 and 253 °C (Table 1-3) by an unusual method consisting in measuring the softening temperature related to the height change of a cellulose powder column. In this study, the cellulose powder was transferred to a glass capillary compressed under constant load and heated at constant rate. The change of height was associated with the collapse of the powder into a solid plug. The thermal treatment causes the material to become rubbery or leather-like due to the glass transition.

Besides, molecular modeling may also be an interesting approach to determine the organisation of cellulose, of its hydrated structure as well as to determine its properties when experimental design failed to do it (Mazeau, 2015; Mazeau & Heux, 2003). Thus, applying

molecular modeling, Mazeau & Heux (2003) used a computational method to model native cellulose, considering it as a bulk native Iα and Iβ crystal phases with 16 (32 cellobiose units) and 18 chains (36 cellobiose units), respectively, and a solid amorphous phase. From this model, they estimated the Tg of dry cellulose around 377 °C (Table *1-3*). Chen *et al*. (2004) also produced models with one cellulose chain of 20 cellobiose repeat units to study the relaxation. The Tg observed in this model was around 227 °C, close to the experimental values reported in the literature (Back & Didriksson, 1969; Goring, 1963).

A Tg lower than with other modeling studies was found around 63 °C by Zhang *et al.* (2012), in exploring a model formed of multiple cellulose chains with 20 glucose units, arranged up and edge-to-edge. A more recent modeling study (Mazeau, 2015) determined the Tg of dry cellulose around 357 °C in a cellulose model similar to that used by Mazeau & Heux (2003), and this temperature decreased to 247 °C with increasing water content at 5% w/w, showing the plasticizing effect of water.

As observed even through modeling, the glass transition temperature of cellulose varies, as this depends on many parameters among which the cellulose structure/model used. A way to approach the high amplitude mobility in cellulose-rich materials, can be to use plasticizers in order to experimentally determine Tg in a temperature range that is non-destructive for the sample.

1.4.1.1. Impact of plasticizers

To overcome the difficulty to determine Tg_{DSC}, the impact of plasticizers has been used to reduce and shift Tg below the temperature of thermal decomposition (Ioelovich, 2016; Paes *et al.*, 2010; Xiao *et al.,* 2003).

Szcześniak *et al*. (2008) investigated the Tg of cellulose powder at different humidities by DSC, obtaining a very low value of Tg (25 °C) at 7 % moisture content (Table 1-3) (Figure 1-5). Salmen & Back (1977) applied a theoretical approach (Kaelbe's approach) to demonstrate the plasticizing effect of water on cellulose. This model is based on the cohesive energy of components and the predicted Tg of cellulose at 11% w/w of water was -33 °C.

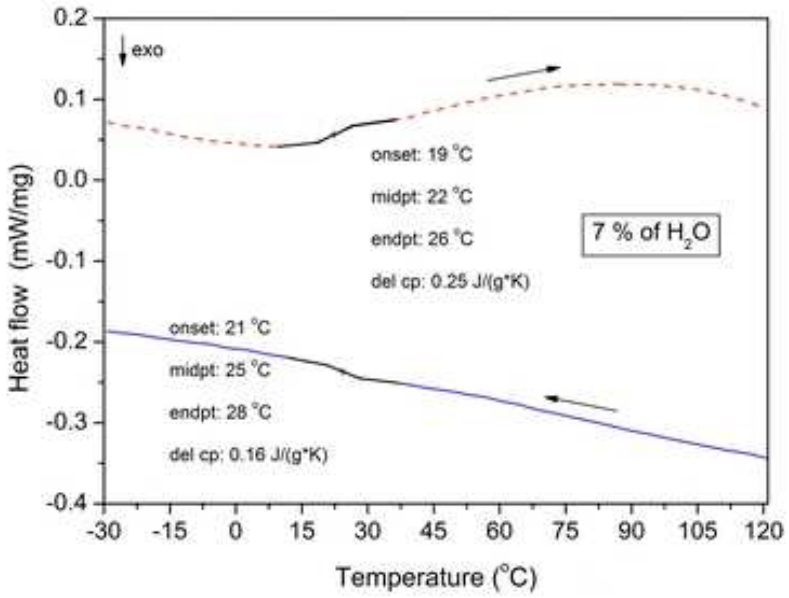

Figure 1-5. DSC measurements of cellulose pellets with 7% moisture content under argon atmosphere for heating (dashed line) and cooling runs (solid line). Reprinted with permission of Szcześniak *et al*. (2008). Copyright 2008, by Springer Nature.

Batzer & Kreibich (1981) investigated the Tg of cellulose from cotton fabric at various hydrations (5 to 60 % w/w water) and applied the Gordon-Taylor equation (*1-1*) to model the plasticizing effect of water although this equation is proposed for binary mixtures. Extrapolating the curve and based on Kargin *et al.* (1960), Tg was measured around 220 °C for dry cellulose and -113 °C for cellulose at 60% w/w water content (Batzer & Kreibich, 1981), but this last calculated value did not take into account the water freezing in the sample, that should induce a cryoconcentration of dry matter.

$$T_{gm} = \frac{x_s . T_{gs} + k_s . x_w . T_{gw}}{x_s + k_s . x_w} \quad (1\text{-}1)$$

Where Tg_m, Tg_s, Tg_w are glass transition temperature (K) of mixture, anhydrous solids, and water, respectively; x_s and x_w are the mass fraction of solids and water, respectively; and k_s is a constant.

Additionally, employing the Gordon Taylor equation in data obtained by Thermal Mechanical Compression (TMCT-DMA), Putri *et al.* (2024) identified the relaxation temperature of anhydrous cellulose-rich material derived from lemon peels. The determined relaxation temperature was around 40°C for anhydrous material, which was not measurable by DSC. Surprisingly, this temperature was significantly lower than expected for a cellulose-rich material characterized at low moisture content. It suggested that the Gordon Taylor equation is not the most suitable model for accurately describing the thermal behavior

(TMCT-DMA data) of this particular material which is not a binary mixture. However, a clear plasticizing effect of water was observed on the curves obtained.

Moreover, ionic liquids are useful plasticizers for polymers (Choi *et al*., 2011; Scott *et al.,* 2002) and can be used to dissolve cellulose-based materials (El Seoud *et al.*, 2021; Heinze, 2016). Wu *et al.* (2015) estimated the Tg of dry cellulose at 183 °C using ionic liquid (1-Butyl-3-methylimidazolium chloride (BmimCl)) as a plasticizer and applying the Gordon-Taylor modeling. Varying the concentration between 30 to 70 % w/w, Tg decreased from 8.7 °C to -18.3 °C. This solvent also increased the heat capacity which made the transition clearer.

Kim *et al.* (2013) determined the Tg of cellulose films by DSC applying step scan mode in which the sample is heated through small temperature increments (5 °C/min) and hold for a short interval, to be able to distinguish reversing heat flow (dependent on rate of change of temperature and heat capacity) and non-reversing heat flow (time and temperature dependent events). Through this method it is possible to detect the weak glass transition (reversing heat flow event) which can be hidden by non-reversing event (enthalpy relaxation, melting) in conventional DSC method (McPhillips *et al*., 1999; Picker & Hoag, 2002; Schick, 2009). The Tg is clearly observed in the reversing heat flow signal measured around 161 °C for HPMC (0.98% w/w water content) (McPhillips *et al.,* 1999). Similarly, Picker & Hoag (2002) found a strong transition at 160 °C for dried MCC.

1.4.2. Mesoscopic scale: exploring the dynamics and behaviours of molecular arrangements

Another experimental alternative to overcome the difficult identification of the glass transition of semi-crystalline materials is to use DMA, because mechanical changes are more pronounced than heat capacity change (Figure 1-6). Consequently, DMA can detect short-range motions (β, γ) before the main relaxation, and identify the onset of main chain motion associated with the glass transition (Paes *et al*., 2010; Patra *et al.,* 2021).

DMA is a dynamic method which measures Tα (with a frequency dependence) while DSC measures Tg (with thermal scanning rate dependence) and even if they are both used to measure the glass transition, they use different solicitations and can result in slight temperature differences (Torres *et al.*, 2019). However, at a frequency of 1 Hz in DMA, and 10 °C/min in DSC the results of both techniques may be comparable (Gracia-Fernández *et al*., 2010; Sakellariou *et al*., 1985).

DMA should always consider sample behavior at different solicitation frequencies, indeed a frequency effect on the relaxation temperature would ascertain the relaxational origin

of an observed phenomenon. The used frequency range allowed the activation energy (Ea) calculation (Equation(1-2) and this value represents the cooperativity of movements in the material: the lower the Ea, the lower the cooperativity of the associated movement, and thus the more local will be the mobility. However, the studies considering the frequency effect on cellulose primary relaxation remain scarce.

$$ln\, f = -\frac{Ea}{RT} + ln\, A \qquad (1\text{-}2)$$

Where f is the frequency (Hz), R is the gas constant (8.314 J/K.mol), T is the temperature (K), and A is a pre-exponential factor.

Kim *et al*. (2013) detected an α-relaxation at 300 °C (corresponding to the temperature of the tan δ maximum) for cellulose films whereas for HPMC, the observed relaxation temperature was below 200 °C (Table 1-3) and increased with increasing molecular weight and/or crystallinity (Kararli *et al.*, 1990). Also, with DMA, Paes *et al.* (2010) investigated the glass transition of ball-milled cellulose from eucalyptus and softwood in a lower temperature range (Figure 1-6b). Indeed, in this study a water-dependent mechanical relaxation was observed between 30 and 100 °C, and another one only weakly water dependent around 117 °C which was associated with an α-relaxation of a rigid fraction less sensitive to water content. The multiple peaks observed in this study suggests the presence of at least 2 domains with different dynamics; this heterogeneity could be correlated to the structure of the cellulose with amorphous zones, and amorphous-crystalline interfaces that have different sensitivities to water. Indeed, dynamics simulations showed cellulose matrices may have at least 3 kinds of organisations: crystalline, amorphous and paracrystalline (interphase regions between crystalline and amorphous zones) differing by their dynamics and physical properties (Kulasinski *et al*., 2014). Among these properties, the affinity for water is expected to decrease from amorphous to paracrystalline suggesting the co-existence of water-rich and water-poor zones in the matrix.

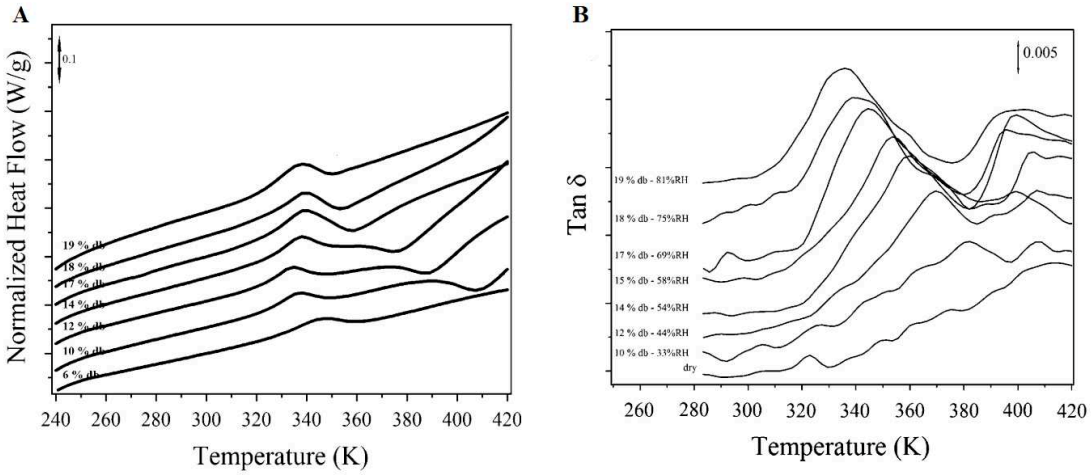

Figure 1-6. DSC analysis for ball milled cellulose (heating rate 10 °C/min) (a); tan delta as a function of temperature (K) from DMA analysis of ball milled cellulose (frequency 10 Hz) (b). Reprinted with permission of Paes *et al.* (2010). Copyright 2010, by Springer Nature.

Among cellulose plasticizers, trimethylphenyl ammonium hydroxide has been investigated at different concentrations using DMA (Kargin *et al*., 1960). The α-relaxation of cellulose with 10% w/w of plasticizer was around 180 °C (by the maximum temperature on the tan δ curve) and reduced to 65 °C with 37% of plasticizer. The Tα of cellulose without plasticizer was determined around 220 °C by extrapolating the solvent dependence of Tα to zero solvent concentration.

As previously observed for the Tg_{DSC} values, the Tα provided by literature spans over a wide range of temperature possibly as a result of a wide diversity of botanical origin, preparation and extraction processes and composition of the cellulose-based materials which are not always precisely given.

Dielectric spectroscopy (DRS) has been also used to study the relaxations of cellulose and its derivatives (Roig *et al.,* 2011; Diogo & Moura-Ramos, 2009; Einfeldt *et al.,* 2001; Einfeldt & Kwasniewski, 2002; Jafarpour *et al.,* 2007; Jafarpour *et al.,* 2009; Zhao *et al.,* 2019). It measures the rate of orientational dynamics distinguishing the molecular units of a polymeric system. The response of dielectric measurement is the sum of all dipolar moments of the system in their present orientation at one given temperature (Einfeldt & Kwasniewski, 2002) .The primary relaxation (α-relaxation) which is usually studied by DMA, and related to the glass transition, could not be observed by DRS for cellulose at low moisture content (Einfeldt *et al.,* 2004), only secondary relaxations were evidenced (Table 1-4).

Table 1-4.Literature values of transitions for cellulose measured by DMA, DRS and TSC methods, and the references citing these data.

	Water content (%w/w)	T_γ (°C)	Ea_γ (kJ/mol)	T_β (°C)	Ea_β (kJ/mol)	Freq (Hz)	Method	Reference
Amorphous cellulose	0	-123	36	-43	85	0.1	DMA	Montès *et al.* (1997)
MCC	0	~ -120	35	-	-	0.1	DRS	Jafarpour *et al.* (2007)
Cellulose	3	~-120	45	-50	75	1	DRS	Roig *et al.* (2011)
MCC	0	-130	~ 32	-70	~ 90	0.1	TSC	Jafarpour *et al.* (2007)
Cellulose	0	-135	~35	-65	~85	1	TSC	Roig *et al.* (2011)

Different varieties of cellulose (amorphous bead cellulose, Valonia cellulose, bacterial cellulose, regenerated cellulosic fiber: viscose and lyocell fiber) were investigated between 10 mHz to 1 MHz and in low temperature (-130 to 20 °C) range. In this frequency range, the predominant relaxation was a β-relaxation associated to local chain dynamics, and also a β_{wet}-relaxation for a collective motion of water-cellulose mixed phase, both were characterised by an activation energy below 100 kJ/mol as expected for secondary relaxations. The β_{wet}-relaxation disappears completely after drying (T>130 °C). At -30 °C, β_{wet}-relaxation of cellulose at 1% w/w of water content is observed at -1 Hz whereas β-relaxation presents a maximum around 5 Hz in a loss spectra obtained by dielectric spectroscopy. In this study, no significant structural influence on the local chain dynamics for different cellulose sources was observed. The relaxation intensity decreased with increasing degree of crystallinity (amorphous bead cellulose>bacterial cellulose>valonia cellulose) as expected from a decreasing amorphous phase contributing to the relaxation (Einfeldt & Kwasniewski, 2002).

A complementary technique for the elucidation of some characteristics of molecular mobility for cellulose-rich materials is thermally stimulated currents (TSC). DRS and TSC are both dielectric techniques, whereas DRS has isothermal nature and covers a wide frequency range, TSC requires a temperature scan and a narrow frequency range. Moreover, TSC is able to resolve a global distributed peak into its individual relaxation modes and determine the temperature-dependent relaxation time (Diogo & Moura-Ramos, 2009).

Contrary to DRS, TSC allows the determination of α-relaxation through the compensation phenomenon since it has been shown to characterize cooperative movements and thus to be related to the glass transition (Lacabanne *et al*., 1994). Cellulose showed a compensation

temperature around 128 °C for hydrated sample and 138 °C for dry sample with an Ea of 320 kJ/mol which corresponds to softening of the vitreous phase upon hydrogen bonds breaking. This result is comparable to the α-relaxation temperature determined by DMA for hydroxypropyl methylcellulose film and ball-milled cellulose shown in Table 1-3 (Jafarpour *et al.*, 2007).

In agreement with DRS (Einfeldt & Kwasniewski, 2002), two relaxations at -130 °C and -70 °C were attributed to γ- (side group reorientation) and β-relaxation (localized movements of the backbone) (Table 1-4) respectively (Jafarpour *et al.*, 2007).

1.4.3. Molecular scale: Dynamics of cellulose-rich products with time domain NMR

Nuclear magnetic resonance (NMR) relaxometry, also called time domain NMR (TD NMR), is a powerful technique to study the dynamics and interactions of molecules in various materials, including plant materials up to pure cellulose. TD NMR, when applied to pure cellulose, provides valuable insights into its molecular dynamics, structure, and interactions, without the complexities introduced by other components of plant cell wall matrix when applied to complex plant-based systems (Garvey *et al*., 2019; Ibbett *et al.*, 2014; Nyström *et al*., 1981; Suekuni *et al.*, 2022; Topgaard & Söderman, 2002).

Proton spin-lattice relaxation (T_1) and spin-spin relaxation (T_2) are the main parameters of TD NMR to characterize proton relaxations. T_1 relaxation correspond to longitudinal relaxation or spin-lattice relaxation and is related to the molecular reorientation or rotational motions of molecule controlled by viscosity at the scale of the proton (the lattice). T_2 relaxation is related to the transverse energy exchange process between close nuclear spins to neighboring other spins, inducing a decay of magnetization. Indeed, T_1 and T_2, reflect the timescales of energy dissipation by motions and the signal decay by magnetization transfer, respectively. Each matrix exhibits distinct T_1 and T_2 values (Figure 1-7). Small molecules undergoing rapid rotation, such as those found in liquids, typically possess extended T_1 and T_2 relaxation times. Conversely, in larger molecules and solid matrices, T_2 tends to decrease while T_1 shows an increase.

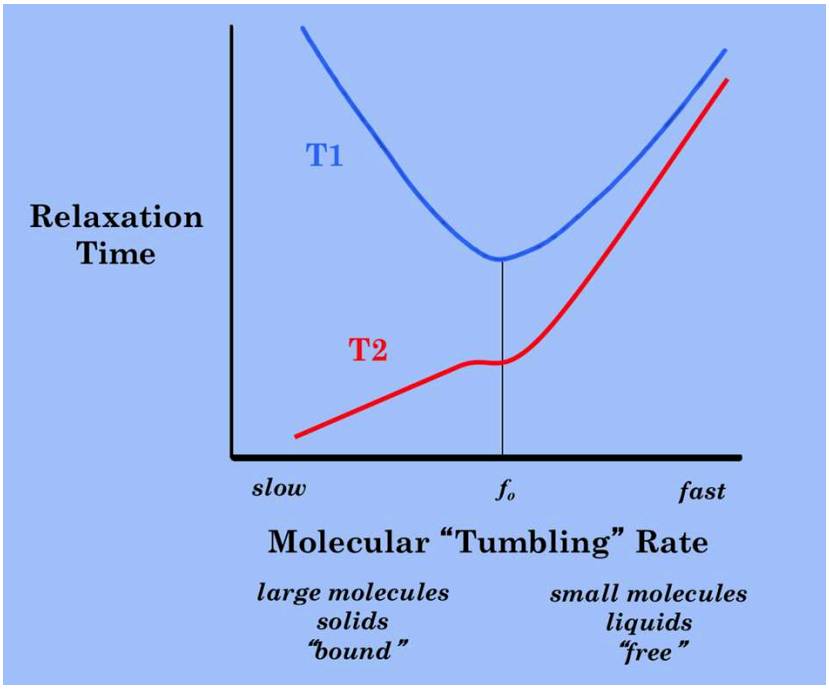

Figure 1-7. T_1 and T_2 as a function of molecular size and tumbling rate.

In cellulose materials, these relaxation times can provide information about the molecular mobility and interactions within the material, and they have been mainly determined to describe the interactions with water molecules. In fact, the main part of the transverse relaxation mechanism (measured by T_2) is proton exchange taking place between water and hydroxyl groups. Additionally, these relaxations T_1 and T_2 may be affected by both the conformation and mobility changes of molecules in the cellulose-rich materials (Hills *et al.*, 1991).

T_1 range reported in literature covers a width of time which depends on the hydration level of the cellulose-rich material: for low hydration levels (below 20% w/w), only one T_1 value is extracted from the NMR signal; it tends to be dependent on water content. For water contents ranging from dry to 7% w/w: the T_1 values decrease *i.e.* from 400 ms to 154 ms for cotton cellulose with an increase in water content (Grunin *et al.*, 2017), then for higher water contents (up to 20%), a reverse tendency can be observed with an increase of T_1 with water amount. Vittadini *et al.* (2001) studied the mobility of water in cellulose by solid-state ^{1}H and high-resolution ^{2}H NMR as a function of moisture content (0-19% dry basis) and found T_1 values increasing from 8 to 43 ms for water content increasing from 6 to 18% w/w. This "V" shape curves tendency of the T_1 as a function of water content was also observed upon material drying with a T_1 minimum for around 10% w/w water amount slightly changing for different cellulose-based materials (Topgaard & Söderman, 2002). The values of T_1 may also widely vary with sample preparation, *i.e.* the intact plant cell wall showing the shortest ^{1}H T_1 (120 ms

at 20% w/w water content), whereas the extracted cell walls at the same water content, exhibited longer T_1's of 900-1400 ms, values closer to bulk water properties (White *et al*., 2014). However, above 20% w/w water content, it was proposed, for complex matrices, that three pools of T_1 could be identified and attributed to water: i) adsorbed on crystals structure, for the first one, with T_1 below 10 ms), ii) in paracrystalline zones (T_1 from 5 to 20 ms), and iii) in fully amorphous zones (from 20 to 200 ms) (Wiesman *et al.*, 2018). These results suggest that the water distribution may be heterogeneous in a cellulose-based matrix according to the structural organization of molecules, even if at low water content, only one value of T_1 can be measured, which probably characterizes more the protons of the matrix solutes than those of water.

The proton NMR relaxation time T_2 enables to study water in cellulose materials bringing information about different water environments and by inference about the internal structure of the cellulosic matrix. Water within cellulose morphologies leads to the appearance of a separate proton NMR signal, which relaxes slower than the signal from the cellulose polymer protons, but quicker than the bulk liquid, as water molecules are able to interact with available cellulose sites (Garvey *et al.,* 2019). T_2 values can also be related to how tight water is bound to matrix hydroxyl groups: the shorter the T_2, the tighter the bonding, suggesting water molecules can be trapped in the interstitial space between the fibrils and thus exhibit limited proton mobility. Zhao *et al*. (2019) showed that, for the cellulosic samples with moisture content of 4.5% and 6.5% w/w, only one proton population with T_2 below 1 ms can be observed, which reveals that all water is adsorbed. Increasing with water content, their T_2 is noticeably larger, suggesting a larger mobility compared to that of anhydrous cellulose. For the samples at 11% and 28% w/w moisture, in addition to a main peak observed at T_2 below 10 ms, a tiny peak can be observed around 40 ms for both samples and an additional peak around 1000 ms only for the sample at 28% w/w. Thus, at high water content, three pools of water coexist in cellulose according to Zhao *et al*. (2019): water in tight interactions, directly bound with hydroxyl groups on cellulose (H-bonds), then water located not far from the cellulose chain, which is non-freezing water, and finally water which should be further away from cellulose molecules, thus able to freeze and that then can be considered as bulk water (Figure *1-8*). The detection of extra-population with different T_2 when water amount reached more than 10% w/w may be in relation with the ability of the material to show two secondary relaxations (β- and β_{wet}-) as detected with DRS. A given pool of water can contribute in quite different ways to a specific relaxation, and it can also play a different role in a variety of relaxations. Bulk water has negligible contribution to secondary relaxations (β-, γ-

relaxations), tightly bound water and non-freezing water are involved in the dynamics by acting as a part of the relaxing unit in β-relaxation and may play a role of plasticizer. However, these water-cellulose interactions and their contribution to relaxation cannot be applied to all kinds of cellulose, because they mainly depend on morphology and crystallinity (Zhao *et al.,* 2019).

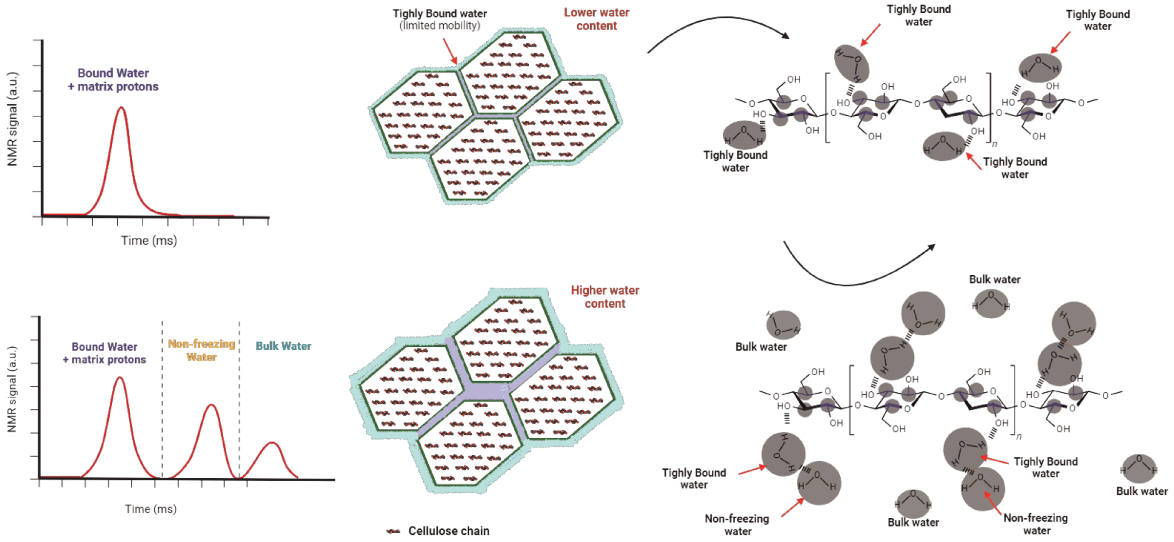

Figure 1-8. Types of protons distributed in the matrix based on Chen *et al*., (2022); Falourd *et al.*, (2022); Rahman *et al.*, (2021); Zhao *et al.,* (2019).

T_2, spin-spin relaxations, were found to slightly increase from 0.1 to 0.15 ms as a function of moisture content from 5 to 11% w/w in the cellulose matrix studied by solid-state H-NMR (Vittadini *et al.,* 2001). However, the relaxation time exhibited a sharp increase (values multiplied by 7) for moisture content varying from 11 to 19% w/w.

The determination of both T_1 and T_2 in cellulose-based materials gives a general view of the different range of mobility as function of water content : below around 5-10% w/w water, we may consider the water as structural water, strongly associated with molecules with a low mobility, then between around 9-19% w/w, the water may be heterogeneously distributed in association with different zones at the molecular level, playing in some zones the role of plasticizer and finally, above 20% w/w, the water shows almost bulk water properties. In cellulose extract, is still difficult to attribute the mobile zone to a specific component (pectin, hemicellulose, cellulose) but is probably more in relation to the physical state (vitreous/rubbery) of these components and to the amorphous/crystalline ratio. Moreover, the supra organisation of plant cell walls can expose spaces where water in high amounts (more

than 20% w/w wide), may be confined between microfibrils by capillary forces with some bulk water properties such as relatively high mobility.

1.4.4. Contribution of other plant cell components on dynamics of cellulose-rich cell wall material

The glass transition of plant cell wall material (CWM) is a complex phenomenon influenced by the contributions of various components. Although in citrus fiber, cellulose is the major component, pectin and xyloglucan play crucial roles in this dynamic process. Hence, investigating the individual glass transition temperatures of these components enhances our understanding of how they collectively influence the overall properties of plant cell wall material.

In contrast to cellulose, pectin is a water-soluble polysaccharide, leading to a pronounced impact of water content on its glass transition. Iijima *et al.* (2000) detected the glass transition of dry pectin at 37 °C and its melting peak (Tm) at 154 °C (Table *1-5*). Surprisingly, Lai *et al*. (2000) detected the Tg of pectin around 96 °C at 14 % w/w water content (Table *1-5*). No huge impact of degree methyl esterification was observed on Tg in both studies.

Xyloglucan has a cellulose-like β-(1,4)-D-glucose backbone with branches of xylose, galactose, and occasionally fucose groups. As a consequence, it has a Tg around 242 °C in dry state close to the degradation temperature (300 °C) (Table *1-5*) (Bergström *et al.*, 2012). This value was similar to that observed by Kochumalayil *et al.* (2010), Tα at 260 °C at a frequency of 1 Hz (Table 1-5).

Table 1-5. Literature values for Tg or Tα for pectin and xyloglucan with the respective methods used and their references.

	Tg (°C)	**Water content (%)**	**Method**		**Reference**
Pectin (high methoxyl)	37	Dry	Experimental	DSC	Iijima *et al*. (2000)
Pectin (intermediate methoxyl)	96	14	Experimental	DSC	Lai *et a*l. (2000)
Xyloglucan	242	Dry	Experimental	DSC	Bergström *et al.* (2012)

Xyloglucan	257	Dry	Experimental	DMA (1Hz)	Kochumalayil *et al.* (2010)

Notably, studies have suggested a strong and intimate interaction between cellulose and xyloglucan, while pectin is thought to engage with the cellulose-xyloglucan network through its pectic sugar side chains. As a consequence, pectin exhibits higher mobility compared to xyloglucan and cellulose. The dynamic properties of xyloglucans fall between the rigidity of cellulose and the increased mobility observed in pectins, highlighting the nuanced nature of these interactions within the intricate matrix of plant cell walls (Zhao *et al.,* 2014; Zykwinska *et al*., 2005).

1.4.5. Enthalpy relaxation

Glassy material is in a nonequilibrium state below Tg, and it will spontaneously approach a more stable state (Figure 1-9). This phenomenon is known as enthalpy relaxation or structural relaxation or physical aging which is induced by the residual local molecular motions of certain molecules or parts of polymer molecules in the glass (Struik, 1977; Yu, 2001). The concept of enthalpy relaxation is crucial when taking into account the physical attributes of an amorphous or semicrystalline material specially because it is accompanied by changes in macroscopic properties such as mechanical properties, density, transport properties (Kim *et al*., 2003).

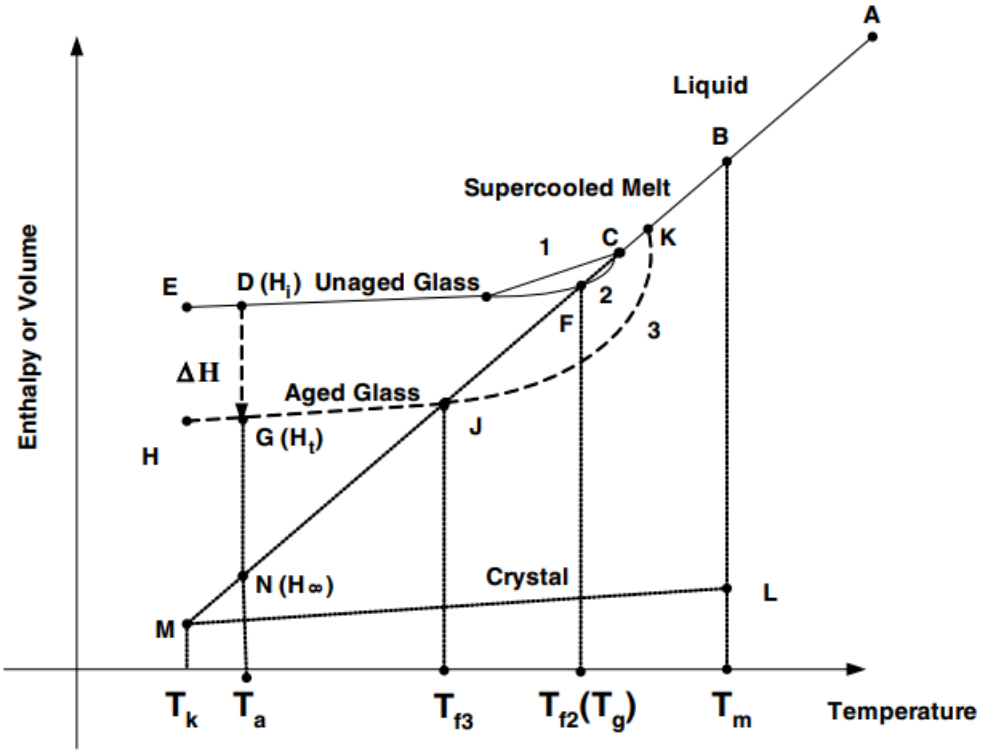

line AB: liquid line (melt)
line BC: supercooled melt line (the melting without crystallization T<Tm)
line BL: isothermal crystallization process at Tm.
line ML: crystal line.
Path ABCDE: cooling process after melting.
Path EDFCBA: reheating process (Tg and delta Cp of unaged sample were determined).
Path DG: isothermal aging process at aging temperature Ta

Figure 1-9. Enthalpy relaxation of amorphous solids. (Tk: Kauzman temperature or zero mobility temperature, where configurational entropy approaches zero, Ta: aging or annealing temperature; Tf_3: glass transition temperature of aged glass, $Tf_2(Tg)$: glass transition temperature of unaged glass; Tm: melting temperature.) Adapted from *Liu et al.,* (2007).

The loss of energy to achieve a more stable state is recovered during reheating of the glassy system by DSC, which allows the measurement of enthalpy relaxation. The size of the endothermic DSC peak is a measure of the amount of energy given up during relaxation in J/g (Liu *et al.*, 2006). Enthalpy relaxation depends on the thermal history, cooling rate to reach the amorphous glassy state, heating rate after aging, water content, aging time and temperature, and type of food components (Borde *et al*., 2002; Yu, 2001).

The enthalpy relaxation is nonexponential and nonlinear. Nonexponential means that the enthalpy relaxation process cannot be described by a simple relaxation function due to the microstructural heterogeneity of matrices. To describe this characteristic a stretched

exponential relaxation function named Kohlrausch-Williams-Watts (KWW) is used (1-3) (Hodge, 1994).

$$\Phi(t) = \exp\left[-\left(\frac{t}{\tau}\right)^{\beta}\right] \quad (1\text{-}3)$$

where Φ is the property of concern as function of time (t) or distribution of relaxation times, τ is the molecular relaxation time and β is a constant representing the distribution of relaxation times within the material ($0 \leq \beta \leq 1$). The smaller the β value, the more heterogeneous the distribution of molecular motion, whereas a β value of 1 corresponds to a single relaxation time with exponential behavior. In general, small molecules have higher β values than polymers (Le Meste *et al*., 2002).

The nonlinearity represents the changes of τ with time, since it depends on temperature and structural state of glass, and it is associated with previous thermal history. The nonlinear behavior of the enthalpy relaxation can be described by Tool-Narayanaswamy-Moynihan (TNM) expression (Equation (1-4)) (Hodge, 1994).

$$\tau = \tau_0 \exp\left(\frac{x.\Delta h}{R.T_a} + \frac{(1-x).\Delta h}{R.T_f}\right) \quad (1\text{-}4)$$

Where τ_0 is the relaxation time in equilibrium at an infinitely high temperature, Δh is the apparent activation energy in the equilibrium state above Tg, R is the ideal gas constant, T_f is the fictive temperature that represents the temperature at which material's structure would be in equilibrium with the liquid state at the actual temperature T (structural state), T_a is the aging temperature, and the parameter x ($0 \leq x \leq 1$) defines the relative contribution of temperature and structure to τ. If x is close to 1, τ mainly depends on the aging temperature (Hodge, 1994).

Enthalpy relaxation phenomena have been observed in the 40-80 °C region, as previously mentioned, on different types of matrices (wheat gluten, breakfast cereals, rice starch, fruits powders) and shown to disappear on subsequent scans (Borde *et al*., 2002). The total enthalpy results from the cumulative effect of various components, and their interactions (Borde *et al*., 2002; Yu, 2001). Thus, low values of enthalpy relaxation may be attributed to the complex structure of food powders due to the interactive forces between the components. For instance, starch and protein-based food have lower enthalpy relaxation compared to the small molecular food components such as sugar. Syamaladevi *et al.*, (2010) evidenced an enthalpy relation of raspberry powder ranging between 0.12-1.76 J/g whereas glucose and fructose ranging between 2-6 J/g.

In general, the enthalpy relaxation amplitude and position (peak temperature) increase with increasing aging time. In addition, the enthalpy relaxation increases nonlinearly and nonexponentially with increasing aging time indicating a kinetic nature of this phenomenon. Regarding the aging temperature, enthalpy relaxation is greater when the aging temperature is close to the Tg onset compared to aging at a temperature far below Tg. This occurs due to the fact that the movement of relaxation components becomes more restricted with increasing distance below Tg (Borde *et al.,* 2002; Hancock et al., 1995; Kim *et al*., 2003; Syamaladevi *et al.,* 2010).

In summary, the "recommended" storage temperature for food materials is significantly influenced by the glass transition temperature. Hancock *et al.* (1995) observed the necessity of cooling to temperatures at least 50 K below the glass transition temperature to minimize molecular motion (*i.e*. the configurational entropy and the free volume tend to zero), thereby stabilizing physicochemical properties during storage. This underscores the importance of controlling both glass transition and enthalpy relaxation to maintain food quality, particularly for amorphous or semi-crystalline solids prone to physical aging phenomena.

1.4.6. Multi-scale real-time techniques for cellulose water dynamics

In addition to the methods previously mentioned in this review, a broad array of key analytical techniques has also significantly enhanced the understanding of water dynamics in cellulose materials (Figure 1-10). The diverse range of analytical methods and protocols developed to investigate interactions between cellulose-rich materials and water reflects the complexity of these interactions and the need to examine them from different perspectives (Solhi *et al.*, 2023).

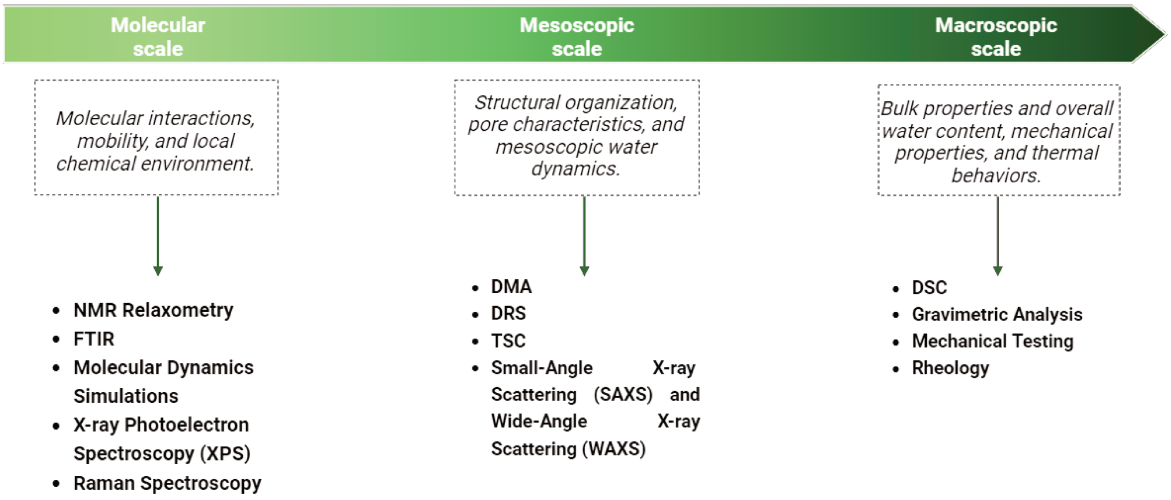

Figure 1-10. Analytical techniques for molecular mobility and dynamics enabling characterization of cellulose-rich materials at different scales. After Solhi *et al*. (2023).

Recent advances include the integration of Small-Angle X-ray Scattering (SAXS) and Wide-Angle X-ray Scattering (WAXS) with complementary techniques such as NMR, DMA, Fourier-Transform Infrared Spectroscopy (FTIR), Atomic Force Microscopy (AFM) and neutron scattering. Small-angle X-ray scattering (SAXS) and small-angle neutron scattering (SANS) are able to provide information on the structure and morphology of cellulose materials on a multiscale length (Liu *et al*., 2023; Okugawa *et al*., 2021; Paajanen *et al*., 2022) (Li *et al.*, 2021; Okugawa *et al.*, 2021; Paajanen *et al.*, 2022). Despite challenges in data interpretation, these methods provide the advantage of monitoring real-time changes: such as changes occurring upon hydration or drying. Moreover, integration of SAXS and WAXS with different methods facilitates a comprehensive understanding of cellulose-rich materials and water interaction spanning various scales (Solhi *et al.,* 2023).

For instance, Liu *et al*. (2023) utilized micro-focusing Grazing-Incidence Small-Angle X-ray Scattering (μGISAXS) along with Atomic Force Microscopy (AFM) to explore structural rearrangements and interphase development of cellulose materials during drying at nano- to microscale level, highlighting strong adhesion due to molecular interdiffusion and structural rearrangement at the interface. Similarly, Paajanen *et al.,* (2022) combined X-ray scattering with molecular simulations to investigate structural changes in wood at different hierarchical levels, providing a comprehensive view of moisture's impact on microfibril packing, orientation, and crystal size, which enhances the interpretation of nanoscale interactions between water and plant cell walls.

Okugawa *et al.* (2021) integrated SAXS, WAXS, and DMA to demonstrate the impact of water on the semicrystalline structure of cellulose. They observed the tan δ peak of regenerated cellulose between 240-279 °C in the dry state. This peak was higher in amplitude in the presence of water compared to organic solvents (ethanol, methanol, propanol, butanol, hexane, heptane, octane), indicating a greater partial loosening of the polymer structure and increased mobility of groups and small chain segments. SAXS experiments showed that the apparent crystal sizes and the width of microfibrils increased from 3.4 nm (dry state) to 6.3 nm (water regain of 100 % by weight), reflecting the influence of water on electron density between microfibrils and inter-microfibril regions. Their findings highlighted how water affects the density in amorphous regions, crystallinity, and mechanical properties such as tan δ, underscoring its critical role in modulating cellulose properties.

These studies collectively highlight the efficacy of integrating multiple analytical techniques to achieve an understanding of water's impact on cellulose-rich material structure and dynamics in real-time at multiple scales (atomic to mesoscale). Furthermore, advanced simulation techniques coupled to experimental data have also been employed to model biomolecular systems, elucidate mechanisms, and explore the interactions within plant cell wall materials (Gurina *et al.,* 2020; Lin & Wang, 2023; Singh & Li, 2019).

1.5. Research gaps and objectives:

Despite a wide range of studies on functionalization and applications of citrus fiber in the literature, little has been done about its stability upon storage. Some studies explore changes in physical properties such as color or microbial development during the storage; changes of functional properties have been in general associated with physical and structural modifications. Only one study addresses the relation of molecular mobility on citrus fiber matrix and storage (Putri *et al.,* 2024). Until now, the mechanism that causes the loss of functional properties of citrus fiber upon storage remains unclear. Hence, the objective of this research project was to investigate the mechanism responsible for functionality loss of citrus fiber upon storage. The originality of this work lies in the study of the physical state and dynamics of this biosystem at different scales (from molecular to macromolecular), with a focus on amorphous phase and its ability to evolve upon storage. The combined effect of temperature and humidity will be considered.

Considering the overall objective and the discerned gaps noted in the review of existing literature, three assumptions were formulated and for each an analytical approach associated:

Assumption a): Movement of segments and/or side groups of amorphous fractions of biopolymers may occur during the storage and facilitated in high relative humidity and temperature and may cause physical and chemical changes can happen in the matrix.

Approach: Investigate the dynamics of molecular mobility of the citrus fiber matrix and its evolution upon storage.

Assumption b): Throughout the storage, certain compounds or side groups of chains might migrate to the surface due to the molecular mobility present within the matrix. As a result, this migration may alter the availability of functional groups on the surface, thereby influencing hydrophilicity/hydrophobicity and charges. Such modifications can have implications for the material's interaction with water.

Approach: Analyze the chemical surface composition.

Assumption c): Chemical reactions such as oxidation, hydrolysis, polymerization, decarbonization, de-esterification may take place during storage, leading to alterations in functional groups. For instance, carbonyl groups may undergo reduction, converting aldehyde groups into carboxylic acids, and chain scissions can occur through the hydrolysis of anhydride linkages. Consequently, these modifications can impact the functional properties of materials. The occurrence of such chemical reactions can be influenced by storage conditions (temperature and water content) and molecular mobility.

Approach: Examine the occurrence of chemical reactions upon storage

Chapter 2. Materials and methods

Chapter 2. Materials and methods

2.1. Samples preparation and storage

Citrus fiber sample (CF) was prepared and provided by Cargill (Baupte, France). CF was extracted with isopropanol/water mixture using high pressure, then dried at pilot-scale, using a fluid-bed drier (GVW 32 / WSG200) for 7 hours with a maximum inlet temperature of 110 °C until product maximum temperature reached 50 °C. Its final dry matter content was 92% and its bulk density 0.41 g/cm^3.

The resulting material is composed of cellulose, hemicellulose, pectin, protein, and ash, in a mass proportion of 53.0 ± 7.4%, 20.0 ± 8.8%, 17.0 ± 2.4%, 5.0 ± 0.4% and 4.0 ± 0.2% g/100 g dry basis, respectively (data provided by the supplier).

To study the storage time effect, CF was stored for 360 days under two different controlled conditions of storage: in accelerated conditions (40 °C and 75% RH) (CF_A) and in room conditions (20 °C and 30% RH) (CF_R). Extensive characterization was done every 45 days to evaluate the effect of storage on its properties (Figure *0-1*Figure *2-1*).

A second set of citrus fiber, CFV corresponds to spent peels processed similarly to CF, but stored in 40-45% isopropanol/water until final drying. Aliquots were dried every 45 days over 360 days at lab-scale, using a Mini Glatt fluid-bed drier for 40-45 min, with an inlet temperature of 50 °C until sample temperature reached 40 °C. Its characteristics were determined in parallel with that of sample CF. All samples were in a powder form, milled and sieved with 50 µm size sieve (Figure *2-1*). Its final dry matter content was 96% and its bulk density 0.29 g/cm^3.

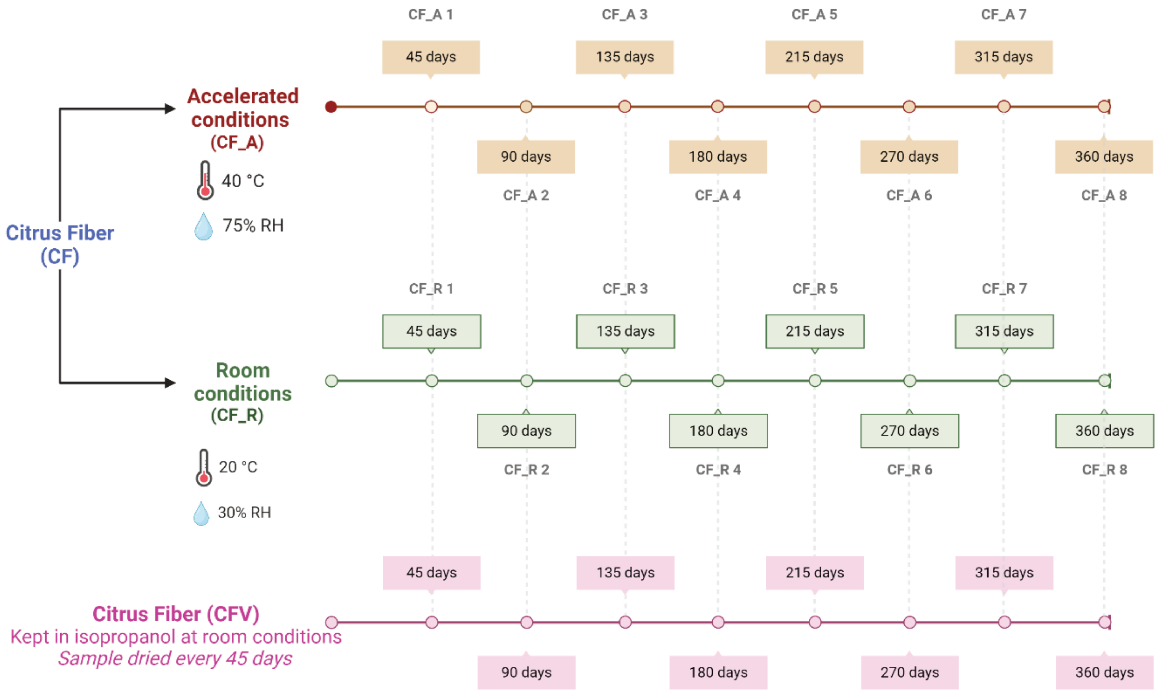

Figure 2-1.Samples preparation and storage.

To study the effect of moisture content on molecular mobility, the citrus fiber was equilibrated at 20.0 ± 0.5 °C in atmospheric chambers with relative humidity controlled by saturated salt-water solutions: P_2O_5 (~0% RH), KCH_3CO_2 (22% RH), $MgCl_2.6H_2O$ (33% RH), K_2CO_3 (46% RH), NaBr (58% RH) and NaCl (75% RH). Samples were used with different water content depending on the method applied, as detailed in each respective section. The water content utilized in this study was determined using vapor sorption analyzer SPS (ProUmid, Ulm, DE). measured on a dry basis.

2.1.1. Addition of plasticizers

In general, plasticizers are employed in order to break the hydrogen bonds between the polymers chains, increasing the molecular mobility, and consequently, reducing the glass transition temperature (Niazi *et al.*, 2013). The plasticizers in this study were chosen so as to interact with hydroxyl groups of cellulose: water, glycerol, glucose, triacetin and triethyl citrate (TEC).

To study the water plasticizing effect, citrus fibers samples were equilibrated for 7 days in different atmospheres controlled by either phosphorus pentoxide (P_2O_5) (0% RH) or

saturated salt-water solutions of potassium carbonate (K_2CO_3) and sodium chloride (NaCl) for RH 46% and 75%, respectively.

To investigate the plasticizing effect of glycerol, two different sample preparations were used. First, the powder sample was mixed with glycerol to form a paste (10% w/w of glycerol in citrus fiber), and this mixture was heated at 120 °C for 30 minutes. This temperature was chosen based on the identification of a potential glass transition in preliminary analysis around 120 °C. By maintaining the sample at this temperature, it facilitated a more open structure, enabling better interaction with the glycerol. Secondly, the mixture between sample and glycerol was made as film (Figure 2-2) with a glycerol/citrus fiber (w/w) and a 2% w/w of citrus fiber in water. The film solution was stirred at 700 rpm for 30 minutes, at room temperature and 100 °C. Afterwards, it was transferred to a polystyrene plate (10 x 10 cm) and dried at 50% RH and 35 °C for 24 hours (Romani *et al.,* 2021). Before the analysis, the samples, used as film or ground as a powder, were equilibrated at 0% RH over P_2O_5.

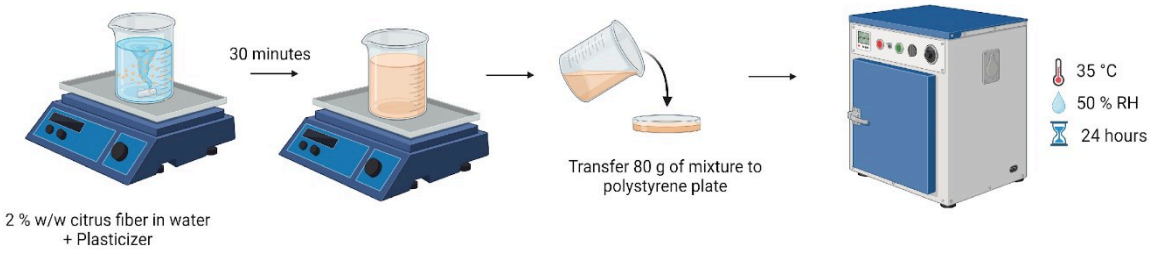

Figure 2-2. Film preparation process.

Similar to the preparation of glycerol films, other citrus fiber films were prepared by mixing citrus fiber powder with either glucose, triacetin or TEC. All of them were prepared at room temperature and at the same concentrations (10% w/w plasticizer/citrus fiber).

2.2. Tablet shaping protocol for viscoelastic measurements

For DMA analysis, the samples were shaped as tablets. The tableting process was performed on a manual hydraulic press (Specac Limited, England, UK), with a diameter of 13 mm. A mass of approximately 500 mg of the equilibrated sample was pressed, applying a compression force of 5 tons (0.4 MPa) (Domínguez-Robles *et al.,* 2019; Medina & Kumar, 2006). The obtained tablet was shaped with a blade and sanded until parallelepiped shape with dimensions approximately of 12 x 9 x 2 mm. Before and after compression, the samples were conditioned in a climatic chamber at 0% RH (over P_2O_5). The samples were coated with silicon oil to limit the dehydration during DMA analysis.

2.3. Characterization of Functional Properties of citrus fiber

2.3.1. pH

The pH of the citrus fibers solution at 2% w/w in distilled water was analyzed in triplicates according to the AOAC Official Method 981.12 (AOAC, 2005) using a pHmeter (PHM210 Radiometer Analytical S.A.; Villeurbanne, FR). Previously, the calibration of electrodes was done with buffer solutions pH 4 (Potassium hydrogen phthalate) and pH 7 (Potassium di-hydrogen phosphate/di-sodium hydrogen phosphate) from VWR chemicals (Pennsylvania, US), at 20°C. To measure the pH the electrode was immersed in the sample solution with constant stirring until the pH stabilized, at 20°C. The electrode was rinsed with distilled water between the calibration and measurements.

2.3.2. Water holding capacity (WHC)

The citrus fiber was used as received (packaged material at around 7% water content). It was suspended at 1% w/w in a buffer solution containing 0.1 M potassium dihydrogen phosphate (pH 6.9), under constant magnetic stirring for 30 min at 700 rpm. Subsequently, the suspension was transferred to a centrifuge tube and centrifuged at 3000 g for 10 min at 25 °C. The WHC was obtained by the weight of centrifuged pellet of hydrated fiber, and the result expressed by the weight of sediment per unit of weight of original dry powder (Equation (*2-1*) (Wallecan *et al.*, 2015; Zhang, *et al.,* 2020b).

$$WHC = \frac{(m_2 - m_1)}{m_0} \qquad (2\text{-}1)$$

where m_0 is the sample weight dried, m_1 is the weight of the centrifuge tube with sample prior to hydration, and m_2 is the weight of centrifuge tube with hydrated fiber. The water content was corrected to the initial dry mass.

2.3.3. Water swelling capacity (WSC)

Citrus fibers powder was dispersed in a buffer containing 0.1 M potassium dihydrogen phosphate (pH 6.9) in a concentration of 0.2% w/w and magnetically stirred for 30 min at 700 rpm. Afterward, the dispersions were transferred into a 100 ml graduated cylinder. The bed volume was measured after 24 h and divided by the initial dry powder weight introduced into the test tube (error of 5%) (Willemsen *et al.,* 2020).

2.3.4. Storage modulus measurement

A rheometer (MCR 302, Anton Paar, Graz, AT) was used to determine the viscoelastic properties of citrus fibers gel with Anton Paar H-PTD 200 device. A concentric cylinder (CC17) with a conical bottom of 16.667 mm diameter and cup of 18.088 mm diameter was used. The gap between the inner bob and the cup was 0.7 mm. For the measurement, a dispersion was prepared with 2% w/w of citrus fibers in a buffer containing 0.1 M potassium dihydrogen phosphate (pH 6.9), under magnetic stirring for 30 min at 700 rpm. Following this step, the solution was homogenized using an IKA Ultra-Turrax T25 Homogenizer (IKA, Staufen, DE) for 10 min at 9500 rpm. Before the analysis, the samples were left to rest for 30 min, at 20 °C. 5 g of solution were loaded in the cup, ensuring the complete immersion of the bob. All the measurements were carried out at 20 °C. The samples were pre-sheared for 30 s to ensure temperature equilibration and avoid possible effects of sample manipulation and loading history. The linear viscoelastic region (LVR) of the samples, the range in which the storage (G') and loss (G") moduli are strain independent at constant angular frequency, was identified with a constant angular frequency of 6.28 rad/s (1 Hz) and a strain sweep from 0.01 to 1000% strain. A similar procedure was carried out to investigate the dependency of the storage and loss moduli (G' and G") on the angular frequency, keeping the strain amplitude of 1% and varying the angular frequency between 628 to 0.628 rad/s (from 100 to 0.1 Hz). The viscoelastic characteristics of CF suspensions were obtained based on G' in a frequency sweep measurement at 6.28 rad/s and 1% strain (Debon *et al.*, 2012; Willemsen *et al.*, 2017). All the measurements were performed in triplicate and mean values are reported with standard deviation.

2.4. Moisture Sorption Isotherm

Sorption isotherms were determined in duplicate by automatic vapor sorption analyzer - SPSx-1µ (ProUmid GmbH & Co., Ulm, DE). Before the measurement, tare was done with empty aluminum dishes Rotilabo PP59.1 (Carl Roth, Karlsruhe, DE) at approximately 3% RH at 25 °C. Dried samples (150 ±1 mg) stored over P_2O_5 for 7 days were transferred onto aluminum dishes, placed in the equipment chamber at 0% RH until they achieved complete desiccation (≈ 0% RH and stable weight). The sample mass measurements were carried out at 25 °C from 0% RH to 90% RH, and then back down to 0% RH for adsorption and desorption processes following 10% RH increments. Two cycles of sorption and desorption were carried out. The minimum time per climate setting was 120 min whereas the maximum time was set at 25 h. Once the mass change was below 0.001%/60 min, the RH was set to the next

programmed humidity stage. The gas used for the analysis was nitrogen with a pressure around 4 bars, and the flux of gas changed according to the humidity of each step. The humidity in each step was also controlled using ultrapure water (Merck KGaA, Darmstadt, DE).

The time effect on water sorption of citrus fibers was evaluated based on parameters provided by the modeling and kinetic study.

2.4.1. Modeling methodology

The Guggenheim-Anderson-de Boer (GAB) model (Equation (*2-2*) was applied to fit equilibrium moisture content (X_{eq}) data against water activity (a_w) (Lewicki, 1997). C and K are model constants, and X_m is the monolayer moisture content (dry basis).

$$X_{eq} = \frac{CkX_m a_w}{(1 - ka_w)(1 - ka_w + Ca_w)} \quad (2\text{-}2)$$

To evaluate the goodness of fit to experiment the mean absolute percentage error modules (p) was calculated (Equation (*2-3*) (Owo *et al.,* 2017).

$$p(\%) = \frac{100}{n}\sum_{i=1}^{n}\frac{|X_{exp} - X_{cal}|}{X_{exp}} \quad (2\text{-}3)$$

where n is the number of experimental data points, X_{exp} are experimental values and X_{cal} are predicted values. It is generally assumed that a good fit is obtained when $p < 10\%$.

2.4.2. Kinetic study

The kinetic curves were obtained by plotting the percentage of mass gain against time. These curves were fitted with a double exponential model in order to extract the characteristics of the phenomenon (Equation (*2-4*) (Hill *et al.*, 2010) using OriginPro software version 2023 (OriginLab, Northampton, US):

$$X_{eq} = X_0 + X_1\left[1 - exp\,(-\frac{t}{t_1})\right] + X_2\left[1 - exp\,(-\frac{t}{t_2})\right] \quad (2\text{-}4)$$

Where X_{eq} is the moisture content after infinite time of exposure of the sample to a constant RH, X_0 is the moisture content of the sample at time zero (previous step), X_1 and X_2 are the moisture contents at infinite time associated with the fast and slow process, and t_1 and t_2 correspond to time constant of a fast and slow processes.

The percentage of X_1 and X_2 was calculated by the ratio of the absolute value of each component (X_1 or X_2) in relation to the sum of both. Moreover, K_1 and K_2 (in h^{-1}) are the inverses of t_1 and t_2.

2.5. Crystallinity index (CI) determination

Citrus fiber sample at time 0 (CF) and CF samples stored in accelerated conditions for 180 and 360 days (CF_A 4 and CF_A 8) were conditioned in a desiccator over P_2O_5 at 0% RH and 20 ± 5 °C for at least one week prior to CI measurement. X-ray diffractometry (XRD) curves were recorded in reflection mode by Bruker D2 Phases XE-T diffractometer (Bruker corporation, Massachusetts, US) at an operating voltage of 30 Kv and current of 10 mA. The angular region was scanned from 5° to 60° with an increment of 0.05° and radiation source of Cu (λ=1.542 nm) (Garvey *et al.,* 2005).

The CI was calculated by Segal method in which the height of the peak (I_{002}) at 2θ= 22.6° and the one at (I_{am}) 2θ=18° (Zain, 2014) are considered to calculate the crystallinity applying Equation ((*2-5*). The deconvolution of the XRD pattern with a Lorentzian-Gaussian function was calculated to obtain the heights of crystalline and amorphous peaks using OriginPro 2023 software (OriginLab, Northampton, US).

$$\text{CI}\ (\%) = \left[\frac{(I_{002} - I_{am})}{I_{002}}\right] x100 \qquad (2\text{-}5)$$

where I_{002} represents crystalline material, while I_{am} represents the amorphous material.

2.6. Identification of glass transition phenomenon in citrus fiber matrix

2.6.1. Differential scanning calorimetry (DSC)

The DSC experiments were performed on equipment DSC Q20 (TA instruments, Inc., New Castle, US), previously calibrated with indium (onset Tm = 156.6 °C). Around 5-10 mg of equilibrated samples were placed in an aluminum Tzero-pan (TA Instruments) which was hermetically sealed. A sealed empty pan was used as a reference. The analysis was carried out in six stages of heating and cooling, under a nitrogen atmosphere of 25 mL/min. Three heating scans were done at 10 °C/min: first, the sample were heated from 25 to 80 °C, to erase the thermal history and to study the endothermic event associated with enthalpy relaxation resulting from their storage; second and third were from -50 to 175 °C, to analyze the reversibility of the observed phase transition and determine the glass transition temperature. The samples were analyzed in triplicate.

The data were treated using Universal Analysis Software 2000 (Version 4.5A, TA Instruments, Inc., New Castle, US). The glass transition temperature of the samples was determined from the midpoint of the heat capacity change observed on the third scan at 10 °C/min.

The first derivative of the heat flow versus temperature was determined for the third heating. A peak analyzer (Origin2023, OriginLab, Northampton, US) was used to fit the heat flow first derivative signal to investigate the presence of different phases (i) and their respective glass transition temperature (Tg_i). The function used was Gaussian distribution functions (Equation (*2-6*). This approach is based on the idea that Gaussian distribution functions characterize the dH/dT versus temperature signal of a pure polymer or polymer fraction at the glass transition (Hourston *et al*., 1999).

$$G_i = \frac{\Delta C_{p,i}}{\Delta T_{g,i}\,(\frac{\pi}{2})^{1/2}} exp\left(-\frac{2(T - T_{g,i})^2}{(\Delta T_{g,i})^2}\right) \qquad (2\text{-}6)$$

The ΔTg,i corresponds to the full width at half maximum (FWHM) for a Gaussian.

2.6.1.1. Contribution of citrus fiber components to the glass transition temperature

Citrus fibers are complex matrices mainly composed of cellulose, hemicellulose (xyloglucan) and pectin and their physical properties such as the glass transition phenomenon for such as multicomponent system reflect the interaction between its components (Tolstoguzov, 2002). Considering it, the contribution of pectin (pectin from citrus peels – galacturonic acid ≥74% db., Sigma Aldrich, US) and xyloglucan (xyloglucan from Tamarind seed, Megazyme, IE) to glass transition temperature was investigated. The powders previously equilibrated at 0% RH (P_2O_5) were analyzed by DSC in the same conditions as citrus fibers.

2.6.2. Dynamical Mechanical Thermal Analysis (DMA)

The DMA analysis was performed with a Metravib VA-2000 Dynamic Mechanical Analysis System (Metravib, Limonest, FR) in tension-compression mode in the frequency range 0.5 – 40 Hz, and from 25 to 200 °C at 1 °C/min and a strain of 0.04%. Sample dimensions were approximately 12 mm of length, 9 mm of width and 2 mm of thickness.

The data were analyzed using Origin 2023 software (OriginLab, Northampton, US). To determine the activation energy (Ea) (J/mol), a curve ln frequency *versus* $1/T_{max}$ (K^{-1}) was

plotted and it was calculated by Arrhenius equation (1-2), T_{max} is temperature of the maximum of tan delta.

2.6.3. Study of molecular mobility at microscopic scale by nuclear magnetic resonance (NMR)

Time domain H-NMR (TD-NMR) was used to determine the water distribution in the sample and understand the mobility of water according to system composition. The measurements were carried out in a low field pulsed NMR Minispec mq20 Brüker (Bruker corporation, Massachusetts, US) with a resonance frequency of 20 MHz.

The citrus fiber at ~0% RH, 22% RH, 46% RH, 58% RH and 75% RH were transferred into a vial with an outer diameter of 8 mm and a height of 35 mm, sealed with a polypropylene cap (Merck KGaA, Darmstadt, GE). The vial containing the sample was then placed inside a glass tube with a 10 mm diameter and a 180 mm length (Bruker Corporation, Massachusetts, US) (Figure 2-3). The glass tube was sealed with a polyethylene cap and wrapped with parafilm to minimize moisture loss. The measurements at different relative humidities were made at 25 °C.

To study the effect of temperature, the analyses were carried out at different temperatures: 25, 40, 50, 60, 70, and 80 °C, at 75% RH. Thermal equilibration was ensured by waiting 10 min for each temperature adjustment before the experiment was started.

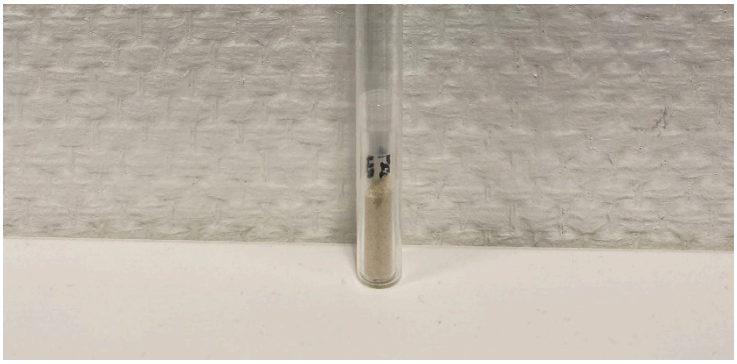

Figure 2-3. Sealed tube NMR with sample.

The spin-spin relaxation time (T_2) was determined using Carr-Purcell-Meiboom-Gill (CPMG) sequence (90-(τ-180- τ)$_n$). The delay time τ between 90° and 180° pulse was 40 µs. The number of echoes (n) was 200, 256 scans were accumulated to improve the signal-to-noise ratio and the recycle delay was 0.4 s (Figure 2-4). Moreover, a Free Induction Decay (FID) sequence was also applied to investigate the protons with low mobility. The FID signal was collected following a single 90° pulse with 64 scans and 2500 data points. The dead time was 14 µs. The acquisition window was 1.6 ms, and the recycle delay 2 s (Figure 2-4).

The spin-lattice relaxation (T_1) was determined with Inversion Recovery sequence. In these experiments, 16 scans were accumulated with a recycle delay of 1 s. The first and final pulse separations were 0.025 and 2000 ms, respectively. The number of points was 32, a sample window of 0.02 ms and with a delay sampling window of 0.05 ms (Figure 2-4). The experiments were replicated three times for each sample.

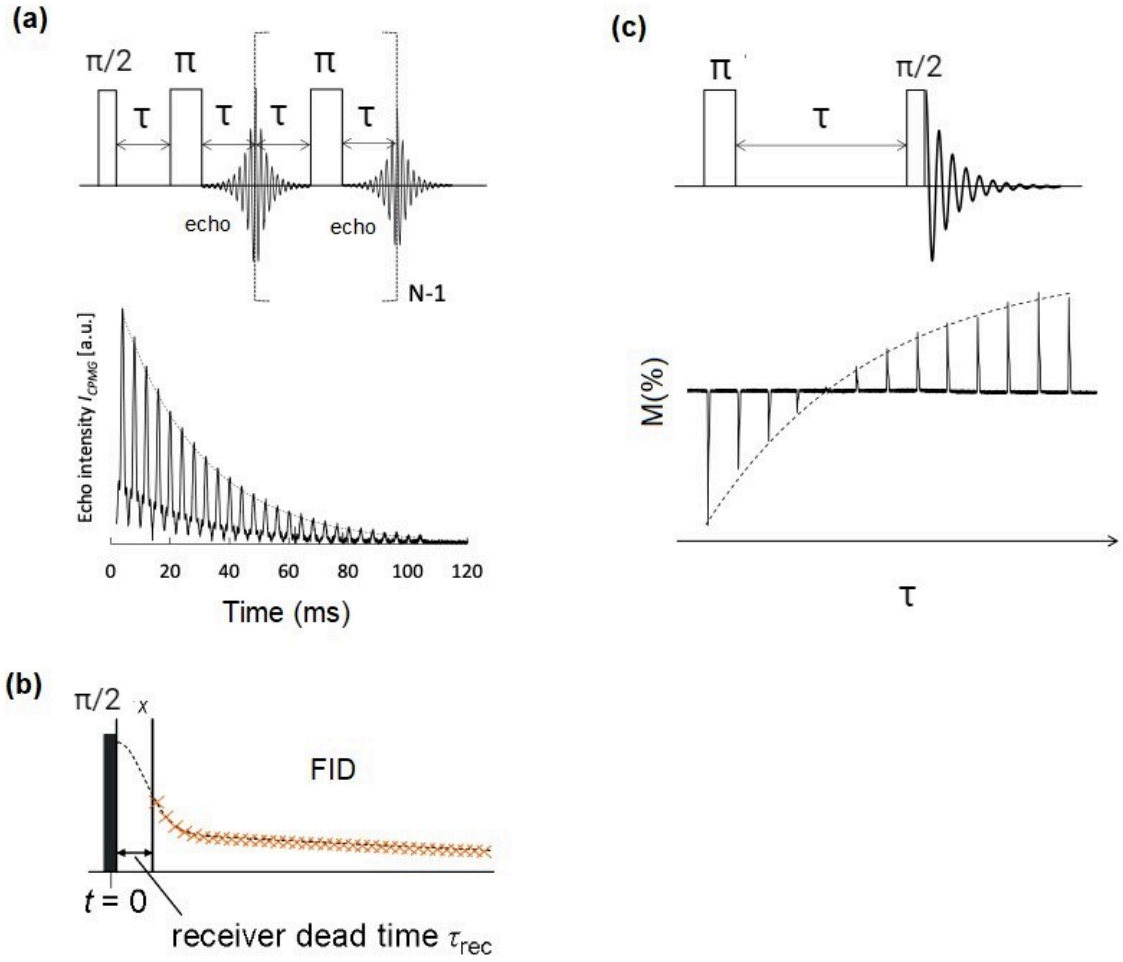

Figure 2-4. Pulse sequence and graphical representation of CPMG (a); FID (b); Inverse Recovery (c). Adapted from JEOL (2022); Schäler (2012).

The curves obtained for T_1 and T_2 were treated using software OriginPro 2023 (OriginLab, Northampton, US). T_2 relaxation decay curves were treated using software OriginPro 2023 (OriginLab, Northampton, US), applying biexponential (2-7) equation fitting the signal intensity to determine T_2 relaxation times. The magnetization decay of FID was fitted with a Gaussian Exponential function (2-8). T_1 was determined by fitting the curve with two exponential growth function (2-9).

$$M(t) = M_1.\exp\left(-\frac{t}{T_{21}}\right) + M_2.\exp\left(-\frac{t}{T_{22}}\right) \quad (2\text{-}7)$$

$$M(t) = S.\exp\left(-2\left(\frac{t}{w}\right)^2\right) + M.\exp\left(-\frac{t}{T_2}\right) \quad (2\text{-}8)$$

$$M(t) = M_1.\exp\left(\frac{t}{T_{11}}\right) + M_2.\exp\left(\frac{t}{T_{12}}\right) \quad (2\text{-}9)$$

where M(t) that represents the NMR signal intensity at time t, T_{11}, T_{12}, T_{21}, T_{22}, T_2 corresponds to the relaxation times measured in the time ranges window 1 and 2, respectively. M_1, M_2, S and M are proportional to the number of protons in the population corresponding to the measured relaxation times. To convert amplitude (a.u.) to percentage, S, M, M_1 and M_2 were divided by the total of protons (S+M or M_1+M_2, according to the signal used FID or CPMG), the resulting relative amplitudes (multiplied by 100 to be expressed in %). w is the standard deviation and controls the width of the Gaussian curve.

To correct M_1 and M_2 versus the total proton population, the percentage of %M_1 was multiplied by the previously determined relative amplitude of mobile fraction (%M). The same calculation was applied to %M_2. The resulting relative amplitudes to the total protons determined for citrus fiber matrix are named M_1' and M_2'.

2.6.3.1. Water contribution in the citrus fiber matrix with deuterium

To study the water contribution in the citrus fiber matrix and explore its structural feature, deuterium was incorporated into samples. To do so, citrus fiber powder was equilibrated at 20.0 ± 0.5 °C by placing the sample in a desiccator over a saturated NaCl in deuterated water (D_2O) for 2 weeks then dried in atmosphere with P_2O_5. This process was repeated two times to guarantee the complete replacement of hydrogen atoms by deuterium ones (Song *et al*., 2021).

Similar to applied to study the molecular mobility in citrus fiber, the curves obtained for T_2 and FID were treated using software OriginPro 2023 (OriginLab, Northampton, US), applying a biexponential (2-7) equation and a Gaussian Exponential function (2-8) to fit the signal.

To calculate the water contribution in the citrus fiber matrix using the FID data, the amplitude of total deuterium protons incorporated in the sample ($\sum A_D = S_D + M_D$) and the

amplitude of total water proton incorporated in the sample at 75% RH ($\sum A_W = S_W + M_W$) were used to determine the total of water proton in the matrix (Pw) (Equation (2-10).

To quantify the water contribution in the solid fraction (P_S), the amplitude of deuterium in the solid fraction (S_D) was subtracted from the amplitude of water in the same fraction (S_W), and the result was divided by the total of water protons in the matrix (Pw) (Equation (2-11). Similarly, to determine the contribution of water in the mobile fraction (P_M), the amplitude of deuterium in the mobile fraction (M_D) was subtracted from the amplitude of water in the same fraction (M_W), and then divided by the total of water protons in the matrix (Pw) (Equation (2-12).

$$P_w = \sum A_W - \sum A_D \quad (2\text{-}10)$$

$$P_S = \frac{S_W - S_D}{P_w} \quad (2\text{-}11)$$

$$P_M = \frac{M_W - M_D}{P_w} \quad (2\text{-}12)$$

The same approach was applied to determine the contribution of water in the two mobile fractions obtained by CPMG signal. The amplitudes used were M_{1D}, M_{2D}, M_{1W}, M_{2W} to determine the P_{WM}. To determine the contribution of water in each fraction M_1 and M_2, named P_{M1} and P_{M2}, the amplitude of deuterium in the less (M_{1D}) and more mobile (M_{2D}) fraction was subtracted from the amplitude of water in the same fraction (M_{1W} and M_{2W}), respectively, and then divided by the total of water protons in the mobile fraction (determined by CPMG sequence) (P_{WM}).

Additionally, to correct P_{M1} and P_{M2} relative to the total water contribution in the matrix, their amplitudes were multiplied by the water contribution in the mobile fraction (P_M). The resulting relative amplitudes (expressed in %) are denoted P_{M1}' and P_{M2}'.

2.7. Chemical characterization of citrus fibers

2.7.1. Chemical Characterization of citrus fiber

Spectral acquisition was performed in Perkin Elmer Spectrum 65 FTIR spectrometer equipped with Spectrum 10 Software version 10.6.2.1159 (Perkin Elmer, Massachusetts, US) and attenuated total reflection (ATR) cell with single reflectance germanium crystal. The spectral resolution was fixed to 4 cm^{-1}, the number of scans to 16 and the selected spectral

range between 4000 to 650 cm^{-1}, with a background spectrum recorded initially. The samples used were in dried powder form (equilibrated during at least 7 days at 0% RH over P_2O_5). The analyses were carried out in triplicate. Baseline corrections were done using the Spectrum software.

2.7.1.1. Principal component analysis

One of the most popular chemometric techniques for data reduction and exploratory analysis of high-dimensional data sets is principal component analysis (PCA). When interpreting FTIR spectra, which display band variety and complexity based on the sample source, this method is particularly helpful (Coimbra *et al*., 1999). Orange Data Mining Software version 3.33.0 (University of Ljubljana, SI) was used to perform PCA analysis. Each spectrum was preprocessed, normalized (standard normal variate (SNV)) and transformed from transmittance to absorbance. This method was applied to identify chemical changes during the storage time in citrus fibers.

2.7.2. Determination of oxidation index and degree of methyl esterification (DM) by Fourier Transform Infrared Spectroscopy (FTIR) analysis

The degree of methyl esterification was determined by FTIR as described by Yu *et al.* (2021) and Fellah *et al*. (2009). FTIR spectra were analyzed by Matlab version R2021a (MathWorks Inc., Massachusetts, US). Initially, the spectra baselines were corrected and transformed to absorbance. The region used to determine the degree of esterification was between 1750 and 1500 cm^{-1}. To determine the number of peaks used for deconvolution, the peaks from the second derivative were correlated with literature (Chatjigakis *et al.*, 1998; Liu *et al.,* 2022; Łojewska *et al.,* 2005). The region from 1750 to 1500 cm^{-1} was deconvoluted using the curve-fitting method with Gaussian function for the peak shapes. The specific bands at 1730 cm^{-1}, corresponding to esterified carboxyl groups (C=O) and 1610 cm^{-1} equivalent to free carboxyl groups (COO^-), were analyzed. The oxidation index and DM were calculated applying the area under the curve in Equations (2-13) and (2-14). The effect of preparation as well as the storage time was analyzed comparing the DM. The oxidation index was also calculated to study the impact of storage.

$$Oxidation\ index = \frac{A_{1730}}{A_{1610}} \quad (2\text{-}13)$$

$$DM\ (\%) = \frac{A_{1730}}{(A_{1730} + A_{1610})} \times 100 \quad (2\text{-}14)$$

Where A_{1730} is the area of the band around 1730 cm^{-1} and A_{1610} is the area of the band around 1610 cm^{-1}.

2.7.3. Determination of degree of methyl esterification (DM) by titration

The DM of samples was determined by the titration method based on Yu *et al*. (2021) with some modifications. 500 mg of samples was transferred to 100 mL of distilled water with 0.2 mL of ethanol. It was magnetically stirred for 30 minutes to complete homogenization. Then, it was titrated with 0.1M NaOH using phenolphthalein as indicator. The volume consumed was recorded as V_1. Afterwards, 10 mL of 0.5 M NaOH was added and stirred for 30 min, promoting the saponification reaction. Then, 10 mL of 0.5M HCl were added and stirred until complete disappearance of the solution pink color. The excess of HCl was titrated with 0.1 M NaOH solution, and the volume consumed was recorded as V_2. V_1 consists in the content of carboxyl without esterification whereas V_2 is the content of esterified carboxyl groups in the sample. The DM was calculated using the Equation (2-15).

$$\mathrm{DM}(\%) = \frac{V_2}{(V_1 + V_2)} x100 \quad (2\text{-}15)$$

2.8. Powder surface characterization by X-ray photoelectron spectroscopy

The elemental surface composition of citrus fiber samples was measured by X-ray Photoelectron Spectroscopy (XPS) Spectra were obtained using an XPS-Auger PHI 5000 VersaProbe (Physical Electronics, Minnesota, US) equipped with a mono-chromatic Al Kα X-ray source (hν = 1486.6 eV) operated at 50 W (15 kV, 3.3 mA). The measurements were performed in ultra-high vacuum (10^{-7} /10^{-8} Pa). The analytical area of analysis is a disc of 200µm of diameter and the analytical information depth between 3 and 4 nm. The spectra were collected at a take-off angle of 45 °.

Before analysis, samples were stored at 0% RH for 7 days, in a desiccator with P_2O_5 to remove the water. Afterward, the samples were outgassed under vacuum for 24 hours and pressed into indium foil.

A procedure was carried out to measure the repeatability of X-ray photoelectron measurement for citrus fiber samples. General spectra were obtained by 2 scans whereas high-resolution analysis of carbon (C 1s) and oxygen (O 1s) were an average of 2, 4 and 6 scans. Four repetitions were performed with the same sample. Because of potential degradation of

the surface during the X-ray exposure in high vacuum, the spectra were collected in the same order such that the extent of exposure was equivalent for all analyzed samples.

XPS spectra were treated using the CasaXPS version 2.3.24 software. The C 1s peak at 285 eV was used to calibrate the binding energy scale. The main elements (C, O, N, Na) detected on the sample's surface were identified by means of their respective binding energy. Besides, the carbon and oxygen peaks were decomposed into their main chemical bonds (C-C/C-H, C-O, C=O, O-C-O, O-C=O).

2.9. Statistical analysis

Values were expressed as means ± standard deviations of triplicate (n=3) and quadruplicate (n=4) determinations. Statistical analyzes of the experimental data were carried out by analysis of variance (ANOVA). Significant differences ($p < 0.05$) between samples were determined by Origin 2023 software (OriginLab, Northampton, US). The level of statistical significance was $p < 0.05$.

Chapter 3. Physicochemical characterization of citrus fiber

Chapter 3. Physicochemical characterization of citrus fiber

3.1. Research background and objectives

Citrus fiber, renowned for its water-binding and gelling properties (Lundberg *et al.*, 2014; Schalow *et al.,* 2018), relies on its composition and physicochemical properties for potential applications (Yapo, 2009). The processing methods can also impact fiber functionality (Nep & Conway, 2011). Characterization becomes imperative for a comprehensive understanding of the physicochemical and thermal properties with a view to defining processing conditions, applications and predicting its storage stability.

The material water vapor uptake at a given water activity, can be monitored by gravimetric method through the determination of sorption isotherm which gives water content as a function of water activity at constant temperature. This isotherm depends on structure and composition of the material, as well as pressure and temperature (Bejar *et al.*, 2012). Understanding sorption behavior is essential in food science and technology for designing and optimizing drying equipment, designing packages, predicting quality, stability, shelf-life, and calculating moisture changes that may occur during storage (Labuza & Hyman, 1998). It also provides insights into water properties and interactions with matrices (Goula *et al.*, 2008). Additionally, comprehending the water activity in relation to moisture content in powders is indispensable to prevent caking or agglomeration during various stages of processing, packaging, and storage (Peleg & Mannheim, 1977).

Additionally, grasping the dynamic properties of food components is of utmost importance, with molecular mobility playing a key role in controlling the thermodynamic and dynamic aspects of aqueous phase elements. These dynamics can be significantly impacted by factors such as hydration and temperature (Roudaut *et al.*, 2004).

Beyond exploring the physical-chemical aspects and water interaction, it is crucial to establish a correlation between this information and the chemical composition of the matrix. The variability of cell walls is influenced by factors such as species, developmental and maturity stages, plant organs, and environmental conditions. In addition, it is completely transformed during the extraction and processing. Infrared spectroscopy (IR) spectroscopy is an important tool to study cell-wall polysaccharides composition and monitor these variabilities (Coimbra *et al.*, 1999). Since there are differences between the surface and bulk composition it is also important to determine the chemical surface composition. X-ray photon electron spectroscopy (XPS) provides valuable insights about surface chemistry, bonding structure and composition of materials surfaces and interfaces (Greczynski & Hultman, 2020;

Johansson & Campbell, 2004). XPS, often combined with other techniques, has been a key technique to study surface composition in cellulose matrices like cotton, kenaf, flax, and hemp, enhancing understanding of material characteristics (Fras *et al*., 2005; Sgriccia *et al.*, 2008).

Hence, in this chapter, we initially determined the water sorption isotherm of citrus fiber and applied mathematical data treatment to investigate the kinetics, equilibrium, and hysteresis, aiming to gain a deeper understanding of moisture distribution in this matrix. Subsequently, the molecular mobility of citrus fiber was assessed at various scales, considering the influence of temperature and moisture content on its mobility. Recognizing the significance of chemical composition and processing history in shaping fiber functionality, the polysaccharide profile and the impact of sample preparation was quantitatively and qualitatively investigated, specifically focusing on the degree of methyl esterification, using IR spectroscopy. Furthermore, we delved into the surface composition of citrus fibers through XPS, taking into account the effects of their preparation, as surface composition is pivotal in influencing functional properties. Physicochemical characterization serves as an initial insight into the matrix, laying the foundation for subsequent exploration into the effects of storage and the associated mechanisms.

3.2. Results and discussion

3.2.1. Water sorption behavior of citrus fiber

The experimental sorption isotherm for citrus fiber is shown in Figure 3-1a. The curve has a sigmoidal shape classified as isotherm type II by Brunauer *et al*. (1940). A similar shape has previously been observed for cotton linter, MCC and α-cellulose (Xie *et al.*, 2011a), papaya seed (Rosa *et al.*, 2021), date pits (Al-Khalili *et al.,* 2023b), cassava starch (Perdomo *et al*., 2009), bacterial cellulose (Cybulska *et al.,* 2023), and rhizome from fresh red water lily (*Nymphaea x rubra*) (Phahom & Roudaut, 2023). It may represent an amorphous and porous structure, and may be associated with multilayers at the internal surface of material (Andrad*e et al*., 2011; Perez-Pirotto *et al.,* 2022). On the opposite, by-products from citrus and other fruits have also shown type III sorption isotherm (Bejar *et al.*, 2012; Castel *et al.*, 2023; Perez-Pirotto *et al*., 2022; Tejada-Ortigoza *et al*., 2017), characteristics of high fiber, sugar and protein content, and it is mainly a result of the weak interactions of vapor with the material surface.

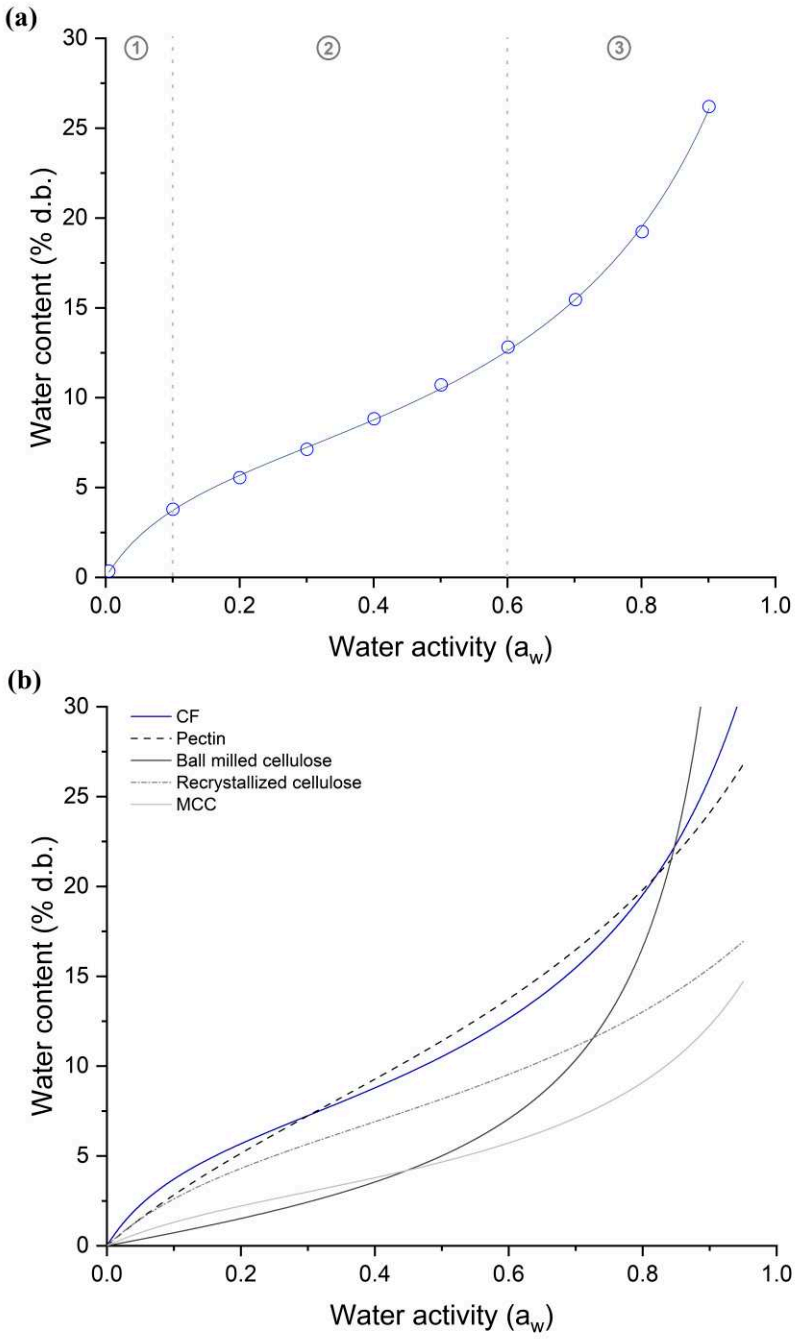

Figure 3-1. Water sorption isotherm of citrus fiber (CF) time 0 at 25 °C and predicted values by GAB model (a); theoretical sorption isotherm of pectin, ball milled cellulose, recrystallized cellulose and MCC calculated by GAB equation compared to experimental sorption isotherm CF time 0 at 25°C (b) (Espino-Pérez *et al.*, 2016; Paes *et al.*, 2010; Panchev *et al.*, 2010).

According to Roos (2006), a sorption isotherm can be divided in three different regions. In the case of citrus fibers (Figure 3-1a), the region 1 (a_w<0.1) represents the water strongly associated with hydrophilic biopolymers (pectins, hemicelluloses and protein), classified as monolayer. The region 2 (around 0.1<a_w<0.6) corresponds to the water with less interactions, named multilayer. The region 3 (a_w> around 0.6) is correlated with the bulk or solvent water

and solvent filling the void capillaries and macro-capillaries when the material is exposed to high moisture content (Hill *et al.,* 2009; Phahom & Roudaut, 2023).

Comparing the predicted values by GAB model of CF, pectin, and different types of cellulose Figure 3-1b, pectin presented the most similar sorption isotherm curve to CF. Recrystallized cellulose and MCC had a type II sorption isotherm like CF and pectin, but with an inferior equilibrium moisture content (EMC) at a_w 0.9. The EMC of pectin at 90% RH was 34% d.b. higher than CF (26.2% d.b.) and cellulose values (ball milled 24.1% d.b., recrystallized cellulose 15.4% d.b. and MCC 12.3% d.b.) (Table 3-1). The intermediate EMC value of CF suggests the contribution of pectin and cellulose in water absorption.

The composition of citrus fiber can influence water adsorption. CF is mostly composed of cellulose which is made of linear chains of glucose aggregated into microfibrillar units. Although cellulose has a high content of OH, only a part of it is available to interact with water (Hatakeyama & Hatakeyama, 2000). The hemicellulose and pectin are predominantly amorphous, consequently, they more easily adsorb water (Einhorn-Stoll *et al.*, 2020; Hill *et al*., 2009).

Besides the influence of each polysaccharide, it is important to consider the overall interaction between them. In the primary cell wall, the network formed between polysaccharides influences the surface, diameter, crystallinity, and organization (structure and conformational rearrangement) of cellulose fibers. Consequently, there is an impact on mechanical and viscoelastic properties as well as on the ability of the material to accumulate water (Cybulska *et al.,* 2023; Szymańska-Chargot *et al.*, 2017).

To better understand the contribution of polysaccharides in water sorption, Cybulska *et al.* (2023) used a biosystem with bacterial cellulose, soluble pectin and several types of hemicellulose (arabinan, rhamnogalacturonan I, arabinoxylan, xyloglucan and glucomannan). From that, they observed that pectin increases the availability of hydrophilic sites instead of increasing the number of it since a system of bacterial cellulose and pectin adsorbs the same quantity of water than only bacterial cellulose, however, in a shorter time. Additionally, xyloglucan showed to have the higher water adsorption capacity compared with different hemicelluloses, reaching 33% d.b. EMC at a_w of 0.95, whereas the others showed water content around 26% d.b..

Determining the crystallinity of the material may provide more information about its structure and aiding understand its behavior concerning water sorption. The amorphous fraction of the samples play an important role on the water interaction (Paes *et al.*, 2010; Xie *et al*., 2011a): EMC at $a_w \geq 0.90$ is inversely proportional to crystallinity index (Table 3-1).

Cotton linter has the highest CI (88%) and the lowest EMC of 14.2% d.b. at a_w 0.95, whereas the EMC of citrus fiber a_w 0.90 was 26.2% d.b. which presents a CI around 71%. It was expected that CF would show a lower EMC based on its CI, close to that observed for α-cellulose (20.6% d.b.), other components such as pectin and hemicellulose, as previously mentioned, might have contributed to increase its water absorption.

Thus, EMC can be influenced by the composition, crystallinity, and organization of the material.

Table 3-1. Crystallinity index and water content at high aw for different cellulose-rich fibers.

Material	**CrI**		**Water content**		
	Value (%)	**Reference**	**A_w**	**Value (% d.b.)**	**Reference**
CF	71 ± 2	-	0.90	26.2	-
Cotton liner	88	Xie *et al.* (2011b)		14.2	
α-cellulose	69	Xie *et al.* (2011b)		20.6	Xie *et al.* (2011b)
MCC	82	Mihranyan *et al.* (2004)		16.9	
Jute	59	Bashar *et al*. (2019)	0.95	24.6	
Flax	67	Simon *et al*. (2022)		19.4	Xie *et al.* (2011a)
Hemp	57	Tanasă *et al.* (2020)		25.0	
Sisal	57	Poletto *et al*. (2014)		25.4	

3.2.1.1. Equilibrium

GAB model was accepted as a good model to describe the sorption data of CF showing a correlation coefficient (r^2) of 0.991 and a p-value around 3.1 ± 0.1 % (Figure 3-1a) and the model allowed the comparison of different plant cell wall components (Figure 3-1b). The monolayer (Xm) indicates the amount of water (Table 3-2) strongly adsorbed to specific sites at the surface, and which can be correlated to the active water sorption sites availability (Owo *et al.,* 2017). CF showed a monolayer value of 7.0 ± 0.0 g of water/g of dry sample; almost the same for recrystallized eucalyptus cellulose, which can be explained by both being semi crystalline materials (Table 3-2).

The Xm value for CF was expected between that of cellulose and pectin due to the contribution of its components in the interaction with water. However, the citrus pectin mentioned in Table 3-2 has a lower Xm, close to that observed for cellulose nanocrystals (CNC). According to Panchev *et al*. (2010), pectin exhibits a complex mechanism of water sorption not only dependent on the polar groups of macromolecular backbone but also on the

chemical composition of its matrix resulting in a lack of correlation between the pectin structural characteristics and water sorption parameters. Moreover, addition of hydrophilic compounds decreases Xm (Poirier-Brulez *et al.*, 2006) so it is not surprising that a lower value for pectin was found because pectin materials can be considered as more hydrophilic than cellulose or CF. Based on the low content of pectin, the studied CF showed a relatively high Xm closer to that of cellulose than pectin. Furthermore, the lack of information in the literature related to the equilibrium of water sorption in xyloglucan (the main hemicellulose present in CF) makes it complex to associate water adsorption as a monolayer in CF with its composition.

Table 3-2. Fitting results of moisture sorption isotherm data with GAB models for citrus fiber in the present study, cellulosic materials (MCC, CNC, paper, eucalyptus cellulose) and pectin from published data.

Sample	**Xm (g H_2O/g d.b.)**	**C**	**K**	**References**
CF	7.0 ± 0.0	10.6 ± 0.1	0.83 ± 0.00	-
Microcrystalline Cellulose (MCC)	3.4	6.1	0.82	Espino-Pérez *et al*. (2016)
Cellulose nanocrystals (CNC)	3.1	6.1	0.98	
Paper	4.1	9.6	0.67	Bedane *et al.* (2015)
Eucalyptus ball milled cellulose	11.0	4.4	0.67	Paes *et al*. (2010)
Recrystallized eucalyptus cellulose	7.0	7.7	0.65	
Citrus pectin	3.96	1.8	0.99	Panchev *et al*. (2010)

The C constant represents the strength of the bond between water molecules of the monolayer and the binding sites on the surface of adsorbent (Chang *et al.*, 2019; Muzaffar & Kumar, 2016). Citrus fiber showed a C value of 10.6 similar to paper and relatively high compared to other celluloses and pectin suggesting strong water binding with surface active sites in the monolayer.

On the other hand, the K value represents the energy of the interaction of water molecules in multilayer with the adsorbent (Chang *et al.*, 2019; Muzaffar & Kumar, 2016). A

K value close to 1 means that the multilayer has properties of bulk water, hence, citrus fiber showed a K of 0.83, indicating a multilayer property more of a bulk liquid.

3.2.1.2. Hysteresis

The hysteresis is the difference between the phenomenon of desorption and adsorption. The hysteresis loop depends on the nature and state of the matrix: structure and conformation change upon sorption/desorption may alter the accessibility of polar sites reflected in differences between the adsorption and desorption isotherms (Al-Muhtaseb *et al*., 2002).

The hysteresis of CF is exhibited in Figure 3-2, at higher water content upon desorption is observed through the whole range: with an increase from the lowest a_w up to 0.4 to reach a maximum value of 2.1%, similarly to the behavior of orange peel (Tejada-Ortigoza *et al.,* 2017). The highest point of hysteresis observed with CF is between that obtained with sugar and/or high pectin-rich matrices such as raisins a_w 0.3 (very high sugar content) and starchy matrix (rice) a_w around 0.7 (Al-Muhtaseb *et al.,* 2002).

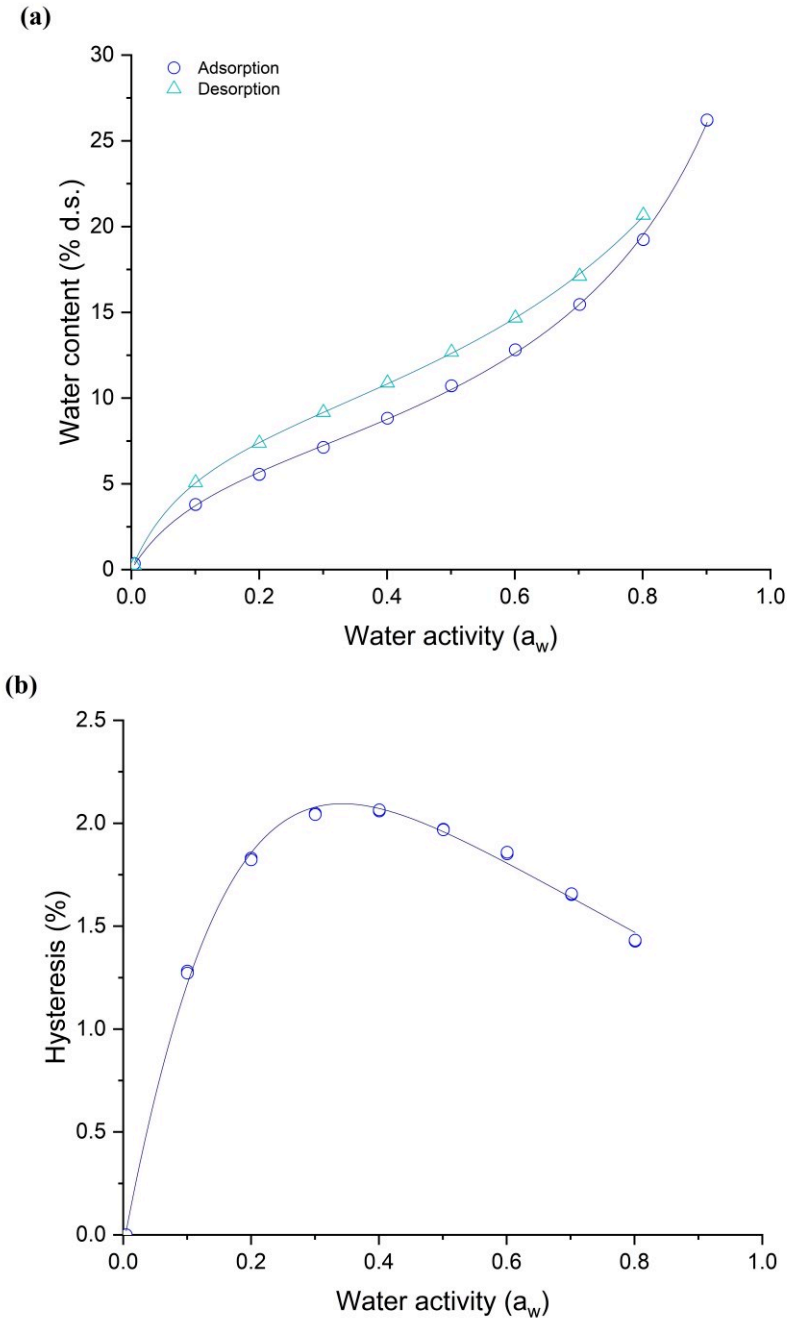

Figure 3-2. Adsorption and desorption points at equilibrium and theoretical GAB curves for CF at 25 °C (a); water content hysteresis (% g/100g d.b.) between sorption and desorption for CF sample time 0 at 25 °C (b).

As previously discussed, during the water adsorption phase, water molecules penetrate the matrix, causing the structure to expand and create nanocapillaries to accommodate them. Conversely, in the desorption phase, the matrix contracts, leading to the collapse of these nanocapillaries as water molecules exit the structure. The water content in equilibrium during desorption exceeds that during adsorption, indicating the formation of a capillary-pore system, increasing hysteresis. However, the decrease of hysteresis at a_w>0.4, possibly occurs due to

the contraction of small pores during equilibrium desorption. This hysteresis strongly suggests changes in the absorbent structure during both processes (Grunin *et al.,* 2019).

The GAB model also describes well the desorption process since p-value is ~2.5% (Table 3-3). Comparing the mathematical modelling of the experimental data of ad/absorption and desorption (Table 3-3), the monolayer moisture content (X_m) of desorption is expectedly higher than for adsorption, signifying a higher number of active sites (specific locations on a material's surface where molecules, such as water or gases, can bind or adsorb) on CF surface in desorption process. The C parameter is higher in desorption than in adsorption, indicating that the quantity of water in monolayer is higher in desorption than in adsorption and it is more strongly bonded in the desorption process than in adsorption. The lower value of k in the desorption process suggests a lower quantity of bulk water in multilayer.

Table 3-3. Values from GAB model applied to adsorption and desorption curve of CF time 0 at 25 °C.

	X_m (g H_2O/g d.b.)	**C**	**k**	**p-value (%)**
CF sample – adsorption	7.03	10.59	0.82	3.15
CF sample – desorption	9.04	13.61	0.73	2.48

A similar behavior was observed in cotton cellulose samples, in which the monolayer capacity increased from adsorption (3.19%) to desorption (3.73%) (X_m value), and the k decreased from 0.71 to 0.66. According to Grunin *et al.* (2019), these changes may be associated with the increase of total specific surface area for a sample subjected to adsorption and subsequent desorption, and a slightly decreased degree of crystallinity.

3.2.1.3. Kinetics

The water sorption of CF sample can be described by two processes (Figure 3-3), in which the amount of water corresponding to a fast and a slow process can be associated with X_1 equal to 72% and X_2 equal to 28% of total water adsorbed, respectively. A greater quantity of sorbed moisture is thus associated with the fast process. X_0 ranged from 1 to 19% depending on a_w. The fast process is generally associated with the adsorption of water in the most accessible sites: such as amorphous regions, polar groups of the external surface and results in the formation of monolayer. The slow process is related to the water sorption onto the inner regions, crystallites and constitution of a multilayer (Cybulska *et al*., 2023).

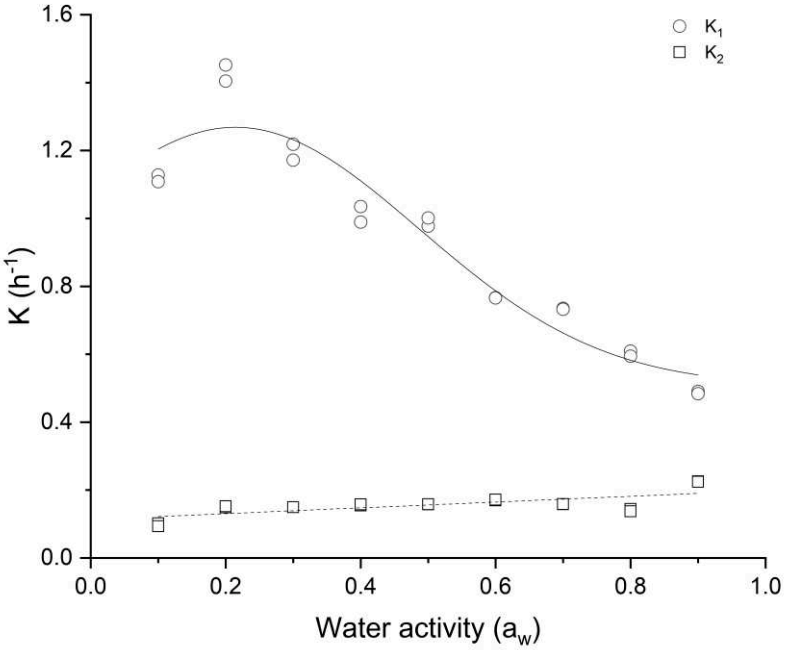

Figure 3-3.Water sorption kinetic constants of CF mathematically (2-4) extracted from sorption data obtained at 25 °C for different water activities.

As can be seen on Figure 3-3, K_1 showed a maximum adsorption rate around a_w 0.2. Afterwards, the adsorption rate dramatically decreased. According to Guillard *et al.* (2004), the decreasing adsorption rate (or diffusivity) can be attributed to the reduction of surface porosity. Water is adsorbed at the surface and forms a gel-like barrier to water diffusion which induces the reduction of K_1. Meanwhile, K_2 slightly increased versus a_w showing that kinetics of water diffusion in the material is the limiting parameter with lower K_2 values compared to K_1 but as expected, this diffusion increases slightly with an increase of water content of the matrix.

3.2.2. Effect of sample shape on physical state

To study the molecular mobility of CF at different scales, three different methods were used: DSC, DMA, and NMR. Each method has a unique principle, as well as requires an adequate sample shape. Based on that, the citrus peel fibers were used either as a powder and film for DSC, as a powder for NMR analysis, or as a tablet for DMA analysis.

To verify the effect of the shaping process on the sample's physicochemical properties, the sample was analyzed in triplicate by DSC for the three different shapes (Figure 3-4). The glass transition temperature (Tg), ranging from 116 to 128 °C, was not statistically different ($p>0.05$) between any shapes.

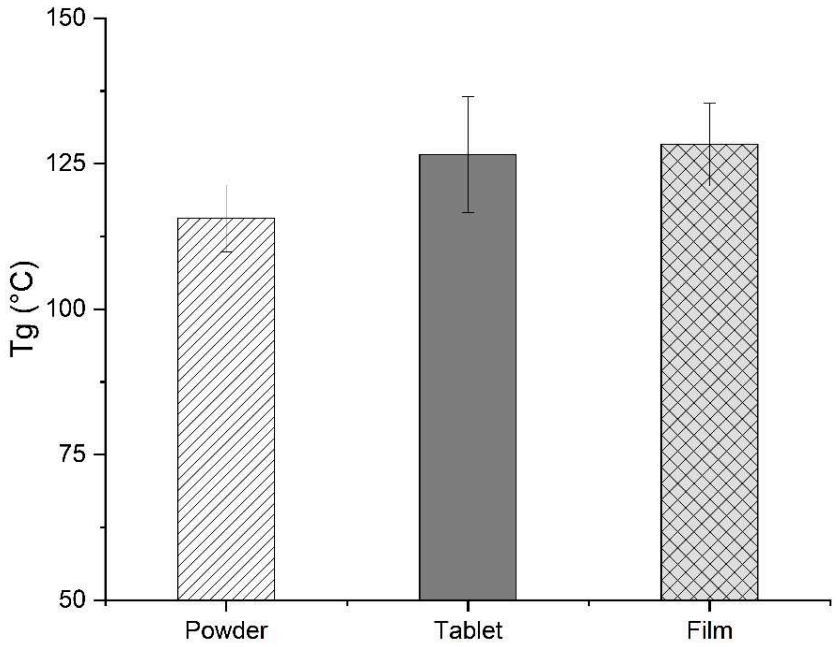

Figure 3-4. Glass transition temperature of citrus fibers as a powder, tablet and film (0.3% d.b. water content) determined by DSC at 10 °C/min during the third heating scan.

The glass transition of the tablet showed the highest standard deviation compared with powders and films reflecting a heterogeneity of the samples possibly caused by the pressure shaping. According to Thapa *et al.* (2017), pressing powder into a tablet induces rearrangement and densification of the particles. However, these physical changes may not happen uniformly in all particles, contributing to the observed variability.

Similarly to tablets, the formed films are heterogeneous with undissolved particles which can explain the standard deviation. During the film formation upon drying, a three-dimensional network is formed by covalent and/or electrostatic, hydrophobic, and ionic interactions. The control of conditions during film production is essential since it can alter kinetic, reaction mechanisms, and final properties (Han & Gennadios, 2005). For instance, solvent evaporation as well as the formation of bonds control the structure and static/dynamic properties of the film. The mobility of the polymer's chains decreases with increasing crosslinking and reduction of solvent concentration. In this case, generally, the Tg of the system increases (Dušková-Smrčková & Dušek, 2002).

Although the standard deviation is different between sample shapes, no significant difference ($p>0.05$) in glass transition temperature was found. It allowed further use of citrus fibers in different shapes for this study without interference in properties.

3.2.3. Identification of glass transition phenomenon in citrus fiber matrix

Initially, citrus fiber powder (0.3% d.b.) was analyzed with a unique DSC run with one heating from -50 °C to 200 °C, 10 °C/min (Figure 3-5). The heat flow curve as function of temperature showed no obvious change in heat flow, except a discrete endothermic peak between 40 and 80 °C (most likely associated with an enthalpy relaxation as a consequence of physical aging), and an endothermic peak at temperature higher than 177 °C which may be attributed to at material melting. The Tg of citrus fibers could not be measured by a unique heating, since Tg could be covered by melting peak and no clear baseline was obtained.

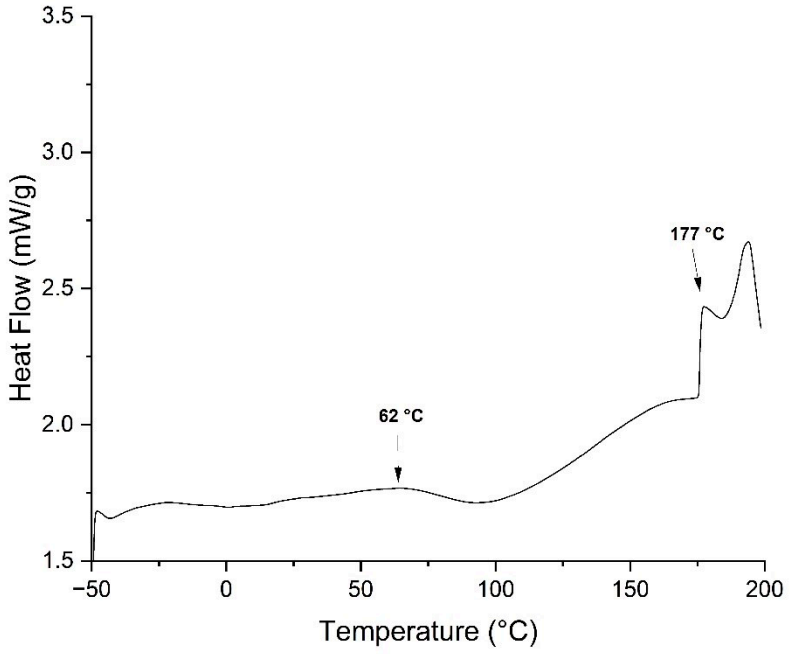

Figure 3-5. DSC heat flow curve (1st scan) heating rate of 10 °C/min of citrus fiber (0.3% d.b. water content).

To investigate further the glass transition, the citrus fiber powder (7.1% d.b. water content) was submitted to four heatings: a first one for the study of enthalpy relaxation, a second one to partially melt the sample, a third one to investigate a glass transition and a last one to verify the reversibility of the latter (Figure 3-6). The first heating showed an endothermic peak between 40 and 80 °C, as observed previously (black arrow – solid line). On the thermogram of the second heating, an endothermic peak starting from 150 °C is associated with a melting peak (T_m) (black arrow – dash line). On the third heating, a change of slope was observed between 80 to 170 °C (gray arrow – solid line). The reversibility of this

event was demonstrated in the fourth heating in the same temperature range which suggested the occurrence of a glass transition (gray and dash line).

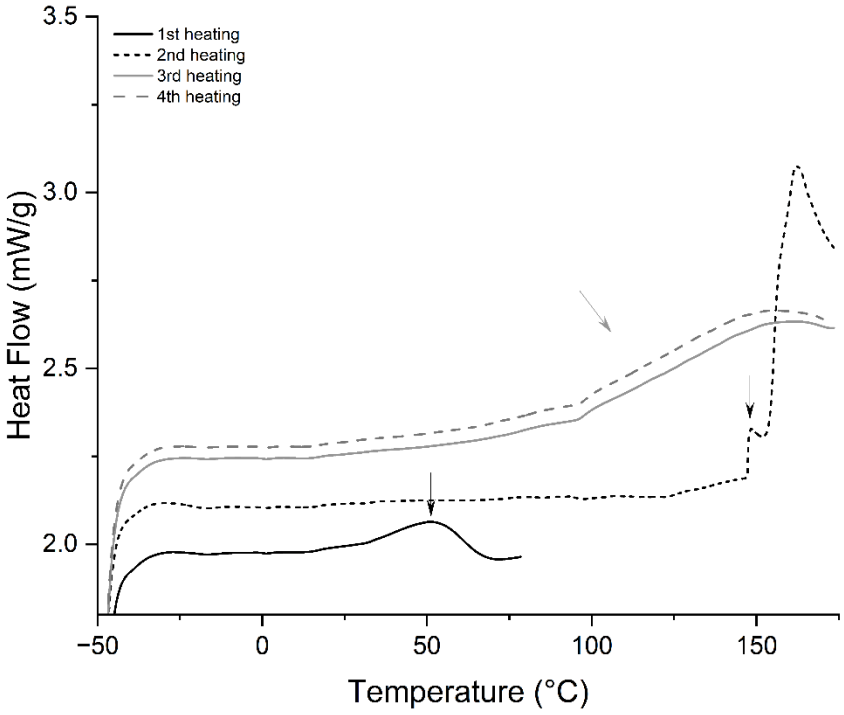

Figure 3-6. DSC heat flow curves at 10 °C/min of CF (7.1 % d.b. water): first heating (a), second heating (b) and third and fourth heatings (c).

3.2.3.1. Enthalpy relaxation

Since the endothermic peak observed on the first heating scan (Figure 3-6) was suggested to result from a physical aging, it was decided to investigate further considering its sensitivity to storage time. CF powder sample at 7.1% d.b. water content was used for this study. The endothermic peak observed on the first heating scan (Figure 3-7) at 55 ± 1 °C with a ΔH of 1.4 ± 0.3 J/g disappeared after the first heating as seen on the thermogram of the immediate second heating which could be considered as a control for rejuvenated sample. The endotherm seemingly reappeared after one week storage at 40 °C, with its maximum observed at higher temperature (76 ± 1 °C), and with an energy of 0.4 ± 0.1 J/g *i.e.* 28% of the original value. The temperature at which these sub-Tg endothermic peaks occur, and their associated energy, are primarily determined by time and the temperature difference between Tg and the sample storage temperature (Borde *et al.,* 2002). These variables can explain the recovery of the enthalpy relaxation peak of CF in higher temperature with lower energy.

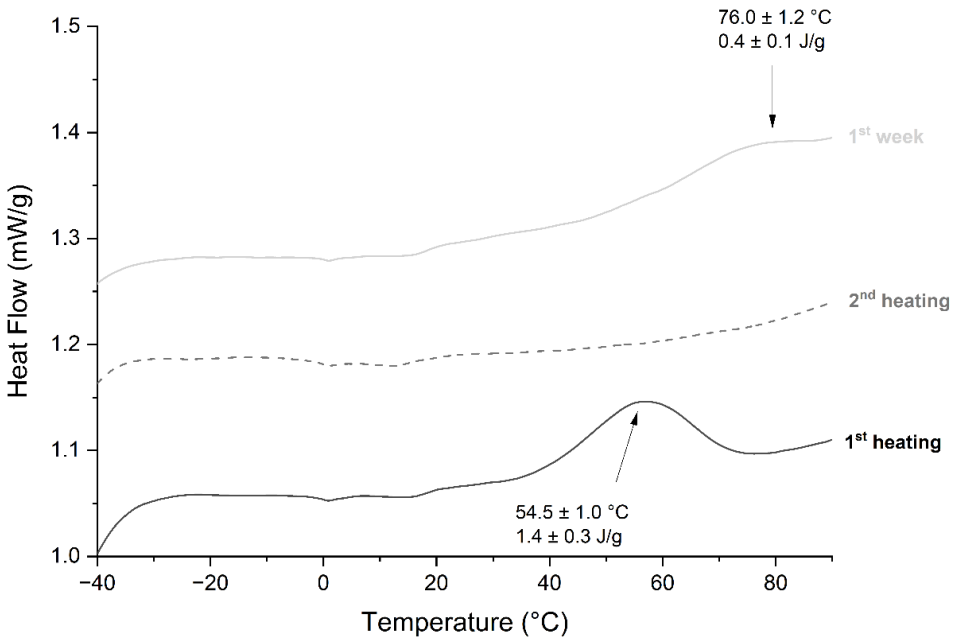

Figure 3-7. DSC thermograms of citrus fiber powder (7.1 % d.b.) showing enthalpy relaxation on first heating (black line), on second subsequent heating (dotted line), on first heating following 1 week 40 °C storage after the original heating (grey line).

The temperature of enthalpy relaxation of CF decreased from 62 ± 1 °C to 53 ± 1°C with increasing water content from 0.3 to 17.3% d.b., and the energy significantly change from 0.3 ± 0.1 J/g (d.b.) to 1.3 ± 0.1 J/g (d.b.) (Figure 3-8). Although, the temperature of enthalpy relaxation peak was significantly different for all water contents, the associated energy was not significantly different between 7.1% (1.4 ± 0.3 J/g (d.b.)) and 17.3% d.b. (1.3 ± 0.1 J/g (d.b.)) in this study. On the opposite to what was observed for other polysaccharides such as starches, pullulan or dextran (Appelqvist *et al.*, 1993). Although the time and difference between Tg and the storage temperature mainly affects the sub-Tg endothermic peak's characteristics, the presence during aging of rigid crystalline zones in the material as well as the presence of more or less water can also modulate the enthalpy relaxation, as a consequence of swelling stress which opposes the volume reduction during aging (Hodge & Berens, 1985).

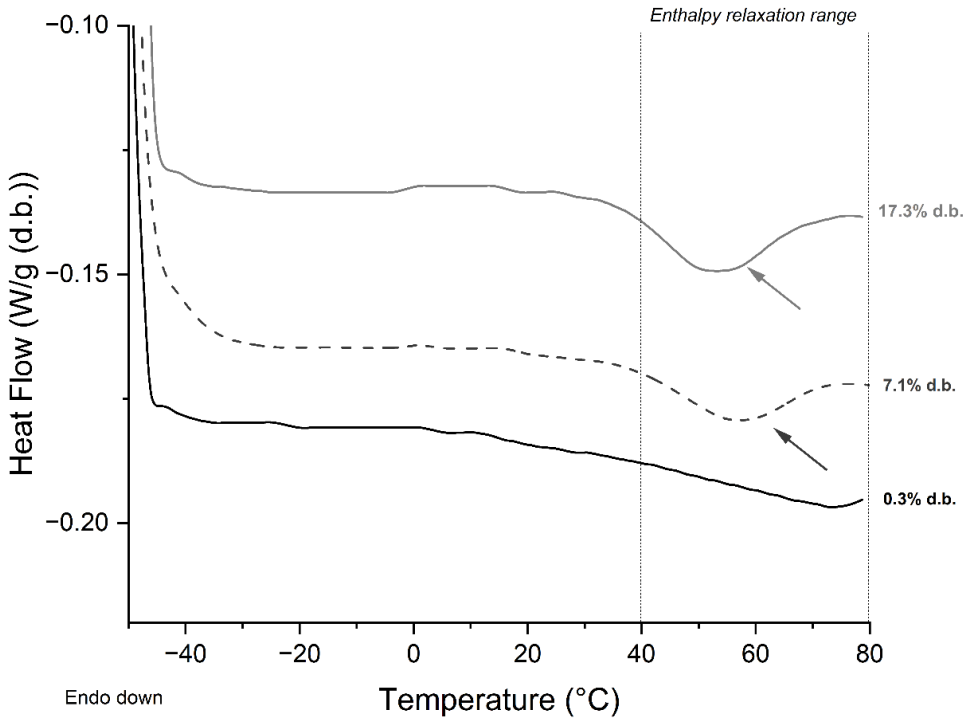

Figure 3-8. Thermal analysis of CF with different water contents (%, d.b.) analyzed by DSC. Arrows indicate the enthalpy relaxation peak, and the lines delimit the endothermic enthalpy relaxation zone.

Regardless of the pattern, the endothermic peak is indicative of the system's molecular mobility in the glass and, the data suggests that the sample swells with increasing both temperature and water content (Rolandelli *et al*., 2022). The increase in water content may also result in the hydration of some components acting as antiplasticizers and limiting both the molecular rearrangement of the glass and the swelling since the enthalpy relaxation energy leveled off above 7.1% d.b. water content.

Appelqvist *et al*. (1993) described the variation of the enthalpy values associated with the endothermic event from 0.6 to 1.4 J/g with moisture content for corn starch at 8.8 to 19.9% wet basis water content. On the other hand, the majority of the enthalpy values for different polysaccharides in this hydration range were found in the range of 2-3.5 J/g. The lower enthalpy relaxation for CF may be attributed to a limited ability of molecular rearrangement due to the presence of rigid crystalline zones expected from cellulose.

3.2.3.2. Glass transition temperature of citrus fiber

The Tg of citrus fiber is difficult to identify due to poor resolution in the third and fourth heatings mainly because this transition appears very spread in temperature and is difficult to

differentiate from the baseline (Figure 3-6). A strategy to identify a thermal event is to use the first derivative of heat flow signal as a function of temperature. Thus, the latter was calculated for the thermogram of the third scan displaying one endothermic event with Tg 116 ± 6 °C with a delta Cp of 0.24 ± 0.10 J/(g/°C) (Figure 3-9). Al-Khalili *et al.* (2023a) found a Tg 136 ± 5 °C with a delta Cp 0.25 J/(g/°C) for date-pits which are mainly composed of fibers comparable to citrus fibers. Putri *et al.* (2024) who also investigated the glass transition of dry lemon peel cell wall material calculated a Tg of 117 °C applying Gordon Taylor model, result in agreement with the present work for citrus fiber. However, in the literature, there is a huge variation of Tg for cellulosic materials reflecting the difficult to determine it (Back & Didriksson, 1969; Goring, 1963; Kargin *et al.*, 1960; Kim *et al.,* 2003; Paes *et al.,* 2010; Szcześniak *et al.*, 2008). The change in specific heat (ΔCp) found for citrus fiber is coherent with usual values given for polysaccharides (0.2 J/g/°C)) (Borde *et al.,* 2002).

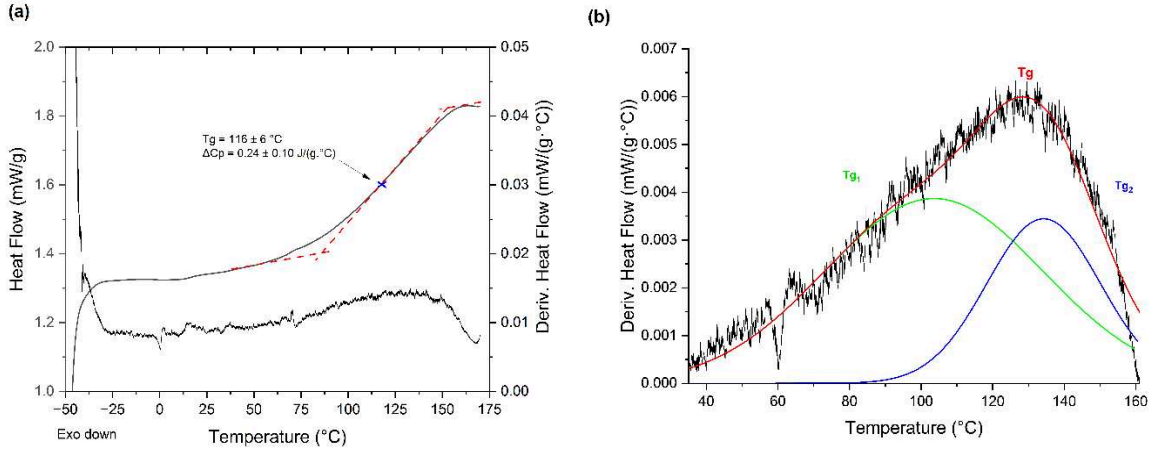

Figure 3-9. DSC curve of citrus fiber (0.3% d.b. water content) a) Heat flow and first derivative of third heating scan; b) Deconvolution of first derivative curve of citrus fiber powder.

The wide glass transition of citrus fiber (between 50 and 170 °C) (Figure 3-9b) resulting from its complex composition suggested the overlap of more than one glass transition. According to Matveev *et al.* (2000), biopolymers mixtures can have a broad transition temperature range or even two transitions. The occurrence of a multiple glass transition is held on terms of compatibility of polymers: a compatible mixture will have a single glass transition with temperature between the Tg values of the mixture components whereas an incompatible mix will exhibit multiple glass transitions (Lai *et al.*, 2000; Roudaut & Wallecan, 2015). To determine the number of transitions and the temperature associated with each one, the derivative curve was fitted with two discrete Gaussian functions (2-6) (Figure 3-9b). The glass transition temperatures were determined with the maximum of each peak. This method has

been applied to identify the glass transition temperature of complex food matrices and also to study the plasticizing effect in different phases (Masavang *et al*., 2019; Roudaut & Wallecan, 2015). Masavang *et al*. (2019) evidenced a dual phenomenon for model breakfast cereals with a low temperature glass transition for a small molecules-rich fraction (water or sugar) and a higher temperature glass transition for a biopolymer (starch and/or protein)-rich fraction.

Due to the complex composition of citrus fibers (cellulose, pectin, hemicellulose and a small amount of proteins and lipids), the evidence of these two different phases suggested heterogeneities in the sample at molecular level. The lower glass transition temperature (Tg_1) 97 ± 4 °C could be related to a less rigid amorphous fraction while the higher glass transition temperature (Tg_2) 134 ± 7 °C would be associated with a more rigid amorphous fraction, Tg_1 could be correlated to the glass transition of citrus fibers components *e.g.* pectin and hemicellulose, as a result of their greater sensivity to water, thus greater plasticization; while Tg_2 could be attributed to the amorphous zone of cellulose.

3.2.3.3. Viscoelastic behavior

Figure 3-10a shows the storage modulus (E'), loss modulus (E") and tan δ as a function of temperature for citrus fiber at 0.3% d.b. water content. The α-relaxation can be revealed through the loss factor peak temperature (tan δ), at the onset of storage modulus (E') drop or at the maximum of loss modulus (E"). The network relaxation is the free vibration of internal microstructure of the material which can be related to glass transition (Liu & Zhang, 2018).

The α-relaxation temperature of the CF sample was detected with the maximum of tan δ at 136 ± 3 °C at 1 Hz (Figure 3-10a). Different results are observed in literature between the Tg or relaxation temperature obtained by DSC and DMA (Al-Khalili *et al.*, 2023a; Fernández-Blázquez *et al.*, 2005; Rahman *et al.*, 2007; Watanabe *et al.,* 1996). These differences may come from the fact that each technique is sensitive to different properties and frequencies (Gracia-Fernández *et al*., 2010).

The temperature of the mentioned event shifted towards higher temperature with increasing frequency sollicitation (Figure 3-10b), as expected for a relaxation (molecular motion). The T_{max} of citrus fiber in the tan δ curve rose from 127 to 149 °C with frequency between 0.5 and 40 Hz. Although there is a difference in the Tg and α-relaxation temperatures, this event is observed by both methods is a similar range from 50 to 170 °C with DSC and from 86 to 180 °C with DMA (based on storage modulus curve temperature before and after the E' drop). It indicates that both techniques are sensitive to the same relaxation process.

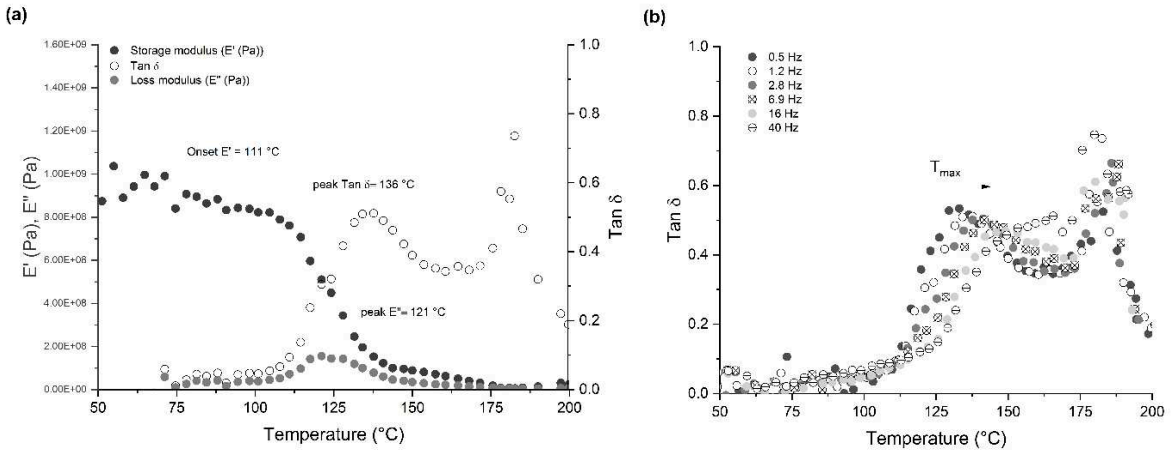

Figure 3-10. Storage (E') and loss (E") moduli, and tan delta at 1 Hz as a function of temperature (a), tan delta as a function of temperature, and for different frequencies between 0.5 and 40 Hz of citrus fibers tablet (0.3 % d.b. water content).

The sensitivity to frequency was used to calculate the activation energy (E_a) of the citrus fiber relaxation using an Arrhenius plot ln of frequency *versus* $1/T_{max}$ (in K) (Figure 3-11) which slope equals -Ea/R, its value 330 kJ/mol was in agreement with the expected values for biopolymers (200 – 400 kJ/mol) (Kalichevsky *et al.,* 1992; Kim *et al.*, 2003).

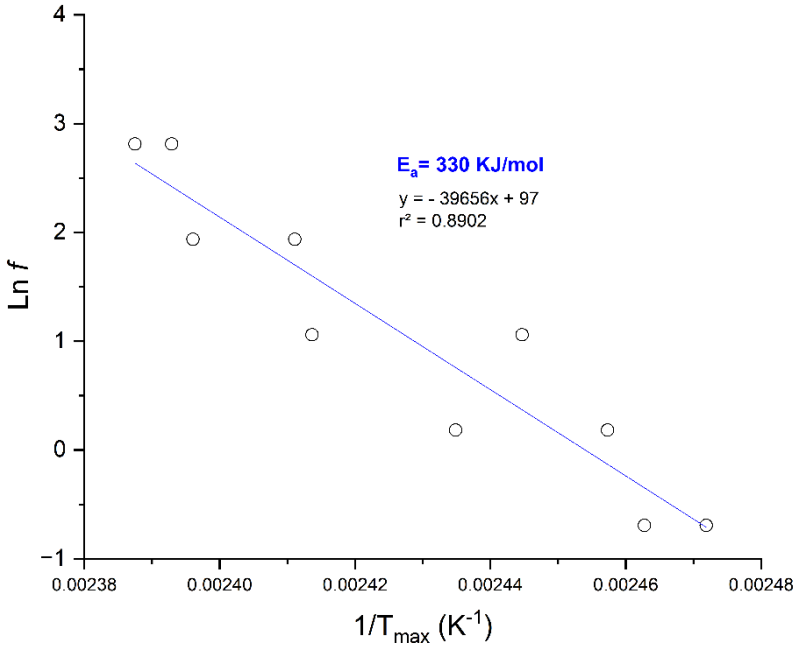

Figure 3-11. Arrhenius curve of ln sollicitation frequency (f) as function of the maximum temperature (T_{max}) of Tan δ for citrus fiber tablet (0.3% d.b. water content).

3.2.3.4. Contribution of citrus fiber components to the glass transition

To investigate the contribution of citrus fibers macromolecules to the overall glass transition, pectin powder from citrus peels (Sigma Aldrich, US) 2.0 ± 0.7 % d.b. water content and xyloglucan powder from Tamarind seed (Megazyme, IE) 1.8 ± 0.5 % d.b. water content were analyzed with the same DSC procedure as citrus fibers (Figure 3-12) (Table 3-4). Pectin and xyloglucan showed a similar enthalpy relaxation peak as citrus fiber (0.3 % d.b.) at 64.8 ± 8.9 °C and 64.1 ± 3.5 °C, respectively. However, the energy of the enthalpy peak of xyloglucan (0.7 ± 0.1 J/g) was higher than citrus fiber and not different from pectin (0.4 ± 0.3 J/g) which peak amplitude was neither different from that of citrus fiber. The glass transition temperature (midpoint) was measured at 112 ± 10 °C, and 106 ± 4 °C (Table 3-4) for pectin and xyloglucan, respectively. No significant difference ($p>0.05$) was observed between Tg values of pectin, xyloglucan, and citrus fibers at similar water content (0-2% d.b.).

Einhorn-Stoll *et al.* (2007) investigated the thermal behavior of pectins. The sample with 3-5% water content showed an endothermic peak between 75 and 105 °C which corroborates with the results of this work. On the other hand, Tg measured for xyloglucan in this present work was found much lower than for xyloglucan film (Bergström *et al*., 2012; Kochumalayil *et al*., 2010) for which the value was 250 °C. The observed variation might result from the extraction techniques applied to obtain these plant extracts. These methods may have retained smaller residual molecules, potentially acting as plasticizers, and consequently reducing the material's Tg.

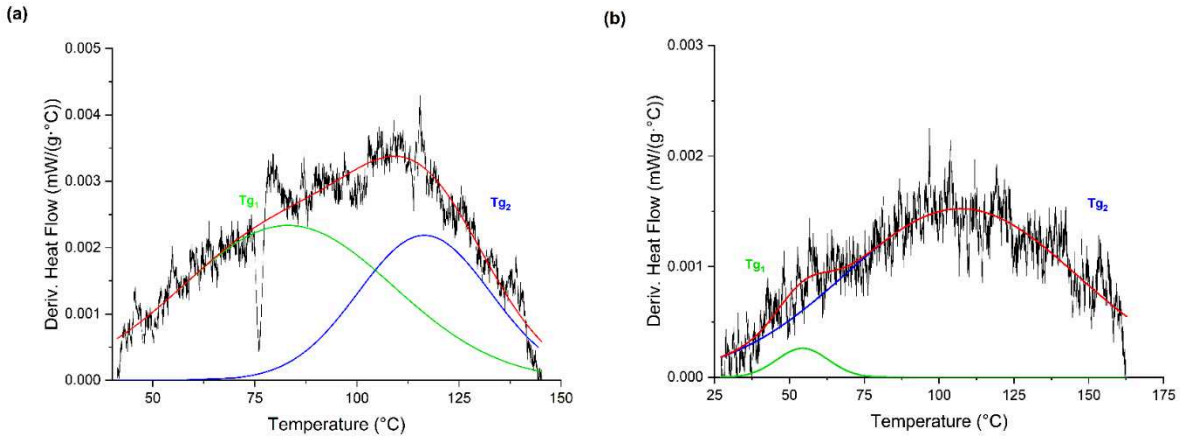

Figure 3-12. Curve fitting plot of first derivative DSC heating curves of pectin powder (2.0 ± 0.7 % d.b water content) (a), and xyloglucan powder (1.8 ± 0.5 % d.b. water content) (b).

The amplitude area of the transitions was also taken into consideration through the surface area of the fitted Gaussian functions of the first derivatives rather than just the

reference temperature with the inflection points Tg_1 and Tg_2 (Table 3-4). The glass transition of citrus fiber displayed a similar profile as pectin, spread over a wider range: with the lower glass transition at 97 ± 14 °C (60%), and the higher transition at 134 ± 7 °C (40%). It suggested that the glass transition of citrus fiber could come from pectin even if pectin represents only 15% of the material.

Table 3-4. Values of enthalpy relaxation (ΔH) peak temperature and energy, glass transition temperature and amplitude by DSC of citrus fiber as a powder (0.3 ± 0.0% d.b.), pectin (2.0 ± 0.7% d.b.) and xyloglucan (1.8 ± 0.2% d.b.).

Sample	ΔH temp. (°C)	ΔH energy (J/g)	Tg (°C) by DSC	Tg_1 (°C)	Amplitude 1 (%)	Tg_2 (°C)	Amplitude 2 (%)
CF	64 ^{a} ± 4	0.3 ^{a} ±0.1	116^{a} ± 6	97 ^{a} ± 14	69 ^{a} ± 14	134 ^{a} ± 7	31 ^{a} ± 14
Pectin	65 ^{a} ± 9	0.4 ^{a,b} ± 0.3	112 ^{a} ± 10	103 ^{a} ± 17	76 ^{a} ± 12	131 ^{a} ± 13	24 ^{a} ± 12
Xyloglucan	64 ^{a} ± 4	0.7 ^{b} ± 0.1	106 ^{a} ± 4	57 ^{b} ± 14	26 ^{b} ± 8	116 ^{b} ± 2	74 ^{b} ±8

Mean ± standard deviation (n=3). Different letters in the same column indicate that values are significantly different ($p < 0.05$).

In addition, pectin and xyloglucan were analyzed by DMA as a tablet shape (Table 3-5). Both samples showed a maximum in the same region of the tan δ curve as citrus fiber, with T_{max} around 130 °C. The E_a of pectin and xyloglucan were in the range mentioned before for main relaxation of biopolymers (between 200 and 400 kJ/mol). There was no significant ($p>0.05$) difference between T_{max} between citrus fiber, pectin, and xyloglucan.

Table 3-5. Temperature of the maximum of tan δ induced by α-relaxation and calculated activation energy of mobility, determined by DMA for citrus fiber, pectin, and xyloglucan with water content <2%.

Sample	Water content (% d.b.)	T_{max} (°C) by DMA 1Hz	Ea (kJ/mol)
Citrus Fiber	0.3 ^{a} ± 0.0	136^{a} ± 3	330
Pectin	2.0 ^{b} ± 0.7	140^{a} ± 6	299
Xyloglucan	1.8 ^{b} ± 0.2	128^{a} ± 4	396

Mean ± standard deviation (n=3). Different letters in the same column indicate that values are significantly different ($p < 0.05$).

In this study, as observed with DSC, it is difficult to clearly assign the contribution of macromolecules to the α-relaxation/glass transition temperature. Citrus fiber is a heterogeneous material with three main components (cellulose, hemicellulose, and pectin), and the glass transition could originate from the interaction of these three components. Even if the glass transition temperature of cellulose is generally given at a higher temperature (above 200 °C) (Al-Khalili *et al.,* 2023a; Paes *et al.*, 2010), in this case, it seems that the contribution of pectin mainly decreased the overall Tg of citrus fiber.

3.2.3.5. Plasticizing effect

Biopolymers are composed of a long, rigid chain with a great number of inter- and intra-molecular interactions, resulting in a high Tg. An effective solvent can reduce the fracture strength, elastic modulus, and viscosity of the biopolymer due to weakening of the inter- and intramolecular interactions, facilitating the molecular motion, and decreasing internal friction through plasticization (Matveev *et al.*, 2000). Plasticizers change the three-dimensional molecular organization, decreasing the energy required for molecular motion (Bocqué *et al.*, 2016).

To investigate the plasticizing effect in citrus fiber, the studied materials were used in film shape. The purpose was to study by DSC the plasticizing effect of water and compare it with different studies and plasticizers. The film was stored at 0% (0.3% water content), 46% (9.8% water content) and 75% (17.3% d.b. water content) relative humidity before analysis. As exposed in Table 3-6, the films at different water content showed Tg between 119 and 128 °C, which were not statistically different ($p>0.05$). This behavior was unexpected since the increase in water content was expected to reduce the Tg as shown for similar matrices in the literature (del Mar Camacho *et al.*, 2021; Moraga *et al.*, 2011; Putri *et al.*, 2024; Szcześniak *et al.*, 2008; Vásquez *et al.*, 2013).

Table 3-6. Glass transition temperature of citrus fiber films at different water content analyzed by DSC: onset, midpoint and endset temperature.

Water content (%) (d.b.)	**Onset (°C)**	**Tg (°C) (midpoint)**	**Endset (°C)**	**Tg_1 (°C)**	**Ampl. 1 (%)**	**Tg_2 (°C)**	**Ampl. 2 (%)**
0.3	99 ^{a} ± 9	128 ^{a} ± 7	157 ^{a} ± 6	114 ^{a} ± 6	66 ^{a} ± 18	142 ^{a} ± 6	34 ^{a} ± 18
9.8	90 ^{a} ± 4	122 ^{a} ± 4	155 ^{a} ± 5	114 ^{a} ± 11	68 ^{a} ± 7	147 ^{a} ± 4	32 ^{a} ± 7
17.3	92 ^{a} ± 11	119 ^{a} ± 8	147 ^{a} ± 6	114 ^{a} ± 11	71 ^{a} ± 4	140 ^{a} ± 7	29 ^{a} ± 4

Mean ± standard deviation (n=3). Different letters in the same column indicate that values are significantly different ($p < 0.05$).

The influence of moisture content on the glass transition temperature was also evaluated regarding the two components of glass transition of citrus fiber (Table 3-6). No significant effect of water was observed on temperature nor on amplitude ($p>0.05$).

The behavior observed in this study may be explained by the complexity of structure and interactions, resulting from the different sources (and thus different composition) and pretreatment of the samples. CF is composed of several biopolymers with individual structures, consequently, the interaction with water is different or only some parts may be interacting with water. As discussed by Matveev *et al.* (2000), each biopolymer has a

particular three-dimensional structure formed by functional and structural groups. The physical properties of a biopolymer are the sum of many contributions of these structural groups in the molecule. Then, the overall glass transition is a range of temperatures corresponding to activation of segmental motion of biopolymers structure: the larger the contributions, the wider the transition.

Although intermolecular hydrogen bonds in cellulosic material can be interrupted by plasticizers such as water, the latter have limited access to cellulose structure (Wu *et al*., 2015). Most aqueous reagents penetrate only in the accessible regions i.e. amorphous regions of cellulose. The water absorption capacity of cellulose fibers largely depends on the availability of free hydroxyl groups. As a considerable number of free hydroxyl groups are also present in non-crystalline regions of cellulose, it is generally considered that water absorption occurs almost entirely in the amorphous regions of cellulose, neglecting the free hydroxyl groups that may be present on the surfaces of the crystallites (Bertran & Dale, 1986). The water content in a cellulosic material is directly related to the crystallinity (Salmen & Back, 1977).

Therefore, some hypotheses can explain the lack of impact of water on the glass transition temperature of citrus fiber. Both the robust hydrogen bonds between cellulose chains and the semi-crystalline nature of cellulose could restrict its interaction with water. Additionally, the intricate composition and structure of citrus fiber may only permit a specific fraction to be accessible for interaction with water. Despite these insights, the inert behavior of citrus fiber in the presence of water remains unclear, warranting further research studies.

Due to this challenging behavior of CF with water, two other plasticizers with different polarities were tested: glycerol and triacetin. Indeed the different chemical polarities should induce different degrees of interaction with biopolymers (Chen *et al.*, 2020).

Glycerol is widely used in the literature and has been found to be particularly effective for hydrophilic polymers (Vieira *et al.*, 2011), and triacetin being water-insoluble and hydrophobic is widely used for hydrophobic and apolar polymers (Bocqué *et al.,* 2016; Chen *et al.*, 2020; Dintcheva *et al.*, 2020; Vinod e*t al.,* 2020). The results with all plasticizers tested were compared in Figure 3-13.

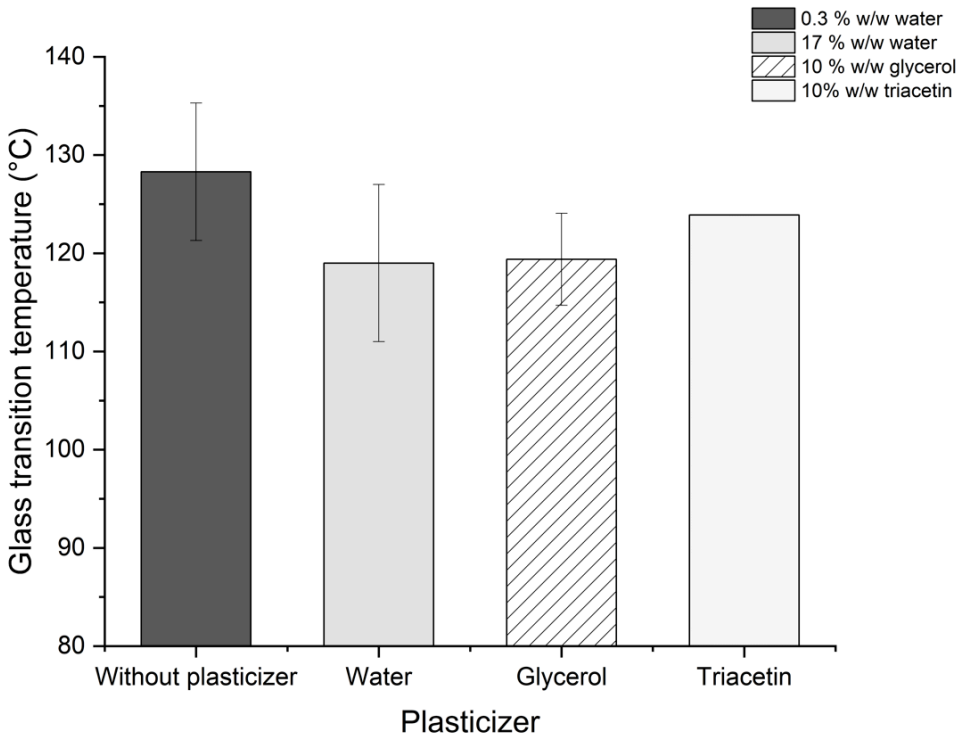

Figure 3-13.Glass transition temperature of citrus fiber plasticized with water, glycerol and triacetin.

No significant effect on Tg was observed for CF with 10 % w/w of any considered plasticizers. Many studies using biopolymer matrices (starch, chitosan, alginate, HPMC, cellulose acetate) showed plasticizing effect of glycerol and triacetin on glass transition temperature and in mechanical properties (Chaudhary *et al.*, 2011; Chen *et al.,* 2020; Gonçalves *et al.*, 2019; Liu *et al.,* 2011; Moraru *et al.,* 2002; Saringat *et al*., 2005). The use of glycerol usually resulted in a decrease of more than 5 °C of Tg depending on the concentration, whereas with triacetin the reduction of Tg was minor. To date, almost no research findings are available on this topic involving cellulosic matrices. Sirviö *et al*. (2018) investigated the effect of single (glycerol, propylene carbonate and ethylene carbonate) and two component plasticizers (deep eutectic solvents (DESs)) on the mechanical and dynamic thermomechanical properties of biocomposites based on natural cellulose fibers and hydroxyethyl cellulose (HEC). Among single plasticizers, only glycerol at high concentration (25 and 37.5% plasticizer relative to the total amount of biopolymers) decreased the T_{max} (Tan δ curve) from 140 °C to 100°C. However, DES (tetrabutylammonium bromide and propylene carbonate) at a concentration of 37.5% was shown to be efficient than glycerol, reducing T_{max} below 100 °C. The lack of studies may reflect the complexity of the plasticizing effect by other components in cellulose-rich materials.

Chen *et al.* (2020) observed the reduction of the α-relaxation of chitosan from 95 °C to 56 °C with 20 % w/w of glycerol. Nevertheless, the addition of 20% w/w of triacetin promoted a slight decrease in α-relaxation down 89 °C. As discussed in some studies, the triacetin may have weaker interactions with biopolymers, showing a limited effect on the main chain mobility. A limited effect of triacetin was also observed (Saringat *et al.*, 2005) on dried hydroxypropyl methylcellulose films which reduced the Tg by 3.6 and 2.8 °C in a concentration of 10 and 20% w/w, respectively.

The absence of a plasticizing effect on CF, observed across various plasticizers regardless of their nature, can be ascribed to the limited interaction between the plasticizer and the matrix. This highlights the complex and rigidity nature of the CF matrix.

3.2.3.6. Study of molecular mobility at microscopic scale by nuclear magnetic resonance (NMR)

In the present work, the spin-spin relaxation time (T_2) and the spin-lattice relaxation time (T_1) were determined using TD-NMR to investigate the water dynamics in citrus fiber as well as the effect of temperature and moisture content on molecular mobility.

Time domain H-NMR (TD-NMR) is a technique generally applied to study the influence of both water content and distribution on the mobility in food at a proton scale. The determination of water distribution in low moisture content matrices is challenging since they count strong molecular interactions and the spins relax fast (Cornillon & Salim, 2000), sometimes faster than the measurement conditions permits to detect due to the dead time of the equipment before to record the NMR signal. It has been applied for many systems at low water content such as starch (Tananuwong & Reid, 2004), biscuits dough (Assifaoui *et al.*, 2006), cellulose (Grunin *et al.,* 2012), polysaccharides (Ozel *et al*., 2017), extruded flour (Sergeev *et al.*, 2021), and wood (Xu *et al.*, 2017b).

3.2.3.6.1. Effect of temperature

The T_1 relaxation time for food systems is expected to be in the order of tens of milliseconds (depending on matrix water content) (Belton, 1995). Two populations of relaxation times were evidenced (Figure 3-14) for citrus fiber: T_{11} which was associated with the less abundant proton population (13% of the total signal) which decreased with increasing temperature (1.9 to 0.7 ms), and T_{12} related to the most abundant proton population (87% of the total signal) which increased with increasing temperature (62 to 80 ms). The presence of these 2 populations suggested the presence of two environments differing by their mobility.

The less mobile population (M_1) became more mobile with increasing temperature, increasing the proton population more mobile (M_2).

The effect of temperature on molecular mobility in citrus fiber was characterized by the apparent activation energy calculated on the basis of an Arrhenius behavior of ln T versus 1/T (K^{-1}) for citrus fiber at 17.3% d.b. water content (Figure 3-14). The apparent activation energy (absolute value) was determined equal 11.8 kJ/mol and 4.2 kJ/mol to T_{11} and T_{12} respectively. These values are significantly lower than for starch (around 21 kJ/mol) and hydrogen bond breakage (≤40 kJ/mol) (Roudaut *et al.,* 2009), suggesting that temperature has a limited impact on molecular mobility of citrus fiber in this temperature range. Despite the slight effect of temperature observed, one fraction of less mobile protons (M_2) became more mobile, while the decrease of T_{11} associated with decrease of M_1, may be explained by stronger interactions between matrix protons or with water protons, reducing the relaxation time.

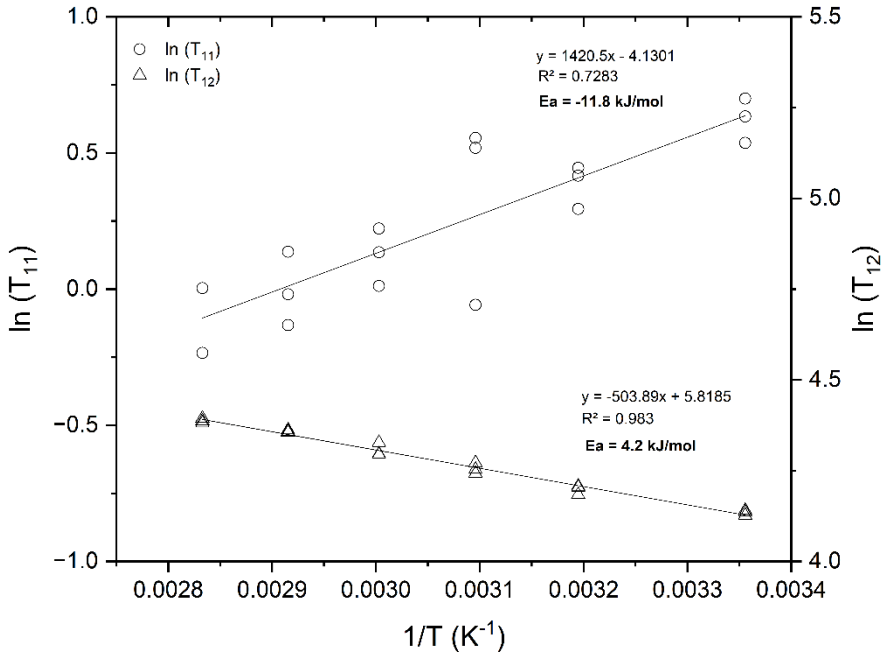

Figure 3-14. Apparent activation energy calculated on the basis of an Arrhenius behavior of ln T *versus* 1/T (K^{-1}): T_{11} and T_{12} for citrus fiber at 17.3% d.b. water content.

Given that citrus fiber was studied in powder form, which restricted molecular mobility likely limits significant orientational changes of proton spins, Free Induction Decay (FID) was used to measure the short relaxation times.

The acquired FID signal exhibited for samples at 25 and 80 °C (Figure 3-15), and at all considered temperatures (40, 50, 60 and 70 °C), a damped sinusoidal shape at approximately

0.04 ms, reflecting strong dipolar interactions between protons in the rigid component, a characteristic commonly observed in many glassy carbohydrates such as starch, maltose, maltodextrins, and amylose (Grattard *et al*., 2002; Partanen *et al.*, 2004; Roudaut *et al.,* 2009; van Den Dries *et al.*, 1998). The sinusoidal pattern slightly decreased with increasing temperature. The sinusoidal pattern is followed by a signal decay at later times (thus corresponding to protons with higher mobility), which was also slightly affected by temperature, indicating some degree of molecular mobility changes. The amount of rigid protons (S) and of more mobile protons (M) changed from 75 to 69% and from 25 to 31% respectively, with an increase in temperature from 25 to 80 °C.

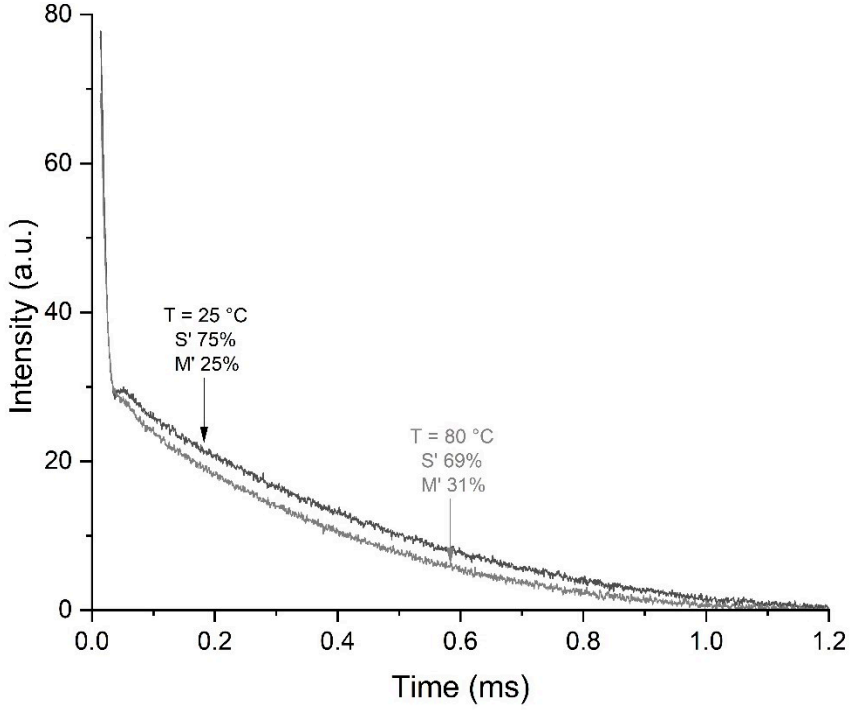

Figure 3-15. FID signal of citrus fiber (17.3% d.b. water content) at 25 °C and 80 °C.

Complementary to FID experiments, the CPMG curves showed two distinct components across all temperatures (Figure 3-16): a rapidly decaying component with an average relaxation time (T_{21}) of 0.14 ms, and a more slowly decaying component with an average relaxation time (T_{22}) of 0.74 ms. This suggests the presence of two fractions of mobile populations with different relaxation rates or degree of mobility (Chen *et al.*, 2010). T_{21} was associated with the more abundant proton population (M_1) (83% of the CPMG signal) and may represent water molecules and hydroxyl groups with protons in interaction with rigid structure of cell wall polysaccharides. T_{22} is related to the least abundant proton population (M_2) (17% of the CPMG signal) and may represent more mobile protons in citrus fiber.

According to Roudaut *et al.* (2009), the assignment of mobile protons is complex due to their varying mobility rates, which can result in one or several populations of mobile protons that cannot be resolved into discrete populations.

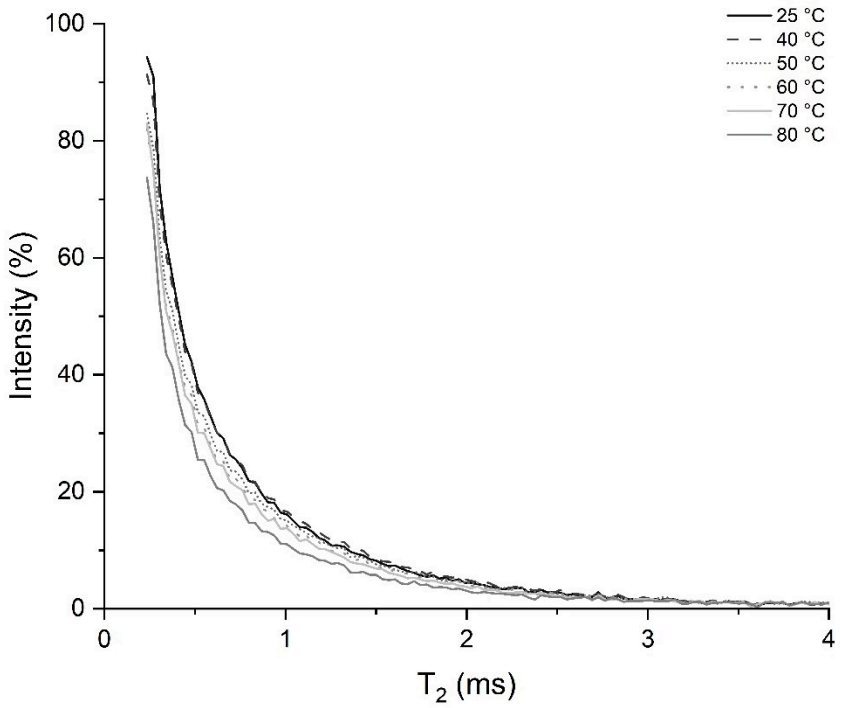

Figure 3-16. TD-NMR whole data for CF sample 17.3% d.b. at different temperatures (25-80 °C) based on CPMG measurements.

As temperatures increased, T_{21} slightly but continuously decreased while T_{22} exhibited a more significant decline (Table 3-7). The decrease in proton populations with increasing temperature (significant only at 80 °C), may result from the increase of mobile fraction interactions with macromolecules or solvation/hydration of molecules (facilitated by higher temperature) slowing down the proton dynamics (Xu *et al.*, 2017a). The changes in the matrix (hydrogen bonds, higher interaction between polysaccharides), may lead to a more constrained environment for water or small molecules protons, and thus to a decrease of T_2 relaxation time while the temperature increase is generally expected to increase.

Table 3-7. TD-NMR T2 relaxation time and proton population values for CF sample 17.3% d.b. at different temperatures (25- 80 °C) based on CPMG measurements.

Temperature (°C)	T_{21} (ms)	T_{22} (ms)	M_1 (%)	M_2 (%)
25	$0.15^{a} \pm 0.00$	$0.77^{a} \pm 0.01$	$81.58^{a} \pm 0.37$	$18.42^{a} \pm 0.37$
40	$0.15^{a,b} \pm 0.00$	$0.79^{b} \pm 0.01$	$81.55^{a} \pm 0.67$	$18.45^{a} \pm 0.67$
50	$0.14^{b,c} \pm 0.00$	$0.76^{a} \pm 0.01$	$82.42^{a} \pm 0.48$	$17.58^{a} \pm 0.48$
60	$0.13^{c,d} \pm 0.01$	$0.73^{c} \pm 0.00$	$83.38^{a} \pm 1.16$	$16.62^{a} \pm 1.16$
70	$0.13^{c,d} \pm 0.01$	$0.71^{d} \pm 0.01$	$83.84^{a,b} \pm 1.22$	$16.16^{a,b} \pm 1.22$
80	$0.12^{d} \pm 0.01$	$0.68^{e} \pm 0.01$	$86.26^{b} \pm 1.24$	$13.74^{b} \pm 1.24$

Data were expressed by means (n=3) ± standard deviation. Values followed by different letters in the same column are significantly different ($p < 0.05$).

Besides, the effect of temperature on molecular mobility for CF at 17.3% d.b. water content, observed on T_2 was also characterized by the apparent activation energy (Figure 3-17). Similarly, to T_1 data, T_2 relaxation times and proton distribution showed slight effect of temperature changes from 25 to 80 °C, showing low apparent activation energies (absolute values): 4.0 kJ/mol for T_{21} (Figure 3-17a) and 2.1 kJ/mol for T_{22} (Figure 3-17b). This confirms the earlier suggestion: T_2 values are not only affected by temperature but also by change in the CF: solvation or better hydration of solid components can explain the decrease in T_{21} and T_{22}, by slowing down the overall mobility of the population.

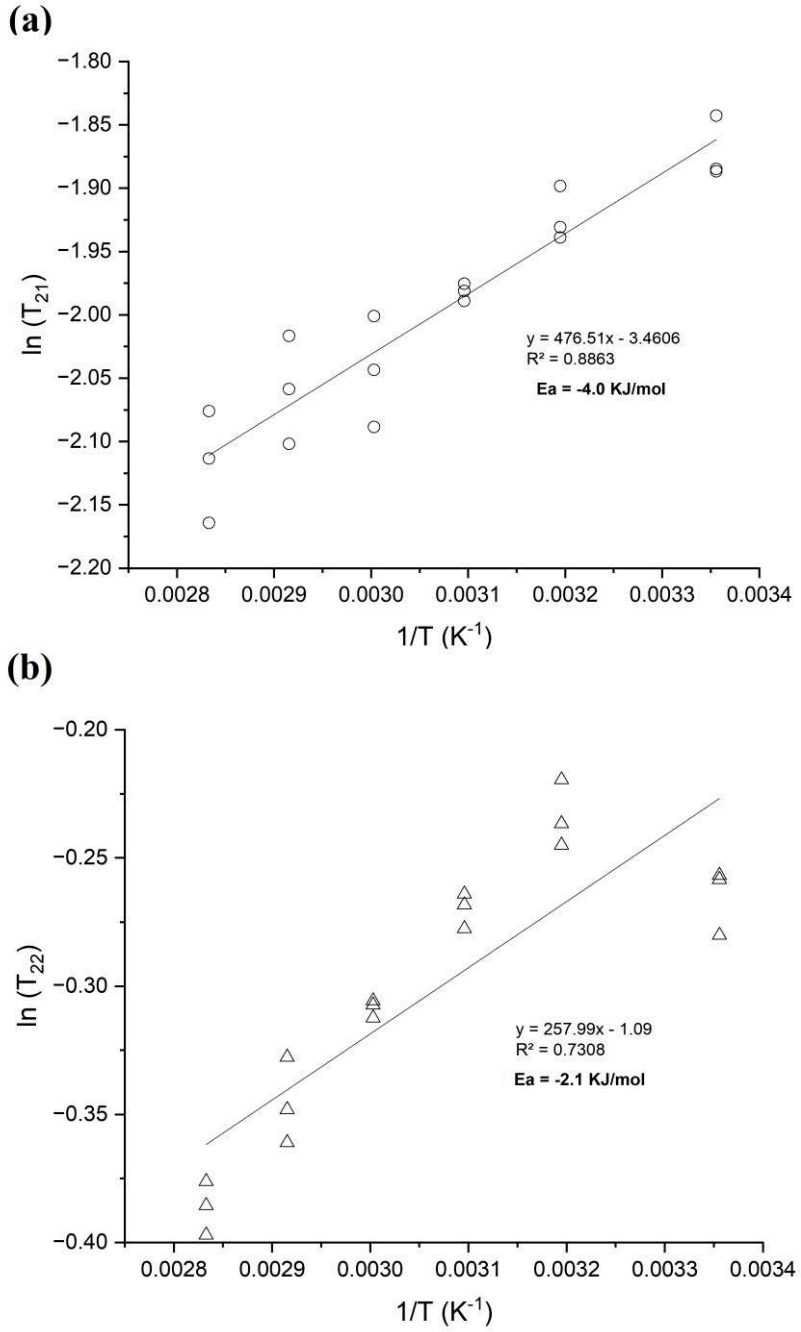

Figure 3-17. Apparent activation energy calculated on the basis of an Arrhenius behavior of ln T versus 1/T (K^{-1}): T_{21} and T_{22} for citrus fiber at 17.3% d.b. water content.

The dynamic behavior of T_{21} values was aligned with observed by enthalpy relaxation: as the temperature increased (the same range of enthalpy relaxation: 40-80 °C), T_{21} values decreased, indicating more extensive molecular rearrangements within the material. The rearrangement of the polymer structures due to the swelling of the sample may prevent or slow down the rotation of glycosidic linkages causing immobilization of polymer chains (Rolandelli *et al*., 2022).

3.2.3.6.2. Effect of moisture content

Figure 3-18 illustrates T_1 relaxation time as a function of moisture content.

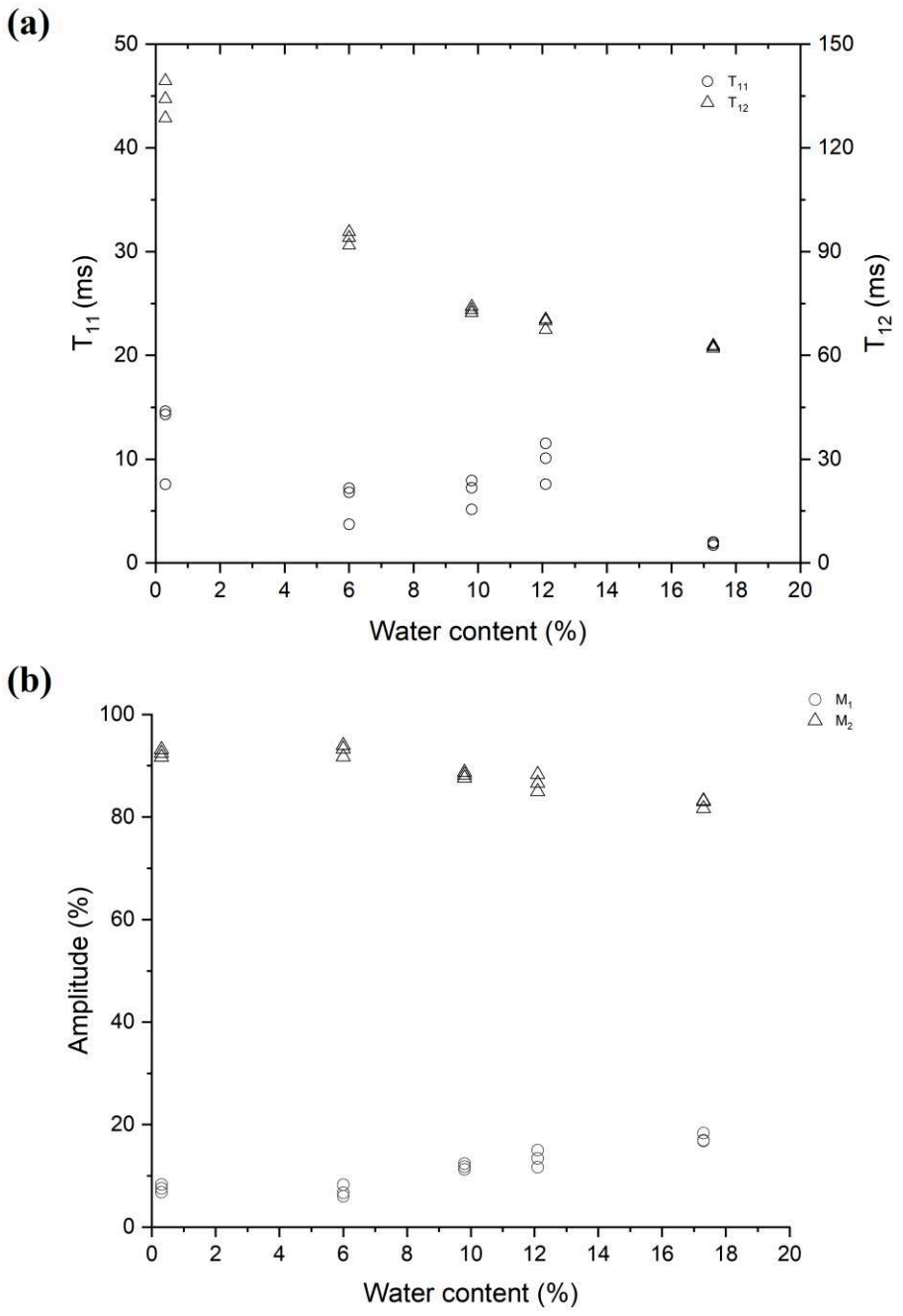

Figure 3-18. Relaxation time as a function of water content (d.b.): T11 (∘) and T12 (△) (a) and amplitude of more mobile population (M_1) and less mobile population (M_2) (b) at 25 °C.

T_{11} oscillated with an increasing moisture content from 0.3 to 17.3 % d.b. (Figure 3-18a), while T_{12} exhibited a sharp decrease with increasing moisture content. A strong water-matrix interaction could limit the mobility of the phase resulting in the decrease of relaxation time. Despite observing an effect of humidity on molecular mobility, the phase distribution

slightly changed. The phase with the higher T_1 (T_{12}) decreased from 92 to 83 %, whereas the phase related to T_{11} increased from 8 to 17%.

Regarding the influence of moisture content on the more rigid fraction determined by FID, the sinusoidal pattern became less pronounced as water content increased (Figure 3-19a). It may be interpreted as a decrease of strength of dipolar interactions between water and mobile small molecules on the one hand and citrus fiber matrix on the other hand (Partanen *et al.*, 2004). The proton distribution changed with increasing water content: rigid protons (S) became more mobile shifting to the more mobile (M) proton population, which rose from 2 to 34 a.u. in the range of 0.3 to 17.3% d.b. of water (Figure 3-19b).

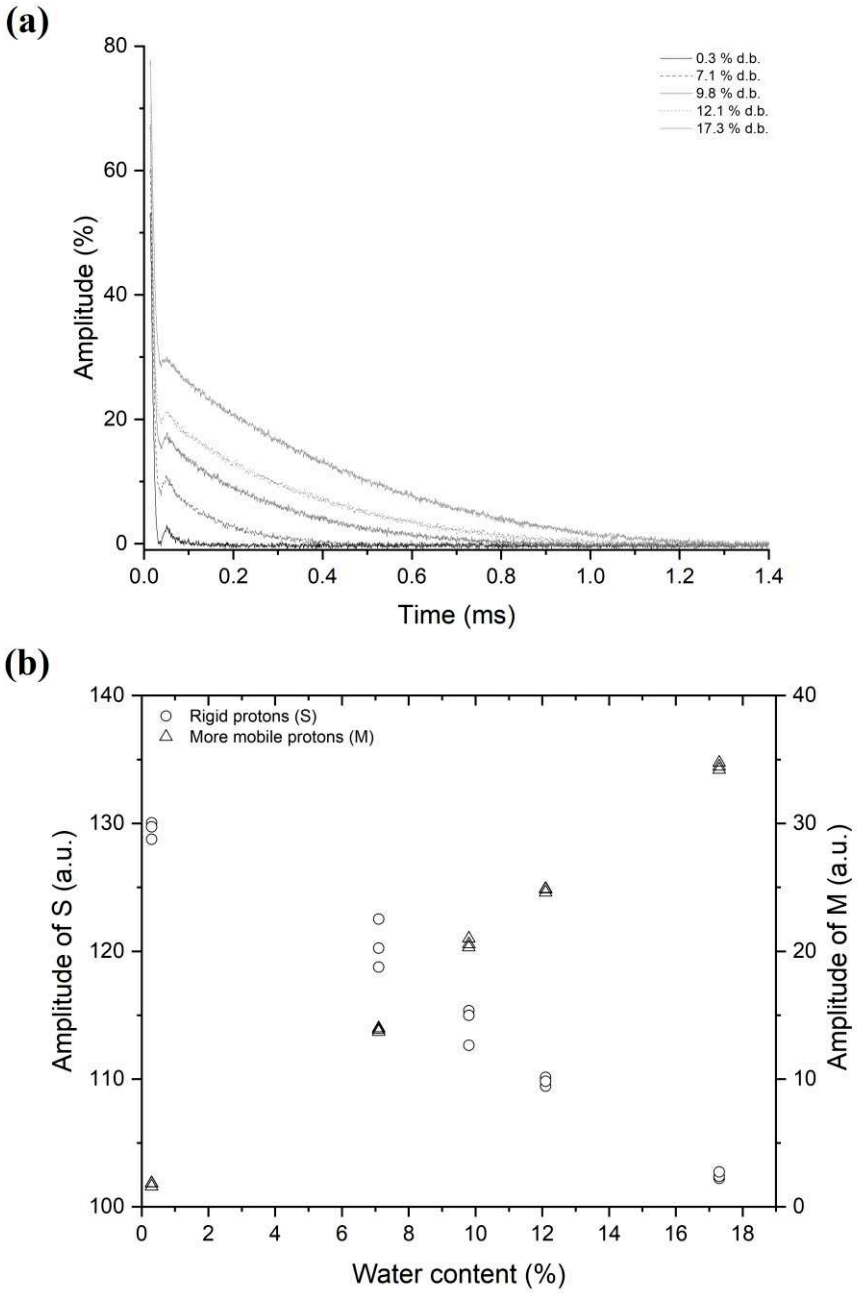

Figure 3-19. FID signal of citrus fiber (a); proton population distribution (b) at different water contents (from 0.3 to 17.3% d.b.) at 25 °C (a).

Many studies have related different proton populations to various water states, such as "bound water", "immobilized water" and "free water" (Rahman *et al.,* 2021; Tananuwong & Reid, 2004; Xu *et al.*, 2014). Furthermore, they can also correspond to the protons from different solute fractions such as fat or sugar (Assifaoui *et al.,* 2006; Sergeev *et al.,* 2021). Vittadini *et al.* (2001) suggested that in cellulose with at least 9% (w/w d.b.) water content, the component with higher relaxation time was related to protons from water molecules reorienting fast and showing a liquid-like behavior, whereas the immobile protons could

represent the "bound" water and cellulose protons. These authors showed also that the cellulose should have a water content of at least 19% (w/w d.b.) to have freezable water.

The TD-NMR T_2 relaxation time curves of CF with different water content (0.3, 9.8 and 17.3% d.b.) at 25 °C are shown in Figure 3-20.

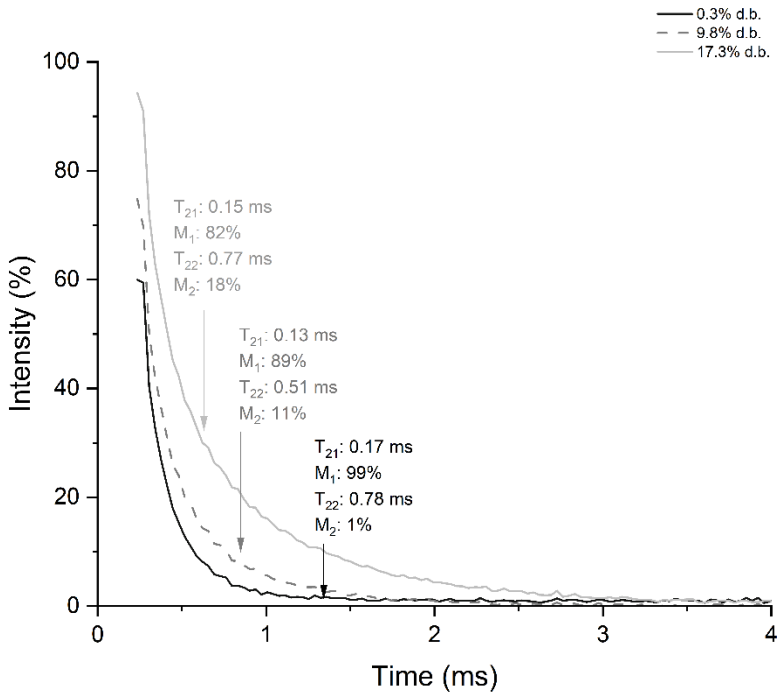

Figure 3-20. CPMG signal of samples with different water content (0.3, 9.8 and 17.3% d.b.) at 25 °C.

The distributed fit for samples with different water content showed two proton components (M_1 and M_2), indicating that even at very low moisture (0.3% d.b.), there was evidence of mobility in the citrus fiber matrix. However, the more mobile proton population (M_2) represents only 1% of protons of the more mobile protons at 0.3% d.b., which is in great agreement with the results of Vittadini *et al.* (2001) who observed a high immobility between 0 and 3% water content. This suggests T_{21} is predominantly associated with protons of macromolecules in the citrus fiber matrix, while T_{22} is linked to protons of both water and more mobile molecules in interaction with water.

The less mobile proton population (M_1), with T_{21} between 0.1 and 0.2 ms, and representing the larger proton population (but only 1-21% of the total protons) was slightly affected by water content. This population was only slightly influenced by water content, as T_{21} remained almost constant with increasing water content. However, a noticeable proton displacement from the less mobile (M_1) to the more mobile population (M_2) was observed.

The more mobile population (M_2) (0-5% of the total proton amount), with higher relaxation times (T_{22}) between 0.4 and 0.8 ms, showed an increase of both T_2 and signal intensity with increasing water content. This indicates that the presence of more water molecules enhances molecular mobility within the material.

T_2 ($T_{11} \approx 0.15$ ms and $T_{12} \approx 0.63$ ms) values are much shorter than T_1 ($T_{11} \approx 7$ ms and $T_{12} \approx 87$ ms). As mentioned by Vittadini *et al.*, (2001), $T_1 >> T_2$ could suggest an effect of cellulose on water mobility: the water-cellulose interactions could prevail over water-water interaction, as a result, a faster relaxation is observed by T_1 relaxation time.

In this study, the two-proton populations identified by the CPMG sequence can be attributed to protons from both the matrix dry matter (probably small molecules) and water, highlighting the heterogeneity of water distribution in the citrus fiber matrix. The FID sequence separates the protons into a rigid (S) and more mobile (M) protons population. The protons visualized by CPMG (M_1 and M_2 populations) correspond to the more mobile protons measured by FID (representing 1% of total protons population at 0.3% d.b. water content and 25% at 17.3% d.b. water content) (Figure 3-21). This indicates that only a small fraction of the sample (5%) has a molecular mobility higher than 0.5 ms (M_2'), which may make the analysis of molecular mobility citrus fiber difficult at higher scales. Although the M_1 amplitude decreased with increasing water content, in opposition with the increase in M observed by FID, this can be explained by the increase in M_2.

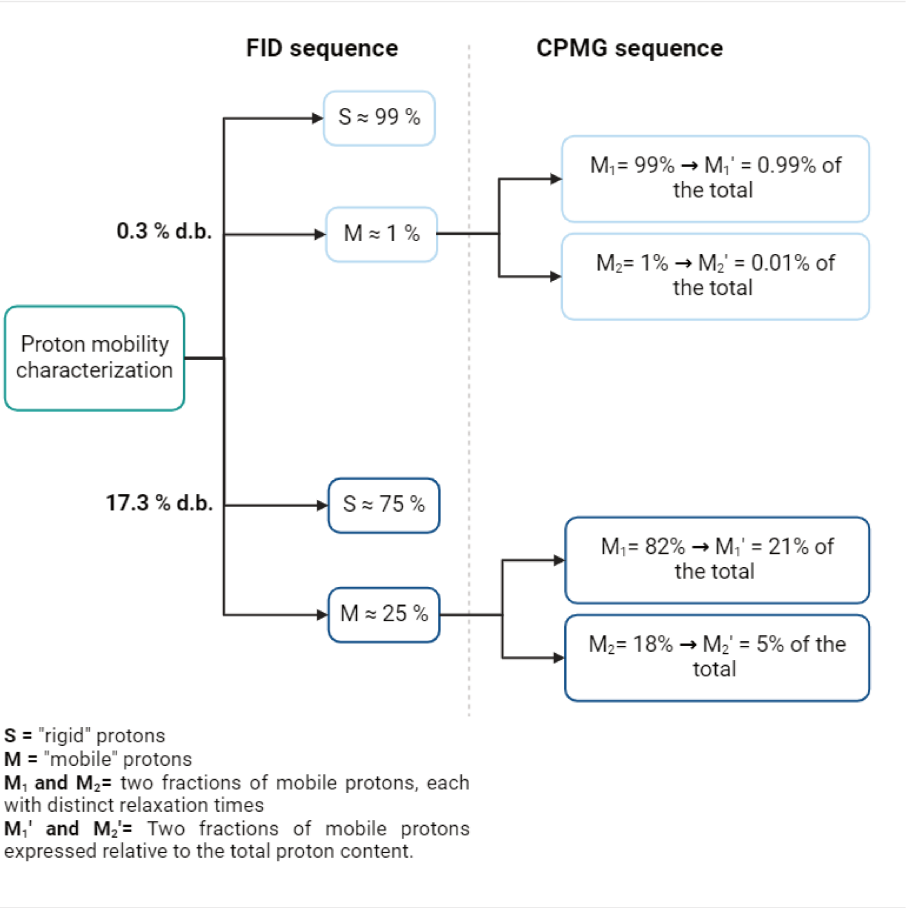

Figure 3-21. Protons matrix characterization: relation between protons determined by FID and CPMG sequence for citrus fiber sample at 0.3 and 17.3 % d.b. water content and 25 °C.

3.2.3.6.3. Water contribution in citrus fiber matrix with deuterium

To gain more insight into the water interactions in the citrus fiber matrix, samples hydrated with water or deuterium were compared through their T_2 relaxation time. The use of deuterium allows to only measure the mobility of non-exchangeable protons of components in the same hydration level (Ibbett *et al*., 2008).

The citrus fiber accessibility related to the hydroxyl protons can be determined from the magnitude of exchanged deuterium and water protons. The percentage difference in proton content between a hydrated sample (17.3% d.b. water content) and a sample equilibrated in deuterium, was calculated relatively to the overall difference in proton content between a hydrated sample and a deuterium-incorporated sample (2-10) (Table 3-8). The contribution of water proton in the rigid fraction (P_S) is 36% whereas in the more mobile fraction (P_M) it is twice as high (64%). When closely analyzing the impact of deuterium exchange on the more mobile fraction (M): the less mobile fraction (P_{M1}') of citrus fiber was 45% while in the more mobile fraction (P_{M2}') it corresponded to 19%. It indicates that most of the water interacts with

the proton population M_1 with some protons becoming more mobile and shifting to the more mobile fraction (M_2), as previously observed.

This indicates that water interacts with the largest mobile proton population in the matrix. Although this interaction does not dramatically increase molecular mobility (T_2<1 ms) —implying a limited plasticizing effect on this matrix—it does show that humidity can influence mobility at 25 °C. Thus, the humidity may be detrimental to maintaining functional properties of citrus fiber over storage.

Table 3-8. Absolute value of amplitude of the proton population corresponding to water or deuterium exchange in the citrus fiber matrix based on CPMG measurements.

Sample	S (a.u.)	M (a.u.)	M_1 (a.u.)	M_2 (a.u.)
CF 75% RH (17.3% d.b. water content)	102	34	248	56
CF 75% RH of deuterium	90	12	181	28

Gathering all information obtained by NMR analysis, an illustrative schema of water dynamics and distribution in citrus fiber matrix is represented in Figure 3-22. The proton population (~15% of total) gathered in the population characterized by T_{11} and T_{22} likely corresponds to the water absorbed within the matrix. The small water-sensitive fraction may correspond to the inside of the matrix, and the absorbed water within it remains in low amounts, creating an environment characterized by low viscosity and enhanced proton molecular mobility. In contrast, T_{12} and T_{21}, associated with greater proton populations (~85% of total), may signify the presence of adsorbed water. The cell wall materials' surface is abundant in hydrophilic groups, fostering a stronger interaction with water. Consequently, the viscosity is reduced, but molecular mobility is constrained due to the water-matrix interaction.

The opposite behavior observed to T_1 and T_2 is common to solid matrices, or large molecules in which the molecular "tumbling" rate is slow (Bloembergen *et al.*, 1948).

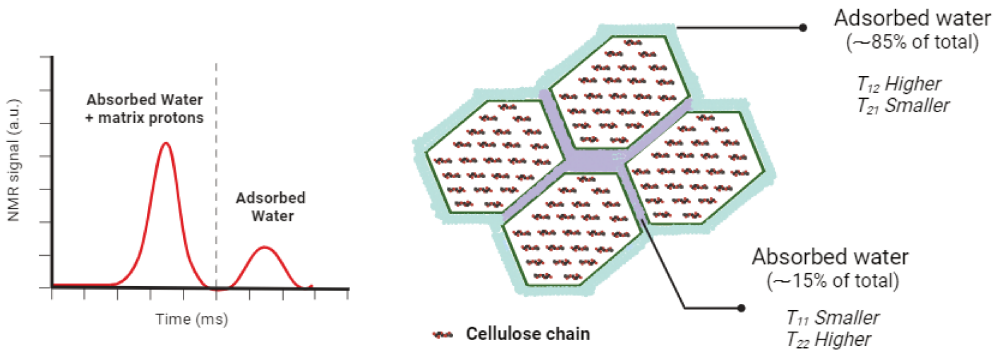

Figure 3-22. Illustrative scheme of water dynamic and distribution in citrus fiber matrix (cellulose-rich material).

3.2.4. Chemical Characterization of citrus fiber

3.2.4.1. Effect of sample preparation in a chemical composition of citrus fiber

FTIR is a useful technique to analyze the chemical composition, molecular structure and chemical bonds of plant cell wall polysaccharides since these properties can be related to different peaks (He *et al.,* 2023; Zhu *et al*., 2021). Thus, FTIR analysis was performed to identify the major functional groups of the sample immediately dried (CF) and the sample kept in isopropanol and finally dried in a different scale (CFV) and their differences (Figure 3-23).

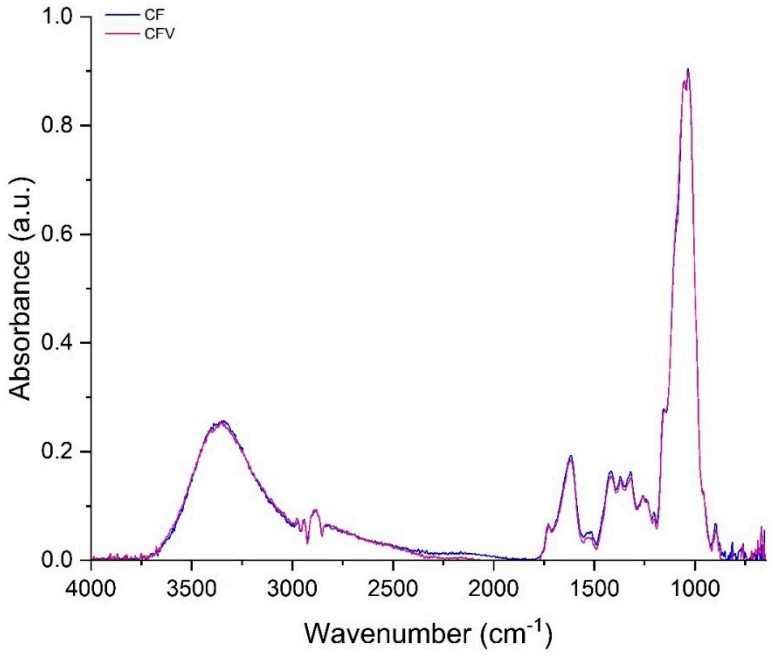

Figure 3-23. FTIR spectra of dry citrus fibers dried in two different conditions: CF and CFV.

Full information of all the vibrational modes present in the spectra is shown in Table *3-9*. The two samples showed very similar spectra with slight intensity differences between some bands in the region 1800-1200 cm^{-1}. The region between 1200 and 850 cm^{-1}, known as fingerprint region, is ascribed to the polysaccharides, and is very complex. Then, it is almost impossible to differentiate and associate specifically these bands to cellulose, hemicellulose and pectin separately (Makarem et al., 2020).

Table 3-9. Assignment of the main absorption bands in FTIR spectra of citrus fibers. FTIR data were interpreted according to investigations issued from (Célino *et al*., 2014; Liu *et al.*, 2021; Szymanska-Chargot & Zdunek, 2013).

Wavelength (cm^{-1})	**Assignment**
3345	Hydrogen bonded of OH stretching
2285	Stretching of C-H bonds from methyl and methylene groups
1730	C=O stretching acetyl or carboxylic acid
1620	COO- antisymmetric stretching
1521	Amid II N–H deformation
1425	Carboxylic acid and carboxylate (COO^-) vibration
1372	CH bending of cellulose (amorphous)
1319	CH_2 bending of cellulose (crystalline)
1245	C–O stretching
1157	Anti-symmetrical deformation of the C-O-C band
1034	C–O stretching, C–C stretching

To explore the differences observed before, a PCA analysis was carried out to compare CF and CFV samples in this region (1800-1200 cm^{-1}) (Figure 3-24). The scores scatter plots PC1 (explaining around 63% of variability) × PC2 (explaining around 26% of variability) were used to obtain separation of each group. PC1 loadings had positive values at 1653, 1560 and 1420 cm^{-1} which may be associate to functional group vibrations in amid I and II groups from proteins and CH_2 symmetric bending of cellulose. The negative PC1 loadings are 1745 and 1227 cm^{-1} corresponding to C=O stretching vibration of alkyl ester and C-O stretching of pectin.

As illustrated in Figure 3-24a, the samples were discriminated along PC1. Based on the peak that presented greater significance in this separation (1745 cm^{-1}), it suggests that the difference between the samples is due to C=O bonds. As reported by Panchev *et al.* (2010), the vibration wavenumber in this region depends on the type of pectin, *e.g.* 1745 cm^{-1} for polygalacturonic acid, 1746 cm^{-1} for sodium pectinate and 1750 cm^{-1} for highly esterified pectin. The influence of the 1745 cm^{-1} band which is more significant for CF may represent a difference in the degree of methylesterification. However, other analysis to investigate these components should be carried out to confirm the effect of sample preparation. Therefore, no major impact of sample preparation (different scale or drying kinetic) was observed in FTIR spectra of the citrus fiber.

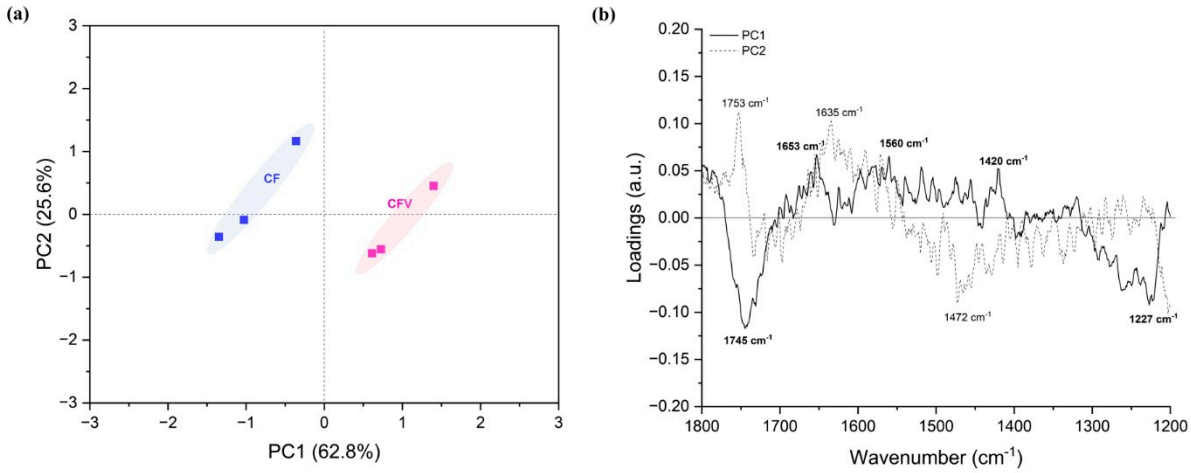

Figure 3-24. PCA score plots images (a) and loading (b) of CF and CFV samples.

3.2.4.2. Determination of degree of methyl esterification (DM)

The degree of methylesterification of pectin plays an important role in the strength and flexibility of the plant cell wall as well as in the functional properties. The most common method for determining the DM is titration. However, FTIR has become more popular to determine the DM since it does not require a pretreatment of the material (Yu *et al.*, 2021).

The carbonyl range of the spectra is complex to study, since it is composed of many overlapping bands. For this reason, some researchers applied deconvolution to deeply investigate it (Chatjigakis *et al*., 1998; Fellah *et al.,* 2009; Łojewska *et al*., 2005). However, it is complex to fit or deconvolute them without any backing from validated tests or theoretical computations (Łojewska *et al.*, 2006). Based on the second derivative of the spectra and suggested peaks in the literature (Boukir *et al*., 2019; Łojewska *et al.*, 2006, 2005), this region was deconvoluted with 7 peaks to determine the degree of esterification (Figure 3-25): 1731 cm^{-1} which can be related to carboxyl group of ester and acetyl; 1695 cm^{-1} associated to ketone; 1650 cm^{-1} related to tautomer of a carbonyl group/enolic group or to amid I C-N stretching from protein; 1610 cm^{-1} representing carboxylate ion stretching bands (COO^-); 1560 cm^{-1}, 1539 cm^{-1} and 1517 cm^{-1} are related to amid I groups of protein.

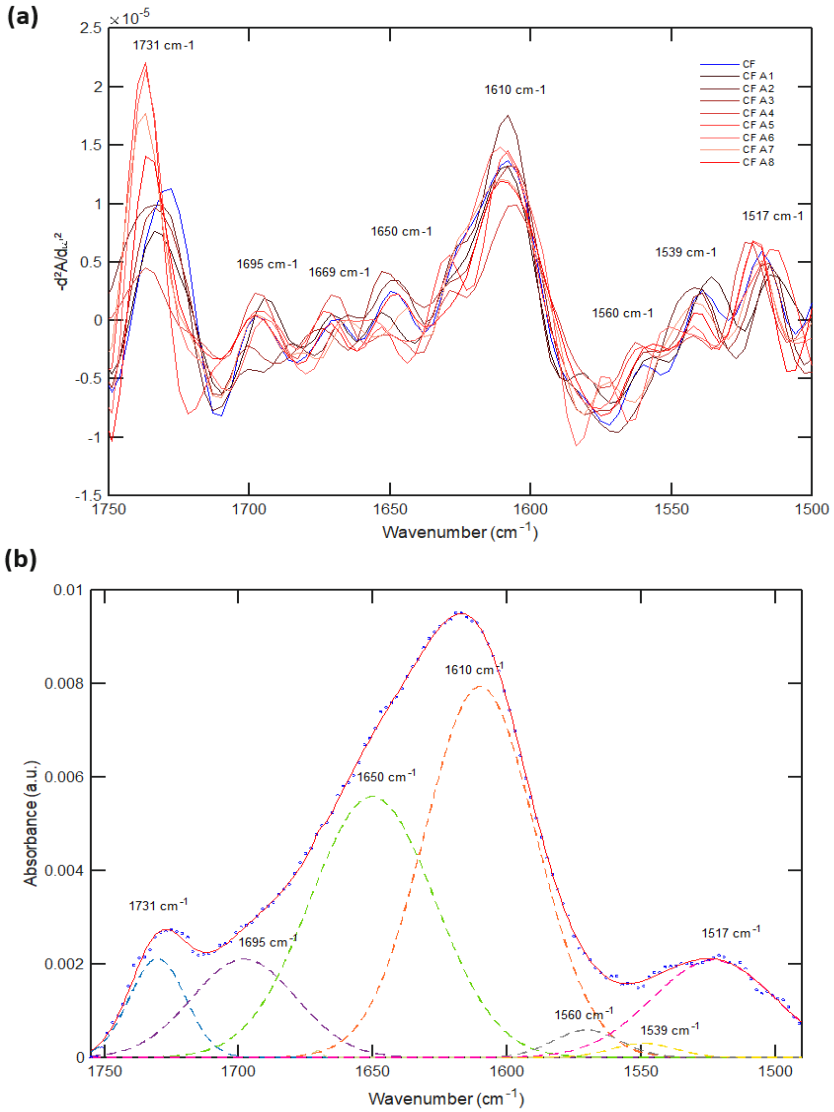

Figure 3-25. Derivative (a) and deconvolution (b) from citrus fiber FTIR spectra in the range from 1750 to 1500 cm^{-1}.

The DM of CF and CFV samples were determined by FTIR, based on the bands around 1731 cm^{-1} and 1610 cm^{-1} corresponding to the esterified carboxyl groups and the free carboxyl group, and by titration (Figure 3-26).

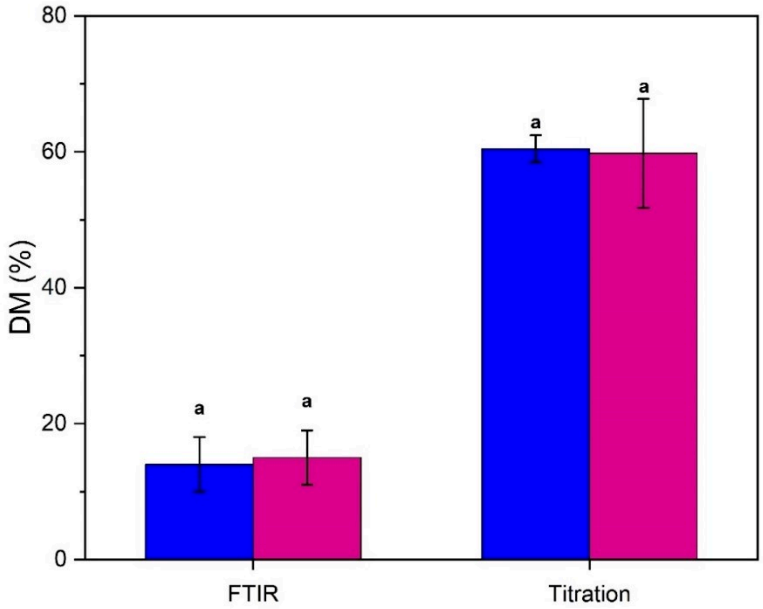

Figure 3-26. Degree of esterification of CF and CFV determined by FTIR and titration.

The value determined by FTIR was lower than 20% for both samples, 14 ± 4% and 15 ± 4% for CF and CFV, respectively, no significant difference was observed between them (Figure 3-26). Furthermore, the degree of methylation (DM) determined by titration for both CF and CFV exhibited a significantly higher percentage (60 ± 2% and 60 ± 8%, respectively) compared to DM determined through FTIR. Notably, no significant difference was observed between the DM values obtained through titration either, in accordance with FTIR results.

The DM of CF and CFV samples determined by titration was similar to those given in the literature for pectin from commercial citrus peels (47.6 – 64.1 %) (Fracasso *et al*., 2018; Yu et al., 2021), and pectin isolated from orange and lemon peels which published values vary between 63 to 75% (Sayah *et al.*, 2016; Willemsen *et al.,* 2017), respectively. The DM may be influenced by the temperature, type of acid and concentration of it used in pectin extraction, *e.g*. the citric acid has a positive effect on DM compared with sulfuric acid. No notable effect of processing was discerned on DM of citrus fiber under the applied conditions and no correlation can be made with the separation observed by PCA analysis. However, the analysis was conducted in a complex matrix (without isolating the pectin), which may explain the difficulty in observing differences in sample preparation or this difference may occur due to other chemical alteration in pectin or even the assay could take into account methylation from other species than pectin.

3.2.5. Chemical surface composition of citrus fibers studied with XPS technique

3.2.5.1. Repeatability of X-ray photoelectron analysis on citrus fibers

In order to evaluate the repeatability of XPS analysis, four repetitions of general spectra of citrus fiber were recorded with 2 scans. In addition, the possible material contamination and/or degradation during the analysis were also investigated since the powder was exposed to the beam for around 37 minutes (comprising the time of general scan and high-resolution scan). Citrus fiber surface is composed of, approximately, 70 % of carbon and 30 % of oxygen with traces of nitrogen (0.6 %) and sodium (0.2 %) as previously discussed (Figure 3-27). Analyzing quantitatively, the standard deviation between the repetitions for all surface components was lower than 0.5 %.

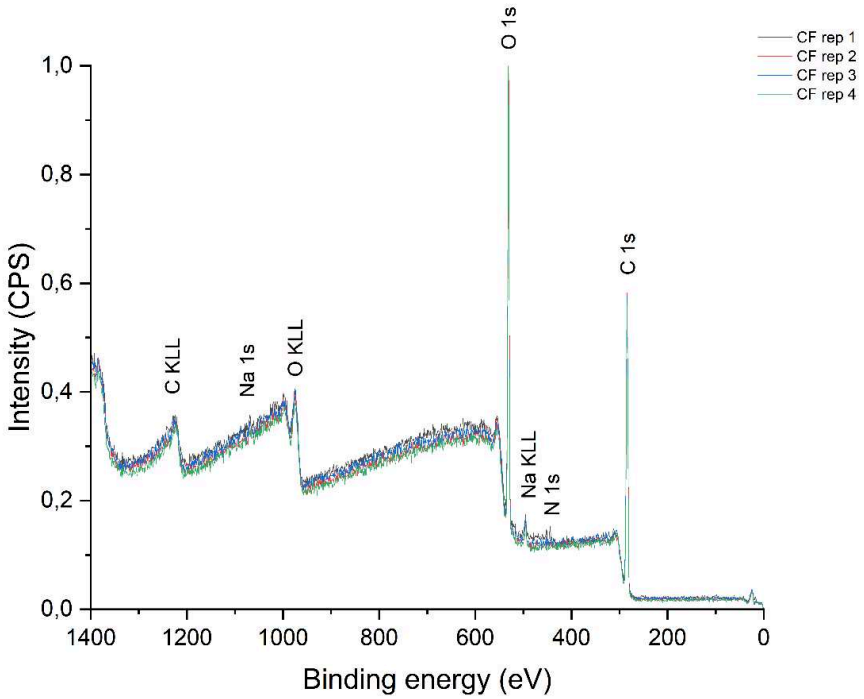

Figure 3-27. XPS citrus fiber spectra for 4 repetitions.

The high-resolution data mode provides the most valuable information about the surface (for quantification and chemical bonding information). In this mode, the sample is submitted to several scans, increasing the risk of charging and decomposition by irradiation. Charging is the greatest challenge for measurement reliability as the non-optimized neutralization parameters can result in slight charging of the surface modifying the peak shapes, and therefore providing a wrong interpretation (Baer *et al.,* 2019; Johansson & Campbell, 2004; Moulder *et al.,* 1992). Another notable issue in XPS measurement is sample degradation when

exposed to radiation, particularly under vacuum conditions. This degradation tends to be time-dependent (Johansson & Campbell, 2004). To check this, the citrus fiber surface was examined using two, four, and six scans.

The energy region of the C 1s signal was decomposed in four peaks corresponding to C-C/C-H, C=O, C-O, and O-C=O in 285 eV, 286.5 eV, 287.9 eV and 289 eV, respectively. The profile of this region slightly changed with increasing scan numbers. Only the area of the peak corresponding to C-C/C-H significantly rose ($p>0.05$) from 24 % for 2 scans to 28% for 6 scans. Then, this modification can be related to light sample charging and/or degradation by irradiation. Regarding the high-resolution binding energy region of the O1s signal, it can be decomposed into two separate peaks around 530 and 532 eV, linked to C=O and C-O, respectively. Contrary to the carbon signal, it does not seem sensitive to charging and nor to degradation of the sample. The O1 (C=O) component was 82.6 ± 1.8 % and the O2 (C-O) component was 17.5 ± 1.8 %. This region showed the same profile and deconvolution parameters independently of the scan numbers.

In summary, only the population related to C-C and/or C-H showed significant variation when the analysis was done with increasing numbers of cycles, with a slight increase ($p>0.05$). The other values were not significantly different ($p < 0.05$). For this reason, all the measurements were done with four scans since it showed an intermediate value of C1 peak. 4 scans corresponded to an intermediate time spent inside the machine which seemed to limit the artifacts and provide a correct signal to noise ratio.

3.2.5.2. The impact of sample preparation on surface composition of citrus fibers

In citrus fiber, the two most common chemical elements detected were carbon at 284.9 eV, and oxygen at 532.9 eV (Table 3-10). Sodium and nitrogen only represent traces. The presence of nitrogen indicates the slight content of protein at the surface (Gaudel *et al.,* 2022). Considering an average conversion factor of 6 for vegetable proteins, the percentage of proteins on the surface would not reach 4%, which is still less than the total protein amount of 5.1%. This observation suggests that the proteins present in the citrus fibers studied, are under-represented on the surface of the fiber particles and therefore more are present in the core of these particles. This can be due to strong interactions of these proteins with other components located in the core. The origin of the sodium atoms may be from the pretreatment of citrus fiber, such as bleaching *i.e.* use of hydrogen peroxide and sodium bisulfite. The carbon and oxygen values observed for sample CF at time 0 were similar to the results

obtained on fruits powders by Gaudel *et al.* (2022). However, sample CF showed lower nitrogen content. On the other hand, the grewia polysaccharide gum presented around 0.5 % of nitrogen on the surface, comparable to citrus fibers (Nep & Conway, 2011).

Table 3-10. Quantitative analysis of surface composition of citrus fibers prepared in two different ways: immediately dried (CF) and kept in IPA for 45 days before drying (CFV) then dried at different scales.

Sample	C (%)	O (%)	N (%)	Na (%)	O/C
CF	68.7 ± 0.7 ^{a}	30.3 ± 0.6 ^{a}	0.6 ± 0.1 ^{a}	0.3 ± 0.1 ^{a}	0.4 ± 0.0 ^{a}
CFV	62.4 ± 0.4 ^{b}	36.5 ± 0.4 ^{b}	0.7± 0.1 ^{a}	0.3 ± 0.2 ^{a}	0.6 ± 0.0 ^{b}

Data were expressed by means (n=9) ± standard deviation. Values followed by different letters in the same column are significantly different ($p < 0.05$).

The ratio O/C obtained for samples CF and CFV were 0.4 and 0.6, respectively. The ratio measured for the samples were lower than the theoretical O/C value for cellulose (0.83), which suggested that their surfaces do not contain pure cellulose in agreement with the composition of the samples (Figure 3-28). A similar value was observed on citrus fiber by Fras *et al.* (2005) for pre-purified cotton specimens. Several studies attributed this low ratio to the presence of lignin and/or waxes (Zafeiropoulos *et al.*, 2003). However, citrus fiber does not contain lignin and the O/C ratio inferior of 0.83 may be due to a complex matrix composition or rearrangement of cellulose, pectin, hemicellulose and low content of protein and ash.

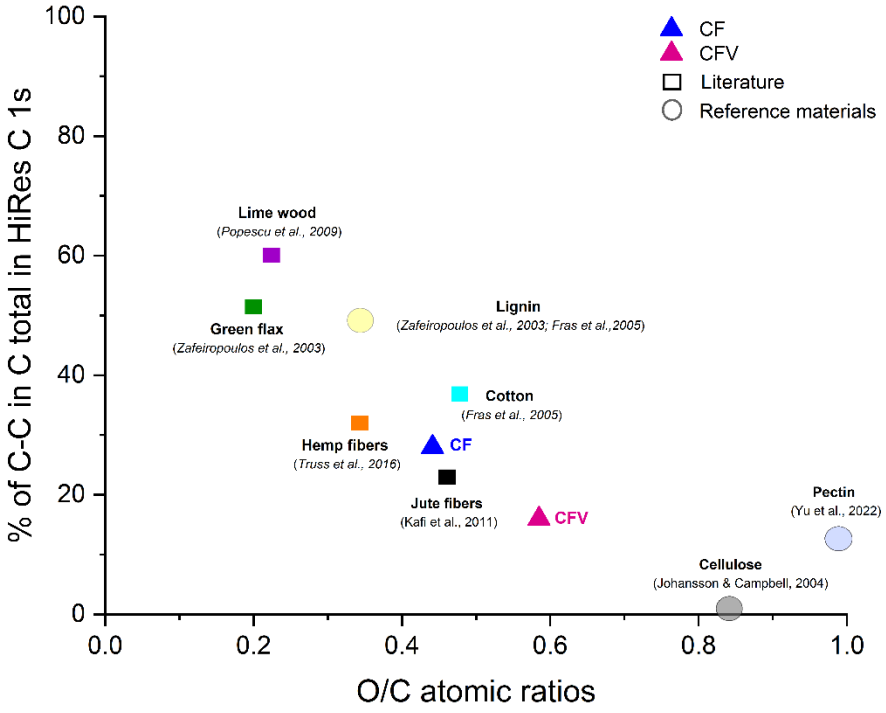

Figure 3-28. Calculated O/C ratios and relative amounts of C-C bonded carbon in samples CF (immediately dried) and CFV (kept in IPA for 45 days and dried with different process conditions), calculated from XPS data, are compared with reference materials (cellulose, pectin and lignin and various literature values).

The greatest difference between samples CF and CFV was in carbon and oxygen content (Table 3-10). Sample CFV showed a lower carbon content and a higher oxygen content, with a difference of 6%.

Several researchers investigated the effect of the drying process on the characteristics and functional properties of carbohydrate powders (Caparino *et al.*, 2012; Mirhosseini & Amid, 2013; Mishra *et al.*, 2009; Nep & Conway, 2011). Nep & Conway (2011) who studied the effect of drying method on the surface composition of grewia gum polysaccharide, only observed significant changes in the relative composition O/C of the air-dried and freeze-dried samples, with lower O/C ratio for air-dried sample compared to freeze-dried. According to Kim *et al*. (2009a), the water diffusion towards the surface is accompanied upon drying by an opposite diffusion of components towards the center. The surface composition depends on the one hand on size of molecules, *i.e* larger molecules diffusing slower than smaller molecules; and on the other hand, on the drying rates and temperatures: *i.e.* lower rates and slow temperature providing the components more time to migrate. Besides, the longer exposition to high temperature may promote degradation, reducing the O/C ratio (Inari *et al.*, 2006).

The samples CF and CFV were dried at different process scales, consequently the exposure for longer drying time (7 hours) and higher temperature (sample temperature 50 °C) of CF sample compared to sample CFV (45 minutes maximum, sample temperature of 40 °C) could have led to more time for component migration to surface, resulting in a different surface composition. Additionally, the components on surface of sample CF may be degraded by the long temperature exposition during drying, reducing the ratio O/C. In addition to the assumptions about the impact of drying, another factor that may explain the difference in the O/C ratio between samples CF and CFV is sample variability. The different latter may correspond to a slight difference in the composition of the citrus fiber samples reflected on surface composition.

Figure 3-29 represents the area of the peaks from deconvolution of C1s and O1s high resolution scans. The C1s spectra was decomposed into 4 components (Figure 3-29a). From these data, the carbon atoms bonded with one oxygen atom (C-O) (C2) was concluded to be the most abundant for CF and CFV, representing between 40-50 % of the total area of C. It most likely corresponds to the presence of polysaccharides on the surface (Truss *et al.,* 2016). C1 can be associated with carbon atoms bonded with other carbon or hydrogen (C-C/C-H) while C3 could be correlated to carbon bonded with two oxygen atoms (C=O/O-C-O). CF had more carbon bonded to another carbon or hydrogen, and carbon single bonded to oxygen than carbon bonded to two different atoms of oxygen. Differently, sample CFV showed a higher quantity of carbon bonded to one or two oxygen atoms. These results agree with the elementary composition, since sample CF had a higher C1 contribution and lower C2 than sample CFV. It may represent the production of by-products with lower oxygen content due the dehydration and/or degradation of biopolymers present in the sample (Inari *et al.,* 2006). In addition, the lowest value of C4 (O-C=O) for samples CFV and CF indicates a lower quantity of acid or ester on the citrus fiber surface (Truss *et al.*, 2016).

Figure 3-29b illustrates the high resolution of O 1s, showing no significant difference between samples CF and CFV regarding carbon-oxygen bonds on the surface, mainly containing C=O bonds.

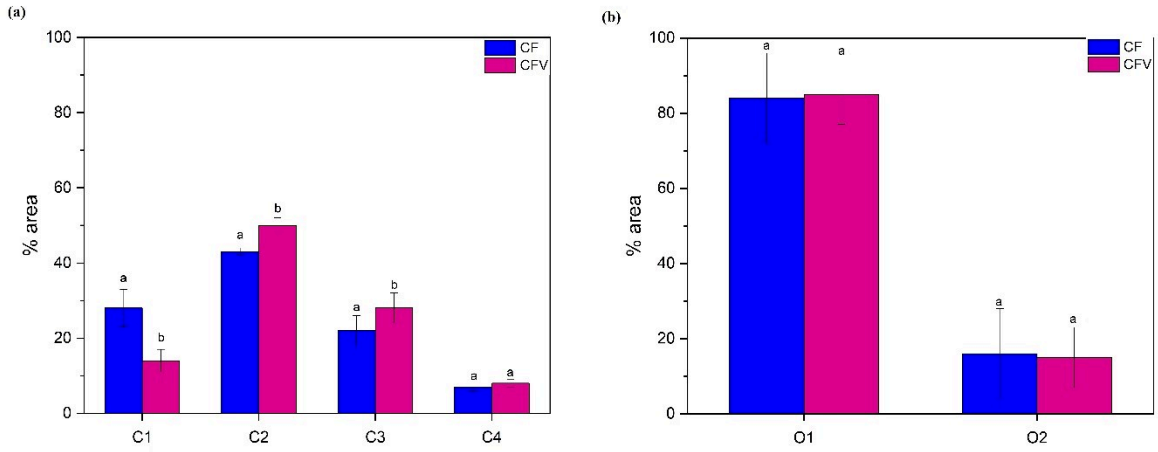

Figure 3-29. C 1s and O 1s peaks for CF and CFV from different drying conditions. Error bars represent standard deviation of the mean (n=9). Means followed by the same letter in each bar group are not significantly different ($p<0.05$).

Another parameter widely used to characterize the surface is the ratio between C-C/C-H and other C bonds. These proportions provide information about the surface hydrophilicity/hydrophobicity. Both samples showed a ratio between 0 and 1 (CF ratio 0.40 ± 0.03 and CFV ratio 0.21 ± 0.02), corresponding to a hydrophilic character of the surface. In general, fruits and polysaccharides powders have hydrophilic a surface (Fournaise *et al.*, 2021). Most of the polysaccharides are hydrophilic which explains the hydrophilic character of the citrus surface (Tang & Huang, 2022). As observed before, CFV has more carbon bonded to oxygen, proving a more hydrophilic character on the surface than CF.

These results showed that the preparation mode of citrus fiber can affect the surface composition resulting in a sample variability, while the drying process could degrade some compounds on the surface depending on the time and temperature. The drying duration may also play a role: longer drying process gives more time for a rearrangement of hydrophobic molecules preferentially at the surface of the particle, than in the core. Then, the control of the sample preparation can be essential to obtain a more hydrophilic surface, to directly control the properties and applications of the product.

3.3. Conclusion

The comprehensive physico-chemical characterization of citrus fibers has provided a deep understanding of their structural attributes, molecular mobility at different scales, water dynamics, chemical composition, and surface chemical composition. The matrix is heterogeneous in its composition and organization. This heterogeneity at the macro, meso, and molecular scales results in different behaviors in response to varying water content and

temperatures (different water sorption kinetic, multiple glass transition, distinct proton populations exhibiting different molecular mobility). Citrus fiber exhibits molecular mobility even at temperatures below the glass transition and with lower water content. Furthermore, water content appears to have a greater impact on the stability of citrus fibers than temperature. Most water interacts with the less mobile fraction of citrus fibers, slightly increasing its molecular mobility, yet the overall plasticizing effect remains limited due to the semi-crystalline structure. Regarding chemical composition and surface chemical composition, these materials are rich in polysaccharides, and the process seems to affect the structure and/or pectin content, as well as the surface composition. This study highlights the importance of the process, which can also influence the stability of citrus fibers during storage.

Chapter 4. Functional properties of citrus fiber and their survey during storage time

Chapter 4. Functional properties of citrus fiber and their survey during storage time

4.1. Research background and objectives

Functional properties in foods arise from intricate interactions involving structure, molecular conformation, and composition within a multi-component physical system. These properties are swelling capacity, water absorption, oil absorption, emulsion activity, stability, foam capacity, and gelatinization (Awuchi *et al.,* 2019). Studying such properties is challenging due to the complex interactions within food systems, reflecting more on the interplay between components than on individual component properties (Tolstoguzov, 2002).

The functional versatility of citrus fiber allows applications as fat and egg replacers, water retention agents, emulsifiers, thickeners improving the stability texture in several food products (bread, cookies, sausages, mayonnaise, and yogurts) (Bugarín & Gómez, 2023; Kohajdová *et al.*, 2011; Korus *et al.*, 2020; Kristensen *et al.,* 2022; Powell *et al.,* 2019; Ruan *et al.,* 2019; Sendra *et al*., 2010; Song *et al.,* 2016; Su *et al.*, 2020).

While studies have explored irreversible changes during drying, leading to reduced functional properties, investigations into the impact of storage time on these properties have been poorly investigated. In the food powders industry, the loss of functional properties upon water reconstitution is a challenge. One plausible reason for the irreversible structural changes during drying is the cross-linking between cellulose microfibrils (Agoda-Tandjawa *et al.*, 2010). Despite some studies on modifications induced by storage in dairy products and fruit powders products (Fernández-López *et al.,* 2009; Fyfe *et al.,* 2011; Gaiani *et al*., 2007; Liu *et al.*, 2010; Masum *et al*., 2020a, 2020b; Staniszewska *et al.,* 2021), detailed examinations of citrus fiber storage effects on functional properties are lacking. Based on this background, this chapter aimed to investigate the pH and functionality (through water holding capacity, water swelling capacity, and gelation) of dried citrus fibers upon storage, considering the combined effect of temperature and humidity.

4.2. Results and discussion

4.2.1. Characterization of functional properties of citrus fiber

The initial pH of CF was 4.78 ± 0.02 whereas CFV showed a pH 4.42 ± 0.05. Low pH represents a high concentration of H^+ ions which could be due the dissociation of carboxylic acid during the processing (*e.g.* drying step) or dissociation of carboxyl group in amino acids

from protein (Rahman e*t al.*, 2019). In the case of CF and CFV the difference may be related to the variation in composition resulting from processing, in polysaccharides or protein fraction. In the literature, the pH of citrus peels is mentioned to be acidic in nature around 4.96 ± 0.01 (Dias *et al.*, 2020; Panwar *et al*., 2023). It was expected that the pH of CF and CFV samples would be similar since they have the same origin, but their different pH could also be justified by different processing. The low pH of citrus derivates makes them resistant to microbial growth, helping keep the quality of the end products.

WHC values of samples CF and CFV at time 0 were 17.6 ± 0.5 g of water/g of dry sample and 17.4 ± 0.4 g of water/g of dry sample, respectively, they were not significantly different (Table 4-1), and in agreement with literature data (Table 1-1).

Table 4-1. Functional properties of samples CF and CFV at time 0.

Samples	**WHC (g / g of sample)**	**WSC (mL / g of sample)**	**G' (Pa)**
CF	$17.6^{a} \pm 0.5$	$63.0^{a} \pm 6.4$	$424^{a} \pm 3$
CFV	$17.4^{a} \pm 0.4$	$52.8^{a} \pm 5.9$	$430^{a} \pm 36$

Data were expressed by means (n=3) ± standard deviation. Values followed by different letters in the same column are significantly different ($p < 0.05$).

The WSC of CF and CFV at time 0 were 63.0 ± 6.4 and 52.8 ± 5.9 mL/ g of sample, respectively (Table 4-1). These values are higher than those observed in the literature which varied from 15 to 36 mL/g (Table 1-1). It could be explained by the different structure (surface, porosity) and chemical composition, known to impact the water swelling capacity (Zhang *et al*., 2020b). Additionally, the measurement protocols are not always the same, notably the sample concentration. However, no significant difference was observed between CF and CFV, in accordance with the results of WHC.

The G' at time 0 (freshly dried sample) was equal to 424 ± 3 Pa for CF and 430 ± 36 Pa for CFV (Table 4-1). No significant difference was observed between CF and CFV samples on WHC, WSC and G' values, indicating that drying at different scales did not impact sample functionality. Thus, CFV can be used as a reference to evaluate the effect of time.

4.2.2. Survey of stability of citrus fiber in long term storage

The pH of citrus fiber stored in accelerated conditions (CF_A) (Figure 4-1) showed fluctuations with increasing storage time, in which the variation was significant ($p>0.05$) with time. Citrus fiber stored at room conditions (CF_R) showed minor fluctuations with storage time compared to the sample stored in accelerated conditions, with no significant difference

($p<0.05$) with time. However, an unsystematic variation was noted, invalidating a relation with storage time.

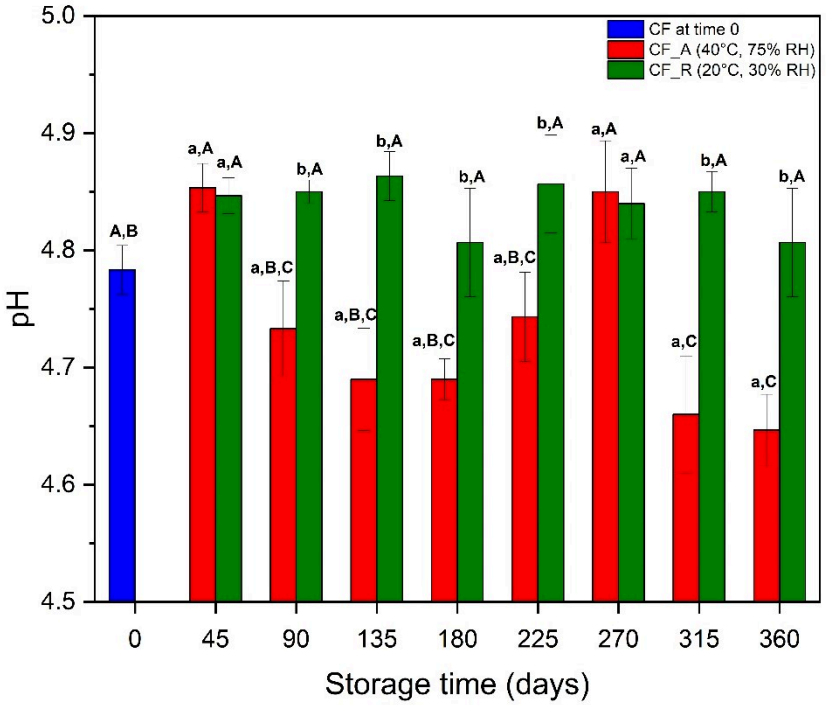

Figure 4-1. The pH of citrus fibers in 2% (g/g) solution after storage of the powder in accelerated aging conditions (CF_A) (40 °C, 75% RH) or room conditions (CF_R) (20 °C, 30% RH).

Data were expressed by means (n=3) ± standard deviation. Values followed by capital letters are significantly different in relation to storage time (each storage condition was compared separately) ($p < 0.05$). Different lower-case letters in the top of each bar denote significant differences between storage conditions ($p < 0.05$).

Liu *et al.* (2010) who investigated the changes in tomato powder during storage, observed a decrease in pH when tomato powder was stored at 25 and 37 °C. This reduction could be attributed to the Maillard reaction, causing the degradation of sugars into acids. Although in this work there is no linear correlation with pH and time, especially the pH after 315 and 360 days of storage, are significantly ($p<0.05$) lower than pH at time 0. It suggested the probability of the Maillard reaction taking place during the storage period in accelerated conditions.

Parrott & Thrall (1978) studied the impact of pH (2.69, 5.20, 7.33) on water-holding capacity (WHC) in different fibers, finding pH variation could alter WHC by up to 40%. Avicel fibers peaked in WHC at pH 7.33, declining in acidity, while peanut hull fibers favored acidic conditions but diminished as pH increased. Schalow *et al.* (2018) observed that WHC of pectin-rich by-products increased with higher pH due to carboxyl group dissociation of pectin. The relation between hydration properties of fibers and pH is more important in the

presence of polyelectrolytes, such as the carboxyl groups of pectin polymers (Willemsen *et al.,* 2020). For this reason, all the analyses were done in a buffer to avoid any pH effect for comparison during the storage experiments.

Figure 4-2 illustrates the variation of WHC values for samples CF_R and CF_A. The sample stored in room conditions (CF_R) only showed significant difference with the value at time 0 after 135 and 270 days of storage in room conditions which indicates a minimal effect of time on WHC. For samples stored under accelerated conditions significantly lower values were observed between WHC at time 0 and 45, 135, 270, 315, and 360 days.

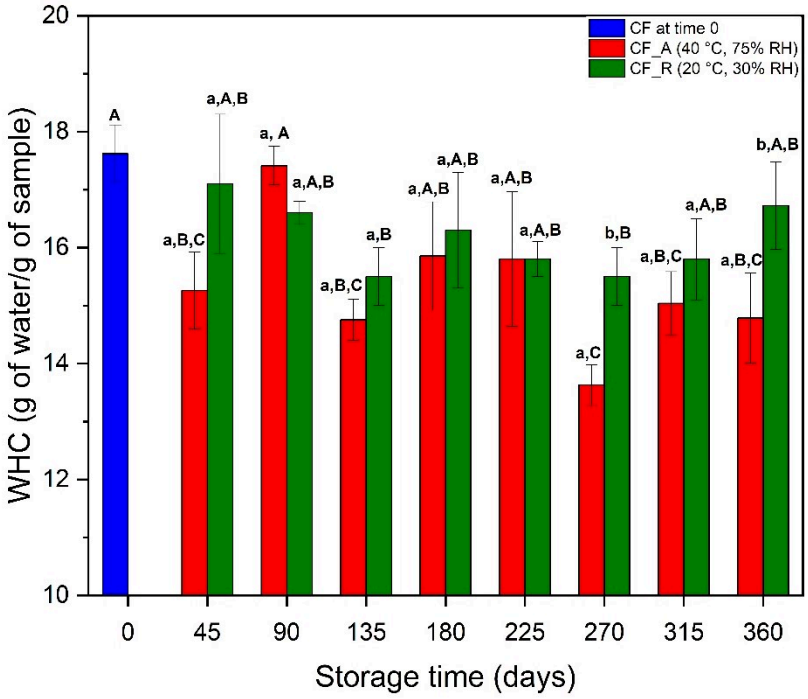

Figure 4-2. WHC values for citrus fibers after storage in accelerated aging conditions (CF_A) (40 °C, 75% RH), or room conditions (CF_R) (20 °C, 30% RH).
Data were expressed by means (n=3) ± standard deviation. Values followed by capital letters are significantly different in relation to storage time (each storage condition was compared separately) ($p < 0.05$). Different lower-case letters in the top of each bar denote significant differences between storage conditions ($p < 0.05$).

When CF was stored in room conditions (CF_R), the WSC decreased from 63 to 28 mL/g of sample (Figure 4-3). When the sample was stored in accelerated aging conditions, WSC decreased from 63 to 23 mL/g of sample during the first 135 days of storage (Figure 4-3). Then, WSC continued to decrease but to a lesser extent. For this functional parameter, keeping the citrus fiber at both milder temperature and humidity conditions helped slow down the evolution observed in the samples during storage.

These data revealed a decrease of the swelling capacity with time meaning that the rehydration of the powder will be limited either by a lower amount of water uptake or/and a

slowdown of swelling kinetics. This may be due to a densification of powder (possibly associated with physical aging) because the storage temperature (40 °C) is only 10 °C below the beginning of the DSC signal detected as Tg_1 (50 °C), this evolution is expected to induce a more stable rearrangement of the amorphous zone of the material.

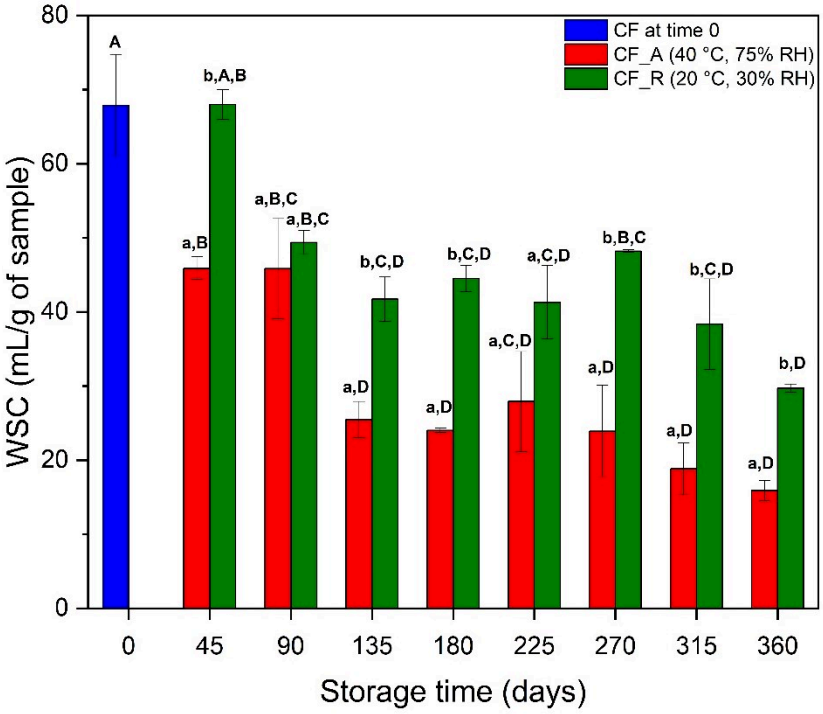

Figure 4-3. Evolution of WSC for citrus fibers after being stored in accelerated aging conditions (CF_A) (40 °C, 75% RH) or room conditions (CF_R) (20 °C, 30% RH).
Data were expressed by means (n=3) ± standard deviation. Values followed by capital letters are significantly different in relation to storage time (each storage condition was compared separately) ($p < 0.05$). Different lower-case letters in the top of each bar denote significant differences between storage conditions ($p < 0.05$).

The storage modulus (G') of CF_A decreased from 424 Pa to 109 Pa (Figure 4-4). It is especially marked after 180 days. Stored in room conditions, the sample's storage modulus remained almost constant until 180 days of storage and also showed a significant decrease (40%) although to a lesser extent than in accelerated conditions (74%). This result was in agreement with the variation of the WSC after storage in the different conditions (Figure 4-3). In accelerated conditions, important changes in the considered properties were observed in early stages of storage, while the mild conditions postponed these quality modifications by 6 months.

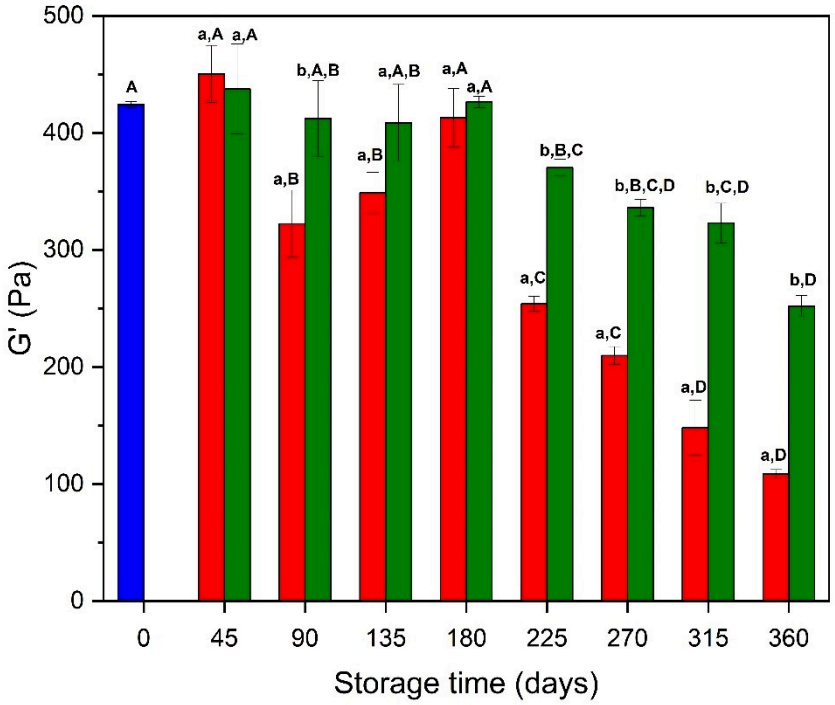

Figure 4-4. Variation of the storage modulus (G') of citrus fibers after being stored in accelerated aging conditions (CF_A) (40 °C, 75% RH) or room conditions (CF_R) (20 °C, 30% RH).

Data were expressed by means (n=3) ± standard deviation. Values followed by capital letters are significantly different in relation to storage time (each storage condition was compared separately) ($p < 0.05$). Different lower-case letters in the top of each bar denote significant differences between storage conditions ($p < 0.05$).

PCA analysis was performed on pH and 3 functional properties (WHC, WSC and storage modulus) to further evaluate their interactions effect (Figure 4-5) and possibly highlight the time effect.

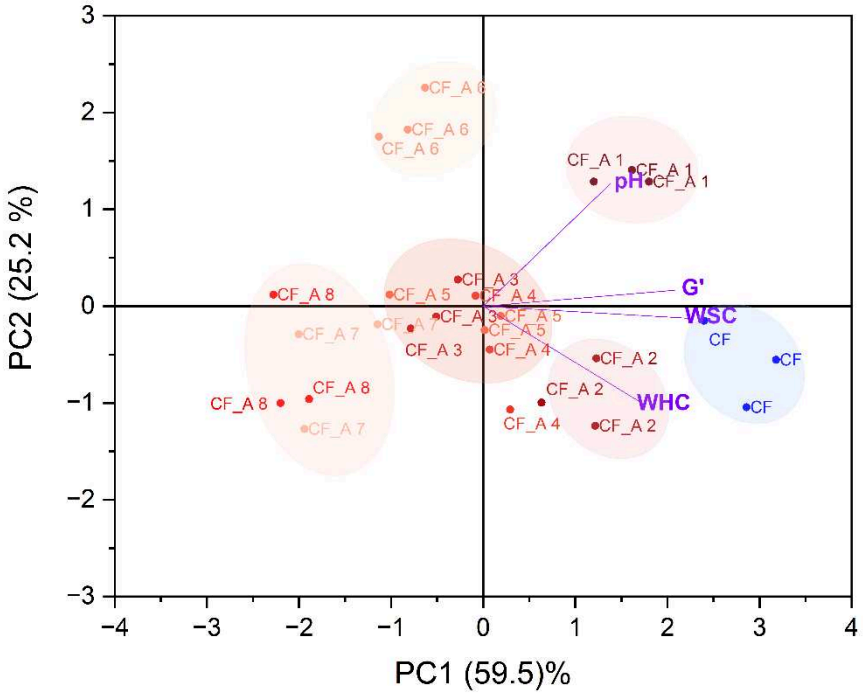

Figure 4-5. Principal component analysis (PCA): simplified loading and score plot for WHC, WSC and G' and CF sample time 0 and after being stored in accelerated aging conditions (CF_A) (40 °C, 75% RH).

The first principal component (PC1) has the higher significance, explaining 59.5% of the total variance whereas the second principal component (PC2) explained 25.2% of the total variance.

PC1 generally separated the samples according to storage time whereas PC2 did not. The CF at time 0 and the samples aged up to 90 days of storage in accelerated aging conditions (CF_A 1 and CF_A 2) were distributed on the positive side of PC1. The samples stored between 90 and 225 days (CF_A 3, CF_A 4, CF_A 5) showed scores close to the crossing of axes, indicating fewer variance in pH and functional properties, whereas those stored for more than 225 days (CF_A 6, CF_A 7 and CF_A 8), stayed in the negative side of PC1. PC1 is most positively influenced by the WSC whereas PC2 was positively influenced by pH and G' values and negatively by WHC.

To further reveal the relationship among different functional properties, the angle of the loading plots of PC1 *versus* PC2 were produced. Pair-wise parameters with small angles had positive correlation among them: suggesting the most positive correlation between WSC and storage modulus (G'), and a positive correlation between pH and storage modulus (G'), and also between WSC and WHC. On the other hand, those with angles close to 90° and 180° had

a neutral and negative relationship, respectively. Then, pH and WHC showed a neutral correlation.

Although there are some studies on food stability during the processing and storage (Harnkarnsujarit & Charoenrein, 2011; Kyomugasho *et al*., 2021; Liu *et al.*, 2006; Ostrowska-Ligęza *et al*., 2014; Roos, 1993), no clear explanation exists for the loss of citrus fibers' functional properties during storage. Several researchers discussed the hornification as a cause of decrease in water absorption for cellulosic matrices (Déléris & Wallecan, 2017; Lovikka *et al.*, 2018; Mo *et al.*, 2022; Šutý *et al.*, 2012). The decrease of hydration capacity with increasing storage time may be related to the decreased capacity of fibers to expand, possibly due to a reallocation of internal hydrogen bonds (Kato & Cameron, 1999).

A better knowledge of storage effects on the physico-chemical properties of citrus fiber remains needed to explain the reduction of functional properties as well as the combined effect of temperature and humidity.

4.3. Conclusion

The processing conditions (drying scales or kinetics) demonstrated to impact the pH of the samples but did not impact the functional properties.

The characterization of the functional properties (WHC, WSC and storage modulus) of dried citrus fiber confirmed the detrimental effect of aging on moisture retention, storage modulus, and rehydration behavior. In addition, a positive correlation was observed between storage modulus and WSC of citrus fiber. The loss in functionality was accelerated at 40 °C and 75% RH compared to 20 °C and 30% RH. These results showed that the water and/or temperature decreased citrus fiber's water holding, water swelling capacities, and storage modulus, affecting the shelf life. These reductions in functional properties can be related to the collapse of pores and changes in particle size and density, in structure of polysaccharides, and surface composition. These modifications may be explained by chemical and/or physical origins. In the next chapters, the assumptions around physical and chemical effects (item 1.5, page 44) will be considered.

Chapter 5. Impact of storage time on physicochemical properties of citrus fibers

Chapter 5. Impact of storage time on physicochemical properties of citrus fibers

5.1. Research background and objectives

Storage-induced changes such as enzymatic and chemical reactions, leading to textural alterations (Massiot *et al.*, 1996; Walter, & Palma, 1996), physiological defects in beans (Chen *et al*., 2021; Kyomugasho *et al*., 2021), degradation of paper and wood (Assifaoui *et al*., 2006; Kato & Cameron, 1999; Łojewska *et al.*, 2006, 2005; Popescu *et al.*, 2009), and loss of functionalities in food powders (Fernández-López *et al.*, 2009; Hedegaard & Skibsted, 2013).

Kato & Cameron (1999) delved into the mechanisms behind cellulose aging, highlighting the significant impact of temperature and humidity on this process. Specifically, elevated temperatures accelerate reaction rates and enhance molecular mobility, whereas heightened humidity markedly increases the potential of hydrolysis. Chemical changes further impact hydration properties, influencing the orientation and rearrangement of water molecules within functional groups (Barbucci *et al*., 2000; Di Gioacchino *et al.*, 2020). Additionally, storage-induced alterations extend to the degree of esterification of pectin, significantly affecting its emulsion stability capacity and gelling mechanism, thus impacting the convenience and utilization of various products (Agoda-Tandjawa *et al.*, 2012; Chatjigakis *et al*., 1998; Ciriminna *et al*., 2017; Humerez-Flores *et al*., 2022).

The alterations induced by storage can be detected through “shifts” in the chemical composition of the surface. Popescu *et al.* (2009) provided, by XPS in particular, insights into the correlation between deterioration and chemical reaction taking place during storage of lime wood. The removal of carbon-rich components, including terpenes, phenolics, and fatty acids, was identified as a consequence of oxidation and hydrolysis reactions.

While studies have investigated the impact of drying on the rehydration behavior of powders (Déléris & Wallecan, 2017; Mo *et al.*, 2020), there is a notable gap in understanding how storage affects functional properties. Most published reports focus on the negative consequences of aging on solubility and hydration properties, particularly in dairy products (Gaiani *et al*., 2007; Kim et al., 2009b, 2009a; Masum *et al.,* 2020a, 2020b), and only few works investigated the impact of storage on functional properties of cell wall materials from citrus (Fernández-López *et al.*, 2009; Putri *et al.,* 2024). Notably, the literature lacks comprehensive investigations into the storage stability of citrus fibers, leaving a significant void in knowledge about the mechanisms underlying storage-induced changes.

This chapter aimed to comprehensively examine the physicochemical properties of citrus fibers after long-term storage, considering the combined influence of temperature and humidity, and understand the underlying mechanisms contributing to the loss of functionalities upon sample rehydration. The impact of storage on water distribution in citrus fibers stored in accelerated aging conditions (40 °C, 75% RH) for 360 days was investigated. Mathematical data analysis was applied to assess vapor sorption kinetics, equilibrium water content, and the hysteresis between sorption and desorption. To study the impact of time on molecular mobility, measurements of the enthalpy relaxation, glass transition and α-relaxation were performed Additionally, chemical reactions that could lead to the loss of functionality in citrus fibers stored under both accelerated aging (40 °C, 75% RH) and room conditions (20 °C, 30% RH) were investigated. Qualitative and quantitative changes in polysaccharide components were evaluated using FTIR, and principal component analysis (PCA) was used to compare samples across different storage durations. Furthermore, the oxidation index and degree of esterification were determined by correlating FTIR data with titration analysis. Lastly, the impact of storage on the chemical surface composition was evaluated by XPS, comparing the two different storage conditions. Understanding how storage-induced changes impact functional properties could offer valuable insights for the food industry.

5.2. Results and discussion

5.2.1. Evolution of moisture distribution during the storage

The adsorption and desorption isotherms curves of citrus fibers (Figure 5-1a) revealed a sensitivity during adsorption for samples stored in accelerated aging conditions (40 °C, 75% RH) for a_w between 0.5 and 0.9, and more obviously at a_w 0.7: the equilibrium water content decreased with increasing storage time (Figure 5-1b).

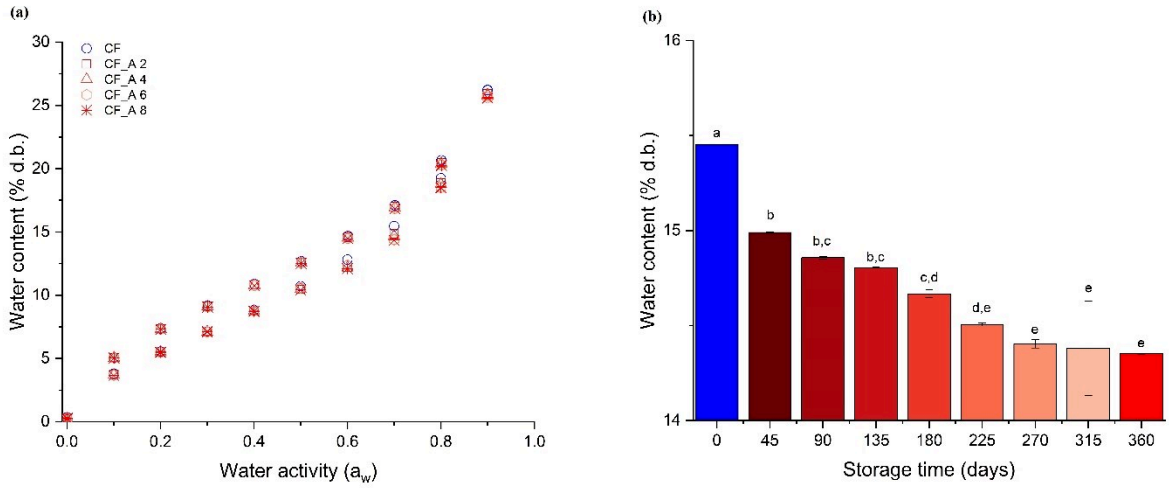

Figure 5-1. Sorption isotherm of citrus fiber after different storage times (stored in accelerated aging conditions (40 °C, 75% RH)) (a); equilibrium water content at aw 0.7 for different storage time in accelerated aging conditions (n=2, different letters represent significant differences ($p<0.05$)) (b).

It suggested changes in the sample during the storage such as reorganization, pore collapse or crystallization, reducing the water sorption capacity. As this reduction is observed at high a_w, probably it is related to changes in capillary pores (shrinks and collapses) instead of in the binding sites (Al-Muhtaseb *et al*., 2002). The storage of the samples at 40 °C and 75% RH, the temperature and/or humidity can soften the biopolymer matrix, and then, the mobility can be enough to allow the formation of an ordered and aggregated structure as a function time. It reduces the water accessibility, similar to the hornification process (Lovikka *et al.*, 2018).

No difference in water interaction was observed in desorption suggesting that the largest alterations in water accessibility took place during adsorption and appeared to be reversible with an exposure to high relative humidity (at least RH 90% in this work). To better understand the time effect on water sorption of citrus fibers, the latter was investigated on the hysteresis and equilibrium.

5.2.1.1. Hysteresis

Citrus fibers upon different storage time deviated from the curve observed to CF at time zero (fresh sample – blue curve) (Figure 5-2a) and also from hysteresis curves observed in the literature (Al-Muhtaseb *et al*., 2002; Espino-Pérez *et al*., 2016; Hill *et al*., 2010; Tejada-Ortigoza *et al*., 2017; Willems, 2014; Xie *et al*., 2011a; Xie *et al.,* 2011b). The maximum of hysteresis shifted from a_w 0.4 for the fresh sample to a_w 0.7 (CF_A 6 to CF_A 8), with an intermediate value of a_w 0.6 for intermediate aged samples (CF_A 2 up to CF_A 5) (Figure

5-2a). At aw 0.7 (Figure 5-2b), this hysteresis dramatically increased between time 0 and 45 days of storage, followed by slight enhancement of hysteresis between 45 days to 270 days, and it then remained constant between 270 to 360 days of storage.

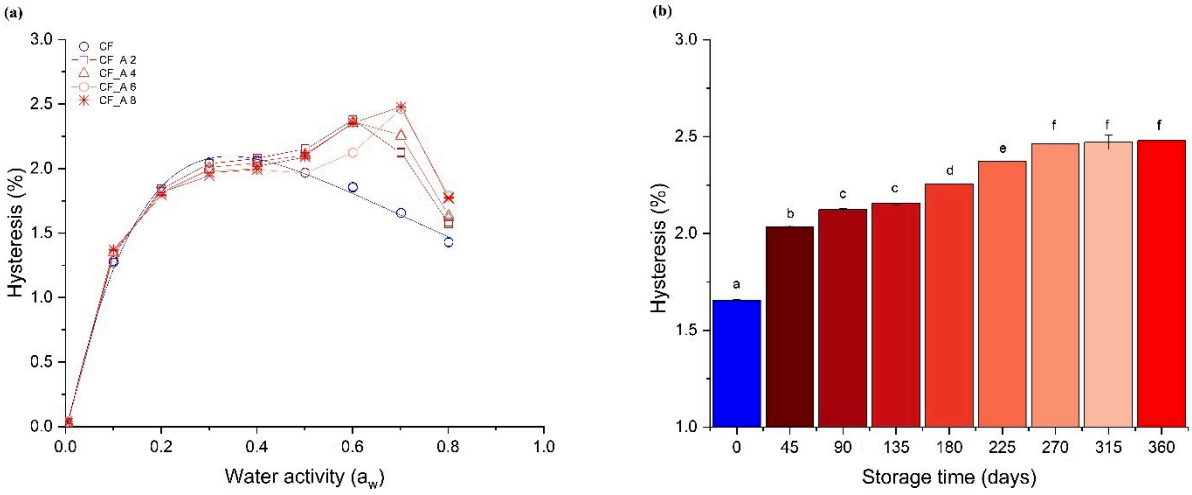

Figure 5-2. Hysteresis of citrus fiber after different storage times in accelerated aging conditions (40 °C, 75% RH) (a); Hysteresis of citrus fiber after different storage times in accelerated aging conditions (40 °C, 75% RH) versus storage time at aw 0.7 (n=2, different letters represent significant differences ($p<0.05$)) (b).

The hysteresis maximum represents the water activity at which sorption and desorption have the greater difference in terms of amount of water. For fresh samples, the hysteresis is lower than for aged ones, meaning that the pressure of water needed to fill the pores has to be higher probably because the material is denser and the access to porosity is more difficult and/or the porosity lower (inducing lower amount of water sorption).

5.2.1.2. Equilibrium

Table 5-1 shows the GAB trendline fitted to the samples stored at 40 °C and 75% RH for 360 days. The saturation of monolayer adsorption sites, measured with monolayer values (X_m), decreased significantly from 7.02 to 6.44 g H_2O/g d.b. after 360 days of storage.

Table 5-1. Parameters of GAB model fitted to the sorption isotherms of citrus fiber after different storage time at 40°C and 75% RH.

Storage days	X_m (g H_2O/g d.b.)	C	K	P-value (%)
0	$7.02^{a} \pm 0.01$	$10.62^{a} \pm 0.07$	$0.8205^{a} \pm 0.0007$	$3.1^{a} \pm 0.1$
45	$6.69^{b} \pm 0.00$	$11.64^{b} \pm 0.00$	$0.8315^{b, c} \pm 0.0007$	$4.7^{b} \pm 0.1$
90	$6.61^{b, c} \pm 0.00$	$12.10^{c} \pm 0.02$	$0.8337^{b, d} \pm 0.0006$	$4.4^{a, b} \pm 0.8$

135	$6.59^{b, c} \pm 0.00$	$12.27^{c, d} \pm 0.04$	$0.8340^{b, d} \pm 0.0000$	$4.8^{b, c} \pm 0.4$
180	$6.55^{c, d, e} \pm 0.01$	$12.48^{d, e} \pm 0.03$	$0.8340^{b, d} \pm 0.0014$	$5.3^{b, c, d} \pm 0.4$
225	$6.61^{b, c} \pm 0.00$	$12.42^{d} \pm 0.01$	$0.8295^{c} \pm 0.0007$	$5.7^{b, c, d} \pm 0.1$
270	$6.55^{c, d} \pm 0.01$	$12.68^{e} \pm 0.11$	$0.8320^{b, c} \pm 0.0010$	$6.2^{b, c, d} \pm 0.3$
315	$6.46^{d, e} \pm 0.12$	$13.20^{f} \pm 0.03$	$0.8355^{d} \pm 0.0007$	$5.6^{b, c, d} \pm 0.4$
360	$6.44^{e} \pm 0.01$	$13.14^{f} \pm 0.07$	$0.8357^{d} \pm 0.0006$	$6.3^{d} \pm 0.2$

Different letters in the same column indicate that values are significantly different (n=2, $p<0.05$).

The parameters C showed a rise of enthalpy involved in monolayer adsorption with increasing storage time, ranging from 10.6 to 13.1. It means that the bonds between water molecules from CF monolayer became stronger with increasing storage time, possibly as a result of greater proximity of two molecules (Muzaffar & Kumar, 2016).

For K values, a significant difference was observed comparing the fresh sample and the sample stored for 360 days. It slightly rose with increasing storage time, suggesting the multilayer became more similar to bulk water after 360 days of storage.

The P-value is below 10% for all storage time which is accepted to be a good fit (Owo *et al.,* 2017). However, it increased with increasing storage time, confirming the change in the water adsorption mechanism upon storage since the GAB model became less adequate to describe the sorption isotherm of citrus fiber.

Paes *et al.* (2010) attributed a similar decrease in X_m (from 11 to 7 g H_2O/g d.b.) for eucalyptus cellulose to recrystallisation as the crystallized fraction would contribute to the water sorption less than the amorphous fraction (Kocherbitov *et al.*, 2008; Paes *et al*., 2010).

5.2.1.3. Crystallization

Because crystallization of citrus fibers may occur during the storage, XRD patterns for dehydrated citrus fibers were measured for different aged samples (0, 180 and 360 days of storage corresponding to CF, CF_A 4 and CF_A 8 samples, respectively) (Figure 5-3). The diffraction of the (200) lattice peak around 21° corresponds to the crystalline fraction and the (110) peak around 18° is equivalent to amorphous fraction of material.

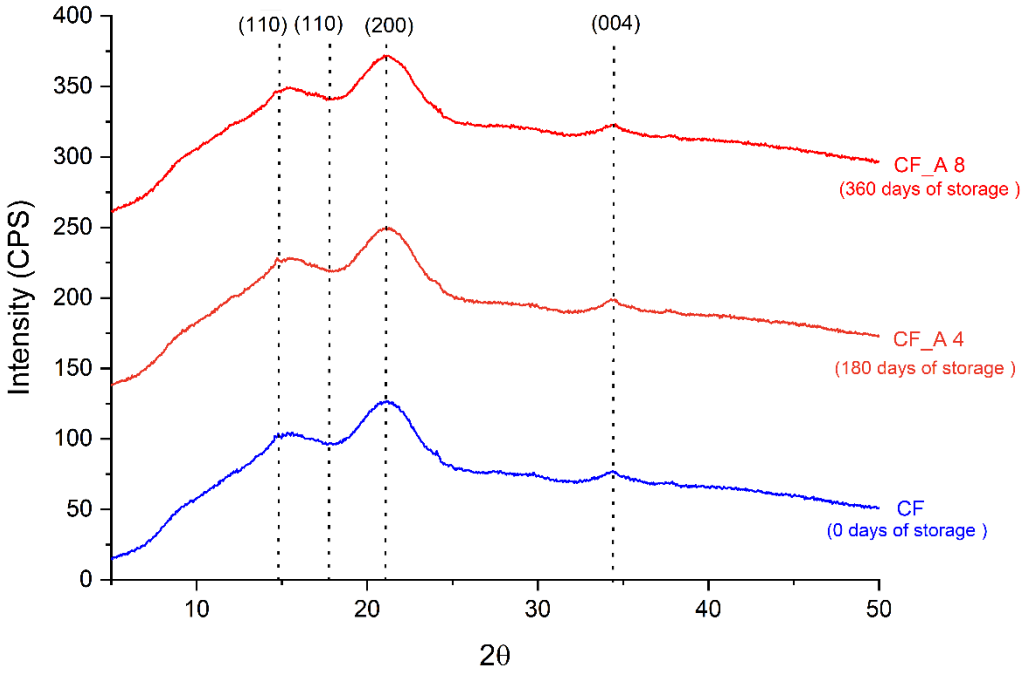

Figure 5-3. X-ray diffraction pattern of citrus fibers at different storage times: 0, 180 and 360 days in 40 °C and 75% RH.

The crystallinity index (CI) was calculated for all samples based on the intensity (height) of the peak (Table 5-2). No significant differences were observed in the intensity of the peaks corresponding to amorphous and crystalline fraction, and consequently, no significant difference was observed in CI. The samples showed a CI between 71 and 77% which is not significantly different between samples, which is lower than expected from literature data (He *et al.*, 2023; Huang *et al.*, 2021; Zain, 2014).

Table 5-2. Crystallinity index of citrus fiber in different storage times in accelerated aging conditions (40 °C, 75% RH).

Storage time (days)	18 °	21 °	CI (%)
0	$14^a \pm 4$	$49^a \pm 1$	$71^a \pm 7$
180	$14^a \pm 1$	$50^a \pm 0$	$72^a \pm 3$
360	$12^a \pm 1$	$50^a \pm 2$	$77^a \pm 3$

Mean ± standard deviation (n=3). Different letters in the same column indicate that values are significantly different ($p < 0.05$).

Deeply analyzing the equilibrium moisture content for the region a_w>0.4 (region with higher hysteresis), the curve of moisture content versus time showed a discrete peak which indicated that some water was adsorbed and subsequently released at constant a_w, and without temperature fluctuation that could explain this phenomenon (Figure 5-4). It was observed mainly at a_w 0.8. This oscillation of water adsorption may also be related to a crystallization

process. Several studies related a similar behavior, at lower a_w, for other products with a greater amplitude, associated with the crystallization of sugars (Bronlund & Paterson, 2004; Huppertz & Gazi, 2016; Omar & Roos, 2007; Roos, 1993) mobilized by increased hydration (Vollenbroek *et al.*, 2010).

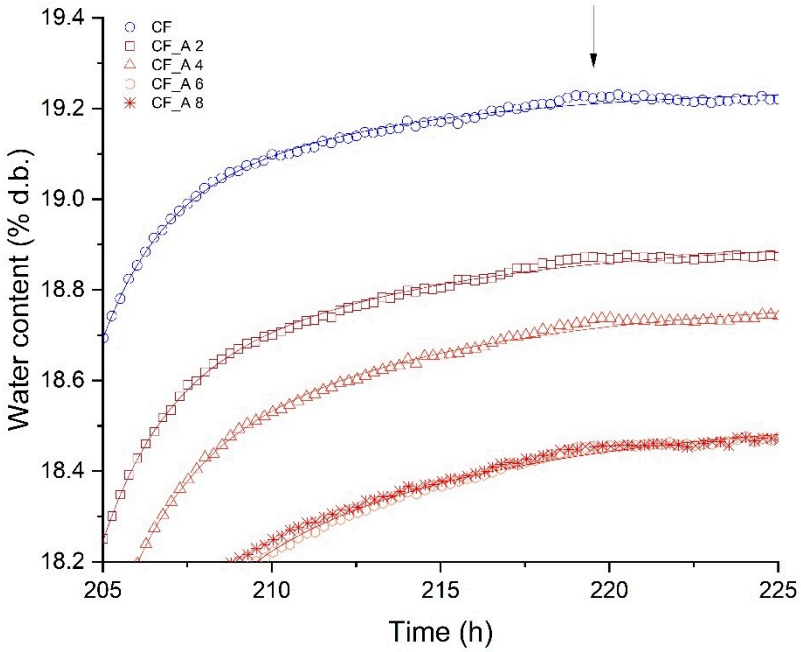

Figure 5-4. Zoom of equilibrium zone of curve water content *versus* time of citrus fiber in different storage times (accelerated conditions (40 °C, 75% RH)) at a_w 0.8.

This loss of adsorbed water was not only observed with dairy products, but also sugars systems including glucose, sucrose, trehalose (Iglesias *et al*., 1997; Makower & Dye, 1956; Schebor *et al.,* 2010) which was attributed to the crystallization of sugar. In this case, sugars such as sucrose can crystallize resulting in a water release into a certain level. However, the polysaccharides present in the mango powder such as pectin which does not crystallize, can adsorb water resulting in a slight increase in the water content. In a higher humidity, these crystallized sugars surrounded by water can be dissolved, recovering total or partial the water adsorption capacity.

For citrus fibers in this study, accelerated storage conditions (40 °C, 75% RH) could have induced small sugars crystallization in CF which was not significant to be detected in XRD. However, it may cause the reduction in water adsorption observed in the sorption experiment (Figure 5-1). The discrete peak observed in equilibrium water sorption plateau occured during the experiment since it was also observed in CF at time 0. Thus, it is not an illustration of what happened during the storage but only when the samples are exposed to high a_w, reducing the water adsorption.

5.2.2. Effect of moisture and temperature on molecular mobility of citrus fiber in long-term storage stability

Food products are complex matrices likely to show recrystallisation, phase separation and component migration during storage, especially in presence of water (Borde *et al.*, 2002). To investigate the influence of storage time on thermal behavior (enthalpy relaxation, thermal transition) and viscoelastic behavior, the "fresh sample" (CF) and the sample stored for 360 days in accelerated conditions (40 °C, 75% RH) (CF_A) were compared.

5.2.2.1. Enthalpy relaxation

Figure 5-5 illustrated the enthalpy relaxation temperature and energy of CF stored for different times at 40 °C and 75% RH. As observed on Figure 5-5a, the peak temperature remained constant with increasing storage time. However, the amplitude of the endothermic peak decreased after 45 days of storage and remained constant between 45 days and 315 days of storage (no significant difference ($p>0.05$)), and then slightly decreased after 360 days (Figure 5-5b). A significant ($p<0.05$) reduction of the energy of the endothermic peak is observed comparing citrus fiber at time 0 and 360 days of storage. As enthalpy relaxation represents the recovery upon heating of the enthalpy lost upon aging, it was expected that the energy would be greater or remained stable with increasing storage time. The diminishing enthalpy relaxation energy implies a hindrance to material relaxation upon heating. It suggests an increase of material stiffness over time, potentially impeding the restoration of the original conformation. The greater rigidity observed in the sample could be attributed to structural rearrangement or densification within the material.

In the case of citrus fibers, the storage at temperature close to the onset of enthalpy relaxation may favor the changes in the matrix. It shows that enthalpy relaxation is a useful parameter to predicting changes in physical properties during storage (Kim *et al.,* 2003).

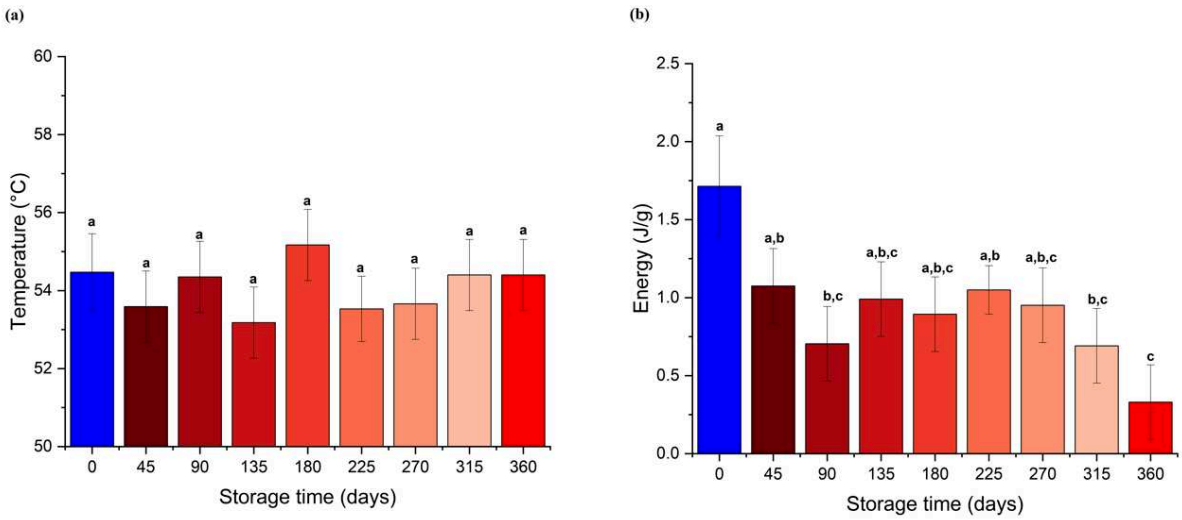

Figure 5-5. Enthalpy relaxation of citrus fibers stored for different times at 40 °C and 75% RH: enthalpy relaxation temperature (a) and enthalpy relaxation energy in J/g of sample (b). *Mean ± standard deviation (n=3). Different letters in the bars indicate that values are significantly different ($p < 0.05$).*

5.2.2.2. Thermal transition behavior

After their storage, aged samples were dried (to ~0% d.b. water) and the glass transition (Tg) values for CF at time 0 and CF_A 8 were determined from the thermogram of the third heating DSC scan (Figure 5-6). Comparing the obtained values, it was observed that they remained constant despite an increase in storage time.

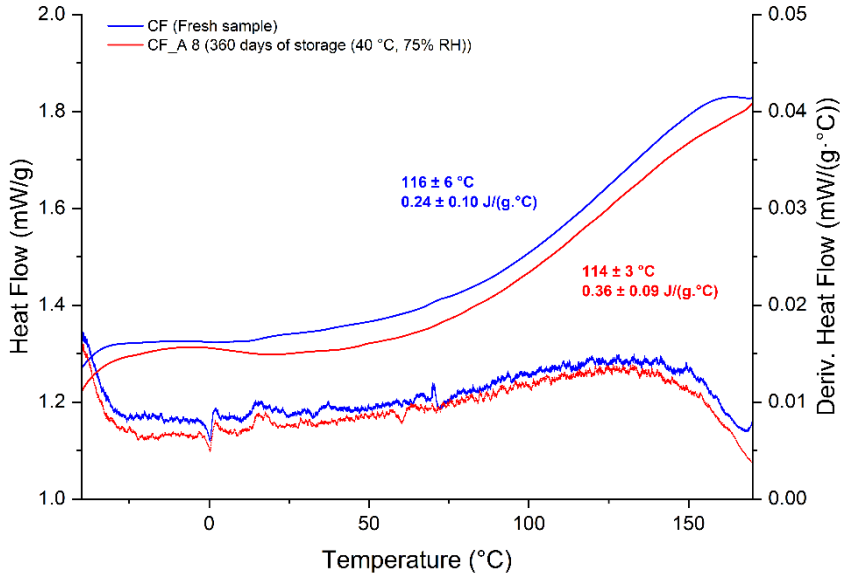

Figure 5-6. Glass transition temperature (Tg) and ΔCp of CF and CF_A 8 (with 0.3% d.b. water content).

Some studies have discussed the impact of time on the glass transition (Chung & Lim, 2004; Liu *et al.*, 2010), which is linked to reduced molecular mobility and matrix densification due to changes in biopolymer chain conformation as free volume decreases. This suggests that the loss of functionality observed during storage can occur even in the glassy state.

The effect of storage on the glass transition temperature depends on whether the storage temperature is below or above the glass transition temperature (Liu *et al.,* 2010; Truong *et al.*, 2004). For example Truong *et al.* (2004) showed that the Tg of fructose increased by 8.6 °C following a storage of 20 days at 22 °C, above the Tg of fructose (16 °C). On the contrary, it decreased with increasing storage time at temperature below Tg (< 7 °C).

In the present study, no effect of time was observed on Tg or ΔCp, probably due to the complexity of this transition, which required three heating scans with DSC for detection.

5.2.2.3. Viscoelastic behavior

Both samples, "fresh sample" (CF) and 360 days aged (CF_A 8) sample, showed an α-relaxation temperature in a range between 115 and 130 °C. T_{max} at 1 Hz for CF and CF_A 8 were 136 ± 3 °C and 134 ± 3 °C, respectively (Figure 5-7a). These results were not significantly different, corroborating with DSC results. Tan δ peak of citrus fiber presented the same intensity as a function of storage time while Chung & Lim (2004) observed its reduction for starch stored for increasing storage time, attributing it to a material stiffening by aging. Additionally, no difference was noted in the activation energy of the transition as a function of storage time (Figure 5-7b).

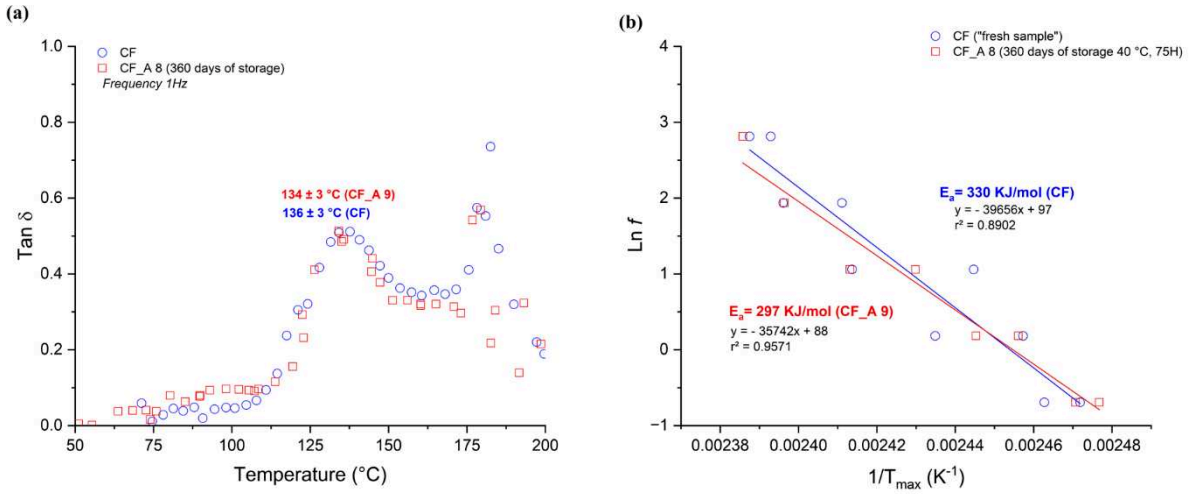

Figure 5-7.Tan δ as a function of temperature comparing initial citrus fiber and after 360 days of storage (40 °C, 75% RH) (a); and activation energy for both samples (b).

The thermal transition and viscoelastic behavior of CF were unaffected by storage, indicating that the loss of functionality over time may be attributed to changes occurring in the glassy state but that do not change Tg or α-relaxation. The local mobility in this material is important enough to induce loss of functionality like the decrease in storage modulus of the gel after reconstitution. More than a real rearrangement of polymers, it is mainly the relationship to water that is impacted with time. The kinetic or process of rehydration may be changed, and the observed change may just be induced by a delayed full rehydration and thus an increased time to form a gel.

Putri *et al*. (2024) who studied a similar material (functionalized lemon peel CWM residue) by thermal mechanical compression test, calculated by Gordon Taylor equation the relaxation temperature around 40 °C for anhydrous material. This relaxation process was well correlated with the loss of functional properties upon storage: when the sample was stored in a temperature higher than the onset of tan δ change (between 25 and 40 °C), the G′ values significantly decreased. The observed physical transformation is likely a consequence of increased molecular mobility, leading to a more viscous state. In this altered state, the structural units of the biopolymer gain increased freedom of movement, facilitating interaction between cellulose microfibrils. This interaction impedes the formation of an open cell wall matrix network, thereby obstructing the entrapment of water during the reconstitution of the material into suspension (Fan *et al*., 2017).

In agreement, the loss of functionality of citrus fiber may be correlated with an increase of molecular mobility below the Tg/α-relaxation.

5.2.3. Effect of long-term storage in a chemical structure of citrus fiber

The FTIR spectra describing time evolution of citrus fiber in different storage conditions are presented in Figure 5-8. Most of the differences between samples stored in accelerated conditions (Figure 5-8a), were observed in three regions in which band intensity “oscillated” with time: i) in the broad band between 3000 to 3750 cm^{-1} associated with -OH stretching of cellulose and hemicellulose; ii) in the band around 3000 and 2850 cm^{-1} corresponding to CH and CH_2 stretching of cellulose and hemicellulose and iii) in the band around 1030 cm^{-1} related to C-O deformation at C6 in cellulose (Célino *et al.*, 2014; Chen *et al.*, 2015).

In addition, a slight increase in the intensity of the band around 1318 cm^{-1} was observed after 180 days of storage, which could suggest an increase in crystallinity. However, this is not supported by a clear reduction in the band around 1337 cm^{-1}, which would indicate a conversion from amorphous to crystalline cellulose (Boukir *et al.*, 2019), nor by the previously

determined crystallinity index. The band around 898 cm^{-1} varied after 225 days of storage in accelerated conditions which may represent a rearrangement of cellulose fraction in CF.

When storage conditions were compared (Figure 5-8b), the overall FTIR spectra appeared similar, suggesting no impact of humidity nor of temperature on chemical bonds.

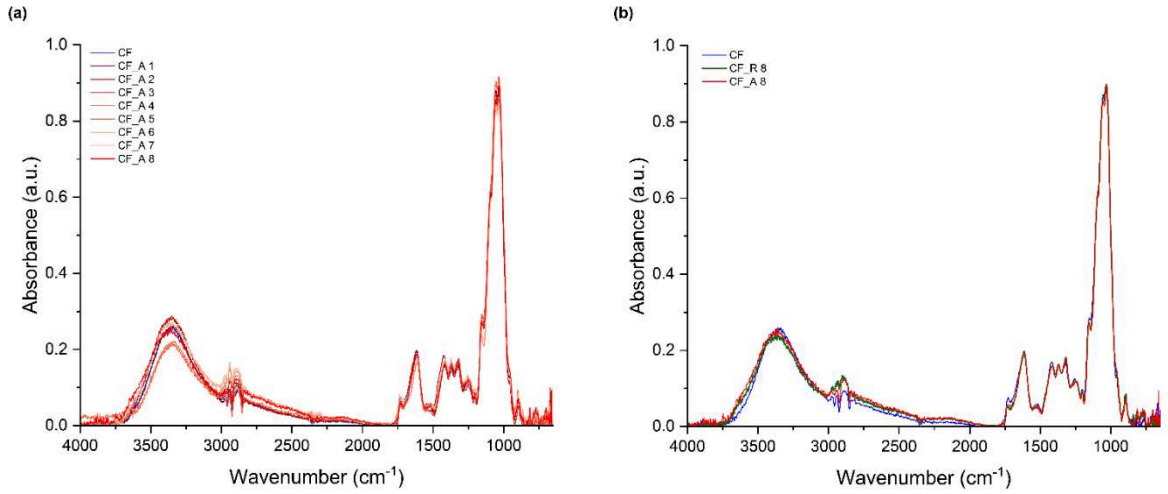

Figure 5-8. FTIR spectra of citrus fibers after different storage times in accelerated conditions (40 °C, 75% RH) (a); and upon two different ways of storage (accelerated aging conditions and room conditions) in the range of 4000–650 cm^{-1} (b).

The water uptake decrease in citrus fiber as a function of time can result from chemical reactions. The main degradation mechanisms of cellulose are oxidation and hydrolysis. The macromolecule of cellulose has three active hydroxyl groups in each glucose ring, which is susceptible to be oxidized (Li *et al*., 2021). The oxidation can promote the formation of C=C double bonds on anhydroglucose ring and of carbonyl groups of cellulose that can be oxidized to carboxylic groups. It can result in depolymerization, breaking of the cellulose chain, or the opening of the rings, making the molecule susceptible to alkaline and acidic attacks. On the other hand, hydrolysis breaks the chain and causes structure fragmentation. It can occur in alkaline and acidic environments, acidic environments being more favorable for it at room temperature (Piantanida *et al*., 2005). The autocatalytic effect in cellulose increases with temperature and moisture (Lewin, 1997).

Most of the studies of stability of cellulosic materials during the storage mentioned changes on the two bands around 1740 cm^{-1} and 1630 cm^{-1}. The differences appeared in both bands positions and intensities. These changes are in general associated with oxidation and/or hydrolysis; however, it is challenging to separate both reactions since they can take place together and affect the same bands (Łojewska *et al*., 2006). Similarly, Li *et al*. (2021) who studied the aging of cellulose fibers, observed changes in the intensity of the peak of carbonyl

(around 1700 cm^{-1}) and carboxyl (around 1600 cm^{-1}) due to the aging of fiber. These modifications were associated with the oxidation reactions.

Besides cellulose, pectin is also susceptible to degradation during storage. Einhorn-Stoll *et al.* (2020) mentioned that pectin degradation can occur by demethoxylation and depolymerization (hydrolysis and/or β-elimination). These reactions can be influenced by the degree of methoxylation, pH, and temperature (accelerated by high temperature) and some of them require water.

Despite all possible modifications described in the literature, identifying changes in the spectrum represented in Figure 5-8 was challenging due to the large number of samples and the variation between repetitions. PCA analysis was applied for a unique storage condition (accelerated conditions) and for different storage times to better investigate the effect of time.

5.2.3.1. Exploratory data analysis of samples stored in accelerated aging conditions

As reported by Szymanska-Chargot & Zdunek (2013), the region between 1200 and 850 cm^{-1} is characteristic of stretching vibration of C-O, C-C, CH_2 of ring structures, and is the one to favor to study carbohydrates. In this region, there is almost no influence of proteins and water absorption. Another interesting region is between 1800 and 1200 cm^{-1} (Ferreira *et al.*, 2001; Hori & Sugiyama, 2003) which can be related to carbonyl esters, and carboxylates from pectin. The PCA analysis was therefore carried out for these two spectra ranges 1800 - 1200 cm^{-1} and 1200 – 850 cm^{-1}, to try and reveal differences between samples with storage time at 40 °C and 75% RH.

Figure 5-9a presents the scores scatter plot PC1 (61.8 %) x PC2 (21.8 %) for data in the 1800 to 1200 cm^{-1} region and demonstrates the differences between samples. The major variability is observed in PC1 which separated the samples for the shortest storage time (CF, CF_A 1, CF_A 2 and CF_A 3) on positive side from the samples stored for long time (CF_A 4, CF_A 5, CF_A 6, CF_A 7) on negative side, while CF_A 8 appeared in the middle. On the other hand, the samples were distributed along PC2, showing no clear distinction based on storage time, except for the CF_A 2 and CF_A 8 samples.

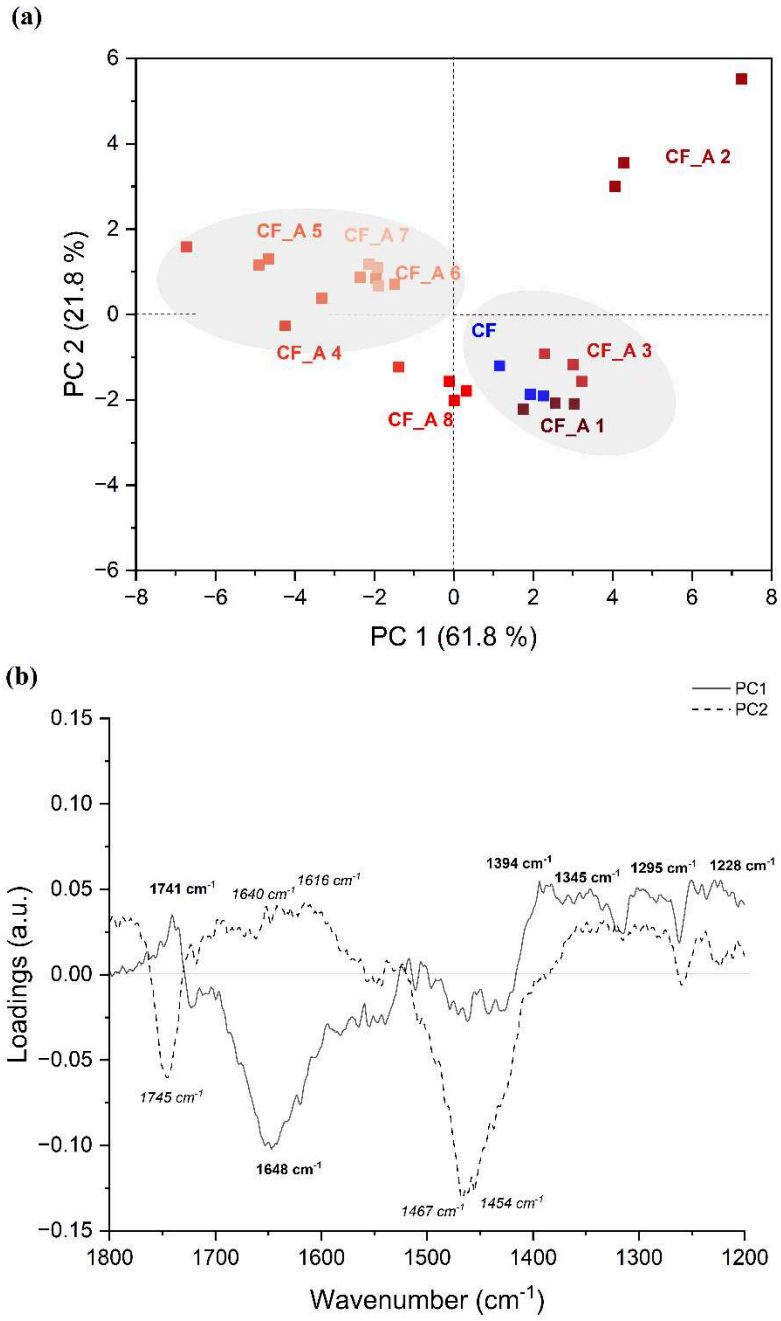

Figure 5-9. PCA scores scatter plot (a) and PCA loadings plot (PC1 and PC2) (b) of citrus fibers FT-IR spectra in the 1800-1200 cm^{-1} region in different storage times.

Variable loadings for PC1 and PC2 were exposed in Figure 5-9b. Positive loadings for PC1 covered the wavenumbers characteristic of pectin (1741, 1394, 1228 cm^{-1}) and one for cellulose and/or hemicellulose (1295 cm^{-1}). Negative loadings for PC1 are limited to the region around 1648 cm^{-1} which may be associated with tautomer carbonyl group/enolic (ketone/aldehyde) or amide I. It suggested changes over storage, mainly in the content and/or structure of pectin or proteins. On the other hand, PC2 positive loadings pattern is characteristic of COO^- antisymmetric stretching polygalacturonic acid (1616 cm^{-1}) and water

(1640 cm^{-1}) while the wavenumbers which negatively influenced PC2 scores are correlated to cellulose or xylose-containing hemicellulose (1467 cm^{-1}) and to esterified carboxyl groups of pectin (1745 cm^{-1}) (Liu *et al.*, 2021; Szymanska-Chargot *et al.,* 2015; Szymanska-Chargot & Zdunek, 2013). Combining the information loadings pattern of PC1 and PC2 suggested that some pectin de-esterification happened during the storage of citrus fiber or alteration in protein structure after 135 days of storage.

Considering the region 1200-850 cm^{-1} (Figure 5-10a), the scores scatter plots PC1 (68.2%) x PC2 (11.0%) showed a spreading of the data along the PC1 axis. PC2 axis seems to separate mainly CF_A 4 and CF_A 8.

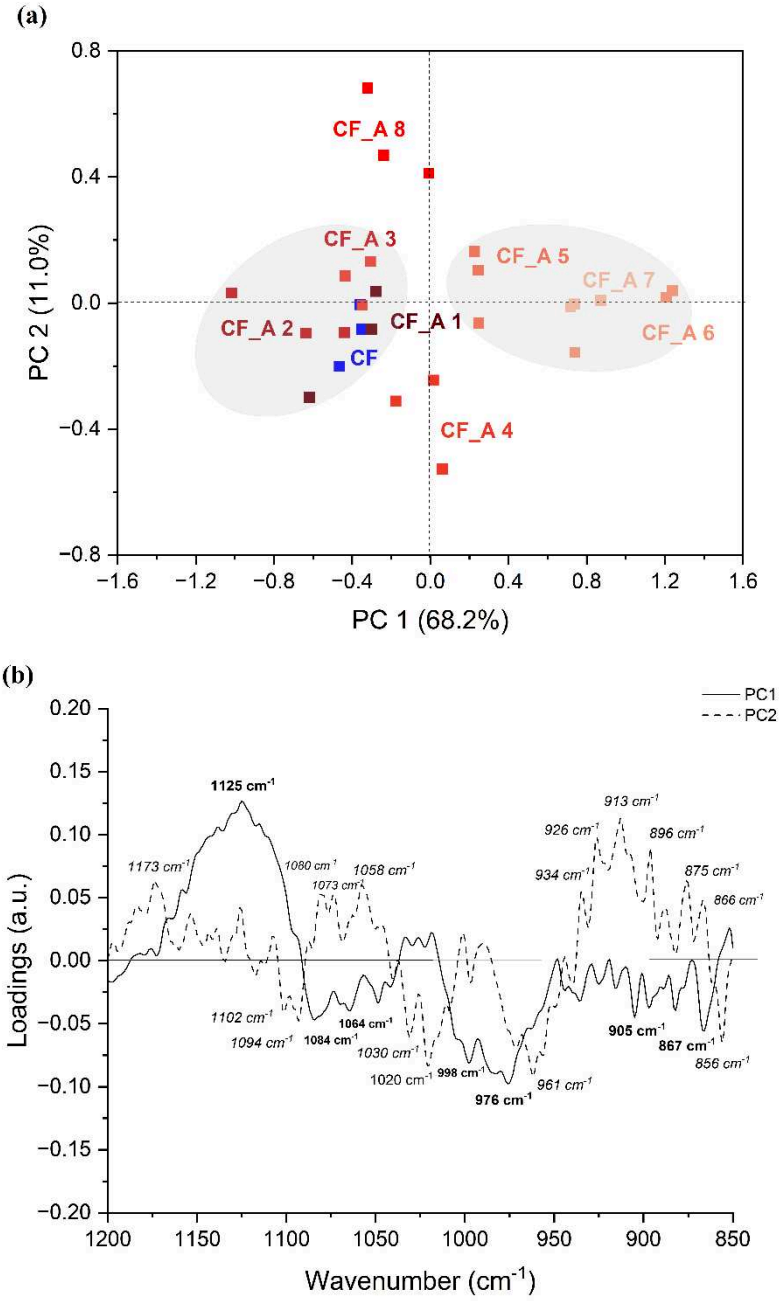

Figure 5-10. PCA scores scatter plot (a) of PCA loadings plot (PC1 and PC2) (b) of citrus fiber FTIR spectra in the 1200-850 cm^{-1} region in different storage times.

PC1 loadings had negative values around 1084 and 976 cm^{-1} characteristic of pectin (C-O and C-C stretching and CO bending) and 1064, 998, 905 and 867 cm^{-1} characteristic of hemicellulose and cellulose (Figure 5-10b) whereas the loadings were only positive for PC1 at 1125 cm^{-1} characteristic of C-O and C-C stretching of cellulose or hemicellulose. Thus, PC1 suggested that after 135 days, the impact of storage became more pronounced, and the samples were mainly differentiated through pectin and cellulose and/or hemicellulose contribution. In the initial period of storage (before 135 days), the sample were separated by

the bands associated with pectin. However, after 135 days, the bands correlated to cellulose and/or hemicellulose became more prominent in their differentiation.

PC2 loadings showed negative and positive values (Figure 5-10b). The wavenumbers which positively influenced the scores are around 1173, 1080, 1073, 1058, 934, 926, 896, 875, 866 cm^{-1}, corresponding to cellulose and hemicellulose and only 913 cm^{-1} related to pectin. The negative influence is in the wavenumbers 1102, 1094, 1020, 961 and 856 cm^{-1} mainly associated with pectin (C-O and C-C stretching, CO bending and ring vibration) and 1030 cm^{-1} correlated to cellulose (Liu *et al.*, 2021; Szymanska-Chargot *et al.,* 2015; Szymanska-Chargot & Zdunek, 2013). Comparing CF_A 4 and CF_A 8, PC2 indicated that CF_A 8 was separated by the bands primarily associated with cellulose and hemicellulose, whereas CF_A 4 was differentiated by bands correlated to both cellulose and pectin.

Although the group separation in the region 1200-850 cm^{-1} is less clear, the PCA analysis underscored a distinct transformation in the chemical structure of citrus fiber over the storage period, with an initial dominance of pectin and/or protein influence transitioning to a greater contribution from cellulose and hemicellulose as storage time increased. This finding suggests that prolonged storage under accelerated conditions significantly affected the composition and structural integrity of citrus fiber.

5.2.3.2. Investigation of oxidation reactions upon storage

The region between 1500 and 1750 cm^{-1} is chosen to evaluate the effect of storage time on the chemical structures of citrus fibers quantitatively comparing different storage times (Figure 5-11). To minimize the influence of water in this region around 1640 cm^{-1}, the samples were equilibrated before the measurement at 0% RH over P_2O_5. In Figure 5-11a, the intensity of the band at 1620 cm^{-1} in the initial storage times was almost constant until 135 days of storage, after 180 days the intensity increased. On the other hand, the intensity of the band around 1730 cm^{-1} decreased until 180 days, afterward, the intensity increased, and it shifted to higher wavenumber. This can be correlated with the results suggested by PCA: samples stored for more than 180 days present a greater intensity of the 1648 cm^{-1} band than before storage, however, the band around 1730 cm^{-1} was more significant for samples up to 135 days while the shift of this band decreased its significance for samples stored for longer time.

Comparing storage conditions (Figure 5-11b), the FTIR spectra showed a remarkable difference in the band around 1730 cm^{-1}: its intensity decreased and shifted to higher wavenumber. These changes may indicate some chemical changes, but it should be quantitatively studied to draw a “stronger” conclusion.

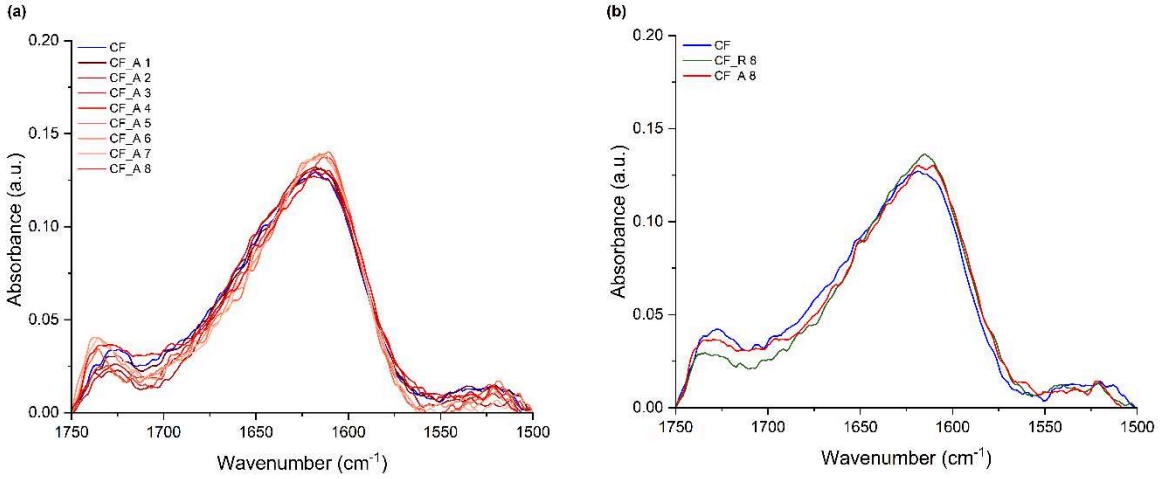

Figure 5-11. FTIR spectra in the range of 1750 to 1500 cm^{-1} for citrus fibers after different storage time (a) and in different storage conditions (b).

To deeply study this region, deconvolution was applied. This region can potentially be deconvoluted by analyzing the wavenumbers of expected products resulting from cellulose oxidation and hydrolysis. Cellulose partial oxidation and hydrolysis results in carbon atoms in various oxygen environments (-COOH, -CHO, -CO), which would originate sub bands in this spectra range. The oxidation is expected to give a variety of different carbonyl groups whereas the hydrolysis would mainly result in aldehydic groups on terminal rings (Li *et al.,* 2021; Łojewska *et al.*, 2006).

Łojewska *et al*. (2005) used nine peaks to fit the region from 1850 to 1500 cm^{-1}: peak 1 at 1780 cm^{-1}; peak 2 at 1745 cm^{-1} equivalent to a final oxidation stage of carbon; peak 3 at 1710 cm^{-1} and peak 6 at 1618 cm^{-1} related to oxidation intermediates; peak 5 at 1660 cm^{-1} assigned to enolic group; peak 7 at 1570 cm^{-1} linked to aryls or conjugated aryl groups; and peak 9 at 1510 cm^{-1}.

The band at 1730 cm^{-1} corresponds to carboxyl groups (1710-1730 cm^{-1}) while the assignment around 1710 cm^{-1} could be related to aldehydic groups (1650-1750 cm^{-1}). The band at 1610 cm^{-1} corresponds to carboxylate groups (1550-1620 cm^{-1}). The peak around 1645 cm^{-1} can be associated with the tautomer of a carbonyl group/enolic group (Ellerbrock & Gerke, 2021; Łojewska et al., 2006).

Boukir *et al.* (2019) found several difficulties to assess the regeneration of oxidized groups in the region 1710-1550 cm^{-1}, due especially to the interference with different type of polar broadbands, such as carbonyl C-O absorptions (1710-1640 cm^{-1}), enol tautomer equilibrium forms towards ketone or aldehyde forms (1680-1540 cm^{-1}), aromatic phenolic

bands: 1620-1550 cm^{-1}), as well as δOH (1640-1620 cm^{-1}) in plane bending vibration of adsorbed water.

The intermediate or final products of oxidation reactions can be associated with the bands in this region (Figure 5-12).

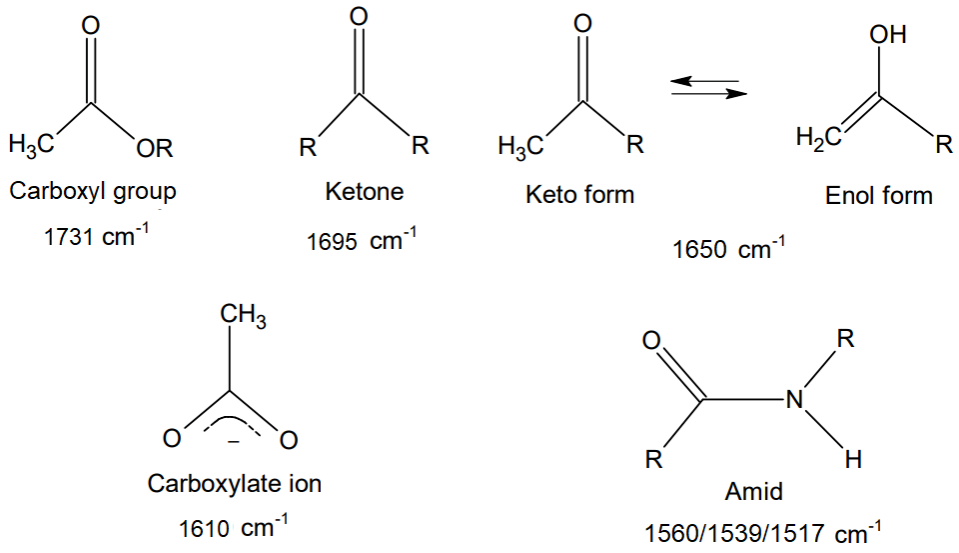

Figure 5-12. Possible products of cellulose partial oxidation presented as functional groups associated with frequencies of their vibrations.

The area ratio of the deconvoluted peaks around 1730 and 1620 cm^{-1}, which can be an indicator of oxidation state of cellulose (Łojewska *et al.*, 2005), was calculated (Figure 5-13). This index varied between 0.1 and 0.25 during storage with a large standard deviation which may have contributed to the lack of significant difference ($p>0.05$).

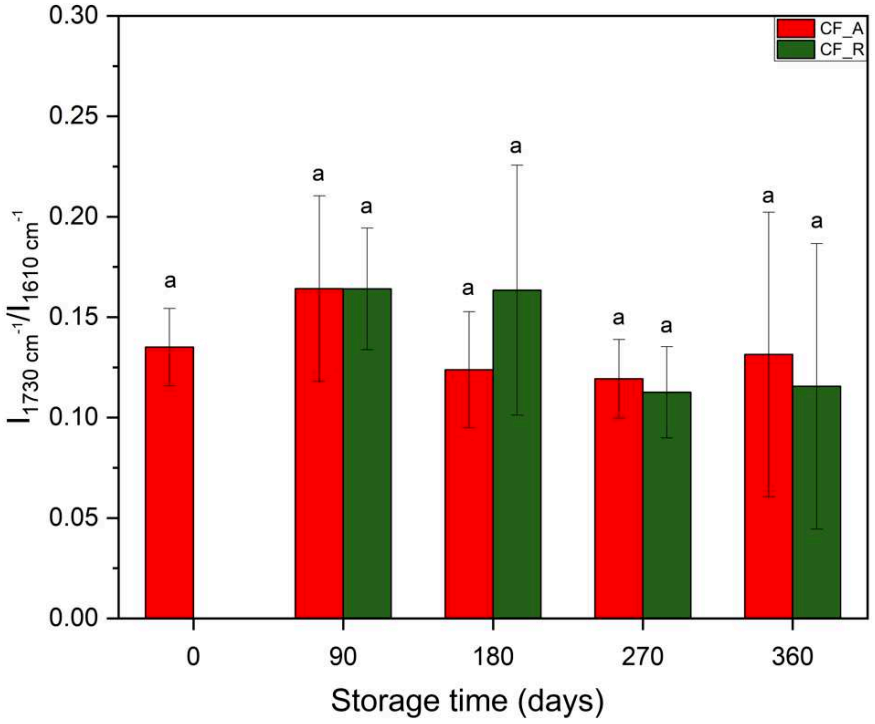

Figure 5-13. Ratio of areas of peaks around 1731 and 1610 cm^{-1} related to the storage time of citrus fibers (p=0.05, n=3).

Łojewska *et al*. (2005) calculated this oxidative index for cellulose from a paper stored at 150 °C for 120 hours, observing an increase of this ratio with increasing time, especially because of considerable rise of band around 1730 cm^{-1} from 0.48 to 1.76. In accordance, Ali *et al.* (2001) noted an increase of intensity of peak around 1710 and 1600 cm^{-1} when paper is aged in air. Besides these bands, Li *et al.* (2021) used the ratio of areas at 1700 cm^{-1} and 1375 cm^{-1}, and 1600 cm^{-1} and 1375 cm^{-1}, as indicators of fiber degradation, showing that aging leads to oxidation of cellulose's hydroxyl, methyl, and methylene groups into carbonyl (C=O) groups.

Unlike what was expected and observed in the literature, if any oxidation reaction had occurred during storage, an increase in the ratio between the two bands was not observed.

Although no significant effect was observed between the area ratio of these two peaks (1735 and 1645 cm^{-1}), this does not eliminate the fact that a chemical reaction occurs during storage. The oxidation reaction occurs predominantly on various C–OH groups on various glucopyranose rings, yielding a diverse array of carbonyl groups, while hydrolysis results mainly on aldehydic groups on terminal rings (Łojewska *et al*., 2006). Quantifying these reactions, especially oxidation, is challenging due to the multitude of resulting products and the complexity of this region in FTIR spectra, where peaks overlap. Additionally, various reactions may occur during storage, impacting these bands as observed by PCA, such as

depolymerization that can occur via elimination, hydrolysis, or decarboxylation; demethoxylation and hydrolysis of acetal bond (Einhorn-Stoll *et al*., 2020; Łojewska *et al.,* 2005). For instance, in the decarboxylation reaction a keto-acid which may be associated with the peak around 1740 cm^{-1} is transformed into a keto-enol tautomer, reflecting in the separation of aged samples by the peak at 1648 cm^{-1}. Furthermore, the hydrolysis of the acetal bond in cellulose can form hemiacetal and aldehyde which is also associated with peak at 1648 cm^{-1}.

Complementary to FTIR analysis, there are other methods to evaluate these chemical changes during storage, such as determination of free galacturonic acid, degree of methyl esterification, intrinsic viscosity, determination of molecular weight, identification of unsaturated uranides, and high-field NMR which might be applied in the future to comprehensively understand the effects of storage on citrus fibers, including the types of reactions occurring and their intensities.

5.2.3.2.4. Determination of degree of methyl esterification (DM)

The region between 1750 and 1500 cm^{-1} in FTIR spectra can also be directly related to the DM of pectin. The DM is one of the most important properties to characterize pectin. Some studies monitor the degree of esterification of pectin during the storage and correlate it with changes in tissue of fruits or defects in beans (Chatjigakis *et al.*, 1998; Chen *et al.*, 2021).

Chatjigakis *et al.* (1998) studied the peaches stored in different conditions for various days and observed significant changes in the carboxylic spectra region. The intensity of the band around 1749 cm^{-1} decreased whereas the band around 1630 cm^{-1} increased, resulting in a diminished degree of esterification of pectin from peach cell wall. In addition, the band around 1630 cm^{-1} shifted to higher wavenumber, reflecting the interaction of carboxylate groups with calcium. Concerning the storage conditions, the rate of decrease of the degree of esterification depended on the storage conditions: at 0 °C, the degree of esterification decreased from 83% to 76% after 35 days of storage, while at higher temperatures, it decreased from 83% to 63% within the same period.

Using the area of the bands corresponding to carbonyl (1731 cm^{-1}) and carboxylate groups (1610 cm^{-1}), the DM of pectin in citrus fiber was calculated (Figure 5-14) and values were between 10 and 15% depending on storage time. These values were inferior to the DM determined by Ciriminna *et al.* (2017) for different citrus fruits, and for different fruit parts using different methods of extraction. Applying FTIR spectroscopy in diffuse reflectance mode (DRIFT), the DM varies between 25 to 40%, depending on the conditions of extraction

and source of pectin. The higher value found by Ciriminna *et al.* (2017) may be attributed to the different method used to calculate the DM which included the component of ester, acid and carboxylate group and the use of KBr to record the spectra instead of ATR device.

There was no significant variation in the DM with increasing storage time in any storage conditions (Figure 5-14). Chen *et al.* (2021), who studied the pectin changes in red haricot beans storage, did not observe any change in the degree of methyl esterification despite the stored beans exhibiting hard-to-cook defects. In this case, the defect developed during storage was more related to calcium and pectates crosslinking at intercellular junction zones (entrapped by hemicellulose and cellulose matrix), and as these interactions are very local, they may not be detectable when DM is measured.

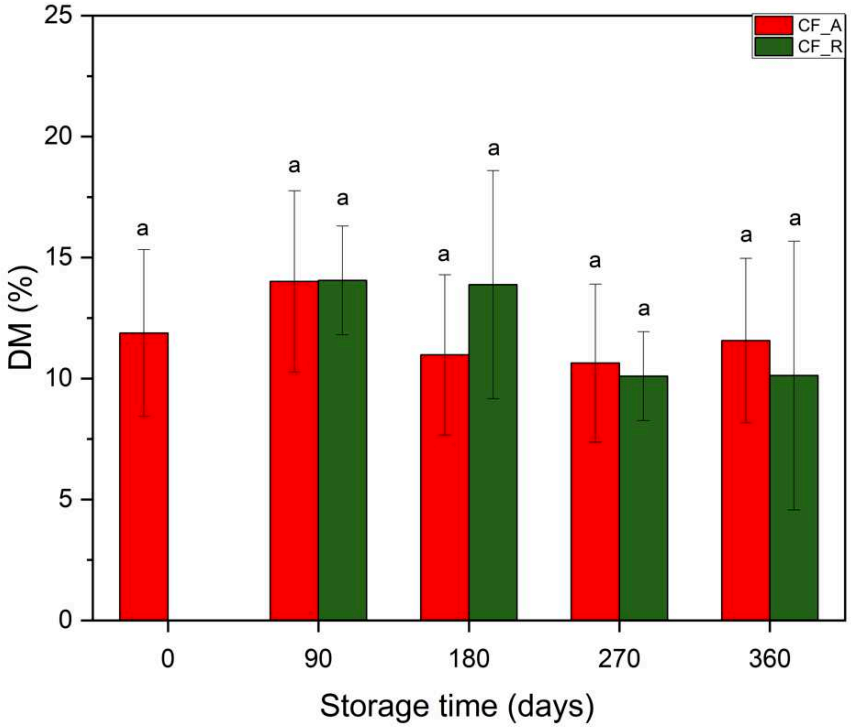

Figure 5-14. Degree of methyl esterification (DM) determined by FTIR for citrus fiber stored in room or accelerated conditions for 360 days.

In spite of a shift and oscillations in the bands around 1610 and 1730 cm^{-1} with increasing storage time, it was not possible to detect any changes in DM. As a result, no conclusion could be drawn from the quantitative analysis (oxidation index and degree of esterification) regarding the effect of time and the effect of water and/or humidity in citrus fiber structure.

5.2.4. The impact of storage time on surface composition of citrus fibers

Apart from chemical reactions, modifications of surface composition can affect the interaction with water. Depending on the composition, mainly carbon and oxygen content, the

surface can be hydrophilic, intermediate hydrophilic, or hydrophobic (Fournaise *et al*., 2021). The surface changes can influence the initial interaction between particles and water upon reconstitution, affecting mainly the wetting and swelling steps (Gaudel *et al.*, 2022).

XPS analysis was performed on sample CF after different storage times and different conditions of storage in order to evaluate the impact of time on the surface composition as well as the impact of temperature and/or humidity. As specified by Popescu *et al.* (2009), polymeric materials age from the surface, then, sensitive methods of investigation on surface modifications are necessary to an accurate representation of the early stages of deterioration.

The data of the surface atomic concentration of chemical elements (Table 5-3) showed no impact of storage time on the surface composition of studied powders.

Table 5-3. Quantitative analysis of surface composition of citrus fiber (CF_A) for different storage time at 75% RH and 40 °C.

Storage time (days)	C (%)	O (%)	N (%)	Na (%)
0	68.4 ± 0.3 ^{a}	30.5 ± 0.4 ^{a}	0.8 ± 0.2 ^{a}	0.4 ± 0.0 ^{a}
45	67.6 ± 0.3 ^{b}	31.1 ± 0.4 ^{a}	0.8 ± 0.2 ^{a}	0.5 ± 0.0 ^{b}
90	70.4 ± 0.3 ^{c}	28.9 ± 0.4 ^{b}	0.6 ± 0.2 ^{a}	0.2 ± 0.0 ^{c}
135	68.7 ± 0.3 ^{a}	30.4 ± 0.4 ^{a}	0.6 ± 0.2 ^{a}	0.3 ± 0.0 ^{d}
180	68.9 ± 0.3 ^{a}	30.3 ± 0.4 ^{a}	0.5 ± 0.2 ^{a}	0.3 ± 0.0 ^{d}
225	69.0 ± 0.3 ^{a}	30.0 ± 0.4 ^{b}	0.7 ± 0.2 ^{a}	0.3 ± 0.0 ^{d}
270	68.5 ± 0.3 ^{a}	30.5 ± 0.4 ^{a}	0.6 ± 0.2 ^{a}	0.4 ± 0.0 ^{a}
315	68.5 ± 0.3 ^{a}	30.8 ± 0.4 ^{a}	0.5 ± 0.2 ^{a}	0.3 ± 0.0 ^{d}
360	68.6 ± 0.3 ^{a}	30.5 ± 0.4 ^{a}	0.6 ± 0.2 ^{a}	0.3 ± 0.0 ^{d}

Data were expressed by means (n=3) ± standard deviation. Values followed by different letters in the same column are significantly different ($p < 0.05$).

Moreover, the analysis of spectra of the samples stored in accelerated (75 % RH, 40 °C) and room conditions (30 % RH, 20 °C) for 360 days, revealed again no significant influence of time, since the spectra of the different samples overlapped each other (data not shown). The humidity and/or temperature conditions upon storage did not impact the surface composition.

Nonetheless, since the samples were dried before analysis (equilibrated at 0% RH), it could mask the effect of prior hydration upon storage.

Using the total area of the carbon and oxygen peaks, the ratio O/C was determined (Table 5-4). The O/C ratio of samples CF_A and CF_R varied between 0.41 to 0.46, with no clear effect of storage time. A slight variation with time was observed, but without any trend versus time on C and O contents. If a hydrolysis and/or oxidation had occurred during storage, this ratio would have risen (Popescu *et al.*, 2009).

As described before, the C 1s spectra was decomposed into 4 bonding states (Table 5-4). The initial relative amounts of different components were 33% of C1, 43% C2, 19% of C3 and 5% C4. CF_A and CF_R showed minimal variation with increasing storage time for all carbon components which was not linearly correlated to storage time, and no significant difference was observed between these two storage conditions. Then, no effect of temperature nor humidity was observed on surface composition upon storage. The high resolution of O1s (Table 5-4), CF had an initial composition of 91% of O1 and 9% of O2. The oxygen components oscillated during the storage more than carbon components, with standard deviation of 10 %. Although this variation was considerable, the same behavior was equally noted for CF_A and CF_R. It validates the results obtained for high-resolution of carbon with no influence of the storage conditions on surface composition.

Table 5-4. Relative amounts of differently bound carbons and oxygen determined from high-resolution carbon C 1s and oxygen O 1s.

Days of storage	**O/C**	**Area (%)**					
CF_A		**C1 (C-C/C-H)**	**C 2 (C-O)**	**C3 (C=O/O-C-O)**	**C4 (O-C=O)**	**O1 (O-C=O)**	**O2 (C-O)**
90	0.41	35.2	43.1	16.4	5.2	95.5	4.5
180	0.44	18.9	42.7	29.5	8.9	59.4	40.6
270	0.45	25.5	44.2	23.2	7.1	80.3	19.7
360	0.44	30.4	43.4	19.9	6.3	88.6	11.4
CF_R							
90	0.43	26.9	44.7	22.0	6.4	77.7	22.3
180	0.46	22.4	44.0	26.2	7.4	69.3	30.7
270	0.46	27.2	41.3	24.5	7.0	89	11.0
360	0.44	28.6	43.3	21.6	6.5	89.3	10.7

According to Fras *et al.* (2005) oxidative reaction would have an obvious effect: increasing C2, which is related to C-O bonds of cellulose, with a simultaneous decrease of C1. Similarly, Popescu *et al*. (2009) observed the variation of C1s components with increasing storage time. The decrease of C1 peak related to extractives and lignin, and the increase of C2 peak

suggested the increase of C-O groups at surface attributed to hydrolysis and oxidation of carbohydrates and lignin. In addition, the variation in high resolution spectra plus the increase of other Cox/Cunox (C2+C3+C4/C1) observed in the same study, showed that XPS was a successful technique to identify modifications in aged samples. In the present study, no oxidation nor hydrolysis seemed to have happened on citrus fibers' surface during storage whatever the conditions of storage.

5.2.5. Reconstitution of aged citrus fiber

As an attempt to reverse the collapse observed in the samples after 360 days of storage in accelerated aging conditions (40 °C, 75% RH) and based on the observations of this study (loss of functionality upon storage, molecular mobility impact, chemical changes in citrus fiber, reduction of adsorption over time), the sample stored for 360 days (CF_A 8) was maintained in a climate chamber at 97% RH for 10 days (final water content was 32% d.b.), and subsequently, rheological analysis were made to measure gelation (storage modulus, G'). The recovered CF_A 8 sample exhibited a G' of 200 Pa (Figure 5-15), intermediate (< 50% of the initial G' value). Exposing the sample to high relative humidity allowed partial recovery of rigidity, suggesting a partial reversibility by hydration of the storage induced changes.

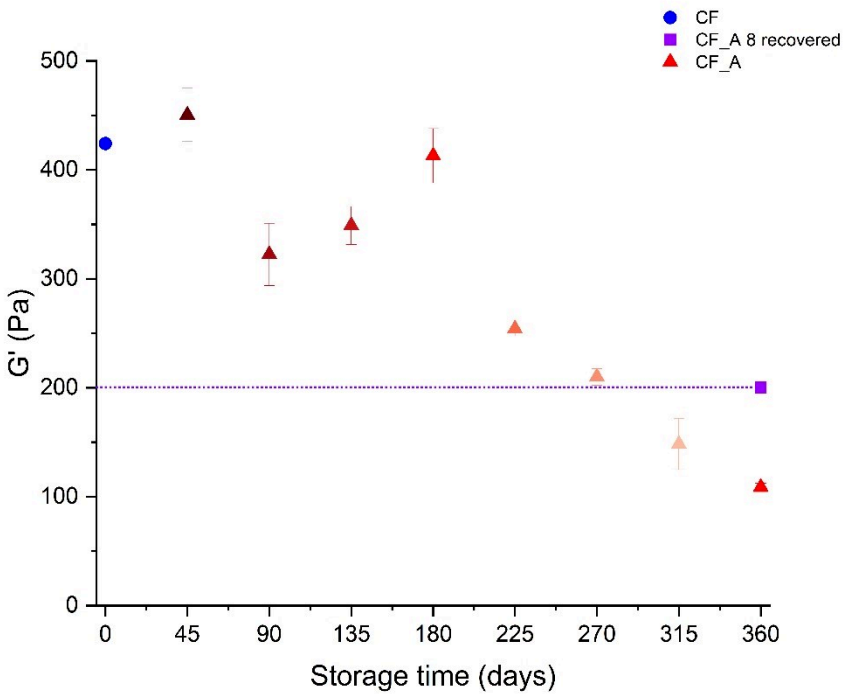

Figure 5-15. Evolution of G' of citrus fiber stored in accelerated aging conditions over time and the regenerated sample (CF_A 8 recovered) after exposition at 97% RH.

Van Audenhove *et al.* (2023), who investigated the impact of drying and storage in pectin-depleted tomato cell wall material, discussed the potential role of a regeneration step after drying using long-time hydration (solution 0.1%, pH 4.5, 24 h) and higher energy input subjecting the sample to high intensity mixing by Silverson mixer after overnight stirring. Applying shear to the system reduces particle size and partially reopens the structure. It has been suggested that the loss of functionality in cell wall materials upon drying occurs at multiple scales, and changes at the small/molecular scale are not reversible by high-intensity mixing. Moreover, the impact on network formation, essential to gel formation, differs from that on water binding capacity (WBC). When the sample was reconstituted after high-intensity mixing, WBC increased significantly, indicating a relationship between WBC and particle aggregation on a larger scale, involving both inter- and intramolecular interactions. However, the same was not observed in the G', which was partially recovered but still considerably lower than the initial. The formation of a network in suspension may be related to the molecular scale.

It suggested that the modification that occurred in CF upon storage may happen at different scales, and by exposition of the sample at high humidity only one scale modification can be reverted. Additionally, the loss of functionality of CF may be related to chemical and/or physical modification in the sample accelerated by water and temperature as previously shown. The exposition of the sample at high humidity (water content 32% d.b.) allows the mobility of the molecules, erasing partially the physical changes and permitting the formation of a "stronger" network. However, other types of modifications, whether on a different scale or chemical in nature, do not appear to be reversible by this method.

Thus, this shows that more than one phenomenon is involved in the loss of functional properties of citrus fibers during storage, and/or these alterations occur at different scales.

5.3. Conclusion

This chapter aimed to understand the cause of the loss of functionality of citrus fiber during storage. Changes in the interaction between water and citrus fiber (CF) over storage time were observed, especially at high humidity levels (>60% RH). These changes included lower moisture adsorption on the surface, stronger bonds between the monolayer and binding sites, and more water in the multilayer with characteristics of bulk water. They suggested a reorganization or aggregation of samples, which reduces capillary pores, and/or crystallization resulting from molecular mobility during storage. The decrease in relaxation enthalpy energy observed by DSC further demonstrated the effect of time, corroborating the hypothesis of

structural reorganization and contributing to the loss of functionality. This may also be attributed to densification which can impede the formation of an expansive biopolymer network, crucial for retaining water when reconstituting suspended materials. Chemical analysis revealed changes in the composition and/or structure of pectin that are not impacted by humidity and temperature, indicating cross-linking between polysaccharides or pectin and cations during storage. Conversely, storage conditions did not affect the elemental composition or carbon-carbon/carbon-oxygen bonds on the surface of citrus fiber, contrary to previous studies suggesting oxidation and hydrolysis.

In summary, the loss of functional properties, elucidated in Chapter 4, may be attributed to more than one mechanism operating within the citrus fibers. The first mechanism, linked to molecular mobility, appears to be relatively affected by water and/or humidity. Consequently, it instigates the reorganization and aggregation of molecules within the citrus fibers, potentially correlated with relaxation below the glass transition temperature. The second mechanism involves crosslinking between molecules and cations within the citrus fibers, showing independence from the tested temperature and humidity conditions. This crosslinking phenomenon likely occurs in conditions below both accelerated and ambient room conditions, suggesting a nuanced interplay of factors influencing the observed changes in functional properties over storage time. The loss of functional properties can be partially recovered when the sample is exposed to higher humidity in agreement with more than one mechanism in citrus fiber aging. Further exploration and research are imperative to untangle the intricate dynamics of these mechanisms and their collective impact on the functional attributes of citrus fibers.

Chapter 6. Conclusion and perspectives

Chapter 6. Conclusion and perspectives

The general objective of this thesis was to understand the physical state and structure of plant-based cell wall materials at various scales, with a specific focus on their evolution during storage and the mechanisms underlying functionality loss over time.

For the physicochemical characterization of the citrus fiber powders (chapter 3), different methodologies and conditions were optimized as well as the most suitable sample shapes for each applied technique. Water sorption analysis revealed distinct kinetics, with faster surface adsorption and slower absorption within the inner regions of fiber particles. The presence of wide glass transitions and α-relaxation phenomena underscored the heterogeneity and dynamic nature of citrus fiber matrices. NMR confirmed the coexistence of two phases, corroborating the multiple glass transitions and reinforcing the matrix's complexity. Chemical characterization of the bulk and surface compositions of citrus fibers underscored the significant impact of processing conditions. This comprehensive characterization revealed structural complexities, water sorption behavior, thermal characteristics, and chemical compositions that provide valuable insights into shelf-life considerations and emphasize the importance of multiple analytical techniques in unraveling molecular dynamics.

Chapter 4 explored the functional properties of dried citrus fibers and showed the impact of processing in pH, but it did not affect the functional properties. This chapter also elucidated the detrimental effects of aging on moisture retention, storage modulus (G'), and rehydration behavior. The observed correlations between storage modulus (G') and water swelling capacity underscored the interplay between structural characteristics and functional attributes. Moreover, the accelerated loss of functionality under elevated temperature and humidity conditions emphasized the importance of storage parameters in preserving citrus fiber quality.

Chapter 5 further elucidated the evolving water-citrus fiber dynamics during storage, delineating the influence of storage conditions on molecular mobility (even below Tg), structural rearrangement, and chemical stability. Long-term storage (>180 days) resulted in densification and structural modifications that correlated with a significant decrease in storage modulus (G'). The physicochemical characterization of aged samples underscored the multifaceted nature of the mechanisms underlying the loss of functional properties over time. Besides, the reconstitution of the aged sample after exposition at high humidity confirmed the occurrence of more than one mechanism during storage. The molecular mobility and crosslinking phenomena were shown to be the potential drivers of functionality loss.

Based on these findings and the semicrystalline nature of CF, the heterogeneity observed suggests that the detected phase corresponds to the amorphous fraction, which can be divided into two phases with distinct characteristics. The first phase exhibits low molecular mobility, a higher glass transition temperature (Tg_i), and lower water affinity, attributed mainly to amorphous cellulose and parts of hemicellulose. The second phase, comprising lower molecular weight components such as pectin, proteins, and a fraction of hemicellulose, shows higher molecular mobility, a lower Tg_i, and greater water affinity. Both phases are surrounded by a crystalline fraction, which mechanically restricts the mobility of the amorphous components, with the first phase being more constrained than the second.

Due to their differing characteristics and mobilities, these phases are susceptible to distinct aging kinetics. The more embedded and constrained fraction likely undergoes slower aging kinetics due to its restricted mobility and higher Tg. Conversely, the less constrained fraction may experience a more rapid aging process and may play a key role in gel network formation due to its higher water affinity. The challenge in measuring and identifying the aging mechanisms, as well as distinguishing between these fractions, lies in their environmental constraints, which often result in combined measurements of both phases.

Although these findings underscore the need for an understanding of the interplay between molecular dynamics, structural characteristics, and environmental factors (humidity and temperature) in influencing the functional properties of citrus fibers during storage, there are still some gaps. Future research endeavors might aim to further investigate the impact of the structure of the main components (crystallinity, degree of methyl esterification, branching) and physical properties (α and β- relaxations) and their interactions in the functionality of citrus fiber and its stability upon storage. Furthermore, it is important to explore the impact of processing techniques associated with the storage strategies tailored to mitigate functionality loss. By advancing understanding of the storage conditions of citrus fibers and their behavior during storage, it is possible to enhance their utilization in various applications unlocking their full potential as versatile and sustainable biomaterials.

Chapter 7. Synthèse de la thèse

Chapter 7. Synthèse de la thèse

Les agrumes représentent l'une des productions de fruits les plus importantes au niveau mondial, environ 104 millions de tonnes en 2022, dont plus de la moitié est destinée à la production de jus d'agrumes (USDA, 2024). Par conséquent, une quantité considérable de coproduits est générée, comme les écorces et les feuilles, qui peuvent être une source potentielle de pectine et d'huiles essentielles (Bejar *et al.*, 2012). Le coproduit des écorces issu de l'extraction de la pectine conserve une composition intéressante avec 80% de glucides, 8% de protéines et une faible quantité de cendres et de lipides, qui peut conférer des propriétés physicochimiques potentielles clé telles que la rétention d'eau, la capacité de gonflement et la capacité de rétention d'huile (He *et al*., 2023; Jiang *et al.,* 2022; Lundberg *et al*., 2014).

Les fibres d'agrumes, valorisées généralement sous forme de poudres, peuvent être utilisées comme substituts de matières grasses et d'œufs, agents de libération contrôlée de saveur, épaississants, agents gélifiants, stabilisants, et même matériau pour l'emballage alimentaire (Kristensen *et al*., 2022; Su *et al.*, 2020). Un des défis majeurs pour l'industrie des poudres alimentaires est la perte des propriétés fonctionnelles lors de la reconstitution avec de l'eau. Plusieurs études ont suggéré que des changements structurels irréversibles, tels que la réticulation entre microfibrilles de cellulose pendant le séchage, pourraient être la cause la plus plausible de la réduction de ces propriétés (Agoda-Tandjawa *et al.,* 2010; Déléris & Wallecan, 2017).

De nombreuses études s'intéressent aux modifications induites par le stockage sur les propriétés de réhydratation des produits issues de lait (Fyfe *et al*., 2011; Gaiani *et al.*, 2007; Masum *et al.*, 2020a). D'autres travaux ont étudié l'impact du stockage sur les poudres de fruits et légumes en se concentrant sur l'effet de l'activité de l'eau et de la température de transition vitreuse sur la stabilité du produit (Liu *et al.*, 2010; Staniszewska *et al.,* 2021). Fernández-López *et al*. (2009) ont étudié les changements des caractéristiques chimiques, microbiologiques et physicochimiques de poudres riches en fibres provenant des oranges, pendant le stockage en explorant différentes conditions d'emballage et de conservation. Néanmoins, à notre connaissance, une seule étude à ce jour a abordé, et ce très récemment, la relation entre la mobilité moléculaire et la stabilité au stockage des matrices de fibres d'agrumes (Putri *et al.*, 2024). Par conséquent, le mécanisme sous-jacent à la perte des propriétés fonctionnelles des fibres d'agrumes pendant le stockage reste mal connu.

Ainsi, le présent travail vise à investiguer i) l'état physique et la dynamique des fibres d'agrumes à différentes échelles (de moléculaire à macromoléculaire) ainsi que les

caractéristiques chimiques (globales et limitées à la surface de la fibre), ii) la capacité des propriétés fonctionnelles des fibres d'agrumes à évoluer lors du stockage, iii) le mécanisme responsable de cette évolution en considérant l'impact de la température et de l'humidité. L'originalité de ce travail réside dans l'étude de l'état physique et de la dynamique de ce biosystème à différentes échelles (de moléculaire à macromoléculaire), en se concentrant sur la phase amorphe et sa capacité à évoluer lors du stockage.

En considérant l'objectif général de projet et l'état actuel des connaissances sur le sujet dans la littérature existante, trois hypothèses ont été formulées, et une approche d'étude proposée pour chacune.

a) Des mouvements de segments et/ou des groupes latéraux des fractions amorphes des biopolymères facilités par des valeurs d'humidité relative et température élevées pourraient se produire pendant le stockage, entraînant des changements physiques et chimiques qui affectent la fonctionnalité des fibres.

Pour vérifier cette hypothèse, une étude de la dynamique moléculaire de la matrice de fibre d'agrumes et son évolution lors du stockage sera conduite.

b) Certains composés ou groupes latéraux des chaînes pourraient, au cours du stockage, migrer vers la surface en raison de la mobilité moléculaire résiduelle dans la matrice. Cette migration pourrait modifier la disponibilité des groupes fonctionnels à la surface, influençant ainsi l'hydrophilie/lipophilie les charges et donc les interactions du matériau avec l'eau. Analyser la composition chimique de surface.

Pour valider cette idée, une analyse de la composition chimique de surface sera réalisée.

c) Des réactions chimiques telles qu'oxydation, hydrolyse, polymérisation, décarbonisation, d'estérification peuvent se produire lors du stockage, et entraîner des altérations des groupes fonctionnels impactant les propriétés fonctionnelles des matériaux. De telles réactions chimiques peuvent être influencées par les conditions de stockage (température et teneur en eau) et la mobilité moléculaire. Examiner la survenue de réactions chimiques lors du stockage.

Une étude de certaines propriétés chimiques des produits frais et après un an de conservation sera menée.

Pour l'ensemble de ses hypothèses, une attention particulière sera portée sur le rôle de l'eau et de la température dans les propriétés des systèmes étudiés.

La caractérisation physicochimique de la fibre d'agrumes au temps initial a été, dans un premier temps, réalisée.

La composition chimique de la fibre d'agrumes est la suivante : cellulose, hémicellulose, pectine, protéine et cendres, dans une proportion massique de 53,0 ± 7,4 %, 20,0 ± 8,8 %, 17,0 ± 2,4 %, 5,0 ± 0,4 % et 4,0 ± 0,2 % g/100 g sur une base sèche, respectivement (données fournies par le fournisseur). De plus, deux méthodes de préparation/traitement des fibres ont été comparées (Table 7-1).

Table 7-1. Méthodes de traitement des fibres d'agrumes.

Échantillon	**CF**	**CFV**
Conditions de traitement	• Extrait avec un mélange d'isopropanol/eau sous haute pression. • Séché à l'échelle pilote : séchoir à lit fluidisé (GVW 32 / WSG200). • Durée du séchage: 7 heures. • Température d'entrée: 110 °C. • Température maximale du produit : 50 °C. • Teneur en matière sèche: 92 %. • Densité apparente: 0,41 g/cm³.	• Préparé de manière similaire au CF mais stocké dans 40-45 % d'isopropanol/eau jusqu'au séchage. • Séché tous les 45 jours sur une période de 360 jours à l'échelle de laboratoire : séchoir à lit fluidisé Mini Glatt. • Durée du séchage : 40-45 min. • Température d'entrée : 50 °C. • Température maximale du produit : 40 °C. • Teneur en matière sèche : 96 %. • Densité apparente : 0,29 g/cm³.

L'isotherme de sorption d'eau des fibres d'agrumes considérées a été déterminée et analysée par un traitement mathématique des données pour étudier les cinétiques de sorption, l'équilibre et l'hystérésis, afin de mieux comprendre les propriétés d'hydratation de cette matrice. La fibre d'agrume présente une isotherme de sorption caractéristique d'une structure amorphe et poreuse qui peut être associée à des multicouches à la surface interne du matériau

(Andrade *et al.,* 2011; Perez-Pirotto *et al*., 2022) telle qu'observée pour le linter de coton, la cellulose microcristalline (MCC) et la α-cellulose (Xie *et al.*, 2011), les graines de papaye (Rosa *et al.*, 2021), les noyaux de dattes (Al-Khalili *et al.*, 2023a), l'amidon de manioc (Perdomo *et al.*, 2009), la cellulose bactérienne (Cybulska *et al*., 2023), et le rhizome de nénuphar rouge (Nymphaea x rubra) (Phahom & Roudaut, 2023).

La sorption d'eau d'une matrice végétale est influencée par la composition, la cristallinité et l'organisation du matériau. Dans le cas de la fibre d'agrumes, la courbe d'adsorption présente un profil similaire à celui de la pectine et une teneur en eau d'équilibre (CEM) (26,2% b.s.) plus élevée que celle attendue pour la cellulose (14,2 – 25,4% b.s.) pour une cristallinité comparable (59 - 88%). Ces observations montrent l'influence prédominante de la pectine dans l'interaction de la fibre d'agrumes avec l'eau.

Pour étudier l'équilibre de la sorption d'eau, le modèle GAB a été appliqué et s'est révélé approprié pour décrire la sorption sur les fibres d'agrumes (valeur P < 10%). La valeur de monocouche (Xm) déterminée par GAB est de 7,0 ± 0,0 g d'eau/g d'échantillon sec, comparable à celle de la cellulose d'eucalyptus recristallisée, ce qui peut être attribué à la leur structure semi-cristalline, induisant des comportements comparables en termes d'interaction avec l'eau. La constante C, représentant la force de liaison de l'eau avec les sites actifs de surface, était de 10,6 pour la CF, indiquant une forte liaison. La valeur K de 0,83 suggère que la multicouche d'eau présente des propriétés similaires à celles d'un liquide.

Concernant la contribution des autres constituants de la CF à la sorption de l'eau, les valeurs de Xm, C et K différaient significativement de celles obtenues pour la pectine d'agrumes. Cependant, le manque d'informations dans la littérature concernant l'équilibre de sorption de l'eau dans le xyloglucane (la principale hémicellulose présente dans la CF) rendent complexe la justification de l'adsorption de l'eau en monocouche dans la CF par sa composition.

L'hystérésis représente la différence entre les teneurs en eau entre désorption et sorption, influencée par la nature et l'état de la matrice. Pour CF, l'hystérésis se caractérise, lors de la désorption, par une teneur en eau plus importante que lors de la sorption, et ce, sur toute la gamme d'activité de l'eau (a_w), elle atteint un maximum de 2,1%, en accord avec les résultats publiés sur de la peau d'orange. La formation et l'effondrement des nano capillaires pendant l'adsorption et la désorption, respectivement, expliquent cette différence. Le modèle GAB décrit bien ces processus, indiquant une plus grande capacité de monocouche (X_m) et une force de liaison (paramètre C) plus élevées en désorption, ce qui suggère une plus grande quantité de sites actifs et une eau en plus forte interaction. Un comportement similaire a été observé

dans des échantillons de cellulose de coton, où la capacité de monocouche et la surface spécifique totale augmentent après adsorption et désorption, tandis que le degré de cristallinité diminue légèrement.

La cinétique de sorption d'eau des échantillons de CF se décrit par deux processus : un rapide (X_1) et concernant 72% de l'eau totale adsorbée, et un autre plus lent (X_2) pour 28% de l'eau totale. Le processus rapide est associé à l'adsorption d'eau sur les sites les plus accessibles, comme les régions amorphes et les groupes polaires de la surface externe, formant une monocouche. Le processus lent concerne l'adsorption d'eau dans les régions internes et les cristallites, conduisant à la formation de multicouches. La vitesse d'adsorption maximale (K_1) est observée à une activité de l'eau (a_w) de 0,2, diminuant ensuite en raison de la réduction de la porosité de surface, à l'origine de l'apparition d'une barrière gélifiée à la diffusion de l'eau. En revanche, K_2, plus faible, augmente légèrement avec l'a_w, indiquant que la diffusion de l'eau est le paramètre limitant, mais augmente avec la teneur en eau de la matrice.

La mobilité moléculaire des fibres d'agrumes a été évaluée à différentes échelles, en considérant l'influence de la température et de la teneur en eau sur la mobilité moléculaire. Pour évaluer la mobilité moléculaire des fibres d'agrumes à différentes échelles, trois méthodes ont été employées : la calorimétrie différentielle à balayage (DSC), l'analyse mécanique dynamique (DMA) et la résonance magnétique nucléaire (RMN). Chaque méthode nécessite une préparation spécifique des échantillons, tels que des poudres, des films ou des comprimés. Les propriétés physicochimiques des échantillons ont été analysées par DSC dans ces différentes formes, révélant des écarts types variés sans différence significative ($p > 0,05$) sur la température de transition vitreuse. Ainsi, les fibres d'agrumes ont pu être utilisées sous diverses formes pour cette étude sans altération notable de leurs propriétés.

Initialement, la mobilité moléculaire a été étudiée à l'échelle macromoléculaire. À cette fin, la poudre de fibres d'agrumes (0,3 % b.s.) analysée par DSC avec un seul chauffage de -50 °C à 200 °C à 10 °C/min, n'a révélé aucun phénomène thermique, à l'exception d'un pic de relaxation enthalpique (endothermique) entre 40 et 80 °C et d'un pic de fusion au-dessus de 177 °C. La Tg des fibres d'agrumes n'était pas mesurable sur le thermogramme du premier chauffage, en raison de l'interférence avec le pic de fusion. Une investigation utilisant quatre chauffages successifs de la poudre de fibres d'agrumes à 7,1% b.s. a montré un pic endothermique (40-80 °C) lors du premier chauffage, un pic de fusion à partir de 150 °C lors du deuxième chauffage, et un changement de pente entre 80 et 170 °C lors du troisième chauffage, qui était réversible au quatrième chauffage, suggérant une transition vitreuse (Tg).

Pour mieux étudier le pic endothermique observé lors du premier balayage thermique, l'effet du temps de stockage sur sa réversibilité a été pris en compte. Un échantillon de poudre de fibres d'agrumes 7,1% d'eau (b.s.) a été utilisé pour cette étude. Le pic à 55 ± 1 °C avec une ΔH de 1,4 ± 0,3 J/g a disparu après le premier chauffage, mais a réapparu après une semaine à 40 °C à une température plus élevée (76 ± 1 °C) avec une énergie de 0,4 ± 0,1 J/g, soit 28% de la valeur initiale. La température et l'énergie du pic de relaxation enthalpique dépendent généralement de la température et du temps de stockage, ainsi que de la complexité de la matrice. Dans ce travail, une valeur de 1,4 J/g a été déterminée, cette valeur est légèrement inférieure aux valeurs généralement publiées pour une variété de différents polysaccharides à une teneur en eau similaire. Comme mentionné précédemment, la faible relaxation de l'enthalpie peut être attribuée à la complexité (semi cristallinité) de la matrice (Syamaladevi *et al.,* 2010) et aussi à la durée du stockage limitée à 7 jours.

Comme mentionné précédemment, la Tg de la fibre d'agrumes est difficile à identifier avec certitude, en raison de l'amplitude limitée du changement de pente lors des troisième et quatrième chauffage, et de son étalement sur une large gamme de température. En utilisant la dérivée première du flux de chaleur en fonction de la température, un événement endothermique associé à une transition vitreuse avec un Tg de 116 ± 6 °C et un ΔCp de 0,24 ± 0,10 J/(g.°C) a été identifié. La transition vitreuse large des fibres d'agrumes (entre 50 et 170 °C) suggère la superposition de plusieurs transitions vitreuses, indiquant des hétérogénéités au niveau moléculaire (Figure 7-1). Deux transitions ont été révélées par déconvolution de l'événement observé dans la dérivée première du signal : Tg_1 à 97 ± 4 °C, probablement liée à une fraction amorphe moins rigide, et Tg_2 à 134 ± 7 °C, associée à une fraction amorphe plus rigide. Ces transitions pourraient correspondre aux composants des fibres d'agrumes, comme la pectine et l'hémicellulose pour le Tg le plus bas, et la zone amorphe de la cellulose pour le Tg le plus élevé.

A l'échelle méso-moléculaire, la température de relaxation α a été mesurée au maximum de tan δ à 136 ± 3 °C à 1 Hz par analyse mécanique dynamique en utilisant les échantillons sous forme de comprimés. La température de cet événement augmente avec la fréquence de sollicitation, passant de 127 à 149 °C entre 0.5 et 40 Hz, indiquant un processus de relaxation lié à la transition vitreuse. Bien que les températures de Tg et de relaxation α diffèrent, la gamme de température observée par DSC (50 à 170 °C) et DMA (86 à 180 °C) est similaire (Figure 7-1), montrant que les deux techniques détectent le même événement. La sensibilité à la fréquence a permis de calculer l'énergie d'activation (Ea) associée à la relaxation des fibres

d'agrumes à 330 kJ/mol, en accord avec les valeurs attendues pour la relaxation principale de biopolymères (200 – 400 kJ/mol) (Kalichevsky *et al*., 1992; Kim *et al*., 2003).

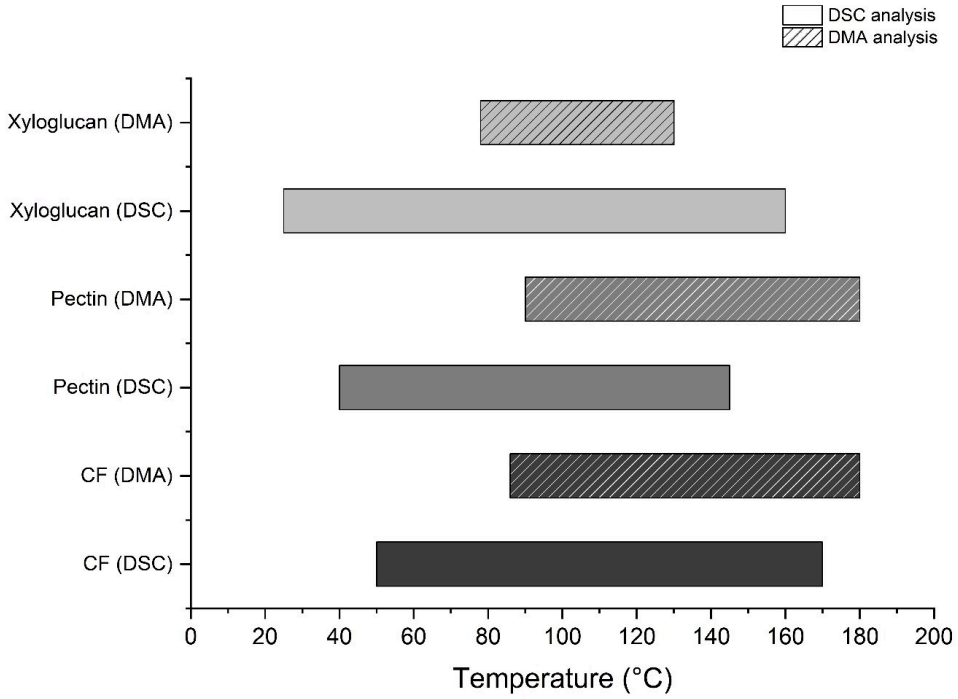

Figure 7-1.Comparaison de l'écart de température de transition vitreuse et de la relaxation α des fibres d'agrumes, de la pectine et du xyloglucane déterminées par DSC et DMA.

Pour étudier la contribution des macromolécules des fibres d'agrumes à la transition vitreuse, comme discuté précédemment, de la poudre de pectine provenant d'agrumes (2,0 ± 0,7 % b.s.) et de la poudre de xyloglucane provenant de tamarin (1,8 ± 0,5 % b.s.) ont été analysées avec la même procédure DSC que la fibre d'agrumes. La pectine et le xyloglucane ont montré un pic de relaxation d'enthalpie similaire à celui des fibres d'agrumes (0,3 % b.s.) à 64,8 ± 8,9 °C et 64,1 ± 3,5 °C, respectivement. Cependant, l'énergie du pic d'enthalpie du xyloglucane (0,7 ± 0,1 J/g) était supérieure à celle des fibres d'agrumes, tandis que celle du pic d'enthalpie de la pectine (0,4 ± 0,3 J/g) n'était pas significativement différente. La température de transition vitreuse a été mesurée à 112 ± 10 °C pour la pectine et à 106 ± 4 °C pour le xyloglucane, sans différence significative avec les fibres d'agrumes à teneur en eau similaire (0-2 % b.s.) (Figure 7-1). La transition vitreuse des fibres d'agrumes pourrait provenir principalement de la pectine, malgré sa faible proportion (15 %) dans le matériau. De plus, la pectine et le xyloglucane ont été analysés par DMA et ont montré un maximum de tan δ dans la même région que les fibres d'agrumes, autour de 130 °C. L'énergie d'activation (Ea) de la pectine et du xyloglucane se situait dans la gamme typique pour les principaux biopolymères (200-400 kJ/mol). La contribution des différentes macromolécules à la

transition vitreuse de CF est complexe à évaluer. Toutefois, il semble que la pectine soit le principal contribuant à la réduction de la Tg globale, car la Tg de la cellulose fournie par la littérature est nettement supérieure à celle mesurée pour CF.

Les biopolymères, constitués de longues chaînes rigides avec de nombreuses interactions inter- et intra- moléculaires, présentent une Tg élevée. Un solvant efficace peut réduire la résistance à la fracture, le module d'élasticité et la viscosité du biopolymère en affaiblissant ces interactions, facilitant ainsi le mouvement moléculaire et diminuant la friction interne, ce qui est appelé l'effet plastifiant. Pour étudier cet effet dans les fibres d'agrumes, des films ont été utilisés et stockés à différentes humidités relatives. Les films avec des teneurs en eau variables ont montré une Tg entre 119 et 128 °C, sans différence statistique notable. Ce résultat inattendu, car une augmentation de l'eau devrait théoriquement réduire la Tg, pourrait s'expliquer par la complexité des interactions structurelles des fibres d'agrumes. D'autres plastifiants, comme le glycérol et le triacétine, ont également été testés, mais n'ont montré aucun effet significatif sur la Tg des fibres d'agrumes. Ce caractère inerte de ces solvants pourrait résulter de la nature complexe et rigide de la matrice des fibres d'agrumes, nécessitant davantage de recherches pour mieux comprendre ces interactions.

La mobilité moléculaire et la dynamique de l'eau dans les fibres d'agrumes ont été étudiées par RMN pulsée (TD-RMN), en évaluant les temps de relaxation spin-spin (T_2) et spin-réseau (T_1). Cette analyse a permis d'explorer l'influence de la température et de la teneur en humidité sur la mobilité moléculaire des échantillons. La matrice de fibres d'agrumes a révélé une hétérogénéité microstructurale, mettant en évidence deux états d'eau distincts caractéristiques par 2 niveaux de mobilités de protons. Bien que la fibre d'agrumes soit majoritairement composée de cellulose, connue pour sa nature rigide, la matrice a montré une certaine mobilité même à de faibles teneurs en eau à 25 °C. Ce résultat confirme la possibilité de changements structuraux pendant le stockage, même dans des conditions sous-vitreuses à de faibles humidités relatives. Si la température n'a eu qu'un léger effet sur la mobilité moléculaire de la matrice en modifiant potentiellement les interactions entre ses composants et ses microstructures, la mobilité moléculaire du système s'est révélée sensible aux changements de teneur en eau.

Corrélant toutes les informations obtenues par analyse RMN, la plus petite population de protons (~15 % du total) qui est la fraction sensible à l'eau, correspond probablement à l'eau absorbée dans la matrice. En revanche, la population de protons la plus élevée (~85 % du total), pourrait être associée à l''eau adsorbée. La majeure partie de l'eau interagit avec la fraction la plus rigide (comme l'eau adsorbée), augmentant sa mobilité moléculaire, mais elle

présente toujours un temps de relaxation court T_2< 1 ms, ce qui suggère un effet plastifiant de l'eau limité. Cela peut être corrélé à la structure semi-cristalline de la fibre d'agrumes : bien qu'il soit connu qu'elle n'ait pas une forte cristallinité, l'arrangement des chaînes et les interactions entre les polysaccharides restreignent sa mobilité moléculaire. De plus, la surface des matériaux de la paroi cellulaire est riche en groupes hydrophiles, favorisant une interaction plus forte avec l'eau. Par conséquent, la mobilité moléculaire est limitée en raison de la liaison des molécules d'eau.

La troisième hypothèse formulée pour expliquer la perte de fonctionnalités suggère un rôle de la composition chimique. Le composition et l'impact de la préparation des échantillons ont été investigués de manière quantitative et qualitative, en utilisant la spectroscopie infra rouge à transformée de Fourier (FTIR). De plus, la composition chimique de la surface des 2 fibres d'agrumes a été étudiée à l'aide de la spectroscopie de photoélectrons X (XPS), car la composition de surface est essentielle pour influencer les propriétés fonctionnelles. La caractérisation physico-chimique sert de premier aperçu de la matrice, jetant les bases pour l'exploration ultérieure des effets du stockage et des mécanismes associés.

Le FTIR a été utilisé pour identifier les principaux groupes fonctionnels de la fibre d'agrumes soumise à deux processus de préparation différents (Table 7-1). Les deux échantillons montrent des spectres très similaires avec de légères différences d'intensité entre certaines bandes entre 1800 et 1200 cm^{-1}. Pour explorer les différences observées, une analyse en composantes principales (ACP) a été réalisée pour comparer les échantillons CF et CFV dans cette région (1800-1200 cm^{-1}), révélant que les échantillons se différencient principalement à cause des bandes à 1745 cm^{-1} associées aux liaisons C=O. Cela suggère une différence dans la teneur et/ou structure de la pectine.

Sur la base du résultat obtenu par ACP et connaissant l'importance du degré de méthylestérification (DM) de la pectine dans ses propriétés, le DM est généralement déterminé par titration, mais la FTIR devient de plus en plus populaire pour cette mesure. Les DM déterminés par FTIR pour CF et CFV étaient inférieurs à 20%, sans différence notable entre les deux échantillons suggérant que la méthode de préparation n'avait pas d'impact notable sur le DM de la fibre d'agrumes. Cependant, l'analyse était réalisée dans une matrice complexe (sans isoler la pectine) ce qui peut justifier la difficulté d'observer la différence de préparation des échantillons.

A la surface des poudres de fibre d'agrumes, les deux éléments chimiques majoritairement détectés étaient le carbone et l'oxygène. Le sodium et l'azote n'étaient présents qu'à l'était de traces. La présence d'azote indique une faible teneur en protéines à la surface.

Avec un facteur de conversion moyen de 6 pour les protéines végétales, le pourcentage de protéines à la surface ne dépasserait pas 4 %, ce qui est inférieur à la teneur totale en protéines de 5,1 %. Cela suggère que les protéines présentes dans la fibre d'agrumes pourraient être sous-représentées à la surface et plus concentrées à l'intérieur des particules, probablement en raison de fortes interactions avec d'autres composants du cœur en raison de la migration de certains composants vers le noyau pendant le séchage. Le sodium pourrait provenir du prétraitement des fibres, à base d'hydrogénosulfite de sodium pour le blanchiment. Le rapport O/C pour les échantillons CF et CFV était respectivement de 0,4 et 0,6, inférieur à la valeur théorique pour la cellulose (0,83), suggérant une surface ne contenant pas de cellulose pure comme prévu en raison de la composition de la fibre d'agrumes mentionnée ci-dessus. La principale différence entre les échantillons CF et CFV résidait dans les contenus en carbone et en oxygène, avec une teneur en carbone plus faible et en oxygène plus élevée pour CFV, ce qui fait que le CFV a une surface plus hydrophile que le CF (Figure 7-2). Les échantillons CF et CFV ont été séchés par des procédés à échelles différentes, la durée de séchage plus longue et à une température plus élevée de CF pouvant entraîner une migration des composants vers la surface. Les résultats montrent que le mode de préparation des fibres d'agrumes peut affecter la composition de surface, avec des différences possibles dues aux variations de production ou au processus de séchage. Le contrôle de la préparation des échantillons est essentiel pour obtenir une surface plus hydrophile, influençant directement les propriétés (notamment de réhydratation) et les applications du produit.

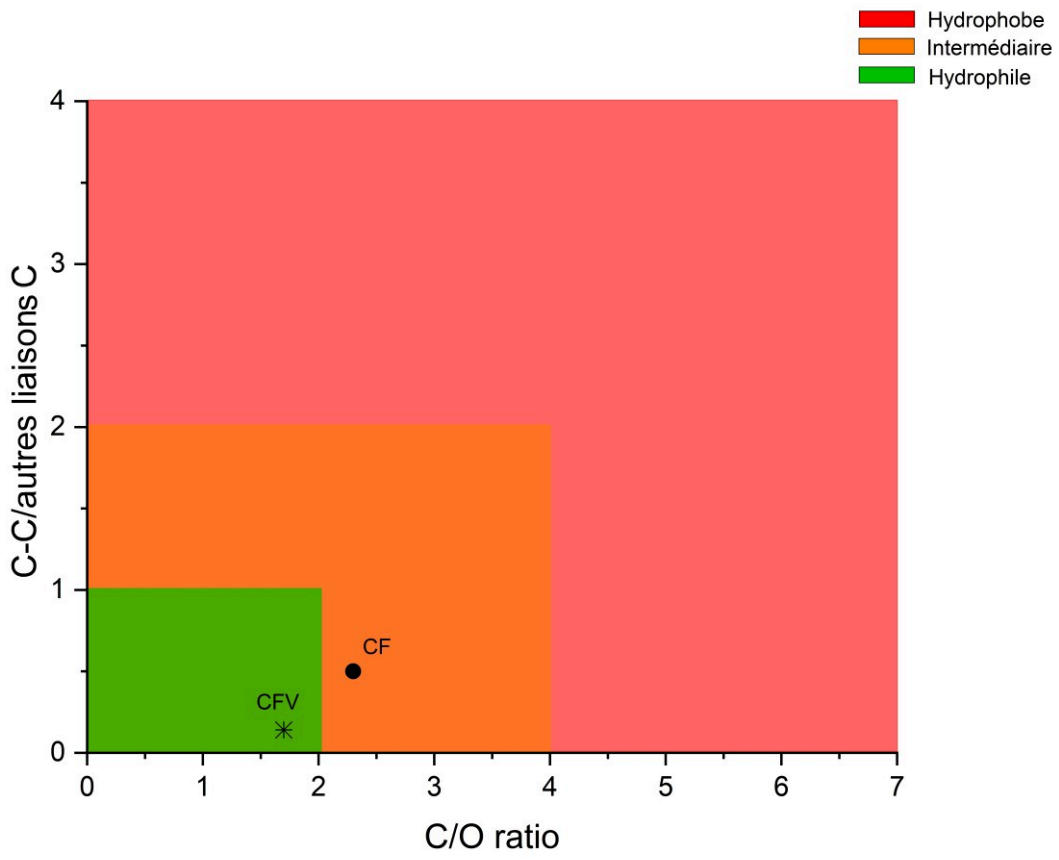

Figure 7-2. Cartographie de l'hydrophobie de surface selon les ratios C-C/autres liaisons C *versus* C/O ratio, et positionnement des deux fibres d'agrumes selon leur mode de préparation (CF et CFV).

La caractérisation des propriétés fonctionnelles des fibres, et leur évolution au cours du stockage ont aussi été analysées. La fonctionnalité (capacité de rétention d'eau, capacité de gonflement de l'eau, fermeté (mesurée par module de cisaillement G')) et le pH des fibres d'agrumes séchés ont été déterminés pendant 360 jours de stockage dans les conditions de vieillissement accéléré (40 °C, 75% HR) et à température ambiante (20 °C, 30% HR).

Le pH initial de CF était de 4,78 ± 0,02, tandis que CFV avait un pH de 4,42 ± 0,05, cette valeur plus basse pourrait être due à la dissociation d'acides carboxyliques ou de groupes carboxyles dans les protéines pendant le traitement. Les échantillons CF et CFV ont montré une WHC de 17,6 ± 0,5 g/g et 17,4 ± 0,4 g/g, respectivement, sans différence significative. La WSC de CF et CFV, 63,0 ± 6,4 mL/g et 52,8 ± 5,9 mL/g respectivement, au temps 0 était supérieure à celle de la littérature (15 – 36 mL/g), probablement en raison de différences de structure et de composition chimique. Le module de stockage (G') était de 424 ± 3 Pa pour CF et de 430 ± 36 Pa pour CFV, montrant que le séchage à différentes échelles n'a pas affecté la fonctionnalité au niveau rhéologique des échantillons.

Le pH et les propriétés fonctionnelles des fibres agglomérées ont été suivis lors du stockage, en tenant compte de l'effet combiné de la température et de l'humidité (Figure 7-3). Le pH des fibres d'agrumes stockées dans des conditions accélérées (CF_A) a montré des fluctuations significatives avec le temps, tandis que les échantillons conservés à température ambiante (CF_R) ont présenté des variations moins marquées et sans effet significatif du temps. La variation des valeurs de capacité de rétention d'eau (WHC) montre que les échantillons stockés dans des conditions accélérées (CF_A) présentent des valeurs significativement plus basses que la WHC au temps 0 pour les jours 45, 135, 270, 315 et 360. En revanche, pour CF_R, des différences significatives n'ont été observées qu'après 135 et 270 jours de stockage, indiquant un effet minimal du temps de conservation à température et RH ambiante sur la WHC. La capacité de gonflement à l'eau (WSC) de CF_R augmenté de 63 à 28 mL/g d'échantillon, tandis que pour CF_A a diminué de 63 à 23 mL/g au cours des premiers 135 jours, avec une diminution continue. Le module de stockage (G') de CF_A a diminué de 424 Pa à 109 Pa, marquant une baisse significative après 180 jours (74%), tandis que CF_R a montré une diminution moindre (40%) sur la même période, en accord avec la variation de la WSC. Dans des conditions de vieillissement accéléré, des changements importants dans les propriétés considérées ont été observés des le début du stockage, tandis que les conditions douces ont décalé ces modifications de 6 mois.

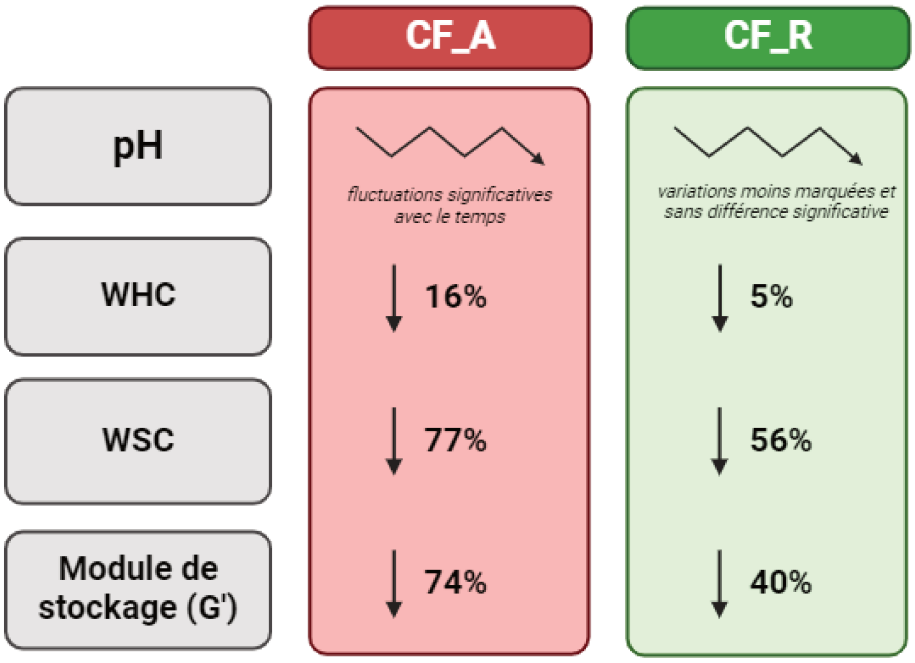

Figure 7-3. Représentation graphique de l'impact du temps (sous différentes conditions de stockage) sur les propriétés fonctionnelles de fibres d'agrumes.

L'ACP a été réalisée sur le pH et trois propriétés fonctionnelles (WHC, WSC et module de stockage) pour évaluer leur effet d'interaction et potentiellement mettre en évidence l'effet du temps. La première composante principale (PC1) est la plus significative, expliquant 59,5 % de la variance totale, tandis que la deuxième composante principale (PC2) en explique 25,2 %. PC1 a principalement séparé les échantillons selon le temps de stockage, tandis que PC2 n'est pas aussi discriminant. Jusqu'à 90 jours de conservation dans des conditions de vieillissement accéléré (CF_A 1 et CF_A 2), les échantillons sont regroupés du côté positif de PC1. Ceux stockés entre 90 et 225 jours (CF_A 3, CF_A 4, CF_A 5) présentent des scores intermédiaires, indiquant une variabilité réduite en pH et en propriétés fonctionnelles, tandis que ceux stockés plus de 225 jours (CF_A 6, CF_A 7 et CF_A 8) sont regroupés du côté négatif de PC1. Pour étudier davantage les relations entre les propriétés fonctionnelles, les angles des plots de « loading » (contribution/coefficient de corrélation) de PC1 par rapport à PC2 ont été analysés. Les paramètres avec de faibles angles reflètent une corrélation positive entre les variables, comme entre WSC et le module de stockage (G'), ainsi qu'entre le pH et le module de stockage (G'), et entre WSC et WHC. En revanche, les angles proches de 90 ° et 180 ° indiquent une corrélation neutre ou négative respectivement, telle qu'entre pH et WHC.

La caractérisation des propriétés fonctionnelles (capacité de rétention d'eau, capacité de gonflement dans l'eau et module de stockage) des fibres d'agrumes séchées a confirmé l'effet préjudiciable du vieillissement sur la rétention d'humidité, le comportement de réhydratation ainsi que la fermeté du gel. Ces résultats montrent que l'eau et/ou la température affecte ces propriétés. Ces réductions des propriétés fonctionnelles peuvent être liées à l'effondrement des pores, aux changements de taille et de densité des particules, à la structure des polysaccharides et à la composition de surface, pouvant avoir des origines chimiques et/ou physiques.

Pour mieux comprendre l'évolution des propriétés fonctionnelles pendant le stockage, la distribution de l'humidité dans la matrice et l'impact de l'humidité et de la température sur la mobilité moléculaire des fibres d'agrumes ont été étudiés. De plus, l'effet du stockage à long terme sur les structures chimiques et la composition de surface des fibres d'agrumes a été déterminé en comparant les échantillons stockés dans les deux conditions.

Les isothermes d'adsorption et de désorption des fibres d'agrumes ont montré une sensibilité au stockage dans des conditions de vieillissement accéléré (40°C, 75% HR). Les niveaux d'adsorption d'eau diminuent à a_w 0,7 avec le temps de stockage. Cela suggère des changements structurels tel qu'une réorganisation, un effondrement des pores ou une cristallisation, réduisant la capacité d'adsorption de l'eau. Par contre, aucune différence dans

la désorption n'a été observée, ce qui suggère que les changements décrits sont réversibles lors d'une exposition à une humidité élevée.

L'effet du temps a également été observé sur la courbe d'hystérésis : la courbe des échantillons vieillis s'écarte de celle de l'échantillon initial, avec un déplacement de l'hystérésis maxima de a_w 0,4 à a_w 0,7 avec le temps. L'hystérésis augmente significativement en 45 jours, puis légèrement jusqu'à 270 jours, se stabilisant ensuite. Cela indique la pression nécessaire pour remplir les pores est plus élevée dans les échantillons conservés sur les temps les plus lents.

L'impact du temps de stockage sur l'équilibre de sorption d'eau est visible sur la diminution des sites d'adsorption de la monocouche (X_m) de 7,02 à 6,44 g H_2O/g s.b. après 360 jours. L'enthalpie d'adsorption de la monocouche (C) a augmenté, impliquant des liaisons plus fortes avec l'eau. La valeur K a aussi augmenté, indiquant une adsorption multicouche plus similaire à celle de l'eau libre. Malgré un "bon" ajustement (valeur P < 10%), l'adéquation du modèle GAB diminue avec le temps. Des tendances semblables ont été observées sur de la cellulose d'eucalyptus recristallisée (par rapport au matériau amorphe), suggérant que la cristallisation pourrait réduire le nombre de sites actifs, limitant l'adsorption de l'eau des fibres d'agrumes.

Pour vérifier cette hypothèse, la cristallinité de la fibre d'agrumes a été analysée à différents temps de stockage. La fibre d'agrumes déshydratée et conservée pendant différentes durées (0, 180 et 360 jours) n'a montré aucun changement significatif de cristallinité, avec un indice de cristallinité (CI) compris entre 71 et 77% pour tous les échantillons. Malgré des attentes d'un CI plus bas (40-60%), la faible teneur en humidité lors de l'analyse a probablement affecté la mesure de la fraction amorphe car l'humidité joue un rôle crucial dans sa stabilisation. Lorsque le matériau est soumis à une faible humidité, les interactions entre les chaînes polymériques peuvent être modifiées, affectant également la densité et la rigidité, ce qui peut influencer les résultats obtenus par des techniques d'analyse telles que la DRX. Les oscillations observées dans l'adsorption d'eau, surtout à une activité de l'eau élevée ($a_w \geq$ 0,7), peuvent être dues à des processus de cristallisation mineurs, similaires à ceux observés dans les produits laitiers et les sucres. Cela pourrait expliquer la réduction de la capacité d'adsorption d'eau sans changements détectables dans les motifs diffraction des rayons X (DRX).

L'impact du temps de stockage sur la mobilité moléculaire a été étudiée à travers le comportement thermique et viscoélastique, en comparant des échantillons frais de fibres d'agrumes (CF) à ceux stockés pendant 360 jours à 40°C et 75% HR (CF_A).

La température de relaxation d'enthalpie est restée constante au fil du temps, mais l'amplitude du pic endothermique a diminué significativement après 45 jours et légèrement plus après 360 jours. Cette diminution a été associée à rigidité accrue du matériau, suggérant un réarrangement structurel ou une densification qui entrave la relaxation d'enthalpie lors du chauffage en DSC et donc une "difficulté" à restaurer la conformation initiale. Comme la température de la relaxation d'enthalpie, la température de transition vitreuse (Tg) des échantillons séchés est restée constante au cours de la période de stockage, malgré la forte humidité de stockage. Cette constance suggère que les changements dans l'échantillon, y compris la perte de fonctionnalité, peuvent se produire dans l'état vitreux sans affecter la Tg.

Le comportement viscoélastique a également été déterminé. La température de relaxation α a varié entre 115 et 130°C pour les échantillons frais et vieillis, sans différences significative sur le T_{max} ou l'intensité du pic Tan δ, indiquant que le stockage n'a pas affecté les propriétés viscoélastiques. L'énergie d'activation de la transition n'a également montré aucune variation avec le temps de stockage. Les résultats suggèrent que, bien que les propriétés thermiques et viscoélastiques restent inchangées.

Contrairement à ce qui a été observé dans l'étude de la mobilité moléculaire, en conditions de stockage accéléré, des changements significatifs ont été observés en FTIR dans plusieurs régions spectrales. Des oscillations d'intensité de bande ont été principalement remarquées dans trois régions : la large bande entre 3000 et 3750 cm^{-1} associée à l'étirement des groupes -OH de la cellulose et de l'hémicellulose, les bandes autour de 3000 et 2850 cm^{-1} correspondant à l'étirement CH et CH_2 de la cellulose et de l'hémicellulose, et la bande autour de 1030 cm^{-1} liée à la déformation C-O en C6 dans la cellulose. Une légère augmentation de l'intensité de la bande autour de 1318 cm^{-1} après 180 jours suggère un renforcement potentiel de la cristallinité, bien que cela ne soit pas confirmé par une réduction claire de la bande autour de 1337 cm^{-1}, indicatrice d'une conversion de la cellulose amorphe en cellulose cristalline. La bande autour de 898 cm^{-1} a également varié après 225 jours, indiquant potentiellement un réarrangement de la fraction de cellulose. L'analyse comparative des conditions de stockage a montré des spectres FTIR globalement similaires, suggérant un impact minimal de l'humidité et/ou de la température sur les liaisons chimiques.

L'ACP sur les régions spectrales de FTIR entre 1800-1200 cm^{-1} et 1200-850 cm^{-1} a été utilisée pour vérifier les effets du temps en conditions de stockage accéléré. Les résultats de l'ACP ont indiqué une variation significative au cours du temps. Les premières périodes de stockage ont mis l'accent sur une variation des bandes liées à la pectine, tandis que les étapes ultérieures ont montré un effet sur les bandes de cellulose et d'hémicellulose, suggérant des

transformations structurelles dans les fibres d'agrumes au cours d'un stockage prolongé en deux temps.

La diminution de la sorption d'eau au fil du temps dans les fibres d'agrumes pourrait être attribuée à des réactions chimiques, notamment l'oxydation et l'hydrolyse de la cellulose, influencées par la température et l'humidité. Des changements dans les bandes spectrales autour de 1740 cm^{-1} et 1630 cm^{-1}, généralement associées à l'oxydation et à l'hydrolyse, ont été notés dans diverses études. Pour vérifier l'occurrence des réactions chimiques, la région spectrale entre 1500 et 1750 cm^{-1} a été analysé. Pour minimiser l'interférence de l'eau, les échantillons ont été équilibrés à 0 % d'humidité relative (en présence de P_2O_5) avant la mesure. L'intensité de la bande à 1620 cm^{-1} est restée initialement, relativement constante, augmentant après 180 jours, tandis que l'intensité de la bande à 1730 cm^{-1} a diminué jusqu'à 180 jours avant de s'intensifier et de se déplacer vers des nombres d'onde plus élevés. En comparant différentes conditions de stockage, des différences notables ont été observées dans l'intensité de la bande à 1730 cm^{-1}, qui a diminué et s'est déplacée vers des nombres d'onde plus élevés pour les deux conditions, suggérant des altérations chimiques nécessitant une investigation quantitative.

La déconvolution a été appliquée pour étudier cette région, révélant des sous-bandes associées aux produits d'oxydation et d'hydrolyse de la cellulose, notamment divers groupes carbonyles et aldéhydiques. Le rapport des pics déconvolués à 1730 cm^{-1} et 1610 cm^{-1}, possiblement indicatif de l'état d'oxydation de la cellulose, a été calculé, fluctuant entre 0,1 et 0,25 avec un écart type important qui peut avoir contribué à l'absence de différence significative ($p>0,05$). Contrairement à certains résultats de la littérature, aucune augmentation de ce rapport n'a été observée, signe de l'absence de détection d'une oxydation. Cela souligne les défis de quantification de telles réactions en raison de la complexité spectrale et du chevauchement des pics.

De plus, l'étude a exploré le degré d'estérification méthylée (DM) de la pectine en utilisant des bandes entre 1750 et 1500 cm^{-1}. Malgré des décalages observés dans les bandes à 1610 cm^{-1} et 1730 cm^{-1} au fil du temps, aucune variation significative du DM n'a été détectée ($p>0,05$), soulignant la nécessité de méthodes analytiques plus sensibles pour évaluer avec précision les transformations chimiques pendant le stockage.

Les modifications de la composition de surface peuvent également avoir un impact sur l'interaction avec l'eau, principalement les étapes de mouillage et de gonflement. Une analyse XPS a été effectuée sur CF après différents temps et conditions de stockage pour évaluer les

changements de composition de surface. Par conséquent, aucune oxydation ou hydrolyse ne s'est produite sur la surface des CF pendant le stockage.

Enfin, pour évaluer une éventuelle réversibilité de la perte de fonctionnalité observée sur les fibres d'agrumes après 360 jours de stockage dans des conditions de vieillissement accéléré (40 °C, 75% HR), un échantillon a été maintenu à 97% HR pendant 10 jours. L'analyse rhéologique a montré une récupération partielle de la valeur module de stockage, G' : à 200 Pa, contre 424 Pa initialement, indiquant que certains changements survenus pendant le stockage sont réversibles avec l'hydratation. Cela suggère que la perte de fonctionnalité se produit à différentes échelles, certaines modifications étant réversibles à haute humidité. Les modifications chimiques et physiques accélérées par l'eau et la température contribuent à la perte de fonctionnalité. L'étude souligne que plusieurs phénomènes à différentes échelles sont impliqués dans la dégradation de fibre d'agrumes pendant le stockage (Table 7-2).

Table 7-2. Relation entre les méthodes utilisées pour évaluer l'impact du stockage dans la fibre d'agrumes, les changements observés et l'hypothèse sur le mécanisme.

Méthode	Changement observé	Mécanisme corrélé
Isotherme de sorption	Réduction de la sorption (vers a_w 0,7) avec le temps de stockage.	Réorganisation, effondrement des pores ou la cristallisation
	Déplacement de l'hystérésis maximum de a_w 0,4 à a_w 0,7 et l'augmentation de l'hystérésis au fil du temps.	Pression nécessaire pour remplir les pores plus élevée dans les échantillons conservés sur des temps longs.
	Diminution des sites d'adsorption de la monocouche et l'augmentation de l'enthalpie d'adsorption de la monocouche (C) et la valeur K.	Cristallisation (réduisant les sites actifs)
Comportement thermique (DSC)	Diminution de la relaxation enthalpique après 45 jours et légèrement plus après 360 jours.	Réarrangement structurel ou densification
Comportement viscoélastique (DMA)	Aucun changement	-
Composition chimique (FTIR)	Changements dans le contenu ou structure de la pectine et de la cellulose/hémicellulose	Réarrangement structural ou réactions chimiques
Composition chimique de surface (XPS)	Aucun changement	-

En résumé, l'étude physico-chimique des fibres d'agrumes a permis la caractérisation de leur complexité, de leur hétérogénéité structurale, de leur comportement à la sorption d'eau, de leurs caractéristiques thermiques et de leur composition chimique, fournissant des informations précieuses pour évaluer leur durée de vie (Figure 7-4). Cette étude souligne l'importance d'utiliser diverses techniques analytiques pour démêler la dynamique moléculaire et la structure des fibres, et aussi ainsi que l'impact des conditions de traitement sur leur composition de surface.

En outre, l'étude de la fonctionnalité des fibres d'agrumes a élucidé les propriétés justifiant sa gamme d'applications et a mesuré l'impact du vieillissement sur la rétention d'humidité, le comportement à la réhydratation et la fermeté de gel (Figure 7-4). Les corrélations observées entre le module de stockage (G') et la capacité de gonflement à l'eau ont souligné l'interaction entre les caractéristiques structurelles et les attributs fonctionnels. De plus, la perte accélérée de fonctionnalités en conditions de température et d'humidité élevées a mis en évidence l'importance des paramètres de stockage pour préserver la qualité des fibres d'agrumes.

Cette étude a également élucidé les dynamiques évolutives entre l'eau et les fibres d'agrumes pendant le stockage, délimitant l'influence des conditions de stockage sur la mobilité moléculaire (même en dessous de Tg), le réarrangement structurel et la stabilité chimique. Les densifications observées et les modifications structurales, principalement après un stockage à long terme (>180 jours), ont été notées. La caractérisation physico-chimique des échantillons vieillis a souligné la nature multifacette des mécanismes sous-jacents à la perte des propriétés fonctionnelles pendant le stockage (Figure 7-4). La mobilité moléculaire et les phénomènes de réticulation se sont révélés être les moteurs potentiels de cette perte de fonctionnalité.

Bien que ces résultats soulignent la nécessité de comprendre l'interaction entre la dynamique moléculaire, les caractéristiques structurales et les facteurs environnementaux (humidité et température) dans l'influence des propriétés fonctionnelles des fibres d'agrumes pendant le stockage, il existe encore des lacunes. Les futures recherches pourraient viser à approfondir l'impact de la structure des composants principaux (cristallinité, degré de méthylation, ramification) et des propriétés physiques : en particulier la mobilité sous-vitreuse (relaxations α et β) et leurs interactions sur la fonctionnalité des fibres d'agrumes et leur stabilité au stockage. De plus, il est important d'explorer l'impact des techniques de traitement associées aux stratégies de stockage visant à atténuer la perte de fonctionnalité. En approfondissant la compréhension des conditions de stockage des fibres d'agrumes et de leur comportement pendant le stockage, il pourrait être possible d'améliorer leur utilisation dans

diverses applications, en libérant leur plein potentiel en tant que biomatériaux polyvalents et durables.

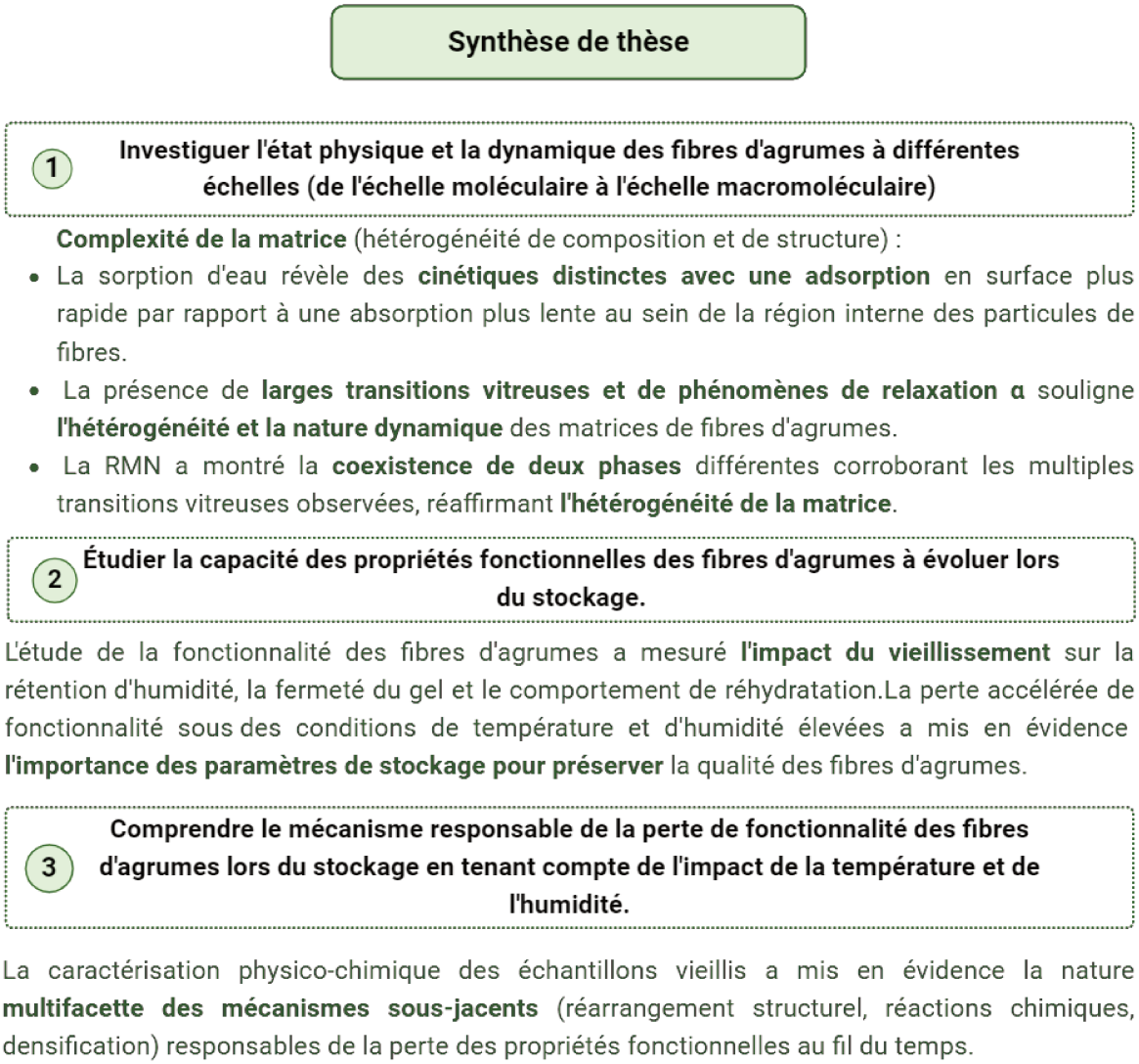

Figure 7-4. Synthèse de la thèse : Conclusions pour chaque objectif de la recherche.

References

References

Agoda-Tandjawa, G., Durand, S., Berot, S., Blassel, C., Gaillard, C., Garnier, C., & Doublier, J. L. (2010). Rheological characterization of microfibrillated cellulose suspensions after freezing. *Carbohydrate Polymers*, *80*(3), 677–686. https://doi.org/10.1016/j.carbpol.2009.11.045

Agoda-Tandjawa, G., Durand, S., Gaillard, C., Garnier, C., & Doublier, J. L. (2012). Properties of cellulose/pectins composites: Implication for structural and mechanical properties of cell wall. *Carbohydrate Polymers*, *90*(2), 1081–1091. https://doi.org/10.1016/j.carbpol.2012.06.047

Al-Khalili, M., Al-Habsi, N., Al-Khusaibi, M., & Rahman, M. S. (2023a). Proton, thermal and mechanical relaxation characteristics of a complex biomaterial (de-fatted date-pits) as a function of temperature. *Journal of Thermal Analysis and Calorimetry*, *148*(9), 3525–3534. https://doi.org/10.1007/s10973-023-11943-6

Al-Khalili, M., Al-Habsi, N., & Rahman, M. (2023b). Moisture sorption isotherms of whole and fractionated date-pits: Measurement and theoretical modelling. *Arabian Journal of Chemistry*, *16*(5), 104678. https://doi.org/10.1016/j.arabjc.2023.104678

Al-Muhtaseb, A. H., McMinn, W. A. M., & Magee, T. R. A. (2002). Moisture sorption isotherm characteristics of food products: A review. *Food and Bioproducts Processing: Transactions of the Institution of of Chemical Engineers, Part C*, *80*(2), 118–128. https://doi.org/10.1205/09603080252938753

Ali, M., Emsley, A. M., Herman, H., & Heywood, R. J. (2001). Spectroscopic studies of the ageing of cellulosic paper. *Polymer*, *42*(7), 2893–2900. https://doi.org/10.1016/S0032-3861(00)00691-1

Anderson, C. T., & Kieber, J. J. (2020). Dynamic Construction, Perception, and Remodeling of Plant Cell Walls. *Annual Review of Plant Biology*, *71*, 39–69. https://doi.org/10.1146/annurev-arplant-081519-035846

Andrade, M. A., Barbosa, C. H., Shah, M. A., Ahmad, N., Vilarinho, F., Khwaldia, K., … Ramos, F. (2023). Citrus By-Products: Valuable Source of Bioactive Compounds for Food Applications. *Antioxidants*, *12*(1), 1–20. https://doi.org/10.3390/antiox12010038

Andrade, R. D. P., Roberto, L. M., & Pérez, C. E. C. (2011). Models of sorption isotherms for food: Uses and limitations. *Vitae*, *18*(3), 325–334.

Anzai, M., Hagiwara, T., Watanabe, M., Komiyama, J., & Suzuki, T. (2011). Relationship between enthalpy relaxation and water sorption of ball-milled potato starch. *Journal of Food Engineering*, *104*(1), 43–48. https://doi.org/10.1016/j.jfoodeng.2010.11.025

AOAC. (2005). *Official Methods of Analysis of AOAC International*. *Association of Official Analysis Chemists International*.

Appelqvist, I. A. M., Cooke, D., Gidley, M. J., & Lane, S. J. (1993). Thermal properties of polysaccharides at low moisture: 1-An endothermic melting process and water-carbohydrate interactions. *Carbohydrate Polymers*, *20*(4), 291–299. https://doi.org/10.1016/0144-8617(93)90102-A

Aravantinos-Zafiris, G., Oreopoulou, V., Tzia, C., & Thomopoulos, C. D. (1994). Fibre fraction from orange peel residues after pectin extraction. *LWT - Food Science and*

Technology. https://doi.org/10.1006/fstl.1994.1094

Assifaoui, A., Champion, D., Chiotelli, E., & Verel, A. (2006). Rheological behaviour of biscuit dough in relation to water mobility. *International Journal of Food Science and Technology*, *41*(supplement 2), 124–128. https://doi.org/10.1111/j.1365-2621.2006.01469.x

Awuchi, C. G., Igwe, V. S., & Echeta, C. K. (2019). The Functional Properties of Foods and Flours. *International Journal of Advanced Academic Research | Sciences*, *5*(11), 2488–9849.

Back, E., & Didriksson, E. (1969). Four secondary and glass transition temperature of cellulose evaluated by sonic pulse technique. *Svensk Papperstidn*, *72*(21), 687–694.

Baer, D. R., Artyushkova, K., Brundle, C. R., Castle, J. E., Engelhard, M. H., Gaskell, K. J., … Smentkowski, V. S. (2019). Practical guides for x-ray photoelectron spectroscopy: First steps in planning, conducting, and reporting XPS measurements. *Journal of Vacuum Science & Technology A*, *37*, 031401. https://doi.org/10.1116/1.5065501

Barbucci, R., Magnani, A., & Consumi, M. (2000). Swelling behavior of carboxymethylcellulose hydrogels in relation to cross-linking, pH, and charge density. *Macromolecules*, *33*(20), 7475–7480. https://doi.org/10.1021/ma0007029

Bashar, M. M., Zhu, H., Yamamoto, S., & Mitsuishi, M. (2019). Highly carboxylated and crystalline cellulose nanocrystals from jute fiber by facile ammonium persulfate oxidation. *Cellulose*, *26*(6), 3671–3684. https://doi.org/10.1007/s10570-019-02363-7

Batzer, H., & Kreibich, U. T. (1981). Influence of water on thermal transition in natural polymers and synthetic polyamides. *Polymer Bulletin*, *5*, 585–590. https://doi.org/https://doi.org/10.1007/BF00255296

Bedane, A. H., Xiao, H., Eić, M., & Farmahini-Farahani, M. (2015). Structural and thermodynamic characterization of modified cellulose fiber-based materials and related interactions with water vapor. *Applied Surface Science*, *351*, 725–737. https://doi.org/10.1016/j.apsusc.2015.06.022

Bejar, A., Mihoubi, N., & Kechaou, N. (2012). Moisture sorption isotherms - Experimental and mathematical investigations of orange (Citrus sinensis) peel and leaves. *Food Chemistry*, *132*(4), 1728–1735. https://doi.org/10.1016/j.foodchem.2011.06.059

Belton, P. S. (1995). NMR in Context. *Annual Reports on NMR Spectroscopy*, *31*, 1–18. https://doi.org/10.1016/S0066-4103(08)60141-6

Bengtsson, H., & Tornberg, E. (2011). Physicochemical characterization of fruit and vegetable fiber suspensions. I: Effect of homogenization. *Journal of Texture Studies*, *42*(4), 268–280. https://doi.org/10.1111/j.1745-4603.2010.00275.x

Bergström, E. M., Salmén, L., Kochumalayil, J., & Berglund, L. (2012). Plasticized xyloglucan for improved toughness-Thermal and mechanical behaviour. *Carbohydrate Polymers*, *87*(4), 2532–2537. https://doi.org/10.1016/j.carbpol.2011.11.024

Bertran, M. S., & Dale, B. E. (1986). Determination of cellulose accessibility by differential scanning calorimetry. *Journal of Applied Polymer Science*, *32*(3), 4241–4253. https://doi.org/10.1002/app.1986.070320335

Bi, C. H., Yan, Z. M., Wang, P. L., Alkhatib, A., Zhu, J. Y., Zou, H. C., … Huang, Z. G.

(2020). Effect of high pressure homogenization treatment on the rheological properties of citrus peel fiber/corn oil emulsion. *Journal of the Science of Food and Agriculture*, *100*(9), 3658–3665. https://doi.org/10.1002/jsfa.10398

Blanshard, J. M. (1995). *The glass transition, its nature and significance in food processing. In ST. Beckett (Ed.), Physico-chemical aspects of food processing*. *Physico-Chemical Aspects of Food Processing*. https://doi.org/10.1007/978-1-4613-1227-7

Bloembergen, N., Purcell, E. M., & Pound, R. V. (1948). Relaxation effects in nuclear magnetic resonance absorption. *Physical Review*, *73*(7), 679–709. https://doi.org/https://doi.org/10.1103/PhysRev.73.679

Bocqué, M., Voirin, C., Lapinte, V., Caillol, S., & Robin, J. J. (2016). Petro-based and bio-based plasticizers: Chemical structures to plasticizing properties. *Journal of Polymer Science, Part A: Polymer Chemistry*, *54*(1), 11–33. https://doi.org/10.1002/pola.27917

Borde, B., Bizot, H., Vigier, G., & Buléon, A. (2002). Calorimetric analysis of the structural relaxation in partially hydrated amorphous polysaccharides. II. Phenomenological study of physical ageing. *Carbohydrate Polymers*, *48*(2), 111–123. https://doi.org/10.1016/S0144-8617(01)00218-1

Bosmans, G. M., Lagrain, B., Ooms, N., Fierens, E., & Delcour, J. A. (2013). Biopolymer interactions, water dynamics, and bread crumb firming. *Journal of Agricultural and Food Chemistry*, *61*(19), 4646–4654. https://doi.org/10.1021/jf4010466

Boukir, A., Fellak, S., & Doumenq, P. (2019). Structural characterization of Argania spinosa Moroccan wooden artifacts during natural degradation progress using infrared spectroscopy (ATR-FTIR) and X-Ray diffraction (XRD). *Heliyon*, *5*(9), e02477. https://doi.org/10.1016/j.heliyon.2019.e02477

Boulos, N. N., Greenfield, H., & Wills, R. B. H. (2000). Water holding capacity of selected soluble and insoluble dietary fibre. *International Journal of Food Properties*, *3*(2), 217–231. https://doi.org/10.1080/10942910009524629

Bronlund, J., & Paterson, T. (2004). Moisture sorption isotherms for crystalline, amorphous and predominantly crystalline lactose powders. *International Dairy Journal*, *14*(3), 247–254. https://doi.org/10.1016/S0958-6946(03)00176-6

Brunauer, S., Deming, L. S., Deming, W. E., & Teller, E. (1940). On a Theory of the van der Waals Adsorption of Gases. *Journal of the American Chemical Society*, *62*(7), 1723–1732. https://doi.org/10.1021/ja01864a025

Bruno, E., Lupi, F. R., Martin-Piñero, M. J., Girimonte, R., Baldino, N., Muñoz, J., & Gabriele, D. (2021). Influence of different dispersing systems on rheological and microstructural properties of citrus fiber suspensions. *LWT - Food Science and Technology*, *152*, 112270. https://doi.org/10.1016/j.lwt.2021.112270

Bugarín, R., & Gómez, M. (2023). Can Citrus Fiber Improve the Quality of Gluten-Free Breads? *Foods*, *12*(7). https://doi.org/10.3390/foods12071357

Cao, Y., & Mezzenga, R. (2020). Design principles of food gels. *Nature Food*, *1*(2), 106–118. https://doi.org/10.1038/s43016-019-0009-x

Caparino, O. A., Tang, J., Nindo, C. I., Sablani, S. S., Powers, J. R., & Fellman, J. K. (2012). Effect of drying methods on the physical properties and microstructures of mango (Philippine "Carabao" var.) powder. *Journal of Food Engineering*, *111*(1), 135–148.

https://doi.org/10.1016/j.jfoodeng.2012.01.010

Castel, A. P. D., Kaufmann, A. I., Endres, C. M., Robazza, W. da S., & Paulino, A. T. (2023). Water sorption isotherms on lyophilized jabuticaba (Myrciaria cauliflora) peel: potential byproduct for the production of dehydrated foods. *Journal of Food Science and Technology*, *60*(1), 419–428. https://doi.org/10.1007/s13197-022-05628-5

Célino, A., Gonçalves, O., Jacquemin, F., & Fréour, S. (2014). Qualitative and quantitative assessment of water sorption in natural fibres using ATR-FTIR spectroscopy. *Carbohydrate Polymers*, *101*(1), 163–170. https://doi.org/10.1016/j.carbpol.2013.09.023

Chang, L. S., Karim, R., Sabo Mohammed, A., Chai, K. F., & Ghazali, H. M. (2019). Moisture sorption isotherm and shelf-life prediction of anticaking agent incorporated spray-dried soursop (Annona muricata L.) powder. *Journal of Food Process Engineering*, *42*(5), 1–10. https://doi.org/10.1111/jfpe.13134

Chatjigakis, A. K., Pappas, C., Proxenia, N., Kalantzi, O., Rodis, P., & Polissiou, M. (1998). FT-IR spectroscopic determination of the degree of esterification of cell wall pectins from stored peaches and correlation to textural changes. *Carbohydrate Polymers*, *37*(4), 395–408. https://doi.org/10.1016/S0144-8617(98)00057-5

Chau, C. F., Wang, Y. T., & Wen, Y. L. (2007). Different micronization methods significantly improve the functionality of carrot insoluble fibre. *Food Chemistry*, *100*(4), 1402–1408. https://doi.org/10.1016/j.foodchem.2005.11.034

Chaudhary, D. S., Adhikari, B. P., & Kasapis, S. (2011). Glass-transition behaviour of plasticized starch biopolymer system - A modified Gordon-Taylor approach. *Food Hydrocolloids*, *25*(1), 114–121. https://doi.org/10.1016/j.foodhyd.2010.06.002

Chen, D., Pham, U. T. T., Van Loey, A., Grauwet, T., Hendrickx, M., & Kyomugasho, C. (2021). Microscopic evidence for pectin changes in hard-to-cook development of common beans during storage. *Food Research International*, *141*, 110115. https://doi.org/10.1016/j.foodres.2021.110115

Chen, F. L., Wei, Y. M., & Zhang, B. (2010). Characterization of water state and distribution in textured soybean protein using DSC and NMR. *Journal of Food Engineering*, *100*(3), 522–526. https://doi.org/10.1016/j.jfoodeng.2010.04.040

Chen, Pan, Wohlert, J., Berglund, L., & Furó, I. (2022). Water as an Intrinsic Structural Element in Cellulose Fibril Aggregates. *Journal of Physical Chemistry Letters*, *13*(24), 5424–5430. https://doi.org/10.1021/acs.jpclett.2c00781

Chen, Pei, Xie, F., Tang, F., & McNally, T. (2020). Unexpected Plasticization Effects on the Structure and Properties of Polyelectrolyte Complexed Chitosan/Alginate Materials. *ACS Applied Polymer Materials*, *2*(7), 2957–2966. https://doi.org/10.1021/acsapm.0c00433

Chen, W., Lickfield, G. C., & Yang, C. Q. (2004). Molecular modeling of cellulose in amorphous state. Part I: Model building and plastic deformation study. *Polymer*, *45*(3), 1063–1071. https://doi.org/10.1016/j.polymer.2003.11.020

Chen, Z., Hu, T. Q., Jang, H. F., & Grant, E. (2015). Modification of xylan in alkaline treated bleached hardwood kraft pulps as classified by attenuated total-internal-reflection (ATR) FTIR spectroscopy. *Carbohydrate Polymers*, *127*, 418–426.

https://doi.org/10.1016/j.carbpol.2015.03.084

Choi, S. Y., Rodriguez, H., Mirjafari, A., Gilpin, D. F., McGrath, S., Malcolm, K. R., … McNally, T. (2011). Dual functional ionic liquids as plasticisers and antimicrobial agents for medical polymers. *Green Chemistry*, *13*, 1527–1535. https://doi.org/https://doi.org/10.1039/C1GC15132K

Chung, H. J., & Lim, S. T. (2004). Physical aging of glassy normal and waxy rice starches: Thermal and mechanical characterization. *Carbohydrate Polymers*, *57*(1), 15–21. https://doi.org/10.1016/j.carbpol.2004.01.010

Ciriminna, R., Fidalgo, A., Delisi, R., Tamburino, A., Carnaroglio, D., Cravotto, G., … Pagliaro, M. (2017). Controlling the Degree of Esterification of Citrus Pectin for Demanding Applications by Selection of the Source. *ACS Omega*, *2*(11), 7991–7995. https://doi.org/10.1021/acsomega.7b01109

Coimbra, M. A., Barros, A., Rutledge, D. N., & Delgadillo, I. (1999). FTIR spectroscopy as a tool for the analysis of olive pulp cell-wall polysaccharide extracts. *Carbohydrate Research*, *317*(1–4), 145–154. https://doi.org/10.1016/S0008-6215(99)00071-3

Cornillon, P., & Salim, L. C. (2000). Characterization of water mobility and distribution in low- and intermediate-moisture food systems. *Magnetic Resonance Imaging*, *18*(3), 335–341. https://doi.org/10.1016/S0730-725X(99)00139-3

Cosgrove, D. J. (1997). Assembly and enlargement of the primary cell wall in plants. *Annual Review of Cell and Developmental Biology*, *13*, 171–201. https://doi.org/10.1146/annurev.cellbio.13.1.171

Cui, J., Zhao, C., Feng, L., Han, Y., Du, H., Xiao, H., & Zheng, J. (2021). Pectins from fruits: Relationships between extraction methods, structural characteristics, and functional properties. *Trends in Food Science and Technology*, *110*, 39–54. https://doi.org/10.1016/j.tifs.2021.01.077

Cybulska, J., Cieśla, J., Kurzyna-Szklarek, M., Szymańska-Chargot, M., Pieczywek, P. M., & Zdunek, A. (2023). Influence of pectin and hemicelluloses on physical properties of bacterial cellulose. *Food Chemistry*, *429*, 136996. https://doi.org/10.1016/j.foodchem.2023.136996

Dassanayake, R. S., Acharya, S., & Abidi, N. (2019). Biopolymer-Based Materials from Polysaccharides: Properties, Processing, Characterization and Sorption Applications. *IntechOpen*. https://doi.org/10.5772/intechopen.80898

de Moraes Crizel, T., Jablonski, A., de Oliveira Rios, A., Rech, R., & Flôres, S. H. (2013). Dietary fiber from orange byproducts as a potential fat replacer. *Lwt*, *53*(1), 9–14. https://doi.org/10.1016/j.lwt.2013.02.002

Debon, S. J. J., Wallecan, J., & Mazoyer, J. (2012). A rapid rheological method for the assessment of the high pressure homogenization of citrus pulp fibres. *Applied Rheology*, *22*(6), 639191–6391911. https://doi.org/10.3933/ApplRheol-22-63919

del Mar Camacho, M., Silva-Espinoza, M. A., & Martínez-Navarrete, N. (2021). Sorption Behavior, Glass Transition and Flowability of Powdered Orange Co-product. *Materials Circular Economy*, *3*(1). https://doi.org/10.1007/s42824-021-00036-0

Déléris, I., & Wallecan, J. (2017). Relationship between processing history and functionality recovery after rehydration of dried cellulose-based suspensions: A critical review.

Advances in Colloid and Interface Science, *246*, 1–12. https://doi.org/10.1016/j.cis.2017.06.013

Denham, C. (2016). *The glass transition of cotton*. Deakin University. https://doi.org/https://dro.deakin.edu.au/articles/thesis/The_glass_transition_of_cotton/21111037

Di Gioacchino, M., Bruni, F., Imberti, S., & Ricci, M. A. (2020). Hydration of Carboxyl Groups: A Route toward Molecular Recognition? *Journal of Physical Chemistry B*, *124*(21), 4358–4364. https://doi.org/10.1021/acs.jpcb.0c03609

Dias, P. G. I., Sajiwanie, J. W. A., & Rathnayaka, R. M. U. S. K. (2020). Chemical Composition, Physicochemical and Technological Properties of Selected Fruit Peels as a Potential Food Source. *International Journal of Fruit Science*, *20*(S2), S240–S251. https://doi.org/10.1080/15538362.2020.1717402

Dintcheva, N. T., Infurna, G., Baiamonte, M., & D'Anna, F. (2020). Natural compounds as sustainable additives for biopolymers. *Polymers*, *12*(4). https://doi.org/10.3390/polym12040732

Diogo, H. P., & Moura-ramos, J. J. (2009). Secondary Molecular Mobility in Amorphous Ethyl Cellulose : Aging Effects and Degree of Co-Operativity. *Journal of Polymer Science Part B: Polymer Physics*, *47*(8), 820–829. https://doi.org/10.1002/polb.21688

Domínguez-Robles, J., Stewart, S. A., Rendl, A., González, Z., Donnelly, R. F., & Larrañeta, E. (2019). Lignin and cellulose blends as pharmaceutical excipient for tablet manufacturing via direct compression. *Biomolecules*, *9*(9). https://doi.org/10.3390/biom9090423

Dušková-Smrčková, M., & Dušek, K. (2002). Processes and states during polymer film formation by simultaneous crosslinking and solvent evaporation. *Journal of Materials Science*, *37*(22), 4733–4741. https://doi.org/10.1023/A:1020843020379

Einfeldt, J., & Kwasniewski, A. (2002). Characterization of different types of cellulose by dielectric spectroscopy. *Cellulose*, *9*(3–4), 225–238. https://doi.org/10.1023/A:1021184620045

Einfeldt, J., Meißner, D., & Kwasniewski, A. (2004). Molecular interpretation of the main relaxations found in dielectric spectra of cellulose - Experimental arguments. *Cellulose*, *11*(2), 137–150. https://doi.org/10.1023/B:CELL.0000025404.61412.d6

Einhorn-Stoll, U., Kastner, H., Fatouros, A., Krähmer, A., Kroh, L. W., & Drusch, S. (2020). Thermal degradation of citrus pectin in low-moisture environment – Investigation of backbone depolymerisation. *Food Hydrocolloids*, *107*, 105937. https://doi.org/10.1016/j.foodhyd.2020.105937

Einhorn-Stoll, U., Kunzek, H., & Dongowski, G. (2007). Thermal analysis of chemically and mechanically modified pectins. *Food Hydrocolloids*, *21*(7), 1101–1112. https://doi.org/10.1016/j.foodhyd.2006.08.004

El Seoud, O. A., Bioni, T. A., & Dignani, M. T. (2021). Understanding cellulose dissolution in ionic liquid-dimethyl sulfoxide binary mixtures: Quantification of the relative importance of hydrogen bonding and hydrophobic interactions. *Journal of Molecular Liquids*, *322*(114848). https://doi.org/10.1016/j.molliq.2020.114848

Ellerbrock, R. H., & Gerke, H. H. (2021). FTIR spectral band shifts explained by OM–cation

interactions. *Journal of Plant Nutrition and Soil Science*, *184*(3), 388–397. https://doi.org/10.1002/jpln.202100056

Espino-Pérez, E., Bras, J., Almeida, G., Relkin, P., Belgacem, N., Plessis, C., & Domenek, S. (2016). Cellulose nanocrystal surface functionalization for the controlled sorption of water and organic vapours. *Cellulose*, *23*(5), 2955–2970. https://doi.org/10.1007/s10570-016-0994-y

Falourd, X., Lahaye, M., & Rondeau-Mouro, C. (2022). Assessment of cellulose interactions with water by ssNMR: 1H->13C transfer kinetics revisited. *Carbohydrate Polymers*, *298*(July), 120104. https://doi.org/10.1016/j.carbpol.2022.120104

Fan, F., Mou, T., Nurhadi, B., & Roos, Y. H. (2017). Water sorption-induced crystallization, structural relaxations and strength analysis of relaxation times in amorphous lactose/whey protein systems. *Journal of Food Engineering*, *196*, 150–158. https://doi.org/10.1016/j.jfoodeng.2016.10.022

Fatimi, A., Tassin, J. F., Turczyn, R., Axelos, M. A. V., & Weiss, P. (2009). Gelation studies of a cellulose-based biohydrogel: The influence of pH, temperature and sterilization. *Acta Biomaterialia*, *5*(9), 3423–3432. https://doi.org/10.1016/j.actbio.2009.05.030

Fellah, A., Anjukandi, P., Waterland, M. R., & Williams, M. A. K. (2009). Determining the degree of methylesterification of pectin by ATR/FT-IR: Methodology optimisation and comparison with theoretical calculations. *Carbohydrate Polymers*, *78*(4), 847–853. https://doi.org/10.1016/j.carbpol.2009.07.003

Fernández-Blázquez, J. P., Bello, A., & Pérez, E. (2005). Dynamic mechanical analysis of the two glass transitions in a thermotropic polymer. *Polymer*, *46*(23), 10004–10010. https://doi.org/10.1016/j.polymer.2005.08.004

Fernández-López, J., Fernández-Ginés, J. M., Aleson-Carbonell, L., Sendra, E., Sayas-Barberá, E., & Pérez-Alvarez, J. A. (2004). Application of functional citrus by-products to meat products. *Trends in Food Science and Technology*, *15*(3–4), 176–185. https://doi.org/10.1016/j.tifs.2003.08.007

Fernández-López, Juana, Sendra-Nadal, E., Navarro, C., Sayas, E., Viuda-Martos, M., & Alvarez, J. A. P. (2009). Storage stability of a high dietary fibre powder from orange by-products. *International Journal of Food Science and Technology*, *44*(4), 748–756. https://doi.org/10.1111/j.1365-2621.2008.01892.x

Ferreira, D., Barros, A., Coimbra, M. A., & Delgadillo, I. (2001). Use of FT-IR spectroscopy to follow the effect of processing in cell wall polysaccharide extracts of a sun-dried pear. *Carbohydrate Polymers*, *45*(2), 175–182. https://doi.org/10.1016/S0144-8617(00)00320-9

Fournaise, T., Petit, J., & Gaiani, C. (2021). Main powder physicochemical characteristics influencing their reconstitution behavior. *Powder Technology*, *383*, 65–73. https://doi.org/10.1016/j.powtec.2021.01.056

Fracasso, A. F., Perussello, C. A., Carpiné, D., Petkowicz, C. L. de O., & Haminiuk, C. W. I. (2018). Chemical modification of citrus pectin: Structural, physical and rheologial implications. *International Journal of Biological Macromolecules*, *109*, 784–792. https://doi.org/10.1016/j.ijbiomac.2017.11.060

Fras, L., Johansson, L. S., Stenius, P., Laine, J., Stana-Kleinschek, K., & Ribitsch, V. (2005).

Analysis of the oxidation of cellulose fibres by titration and XPS. *Colloids and Surfaces A: Physicochemical and Engineering Aspects*, *260*(1–3), 101–108. https://doi.org/10.1016/j.colsurfa.2005.01.035

Fyfe, K. N., Kravchuk, O., Le, T., Deeth, H. C., Nguyen, A. V., & Bhandari, B. (2011). Storage induced changes to high protein powders: Influence on surface properties and solubility. *Journal of the Science of Food and Agriculture*, *91*(14), 2566–2575. https://doi.org/10.1002/jsfa.4461

Gaiani, C., Scher, J., Ehrhardt, J. J., Linder, M., Schuck, P., Desobry, S., & Banon, S. (2007). Relationships between dairy powder surface composition and wetting properties during storage: importance of residual lipids. *Journal of Agricultural and Food Chemistry*, *55*(16), 6561–6567. https://doi.org/10.1021/jf070364b

Garau, M. C., Simal, S., Rosselló, C., & Femenia, A. (2007). Effect of air-drying temperature on physico-chemical properties of dietary fibre and antioxidant capacity of orange (Citrus aurantium v. Canoneta) by-products. *Food Chemistry*, *104*(3), 1014–1024. https://doi.org/10.1016/j.foodchem.2007.01.009

Garvey, C. J., Parker, I. H., & Simon, G. P. (2005). On the interpretation of X-ray diffraction powder patterns in terms of the nanostructure of cellulose I fibres. *Macromolecular Chemistry and Physics*, *206*(15), 1568–1575. https://doi.org/10.1002/macp.200500008

Garvey, C. J., Simon, G. P., Whittaker, A. K., & Parker, I. H. (2019). Moisture-activated dynamics on crystallite surfaces in cellulose. *Colloid and Polymer Science*, *297*(4), 521–527. https://doi.org/10.1007/s00396-018-04464-4

Gaudel, N., Gaiani, C., Harshe, Y. M., Kammerhofer, J., Pouzot, M., Desobry, S., & Burgain, J. (2022). Reconstitution of fruit powders: A process – structure – function approach. *Journal of Food Engineering*, *315*, 110800. https://doi.org/10.1016/j.jfoodeng.2021.110800

Goff, D., & Guo, Q. (2019). Food Structure Development : The Interplay Between Processing Routes and Formulation Elements. *Part A Food Structure Development: The Interplay Between Processing Routes and Formulation Elements*, 1–28.

Gonçalves, S. M., dos Santos, D. C., Motta, J. F. G., Santos, R. R. dos, Chávez, D. W. H., & Melo, N. R. de. (2019). Structure and functional properties of cellulose acetate films incorporated with glycerol. *Carbohydrate Polymers*, *209*, 190–197. https://doi.org/10.1016/j.carbpol.2019.01.031

Goring, D. A. I. (1963). *Thermal Softening of Lignin, Hemicellulose and Cellulose*. Pulp and Paper in Canada.

Goula, A. M., Karapantsios, T. D., Achilias, D. S., & Adamopoulos, K. G. (2008). Water sorption isotherms and glass transition temperature of spray dried tomato pulp. *Journal of Food Engineering*, *85*(1), 73–83. https://doi.org/10.1016/j.jfoodeng.2007.07.015

Gracia-Fernández, C. A., Gómez-Barreiro, S., López-Beceiro, J., Tarrío Saavedra, J., Naya, S., & Artiaga, R. (2010). Comparative study of the dynamic glass transition temperature by DMA and TMDSC. *Polymer Testing*, *29*(8), 1002–1006. https://doi.org/10.1016/j.polymertesting.2010.09.005

Grattard, N., Salaün, F., Champion, D., Roudaut, G., & Le Meste, M. (2002). Influence of physical state and molecular mobility of freeze-dried maltodextrin matrices on the

oxidation rate of encapsulated lipids. *Journal of Food Science*, *67*(8), 3002–3010. https://doi.org/10.1111/j.1365-2621.2002.tb08851.x

Greczynski, G., & Hultman, L. (2020). Progress in Materials Science X-ray photoelectron spectroscopy : Towards reliable binding energy referencing. *Progress in Materials Science*, *107*, 100591. https://doi.org/10.1016/j.pmatsci.2019.100591

Grigelmo-Miguel, N., & Martín-Belloso, O. (1998). Characterization of dietary fiber from orange juice extraction. *Food Research International*, *31*(5), 355–361. https://doi.org/10.1016/S0963-9969(98)00087-8

Grunin, L. Y., Grunin, Y. B., Nikolskaya, E. A., Sheveleva, N. N., & Nikolaev, I. A. (2017). An NMR relaxation and spin diffusion study of cellulose structure during water adsorption. *Biophysics (Russian Federation)*, *62*(2), 198–206. https://doi.org/10.1134/S0006350917020087

Grunin, Y. B., Grunin, L. Y., Nikol'Skaya, E. A., & Talantsev, V. I. (2012). Microstructure of cellulose: NMR relaxation study. *Polymer Science - Series A*, *54*(3), 201–208. https://doi.org/10.1134/S0965545X12030030

Grunin, Y. B., Ivanova, M. S., Masas, D. S., & Grunin, L. Y. (2019). The Nature of the Supramolecular Structural Variation and Hydrophilic Properties of Cellulose during Water Sorption. *Biophysics*, *64*(6), 1066–1070. https://doi.org/10.1134/S0006350919060071

Guillard, V., Broyart, B., Guilbert, S., Bonazzi, C., & Gontard, N. (2004). Moisture diffusivity and transfer modelling in dry biscuit. *Journal of Food Engineering*, *64*(1), 81–87. https://doi.org/10.1016/j.jfoodeng.2003.09.014

Gurina, D., Surov, O., Voronova, M., & Zakharov, A. (2020). Molecular dynamics simulation of polyacrylamide adsorption on cellulose nanocrystals. *Nanomaterials*, *10*(7), 1–15. https://doi.org/10.3390/nano10071256

Han, J. H., & Gennadios, A. (2005). Edible Films and Coatings: a review. In J. H. Han (Ed.), *Innovations in Food Packaging* (pp. 239–262). Elsevier. https://doi.org/https://doi.org/10.1016/B978-0-12-311632-1.X5031-1

Hancock, B. C., Shamblin, S. L., & Zografi, G. (1995). Molecular Mobility of Amorphous Pharmaceutical Solids Below Their Glass Transition Temperatures. *Pharmaceutical Research: An Official Journal of the American Association of Pharmaceutical Scientists*. https://doi.org/10.1023/A:1016292416526

Harnkarnsujarit, N., & Charoenrein, S. (2011). Effect of water activity on sugar crystallization and β-carotene stability of freeze-dried mango powder. *Journal of Food Engineering*, *105*(4), 592–598. https://doi.org/10.1016/j.jfoodeng.2011.03.026

Hatakeyama, H., & Hatakeyama, T. (2000). Interaction between cellulosic polysaccharides and water. *Hydrocolloids*, 261–270. https://doi.org/10.1016/b978-044450178-3/50032-9

He, C. ai, Qi, J. ru, Liao, J. song, Song, Y. ting, & Wu, C. lin. (2023). Excellent hydration properties and oil holding capacity of citrus fiber: Effects of component variation and microstructure. *Food Hydrocolloids*, *144*, 108988. https://doi.org/10.1016/j.foodhyd.2023.108988

Hedegaard, R. V., & Skibsted, L. H. (2013). *Shelf-life of food powders*. (B. Bhandari, N. Bansal, M. Zhang, & P. Schuck, Eds.), *Handbook of Food Powders: Processes and*

Properties. Elsevier. https://doi.org/10.1533/9780857098672.2.409

Heinze, T. (2016). Cellulose: Structure and Properties. In O. J. Rojas (Ed.), *Cellulose Chemistry and Properties: Fibers, Nanocelluloses and Advanced Materials* (pp. 1–52). Cham: Springer International Publishing. https://doi.org/10.1007/12_2015_319

Hill, C. A. S., Norton, A., & Newman, G. (2009). The Water Vapor Sorption Behavior of Natural Fibers Callum. *Journal of Applied Polymer Science*, *112*, 1524–1537. https://doi.org/10.1002/app

Hill, C. A. S., Norton, A., & Newman, G. (2010). The Water Vapor Sorption Behavior of Flax Fibers— Analysis Using the Parallel Exponential Kinetics Model and Determination of the Activation Energies of Sorption. *Journal of Applied Polymer Science*, *116*(5), 2166–2173. https://doi.org/10.1002/app.31819

Hills, B. P., Cano, C., & Belton, P. S. (1991). Proton NMR Relaxation Studies of Aqueous Polysaccharide Systems. *Macromolecules*, *24*(10), 2944–2950. https://doi.org/10.1021/ma00010a047

Hodge, I. M. (1994). Enthalpy relaxation and recovery in amorphous materials. *Journal of Non-Crystalline Solids*, *169*, 211–266. https://doi.org/10.1016/0022-3093(94)90321-2

Hodge, I. M., & Berens, A. R. (1985). Effects of Annealing and Prior History on Enthalpy Relaxation in Glassy Polymers. 5. Mathematical Modeling of Nonthermal Preaging Perturbations. *Macromolecules*, *18*(10), 1980–1984. https://doi.org/10.1021/ma00152a030

Holloway, W. D., & Greig, R. I. (1984). Water Holding Capacity of Hemicelluloses from Fruits, Vegetables and Wheat Bran. *Journal of Food Science*, *49*(6), 1632–1633. https://doi.org/10.1111/j.1365-2621.1984.tb12867.x

Hori, R., & Sugiyama, J. (2003). A combined FT-IR microscopy and principal component analysis on softwood cell walls. *Carbohydrate Polymers*, *52*(4), 449–453. https://doi.org/10.1016/S0144-8617(03)00013-4

Hourston, D. J., Song, M., Schafer, F. U., Pollock, H. M., & Hammiche, A. (1999). Modulated-temperature differential scanning calorimetry: 15. Crosslinking in polyurethane-poly(ethyl methacrylate) interpenetrating polymer networks. *Polymer*, *40*(17), 4769–4775. https://doi.org/10.1016/S0032-3861(98)00706-X

Howard, K. R., Runyan, C. L., Poe, A. B., Cassens, A. M., & Kinman, L. A. (2024). Evaluation of citrus fiber as a natural alternative to sodium tripolyphosphate in marinated boneless broiler chicken breast and inside beef skirt (transversus abdominis). *Animal Bioscience*, *37*(1), 116–122. https://doi.org/10.5713/ab.22.0145

Huang, J. yi, Liao, J. song, Qi, J. ru, Jiang, W. xin, & Yang, X. quan. (2021). Structural and physicochemical properties of pectin-rich dietary fiber prepared from citrus peel. *Food Hydrocolloids*, *110*, 106140. https://doi.org/10.1016/j.foodhyd.2020.106140

Humerez-Flores, J. N., Verkempinck, S. H. E., Van Loey, A. M., Moldenaers, P., & Hendrickx, M. E. (2022). Targeted modifications of citrus pectin to improve interfacial properties and the impact on emulsion stability. *Food Hydrocolloids*, *132*, 107841. https://doi.org/10.1016/j.foodhyd.2022.107841

Huppertz, T., & Gazi, I. (2016). Lactose in dairy ingredients: Effect on processing and storage stability. *Journal of Dairy Science*, *99*(8), 6842–6851. https://doi.org/10.3168/jds.2015-

10033

Ibbett, R., Taylor, J., Schuster, K. C., & Cox, M. (2008). Interpretation of relaxation and swelling phenomena in lyocell regenerated cellulosic fibres and textiles associated with the uptake of solutions of sodium hydroxide. *Cellulose*, *15*(3), 393–406. https://doi.org/10.1007/s10570-007-9180-6

Ibbett, R., Wortmann, F., Varga, K., & Schuster, K. C. (2014). A morphological interpretation of water chemical exchange and mobility in cellulose materials derived from proton NMR T2 relaxation. *Cellulose*, *21*(1), 139–152. https://doi.org/10.1007/s10570-013-0106-1

Iglesias, H. A., Chirife, J., & Buera, M. P. (1997). Adsorption isotherm of amorphous trehalose. *Journal of the Science of Food and Agriculture*, *75*(2), 183–186. https://doi.org/https://doi.org/10.1002/(SICI)1097-0010(199710)75:2<183::AID-JSFA860>3.0.CO;2-T

Iijima, M., Nakamura, K., Hatakeyama, T., & Hatakeyama, H. (2000). Phase transition of pectin with sorbed water. *Carbohydrate Polymers*, *41*(1), 101–106. https://doi.org/10.1016/S0144-8617(99)00116-2

Inari, N. G., Petrissans, M., Lambert, J., Ehrhardt, J. J., & Férardin, P. (2006). XPS characterization of wood chemical composition after heat-treatment. *Surface and Interface Analysis*, *38*, 1336–1342. https://doi.org/10.1002/sia.2455

Ioelovich, M. (2016). Isophase Transitions of Cellulose – A Short Review. *Athens Journal of Sciences*, *3*(4), 309–322. https://doi.org/10.30958/ajs.3-4-4

Ioelovich, M. (2021). Adjustment of hydrophobic properties of cellulose materials. *Polymers*, *13*(8). https://doi.org/10.3390/polym13081241

Jafarpour, G., Dantras, E., Boudet, A., & Lacabanne, C. (2007). Study of dielectric relaxations in cellulose by combined DDS and TSC. *Journal of Non-Crystalline Solids*, *353*(44–46), 4108–4115. https://doi.org/10.1016/j.jnoncrysol.2007.06.026

JEOL. (2022). *Magnetic nanoparticles and superparamagnetic resonance - Magnetic relaxation of magnetic nanoparticles and fluid*. Tokyo.

Jiang, Z., Zhang, M., Huang, Y., Ma, C., Mu, S., Li, H., … Hou, J. (2022). Comparison and Characterization of the Structure and Physicochemical Properties of Three Citrus Fibers: Effect of Ball Milling Treatment. *Foods*, *11*(17). https://doi.org/10.3390/foods11172665

Johansson, L. S., & Campbell, J. M. (2004). Reproducible XPS on biopolymers: Cellulose studies. *Surface and Interface Analysis*, *36*(8), 1018–1022. https://doi.org/10.1002/sia.1827

Kalichevsky, M. T., Jaroszkiewicz, E. M., Ablett, S., Blanshard, J. M. V., & Lillford, P. J. (1992). The glass transition of amylopectin measured by DSC, DMTA and NMR. *Carbohydrate Polymers*, *18*(2), 77–88. https://doi.org/10.1016/0144-8617(92)90129-E

Kalla-Bertholdt, A. M., Baier, A. K., & Rauh, C. (2023). Potential of Modification of Techno-Functional Properties and Structural Characteristics of Citrus, Apple, Oat, and Pea Dietary Fiber by High-Intensity Ultrasound. *Foods*, *12*(19). https://doi.org/10.3390/foods12193663

Kararli, T. T., Hurlbut, J. B., & Needham, T. E. (1990). Glass–rubber transitions of cellulosic

polymers by dynamic mechanical analysis. *Journal of Pharmaceutical Sciences*, *79*(9), 845–848. https://doi.org/10.1002/jps.2600790922

Karel, M., Anglea, S., Buera, P., Karmas, R., Levi, G., & Roos, Y. (1994). Stability-related transitions of amorphous foods. *Thermochimica Acta*, *246*(2), 249–269. https://doi.org/10.1016/0040-6031(94)80094-4

Kargin, V. A., Kozlov, P. V., & Nai-chan, W. (1960). Classification temperature of cellulose. *Dokl. Akad. Nauk SSSR*, *130*(2), 356–358. https://doi.org/http://mi.mathnet.ru/dan39549

Kato, K. L., & Cameron, R. E. (1999). A review of the relationship between thermally-accelerated ageing of paper and hornification. *Cellulose*, *6*(1), 23–40. https://doi.org/10.1023/A:1009292120151

Khodayari, A., Thielemans, W., Hirn, U., Van Vuure, A. W., & Seveno, D. (2021). Cellulose-hemicellulose interactions - A nanoscale view. *Carbohydrate Polymers*, *270*, 118364. https://doi.org/10.1016/j.carbpol.2021.118364

Kim, E. H. J., Chen, X. D., & Pearce, D. (2009a). Surface composition of industrial spray-dried milk powders. 2. Effects of spray drying conditions on the surface composition. *Journal of Food Engineering*, *94*, 169–181. https://doi.org/10.1016/j.jfoodeng.2008.10.020

Kim, E. H. J., Chen, X. D., & Pearce, D. (2009b). Surface composition of industrial spray-dried milk powders. 3. Changes in the surface composition during long-term storage. *Journal of Food Engineering*, *94*, 182–191. https://doi.org/10.1016/j.jfoodeng.2008.12.001

Kim, J. W., Park, S., Harper, D. P., & Rials, T. G. (2013). Structure and thermomechanical properties of stretched cellulose films. *Journal of Applied Polymer Science*, *128*(1), 181–187. https://doi.org/10.1002/app.38149

Kim, Y. J., Hagiwara, T., Kawai, K., Suzuki, T., & Takai, R. (2003). Kinetic process of enthalpy relaxation of glassy starch and effect of physical aging upon its water vapor permeability property. *Carbohydrate Polymers*, *53*(3), 289–296. https://doi.org/10.1016/S0144-8617(03)00075-4

Kocherbitov, V., Ulvenlund, S., Kober, M., Jarring, K., & Arnebran, T. (2008). Hydration of microcrystalline cellulose and milled cellulose studied by sorption calorimetry. *Journal of Physical Chemistry B*, *112*(12), 3728–3734. https://doi.org/10.1021/jp711554c

Kochumalayil, J., Sehaqui, H., Zhou, Q., & Berglund, L. A. (2010). Tamarind seed xyloglucan - A thermostable high-performance biopolymer from non-food feedstock. *Journal of Materials Chemistry*, *20*(21), 4321–4327. https://doi.org/10.1039/c0jm00367k

Kohajdová, Z., Karovičóvá, J., Jurasová, M., & Kukurová, K. (2011). Application of citrus dietary fibre preparations in biscuit production. *Journal of Food and Nutrition Research*, *50*(3), 182–190.

Korese, J. K., Achaglinkame, M. A., & Adzitey, F. (2022). Effect of different packaging materials on storage stability of Gardenia erubescens Stapf. & Hutch. dried fruits and powder. *Applied Food Research*, *2*(2), 100143. https://doi.org/10.1016/j.afres.2022.100143

Korus, J., Juszczak, L., Witczak, M., & Ziobro, R. (2020). Effect of citrus fiber on the rheological properties of dough and quality of the gluten-free bread. *Applied Sciences*,

10(19). https://doi.org/10.3390/APP10196633

Kristensen, K., Warne, G., Agarwal, D., & Foster, T. J. (2022). Effects of different moisture contents on the structural and functional properties of cellulose with cell wall components in different citrus fibres. *Food & Function*, *13*(5), 2756–2767. https://doi.org/10.1039/d1fo02808a

Kulasinski, K., Keten, S., Churakov, S. V., Derome, D., & Carmeliet, J. (2014). A comparative molecular dynamics study of crystalline, paracrystalline and amorphous states of cellulose. *Cellulose*, *21*(3), 1103–1116. https://doi.org/10.1007/s10570-014-0213-7

Kyomugasho, C., Kamau, P. G., Aravindakshan, S., & Hendrickx, M. E. (2021). Evaluation of storage stability of low moisture whole common beans and their fractions through the use of state diagrams. *Food Research International*, *140*, 109794. https://doi.org/10.1016/j.foodres.2020.109794

Labuza, T. P., & Hyman, C. R. (1998). Moisture migration and control in multi-domain foods. *Trends in Food Science and Technology*, *9*(2), 47–55. https://doi.org/10.1016/S0924-2244(98)00005-3

Lacabanne, C., Lamure, A., Teyssedre, G., Bernes, A., & Mourgues, M. (1994). Study of cooperative relaxation modes in complex systems by thermally stimulated current spectroscopy. *Journal of Non-Crystalline Solids*, *172–174*(Part 2), 884–890. https://doi.org/10.1016/0022-3093(94)90593-2

Lai, Y.-C., Sung, P.-H., & Chien, J. T. (2000). Evaluation of Compatibility of Rice Starch and Pectins by Glass Transition and Sub-Tg Endotherms. *Cereal Chemistry*, *77*(5), 544–550. https://doi.org/https://doi.org/10.1094/CCHEM.2000.77.5.544

Le Meste, M., Champion, D., Roudaut, G., Blond, G., & Simatos, D. (2002). Glass transition and food technology: A critical appraisal. *Journal of Food Science*, *67*(7), 2444–2458. https://doi.org/10.1111/j.1365-2621.2002.tb08758.x

Lee, J. S., Hwang, G. H., Kwon, Y. S., & Jeong, Y. G. (2020). Impacts of cellulose nanofibril and physical aging on the enthalpy relaxation behavior and dynamic mechanical thermal properties of Poly(lactic acid) composite films. *Polymer*, *202*, 122677. https://doi.org/10.1016/j.polymer.2020.122677

Lewicki, P. P. (1997). The applicability of the GAB model to food water sorption isotherms. *International Journal of Food Science and Technology*, *32*(6), 553–557. https://doi.org/10.1111/j.1365-2621.1997.tb02131.x

Lewin, M. (1997). Oxidation and aging of cellulose. *Macromolecular Symposia*, *118*, 715–724. https://doi.org/10.1002/masy.19971180192

Li, H., Roth, S. V., Freychet, G., Zhernenkov, M., Asta, N., Wågberg, L., & Pettersson, T. (2021). Structure Development of the Interphase between Drying Cellulose Materials Revealed by in Situ Grazing-Incidence Small-Angle X-ray Scattering. *Biomacromolecules*, *22*(10), 4274–4283. https://doi.org/10.1021/acs.biomac.1c00845

Li, N., Zhan, H., Yu, X., Tang, W., & Xue, Q. (2021). Investigation of the aging behavior of cellulose fiber in reclaimed asphalt pavement. *Construction and Building Materials*, *271*, 121559. https://doi.org/10.1016/j.conbuildmat.2020.121559

Lin, K., & Wang, Z. (2023). Multiscale mechanics and molecular dynamics simulations of the durability of fiber-reinforced polymer composites. *Communications Materials*, *4*(1), 1–

16. https://doi.org/10.1038/s43246-023-00391-2

Liu, F., Cao, X., Wang, H., & Liao, X. (2010). Changes of tomato powder qualities during storage. *Powder Technology*, *204*(1), 159–166. https://doi.org/10.1016/j.powtec.2010.08.002

Liu, H., Chaudhary, D., Ingram, G., & John, J. (2011). Interactions of hydrophilic plasticizer molecules with amorphous starch biopolymer-an investigation into the glass transition and the water activity behavior. *Journal of Polymer Science, Part B: Polymer Physics*, *49*(14), 1041–1049. https://doi.org/10.1002/polb.22275

Liu, P., Yu, L., Liu, H., Chen, L., & Li, L. (2009). Glass transition temperature of starch studied by a high-speed DSC. *Carbohydrate Polymers*, *77*(2), 250–253. https://doi.org/10.1016/j.carbpol.2008.12.027

Liu, R., Liu, G., Yousaf, B., Niu, Z., & Abbas, Q. (2022). Novel investigation of pyrolysis mechanisms and kinetics for functional groups in biomass matrix. *Renewable and Sustainable Energy Reviews*, *153*, 111761. https://doi.org/10.1016/j.rser.2021.111761

Liu, W., & Zhang, L. (2018). Mechanisms of the complex thermo-mechanical behavior of polymer glass across a wide range of temperature variations. *Polymers*, *10*(10), 1153. https://doi.org/10.3390/polym10101153

Liu, X., Le Bourvellec, C., & Renard, C. M. G. C. (2020). Interactions between cell wall polysaccharides and polyphenols: Effect of molecular internal structure. *Comprehensive Reviews in Food Science and Food Safety*, *19*(6), 3574–3617. https://doi.org/10.1111/1541-4337.12632

Liu, X., Renard, C. M. G. C., Bureau, S., & Le Bourvellec, C. (2021). Revisiting the contribution of ATR-FTIR spectroscopy to characterize plant cell wall polysaccharides. *Carbohydrate Polymers*, *262*, 117935. https://doi.org/10.1016/j.carbpol.2021.117935

Liu, Yang, Tian, F., Zhou, P., Zhu, H., Zhong, J., Chen, M., … Bian, F. (2023). A novel in situ sample environment setup for combined small angle x-ray scattering (SAXS), wide-angle x-ray scattering (WAXS), and Fourier transform infrared spectrometer (FTIR) simultaneous measurement. *Review of Scientific Instruments*, *94*(3), 33103. https://doi.org/10.1063/5.0128211

Liu, Yeting, Bhandari, B., & Zhou, W. (2006). Glass transition and enthalpy relaxation of amorphous food saccharides: A review. *Journal of Agricultural and Food Chemistry*, *54*(16), 5701–5717. https://doi.org/10.1021/jf060188r

Liu, Yeting, Bhandari, B., & Zhou, W. (2007). Study of glass transition and enthalpy relaxation of mixtures of amorphous sucrose and amorphous tapioca starch syrup solid by differential scanning calorimetry (DSC). *Journal of Food Engineering*, *81*(3), 599–610. https://doi.org/10.1016/j.jfoodeng.2006.12.017

Łojewska, J., Lubańska, A., Miśkowiec, P., Łojewski, T., & Proniewicz, L. M. (2006). FTIR in situ transmission studies on the kinetics of paper degradation via hydrolytic and oxidative reaction paths. *Applied Physics A: Materials Science and Processing*, *83*(4), 597–603. https://doi.org/10.1007/s00339-006-3529-9

Łojewska, J., Miśkowiec, P., Łojewski, T., & Proniewicz, L. M. (2005). Cellulose oxidative and hydrolytic degradation: In situ FTIR approach. *Polymer Degradation and Stability*, *88*(3), 512–520. https://doi.org/10.1016/j.polymdegradstab.2004.12.012

Lopez-Sanchez, P., Martinez-Sanz, M., Bonilla, M. R., Wang, D., Gilbert, E. P., Stokes, J. R., & Gidley, M. J. (2017). Cellulose-pectin composite hydrogels: Intermolecular interactions and material properties depend on order of assembly. *Carbohydrate Polymers*, *162*, 71–81. https://doi.org/10.1016/j.carbpol.2017.01.049

Lopez-Sanchez, P., Martinez-Sanz, M., Bonilla, M. R., Wang, D., Walsh, C. T., Gilbert, E. P., … Gidley, M. J. (2016). Pectin impacts cellulose fibre architecture and hydrogel mechanics in the absence of calcium. *Carbohydrate Polymers*, *153*, 236–245. https://doi.org/10.1016/j.carbpol.2016.07.113

Lovikka, V. A., Rautkari, L., & Maloney, T. C. (2018). Changes in the hygroscopic behavior of cellulose due to variations in relative humidity. *Cellulose*, *25*(1), 87–104. https://doi.org/10.1007/s10570-017-1570-9

Lundberg, B., Pan, X., White, A., Chau, H., & Hotchkiss, A. (2014). Rheology and composition of citrus fiber. *Journal of Food Engineering*, *125*(1), 97–104. https://doi.org/10.1016/j.jfoodeng.2013.10.021

Makarem, M., Kim, H., Emami, P., Melendez, J., Steinbach, A., Lipkie, T., … Kim, S. H. (2020). Impact of Drying on Meso-and Nanoscale Structures of Citrus Fiber: A Study by SFG, ATR-IR, XRD, and DLS. *Industrial and Engineering Chemistry Research*, *59*(7), 2718–2724. https://doi.org/10.1021/acs.iecr.9b06194

Makower, B., & Dye, W. B. (1956). Equilibrium moisture content and crystallization of amorphous sucrose and glucose. *Journal of Agricultural and Food Chemistry*, *4*(1), 72–77. https://doi.org/10.1021/jf60059a010

Maqbool, Z., Khalid, W., Atiq, H. T., Koraqi, H., Javaid, Z., Alhag, S. K., … AL-Farga, A. (2023). Citrus Waste as Source of Bioactive Compounds: Extraction and Utilization in Health and Food Industry. *Molecules*, *28*(4). https://doi.org/10.3390/molecules28041636

Masavang, S., Roudaut, G., & Champion, D. (2019). Identification of complex glass transition phenomena by DSC in expanded cereal-based food extrudates: Impact of plasticization by water and sucrose. *Journal of Food Engineering*, *245*, 43–52. https://doi.org/10.1016/j.jfoodeng.2018.10.008

Massiot, P., Baron, A., & Drilleau, J. F. (1996). Effect of storage of apple on the enzymatic hydrolysis of cell wall polysaccharides. *Carbohydrate Polymers*, *29*(4), 301–307. https://doi.org/10.1016/S0144-8617(96)00043-4

Masum, A. K. M., Chandrapala, J., Huppertz, T., Adhikari, B., & Zisu, B. (2020a). Effect of storage conditions on the physicochemical properties of infant milk formula powders containing different lactose-to-maltodextrin ratios. *Food Chemistry*, *319*, 126591. https://doi.org/10.1016/j.foodchem.2020.126591

Masum, A. K. M., Chandrapala, J., Huppertz, T., Adhikari, B., & Zisu, B. (2020b). Influence of drying temperatures and storage parameters on the physicochemical properties of spray-dried infant milk formula powders. *International Dairy Journal*, *105*, 104696. https://doi.org/10.1016/j.idairyj.2020.104696

Matveev, Y. I., Grinberg, V. Y., & Tolstoguzov, V. B. (2000). The plasticizing effect of water on proteins, polysaccharides and their mixtures. Glassy state of biopolymers, food and seeds. *Food Hydrocolloids*, *14*(5), 425–437. https://doi.org/10.1016/S0268-005X(00)00020-5

Mazeau, K. (2015). The hygroscopic power of amorphous cellulose: A modeling study. *Carbohydrate Polymers*, *117*, 585–591. https://doi.org/10.1016/j.carbpol.2014.09.095

Mazeau, K., & Heux, L. (2003). Molecular dynamics simulations of bulk native crystalline and amorphous structures of cellulose. *Journal of Physical Chemistry B*, *107*(10), 2394–2403. https://doi.org/10.1021/jp0219395

McPhillips, H., Craig, D. Q. M., Royall, P. G., & Hill, V. L. (1999). Characterisation of the glass transition of HPMC using modulated temperature differential scanning calorimetry. *International Journal of Pharmaceutics*, *180*(1), 83–90. https://doi.org/10.1016/S0378-5173(98)00407-4

Medina, M. de la L. R., & Kumar, V. (2006). Evaluation of cellulose II powders as a potential multifunctional excipient in tablet formulations. *International Journal of Pharmaceutics*, *322*(1–2), 31–35. https://doi.org/10.1016/j.ijpharm.2006.05.033

Mihranyan, A., Llagostera, A. P., Karmhag, R., Strømme, M., & Ek, R. (2004). Moisture sorption by cellulose powders of varying crystallinity. *International Journal of Pharmaceutics*, *269*(2), 433–442. https://doi.org/10.1016/j.ijpharm.2003.09.030

Mirhosseini, H., & Amid, B. T. (2013). Effect of different drying techniques on flowability characteristics and chemical properties of natural carbohydrate-protein Gum from durian fruit seed. *Chemistry Central Journal*, *7*(1), 1–14. https://doi.org/10.1186/1752-153X-7-1

Mishra, P., Srivastava, V., Verma, D., Chauhan, O. P., & Rai, G. K. (2009). Physico-chemical properties of Chakiya variety of Amla (Emblica officinalis) and effect of different dehydration methods on quality of powder. *African Journal of Food Science*, *3*(10), 303–306. Retrieved from http://www.academicjournals.org/ajfs

Mo, W., Chen, K., Yang, X., Kong, F., Liu, J., & Li, B. (2022). Elucidating the hornification mechanism of cellulosic fibers during the process of thermal drying. *Carbohydrate Polymers*, *289*, 1–7. https://doi.org/10.1016/j.carbpol.2022.119434

Mo, W., Li, B., & Chai, X. S. (2020). Impact of fiber initial water content on the water retention capacity of poplar APMP fibers during the thermal drying. *Wood Science and Technology*, *54*(1), 227–235. https://doi.org/10.1007/s00226-019-01148-2

Molnár, J., Zuba, Z., Sepsi, Ujhelyi, F., Erdei, G., Lenk, S., & Menyhárd, A. (2021). Structural investigation of semicrystalline polymers. *Polymer Testing*, *95*, 107098. https://doi.org/10.1016/j.polymertesting.2021.107098

Monnier, X., Maigret, J. E., Lourdin, D., & Saiter, A. (2017). Glass transition of anhydrous starch by fast scanning calorimetry. *Carbohydrate Polymers*, *173*, 77–83. https://doi.org/10.1016/j.carbpol.2017.05.042

Montès, H., Mazeau, K., & Cavaillé, J. Y. (1997). Secondary mechanical relaxations in amorphous cellulose. *Macromolecules*, *30*(22), 6977–6984. https://doi.org/10.1021/ma9611329

Moraga, G., Talens, P., Moraga, M. J., & Martínez-Navarrete, N. (2011). Implication of water activity and glass transition on the mechanical and optical properties of freeze-dried apple and banana slices. *Journal of Food Engineering*, *106*(3), 212–219. https://doi.org/10.1016/j.jfoodeng.2011.05.009

Moraru, C. I., Lee, T. C., Karwe, M. V., & Kokini, J. L. (2002). Plasticizing and

antiplasticizing effects of water and polyols on a meat-starch extruded matrix. *Journal of Food Science*, *67*(9), 3396–3401. https://doi.org/10.1111/j.1365-2621.2002.tb09596.x

Morris, G. A., Castile, J., Smith, A., Adams, G. G., & Harding, S. E. (2010). The effect of different storage temperatures on the physical properties of pectin solutions and gels. *Polymer Degradation and Stability*, *95*(12), 2670–2673. https://doi.org/10.1016/j.polymdegradstab.2010.07.013

Moulder, J. F., Stickle, W. F., Sobol, P. E., & Bomben, K. D. (1992). *Handbook of X-ray Photoelectron Spectroscopy Edited by*. (J. Chastain, Ed.). Minnesota: Perkin-Elmer Corporation.

Muzaffar, K., & Kumar, P. (2016). Moisture sorption isotherms and storage study of spray dried tamarind pulp powder. *Powder Technology*, *291*, 322–327. https://doi.org/10.1016/j.powtec.2015.12.046

Nam, S., Hillyer, M. B., & Condon, B. D. (2020). Method for identifying the triple transition (glass transition-dehydration-crystallization) of amorphous cellulose in cotton. *Carbohydrate Polymers*, *228*, 115374. https://doi.org/10.1016/j.carbpol.2019.115374

Nasser, S., Moreau, A., Jeantet, R., Hédoux, A., & Delaplace, G. (2017). Influence of storage conditions on the functional properties of micellar casein powder. *Food and Bioproducts Processing*, *106*, 181–192. https://doi.org/10.1016/j.fbp.2017.09.004

Nep, E. I., & Conway, B. R. (2011). Physicochemical characterization of grewia polysaccharide gum: Effect of drying method. *Carbohydrate Polymers*, *84*(1), 446–453. https://doi.org/10.1016/j.carbpol.2010.12.005

Niazi, M. B. K., Zijlstra, M., & Broekhuis, A. A. (2013). Understanding the role of plasticisers in spray-dried starch. *Carbohydrate Polymers*, *97*(2), 571–580. https://doi.org/10.1016/j.carbpol.2013.04.074

Noguerol, A. T., Igual, M., & Pagán-Moreno, M. J. (2021). Nutritional, physico-chemical and mechanical characterization of vegetable fibers to develop fiber-based gel foods. *Foods*, *10*(5). https://doi.org/10.3390/foods10051017

Nyström, B., Moseley, M. E., Brown, W., & Roots, J. (1981). Molecular motion of small molecules in cellulose gels studied by NMR. *Journal of Applied Polymer Science*, *26*(10), 3385–3393. https://doi.org/10.1002/app.1981.070261018

Okugawa, A., Yuguchi, Y., & Yamane, C. (2021). Relaxation phenomenon and swelling behavior of regenerated cellulose fibers affected by organic solvents. *Carbohydrate Polymers*, *259*, 117656. https://doi.org/10.1016/j.carbpol.2021.117656

Omar, A. M. E., & Roos, Y. H. (2007). Water sorption and time-dependent crystallization behaviour of freeze-dried lactose–salt mixtures. *LWT - Food Science and Technology*, *40*(3), 520–528. https://doi.org/https://doi.org/10.1016/j.lwt.2005.12.006

Ostrowska-Ligęza, E., Jakubczyk, E., Górska, A., Wirkowska, M., & Bryś, J. (2014). The use of moisture sorption isotherms and glass transition temperature to assess the stability of powdered baby formulas. *Journal of Thermal Analysis and Calorimetry*, *118*(2), 911–918. https://doi.org/10.1007/s10973-014-3846-8

Owo, H. O., Adebowale, A. A., Sobukola, O. P., Obadina, A. O., Kajihausa, O. E., Adegunwa, M. O., … Tomlins, K. (2017). Adsorption isotherms and thermodynamics properties of water yam flour. *Quality Assurance and Safety of Crops and Foods*, *9*(2), 221–227.

https://doi.org/10.3920/QAS2015.0655

Ozel, B., Uguz, S. S., Kilercioglu, M., Grunin, L., & Oztop, M. H. (2017). Effect of different polysaccharides on swelling of composite whey protein hydrogels: A low field (LF) NMR relaxometry study. *Journal of Food Process Engineering*, *40*(3), 1–9. https://doi.org/10.1111/jfpe.12465

Paajanen, A., Zitting, A., Rautkari, L., Ketoja, J. A., & Penttilä, P. A. (2022). Nanoscale Mechanism of Moisture-Induced Swelling in Wood Microfibril Bundles. *Nano Letters*, *22*(13), 5143–5150. https://doi.org/10.1021/acs.nanolett.2c00822

Pacheco, C., García-Martínez, E., Moraga, G., Piña, J., Nazareno, M. A., & Martínez-Navarrete, N. (2020). Development of dried functional foods: Stabilization of orange pulp powder by addition of biopolymers. *Powder Technology*, *362*, 11–16. https://doi.org/10.1016/j.powtec.2019.11.116

Paes, S. S., Sun, S., MacNaughtan, W., Ibbett, R., Ganster, J., Foster, T. J., & Mitchell, J. R. (2010). The glass transition and crystallization of ball milled cellulose. *Cellulose*, *17*(4), 693–709. https://doi.org/10.1007/s10570-010-9425-7

Panchev, I. N., Slavov, A., Nikolova, K., & Kovacheva, D. (2010). On the water-sorption properties of pectin. *Food Hydrocolloids*, *24*(8), 763–769. https://doi.org/10.1016/j.foodhyd.2010.04.002

Panwar, D., Panesar, P. S., & Chopra, H. K. (2019). Recent Trends on the Valorization Strategies for the Management of Citrus By-products. *Food Reviews International*, *37*(1), 91–120. https://doi.org/10.1080/87559129.2019.1695834

Panwar, D., Panesar, P. S., & Chopra, H. K. (2023). Evaluation of nutritional profile, phytochemical potential, functional properties and anti-nutritional studies of Citrus limetta peels. *Journal of Food Science and Technology*, *60*(8), 2160–2170. https://doi.org/10.1007/s13197-023-05743-x

Parrott, M. E., & Thrall, B. E. (1978). Functional properties of various fibers: physical properties. *Journal of Food Science*, *43*, 759–764.

Partanen, R., Marie, V., MacNaughtan, W., Forssell, P., & Farhat, I. (2004). 1H NMR study of amylose films plasticised by glycerol and water. *Carbohydrate Polymers*, *56*(2), 147–155. https://doi.org/10.1016/j.carbpol.2004.01.001

Patil, D. A., Tated, S., & Mhaske, S. T. (2021). Plasticized kafirin-based films: analysis of thermal, barrier and mechanical properties. *Polymer Bulletin*, *78*(3), 1721–1733. https://doi.org/10.1007/s00289-020-03179-3

Patra, S., Ajayan, P. M., & Narayanan, T. N. (2021). Dynamic mechanical analysis in materials science: The Novice's Tale. *Oxford Open Materials Science*, *1*(1), 1–12. https://doi.org/10.1093/oxfmat/itaa001

Peleg, M., & Mannheim, C. H. (1977). The mechanism of caking of powdered onion. *Journal of Food Processing and Preservation*, *1*(1), 3–11. https://doi.org/https://doi.org/10.1111/j.1745-4549.1977.tb00309.x

Perdomo, J., Cova, A., Sandoval, A. J., García, L., Laredo, E., & Müller, A. J. (2009). Glass transition temperatures and water sorption isotherms of cassava starch. *Carbohydrate Polymers*, *76*(2), 305–313. https://doi.org/10.1016/j.carbpol.2008.10.023

Pereira, P. H. F., Ornaghi, H. L., Arantes, V., & Cioffi, M. O. H. (2021). Effect of chemical treatment of pineapple crown fiber in the production, chemical composition, crystalline structure, thermal stability and thermal degradation kinetic properties of cellulosic materials. *Carbohydrate Research*, *499*, 108227. https://doi.org/10.1016/j.carres.2020.108227

Perez-Pirotto, C., Moraga, G., Hernando, I., Cozzano, S., & Arcia, P. (2022). Sorption Isotherms, Glass Transition and Bioactive Compounds of Ingredients Enriched with Soluble Fibre from Orange Pomace. *Foods*, *11*(22), 3615. https://doi.org/10.3390/foods11223615

Phahom, T., & Roudaut, G. (2023). Moisture sorption characteristics and dynamic mechanical thermal analysis of dried petiole and rhizome of red water lily (Nymphaea x rubra). *Heat and Mass Transfer*, *59*(2), 309–328. https://doi.org/10.1007/s00231-022-03258-3

Piantanida, G., Bicchieri, M., & Coluzza, C. (2005). Atomic force microscopy characterization of the ageing of pure cellulose paper. *Polymer*, *46*(26), 12313–12321. https://doi.org/10.1016/j.polymer.2005.10.015

Picker, K. M., & Hoag, S. W. (2002). Characterization of the thermal properties of microcrystalline cellulose by modulated temperature differential scanning calorimetry. *Journal of Pharmaceutical Sciences*, *91*(2), 342–349. https://doi.org/10.1002/jps.10018

Poirier-Brulez, F., Roudaut, G., Champion, D., Tanguy, M., & Simatos, D. (2006). Influence of sucrose and water content on molecular mobilityin starch-based glasses. *Biopolymers*, *81*, 63–73. https://doi.org/10.1002/bip.20358

Poletto, M., Ornaghi Júnior, H. L., & Zattera, A. J. (2014). Native cellulose: Structure, characterization and thermal properties. *Materials*, *7*(9), 6105–6119. https://doi.org/10.3390/ma7096105

Popescu, C. M., Tibirna, C. M., & Vasile, C. (2009). XPS characterization of naturally aged wood. *Applied Surface Science*, *256*(5), 1355–1360. https://doi.org/10.1016/j.apsusc.2009.08.087

Powell, M. J., Sebranek, J. G., Prusa, K. J., & Tarté, R. (2019). Evaluation of citrus fiber as a natural replacer of sodium phosphate in alternatively-cured all-pork Bologna sausage. *Meat Science*, *157*(July), 1–7. https://doi.org/10.1016/j.meatsci.2019.107883

Putri, N. I., Van Audenhove, J., Kyomugasho, C., Van Loey, A., & Hendrickx, M. (2024). Relaxation temperature and storage stability of the functionalized cell wall material residue from lemon peel. *Food Hydrocolloids*, *150*, 109711. https://doi.org/10.1016/j.foodhyd.2023.109711

Rahman, M. S., Al-Marhubi, I. M., & Al-Mahrouqi, A. (2007). Measurement of glass transition temperature by mechanical (DMTA), thermal (DSC and MDSC), water diffusion and density methods: A comparison study. *Chemical Physics Letters*, *440*(4–6), 372–377. https://doi.org/10.1016/j.cplett.2007.04.067

Rahman, M. S., Suresh, S., & Al-Habsi, N. (2021). Proton relaxation in freeze-dried broccoli as measured by low-frequency nuclear magnetic resonance (LF-NMR) and its relationship with the thermal glass transition. *Journal of Thermal Analysis and Calorimetry*, *143*(4), 3147–3159. https://doi.org/10.1007/s10973-020-09401-8

Rahman, N. F. A., Ismail, A., Shah, N. N. A. K., Varith, J., & Shamsudin, R. (2019). Effect

of drying temperature on Malaysia pomelo (Citrus grandis (L.) osbeck) pomace residue under vacuum condition. *Pertanika Journal of Science and Technology*, *27*(S1), 57–66.

Ramasamy, U. R. (2014). *Water holding capacity and enzymatic modification of pressed potato fibres*. Wageningen University.

Rivas, M. Á., Casquete, R., Córdoba, M. de G., Ruíz-Moyano, S., Benito, M. J., Pérez-Nevado, F., & Martín, A. (2021). Chemical composition and functional properties of dietary fibre concentrates from winemaking by-products: Skins, stems and lees. *Foods*, *10*(7). https://doi.org/10.3390/foods10071510

Roig, F., Dantras, E., Dandurand, J., & Lacabanne, C. (2011). Influence of hydrogen bonds on glass transition and dielectric relaxations of cellulose. *Journal of Physics D: Applied Physics*, *44*(4). https://doi.org/10.1088/0022-3727/44/4/045403

Rolandelli, G., Farroni, A. E., & Buera, M. del P. (2022). Analysis of molecular mobility in corn and quinoa flours through 1H NMR and its relationship with water distribution, glass transition and enthalpy relaxation. *Food Chemistry*, *373*, 131422. https://doi.org/10.1016/j.foodchem.2021.131422

Romani, V. P., Martins, V. G., da Silva, A. S., Martins, P. C., Nogueira, D., & Carbonera, N. (2021). Amazon-sustainable-flour from a a seeds added to starch films to develop. *Journal of Applied Polymer Science*, *139*, 51579. https://doi.org/10.1002/app.51579

Rongpipi, S., Ye, D., Gomez, E. D., & Gomez, E. W. (2019). Progress and opportunities in the characterization of cellulose – an important regulator of cell wall growth and mechanics. *Frontiers in Plant Science*, *9*. https://doi.org/10.3389/fpls.2018.01894

Roos, Y. H. (1993). Water activity and physical state effects on amorphous food stability. *Journal of Food Processing and Preservation*, *16*(6), 433–447. https://doi.org/10.1111/j.1745-4549.1993.tb00221.x

Roos, Y. H. (2006). *Phase Transitions and Transformations in Food Systems*. (D. R. Heldman & D. B. Lund, Eds.), *Handbook of food engineering* (2nd ed.). Boca Raton: CRC Press.

Rosa, D. P., Evangelista, R. R., Borges Machado, A. L., Sanches, M. A. R., & Telis-Romero, J. (2021). Water sorption properties of papaya seeds (Carica papaya L.) formosa variety: An assessment under storage and drying conditions. *Lwt*, *138*, 110458. https://doi.org/10.1016/j.lwt.2020.110458

Roudaut, Gaëlle, Farhat, I., Poirier-Brulez, F., & Champion, D. (2009). Influence of water, temperature and sucrose on dynamics in glassy starch-based products studied by low field 1H NMR. *Carbohydrate Polymers*, *77*(3), 489–495. https://doi.org/10.1016/j.carbpol.2009.01.029

Roudaut, Gaelle, Simatos, D., Champion, D., Contreras-Lopez, E., & Le Meste, M. (2004). Molecular mobility around the glass transition temperature: A mini review. *Innovative Food Science and Emerging Technologies*, *5*(2), 127–134. https://doi.org/10.1016/j.ifset.2003.12.003

Roudaut, Gaëlle, & Wallecan, J. (2015). New insights on the thermal analysis of low moisture composite foods. *Carbohydrate Polymers*, *115*, 10–15. https://doi.org/10.1016/j.carbpol.2014.08.066

Ruan, Q., Yang, X., Zeng, L., & Qi, J. (2019). Physical and tribological properties of high internal phase emulsions based on citrus fibers and corn peptides. *Food Hydrocolloids*,

95(April), 53–61. https://doi.org/10.1016/j.foodhyd.2019.04.014

Sablani, S. S., Kasapis, S., & Rahman, M. S. (2007). Evaluating water activity and glass transition concepts for food stability. *Journal of Food Engineering*, *78*(1), 266–271. https://doi.org/10.1016/j.jfoodeng.2005.09.025

Sakellariou, P., Rowe, R. C., & White, E. F. T. (1985). The thermomechanical properties and glass transition temperatures of some cellulose derivatives used in film coating. *International Journal of Pharmaceutics*, *27*(2), 267–277. https://doi.org/10.1016/0378-5173(85)90075-4

Salmen, N. L., & Back, E. L. (1977). The influence of water on the glass transition temperature of cellulose. *In Fibre-Water Interactions in Paper-Making, Trans. of the VIth Fund. Res. Symp. Oxford*, 683–690. https://doi.org/10.1063/1.3633242

Santivarangkna, C., Aschenbrenner, M., Kulozik, U., & Foerst, P. (2011). Role of Glassy State on Stabilities of Freeze-Dried Probiotics. *Journal of Food Science*, *76*(8). https://doi.org/10.1111/j.1750-3841.2011.02347.x

Saringat, H. B., Alfadol, K. I., & Khan, G. M. (2005). The influence of different plasticizers on some physical and mechanical properties of hydroxypropyl methylcellulose free films. *Pakistan Journal of Pharmaceutical Sciences*, *18*(3), 25–38.

Sayah, M. Y., Chabir, R., Benyahia, H., Kandri, Y. R., Chahdi, F. O., Touzani, H., & Errachidi, F. (2016). Yield, esterification degree and molecular weight evaluation of pectins isolated from orange and grapefruit peels under different conditions. *Plos One*, *11*(9), 1–16. https://doi.org/10.1371/journal.pone.0161751

Schäler, K. (2012). *Low-Field Nmr Studies of Structure and Dynamics in Semicrystalline Polymers*. Martin Luther University Halle-Wittenberg. Retrieved from http://d-nb.info/1033306622/34

Schalow, S., Baloufaud, M., Cottancin, T., Fischer, J., & Drusch, S. (2018). Orange pulp and peel fibres: pectin-rich by-products from citrus processing for water binding and gelling in foods. *European Food Research and Technology*, *244*, 235–244. https://doi.org/https://doi.org/10.1007/s00217-017-2950-y

Schebor, C., Mazzobre, M. F., & Buera, M. del P. (2010). Glass transition and time-dependent crystallization behavior of dehydration bioprotectant sugars. *Carbohydrate Research*, *345*(2), 303–308. https://doi.org/10.1016/j.carres.2009.10.014

Schick, C. (2009). Differential scanning calorimetry (DSC) of semicrystalline polymers. *Analytical and Bioanalytical Chemistry*, *395*, 1589–1611. https://doi.org/10.1007/s00216-009-3169-y

Scott, M. P., Brazel, C. S., Benton, M. G., Mays, J. W., Holbrey, J. D., & Rogers, R. D. (2002). Application of ionic liquids as plasticizers for poly(methyl methacrylate). *Chemical Communications*, *2*(13), 1370–1371. https://doi.org/10.1039/b204316p

Sendra, E., Kuri, V., Fernández-López, J., Sayas-Barberá, E., Navarro, C., & Pérez-Alvarez, J. A. (2010). Viscoelastic properties of orange fiber enriched yogurt as a function of fiber dose, size and thermal treatment. *LWT - Food Science and Technology*, *43*(4), 708–714. https://doi.org/10.1016/j.lwt.2009.12.005

Sergeev, A., Mettu, S., & Zaborova, V. (2021). The influence of extruded flour on water content and retrogradation process in muffins during storage: NMR relaxation study.

Journal of Food Science and Technology, *58*(5), 2028–2033. https://doi.org/10.1007/s13197-020-04921-5

Sgriccia, N., Hawley, M. C., & Misra, M. (2008). Composites : Part A Characterization of natural fiber surfaces and natural fiber composites. *Composites Part A: Applied Science and Manufacturing*, *39*, 1632–1637. https://doi.org/10.1016/j.compositesa.2008.07.007

Simon, M., Fulchiron, R., & Gouanvé, F. (2022). Water Sorption and Mechanical Properties of Cellulosic Derivative Fibers. *Polymers*, *14*, 2836. https://doi.org/10.3390/polym14142836

Singh, N., & Li, W. (2019). Recent advances in coarse-grained models for biomolecules and their applications. *International Journal of Molecular Sciences*, *20*(15). https://doi.org/10.3390/ijms20153774

Sirviö, J. A., Visanko, M., Ukkola, J., & Liimatainen, H. (2018). Effect of plasticizers on the mechanical and thermomechanical properties of cellulose-based biocomposite films. *Industrial Crops and Products*, *122*, 513–521. https://doi.org/10.1016/j.indcrop.2018.06.039

Solhi, L., Guccini, V., Heise, K., Solala, I., Niinivaara, E., Xu, W., … Kontturi, E. (2023). Understanding Nanocellulose-Water Interactions: Turning a Detriment into an Asset. *Chemical Reviews*, *123*(5), 1925–2015. https://doi.org/10.1021/acs.chemrev.2c00611

Song, J., Pan, T., Wu, J., & Ren, F. (2016). The improvement effect and mechanism of citrus fiber on the water-binding ability of low-fat frankfurters. *Journal of Food Science and Technology*, *53*(12), 4197–4204. https://doi.org/10.1007/s13197-016-2407-5

Song, Y., Jiang, W., Ben, H., Zhang, Y., Han, G., & Ragauskas, A. J. (2021). The preparation and characterization of chemically deuterium incorporated cotton fibers. *Cellulose*, *28*(9), 5351–5361. https://doi.org/10.1007/s10570-021-03869-9

Staniszewska, I., Dzadz, L., Nowak, K. W., & Zielinska, M. (2021). Evaluation of storage stability of dried powdered coriander, parsley and celery leaves based on the moisture sorption isotherms and glass transition temperature. *LWT - Food Science and Technology*, *146*, 111440. https://doi.org/10.1016/j.lwt.2021.111440

Struik, L. C. E. (1977). *Physical aging in amorphous polymers and other materials*. Delft University of Technology. https://doi.org/10.1016/0040-6031(82)85085-5

Su, D., Zhu, X., Wang, Y., Li, D., & Wang, L. (2019). Effects of high-pressure homogenization on physical and thermal properties of citrus fiber. *LWT - Food Science and Technology*, *116*, 108573. https://doi.org/10.1016/j.lwt.2019.108573

Su, D., Zhu, X., Wang, Y., Li, D., & Wang, L. (2020). Effect of high-pressure homogenization on rheological properties of citrus fiber. *LWT - Food Science and Technology*, *127*, 109366. https://doi.org/10.1016/j.lwt.2020.109366

Suekuni, M. T., D'Souza, N., & Allgeier, A. M. (2022). NMR Relaxometry Studies on the Drying Kinetics of Cellulose Nanofibers. *Industrial and Engineering Chemistry Research*, *61*(16), 5475–5483. https://doi.org/10.1021/acs.iecr.1c04878

Suri, S., Singh, A., & Nema, P. K. (2022). Current applications of citrus fruit processing waste: A scientific outlook. *Applied Food Research*, *2*(1), 100050. https://doi.org/10.1016/j.afres.2022.100050

Šutý, Š., Petriláková, K., Katuščák, S., Kirschnerová, S., Jablonský, M., Vizarová, K., & Vrška, M. (2012). Change in the capability of cellulose fibres to retain water during thermally accelerated ageing of paper. *Cellulose Chemistry and Technology*, *46*(9–10), 631–635.

Syamaladevi, R. M., Sablani, S. S., & Swanson, B. G. (2010). Aging of amorphous raspberry powder: Enthalpy relaxation and fragility. *Journal of Food Engineering*, *101*(1), 32–40. https://doi.org/10.1016/j.jfoodeng.2010.06.006

Szcześniak, L., Rachocki, A., & Tritt-Goc, J. (2008). Glass transition temperature and thermal decomposition of cellulose powder. *Cellulose*, *15*(3), 445–451. https://doi.org/10.1007/s10570-007-9192-2

Szymańska-Chargot, M., Chylińska, M., Cybulska, J., Kozioł, A., Pieczywek, P. M., & Zdunek, A. (2017). Simultaneous influence of pectin and xyloglucan on structure and mechanical properties of bacterial cellulose composites. *Carbohydrate Polymers*, *174*, 970–979. https://doi.org/10.1016/j.carbpol.2017.07.004

Szymanska-Chargot, M., Chylinska, M., Kruk, B., & Zdunek, A. (2015). Combining FT-IR spectroscopy and multivariate analysis for qualitative and quantitative analysis of the cell wall composition changes during apples development. *Carbohydrate Polymers*, *115*, 93–103. https://doi.org/10.1016/j.carbpol.2014.08.039

Szymanska-Chargot, Monika, & Zdunek, A. (2013). Use of FT-IR Spectra and PCA to the Bulk Characterization of Cell Wall Residues of Fruits and Vegetables Along a Fraction Process. *Food Biophysics*, *8*(1), 29–42. https://doi.org/10.1007/s11483-012-9279-7

Tananuwong, K., & Reid, D. S. (2004). DSC and NMR relaxation studies of starch-water interactions during gelatinization. *Carbohydrate Polymers*, *58*(3), 345–358. https://doi.org/10.1016/j.carbpol.2004.08.003

Tanasă, F., Zănoagă, M., Teacă, C. A., Nechifor, M., & Shahzad, A. (2020). Modified hemp fibers intended for fiber-reinforced polymer composites used in structural applications—A review. I. Methods of modification. *Polymer Composites*, *41*(1), 5–31. https://doi.org/10.1002/pc.25354

Tang, Q., & Huang, G. (2022). Improving method, properties and application of polysaccharide as emulsifier. *Food Chemistry*, *376*, 131937. https://doi.org/10.1016/j.foodchem.2021.131937

Tejada-Ortigoza, V., Garcia-Amezquita, L. E., Serment-Moreno, V., Torres, J. A., & Welti-Chanes, J. (2017). Moisture sorption isotherms of high pressure treated fruit peels used as dietary fiber sources. *Innovative Food Science and Emerging Technologies*, *43*, 45–53. https://doi.org/10.1016/j.ifset.2017.07.023

Termonia, Y. (1995). Chain Conformations at Semicrystalline Interphases. *Macromolecules*, *28*(23), 7667–7670. https://doi.org/10.1021/ma00127a012

Thapa, P., Lee, A. R., Choi, D. H., & Jeong, S. H. (2017). Effects of moisture content and compression pressure of various deforming granules on the physical properties of tablets. *Powder Technology*, *310*, 92–102. https://doi.org/10.1016/j.powtec.2017.01.021

Thomas, M. E. C., Scher, J., Desobry-Banon, S., & Desobry, S. (2004). Milk powders ageing: Effect on physical and functional properties. *Critical Reviews in Food Science and Nutrition*, *44*(5), 297–322. https://doi.org/10.1080/10408690490464041

Thygesen, A., Oddershede, J., Lilholt, H., Thomsen, A. B., & Ståhl, K. (2005). On the determination of crystallinity and cellulose content in plant fibres. *Cellulose*, *12*(6), 563–576. https://doi.org/10.1007/s10570-005-9001-8

Tolstoguzov, V. (2002). Thermodynamic aspects of biopolymer functionality in biological systems, foods, and beverages. *Critical Reviews in Biotechnology*, *22*(2), 89–174. https://doi.org/10.1080/07388550290789478

Topgaard, D., & Söderman, O. (2002). Changes of cellulose fiber wall structure during drying investigated using NMR self-diffusion and relaxation experiments. *Cellulose*, *9*(2), 139–147. https://doi.org/10.1023/A:1020158524621

Torres, F. G., Mayorga, J. P., Vilca, C., Arroyo, J., Castro, P., & Rodriguez, L. (2019). Preparation and characterization of a novel starch–chestnut husk biocomposite. *SN Applied Sciences*, *1*(10), 1–7. https://doi.org/10.1007/s42452-019-1204-y

Truong, V., Bhandari, B. R., Howes, T., & Adhikari, B. (2004). Glass transition behaviour of fructose. *International Journal of Food Science and Technology*, *39*(5), 569–578. https://doi.org/10.1111/j.1365-2621.2004.00817.x

Truss, R. W., Wood, B., & Rasch, R. (2016). Quantitative surface analysis of hemp fibers using XPS, conventional and low voltage in-lens SEM. *Journal of Applied Polymer Science*, *133*(8), 1–9. https://doi.org/10.1002/app.43023

USDA. (2024). Citrus: World Markets and Trade. *United States*.

Van Audenhove, J., Putri, N. I., Caveye, I., Van Loey, A. M., & Hendrickx, M. E. (2024). The impact of drying and storage in the semi-dry state on the texturizing potential of partially pectin-depleted tomato cell wall material functionalised by high-pressure homogenisation. *Food Hydrocolloids*, *150*, 109653. https://doi.org/10.1016/j.foodhyd.2023.109653

Van Buggenhout, S., Wallecan, J., Christiaens, S., Debon, S. J. J., Desmet, C., Van Loey, A., … Mazoyer, J. (2015). Influence of high-pressure homogenization on functional properties of orange pulp. *Innovative Food Science and Emerging Technologies*, *30*, 51–60. https://doi.org/10.1016/j.ifset.2015.05.004

Van Den Dries, I. J., Van Dusschoten, D., & Hemminga, M. A. (1998). Mobility in maltose-water glasses studied with 1H NMR. *Journal of Physical Chemistry B*, *102*(51), 10483–10489. https://doi.org/10.1021/jp982718v

Vásquez, C., Díaz-Calderón, P., Enrione, J., & Matiacevich, S. (2013). State diagram, sorption isotherm and color of blueberries as a function of water content. *Thermochimica Acta*, *570*, 8–15. https://doi.org/10.1016/j.tca.2013.07.029

Vieira, M. G. A., Da Silva, M. A., Dos Santos, L. O., & Beppu, M. M. (2011). Natural-based plasticizers and biopolymer films: A review. *European Polymer Journal*, *47*(3), 254–263. https://doi.org/10.1016/j.eurpolymj.2010.12.011

Vinod, A., Sanjay, M. R., Suchart, S., & Jyotishkumar, P. (2020). Renewable and sustainable biobased materials: An assessment on biofibers, biofilms, biopolymers and biocomposites. *Journal of Cleaner Production*, *258*, 120978. https://doi.org/10.1016/j.jclepro.2020.120978

Vittadini, E., Dickinson, L. C., & Chinachoti, P. (2001). 1H and 2H NMR mobility in cellulose. *Carbohydrate Polymers*, *46*(1), 49–57. https://doi.org/10.1016/S0144-

8617(00)00282-4

Vollenbroek, J., Hebbink, G. A., Ziffels, S., & Steckel, H. (2010). Determination of low levels of amorphous content in inhalation grade lactose by moisture sorption isotherms. *International Journal of Pharmaceutics*, *395*(1–2), 62–70. https://doi.org/10.1016/j.ijpharm.2010.04.035

Walczak, M. (2012). *Role and properties of the confined amorphous phase of polymers.* Ecole nationale supérieure d'arts et métiers (ENSAM). Retrieved from https://pastel.archives-ouvertes.fr/pastel-00839174

Wallecan, J., McCrae, C., Debon, S. J. J., Dong, J., & Mazoyer, J. (2015). Emulsifying and stabilizing properties of functionalized orange pulp fibers. *Food Hydrocolloids*, *47*, 115–123. https://doi.org/10.1016/j.foodhyd.2015.01.009

Walter, W. M., & Palma, C. S. (1996). Effect of Long-Term Storage on Cell Wall Neutral Sugars and Galacturonic Acid of Two Sweetpotato Cultivars. *Journal of Agricultural and Food Chemistry*, *44*(1), 278–281. https://doi.org/10.1021/jf950101u

Wang, C., Qiu, W. Y., Chen, T. T., & Yan, J. K. (2021). Effects of structural and conformational characteristics of citrus pectin on its functional properties. *Food Chemistry*, *339*(May 2020), 128064. https://doi.org/10.1016/j.foodchem.2020.128064

Wang, S., Luo, S., Wang, H., Zhang, S., Wang, X., Yang, X., & Guo, Y. (2024). Strong gelation capacity of a pectin-like polysaccharide in the presence of K+ ion. *International Journal of Biological Macromolecules*, *256*, 128395. https://doi.org/10.1016/j.ijbiomac.2023.128395

Watanabe, H., Tang, C. Q., Suzuki, T., & Mihori, T. (1996). Fracture stress of fish meat and the glass transition. *Journal of Food Engineering*, *29*(3–4), 317–327. https://doi.org/10.1016/0260-8774(95)00077-1

Wiesman, Z., Linder, C., Resende, M. T., Ayalon, N., Levi, O., Bernardinelli, O. D., … Jackman, R. (2018). 2D and 3D Spectrum Graphics of the Chemical-Morphological Domains of Complex Biomass by Low Field Proton NMR Energy Relaxation Signal Analysis. *Energy and Fuels*, *32*(4), 5090–5102. https://doi.org/10.1021/acs.energyfuels.7b03339

Willems, W. (2014). The water vapor sorption mechanism and its hysteresis in wood: The water/void mixture postulate. *Wood Science and Technology*, *48*(3), 499–518. https://doi.org/10.1007/s00226-014-0617-4

Willemsen, K. L. D. D., Panozzo, A., Moelants, K., Debon, S. J. J., Desmet, C., Cardinaels, R., … Hendrickx, M. E. G. (2017). Physico-chemical and viscoelastic properties of high pressure homogenized lemon peel fiber fraction suspensions obtained after sequential pectin extraction. *Food Hydrocolloids*, *72*, 358–371. https://doi.org/10.1016/j.foodhyd.2017.06.020

Willemsen, K. L. D. D., Panozzo, A., Moelants, K., Wallecan, J., & Hendrickx, M. (2020). Towards improved understanding of the viscoelastic properties of functionalized lemon peel fibers in suspension based on microstructure, hydration value and swelling volume. *Journal of Food Engineering*, *278*, 109950. https://doi.org/10.1016/j.jfoodeng.2020.109950

Wu, J., Bai, J., Xue, Z., Liao, Y., Zhou, X., & Xie, X. (2015). Insight into glass transition of

cellulose based on direct thermal processing after plasticization by ionic liquid. *Cellulose*, *22*(1), 89–99. https://doi.org/10.1007/s10570-014-0502-1

Xiao, C., Zhang, Z., Zhang, J., Lu, Y., & Zhang, L. (2003). Properties of regenerated cellulose films plasticized with α-monoglycerides. *Journal of Applied Polymer Science*, *89*(13), 3500–3505. https://doi.org/10.1002/app.12509

Xie, Yanjum, Hill, C., Jalaludin, Z., & Sun, D. (2011a). The water vapour sorption behaviour of three celluloses: Analysis using parallel exponential kinetics and interpretation using the Kelvin-Voigt viscoelastic model. *Cellulose*, *18*(3), 517–530. https://doi.org/10.1007/s10570-011-9512-4

Xie, Yanjun, Callum, H., Jalaludin, Z., Curling, S., Anandjiwala, R., Norton, A., & Newman, G. (2011b). The dynamic water vapour sorption behaviour of natural fibres and kinetic analysis using the parallel exponential kinetics model. *Journal of Materials Science*, *46*(2), 479–489. https://doi.org/10.1007/s10853-010-4935-0

Xu, C., Li, Y., & Yu, H. (2014). Effect of far-infrared drying on the water state and glass transition temperature in carrots. *Journal of Food Engineering*, *136*, 42–47. https://doi.org/10.1016/j.jfoodeng.2014.03.022

Xu, F., Jin, X., Zhang, L., & Chen, X. D. (2017a). Investigation on water status and distribution in broccoli and the effects of drying on water status using NMR and MRI methods. *Food Research International*, *96*, 191–197. https://doi.org/10.1016/j.foodres.2017.03.041

Xu, K., Lu, J., Gao, Y., Wu, Y., & Li, X. (2017b). Determination of moisture content and moisture content profiles in wood during drying by low-field nuclear magnetic resonance. *Drying Technology*, *35*(15), 1909–1918. https://doi.org/10.1080/07373937.2017.1291519

Yang, X., Li, A., Li, X., Sun, L., & Guo, Y. (2020). An overview of classifications, properties of food polysaccharides and their links to applications in improving food textures. *Trends in Food Science and Technology*, *102*, 1–15. https://doi.org/10.1016/j.tifs.2020.05.020

Yapo, B. M. (2009). Pectin quantity, composition and physicochemical behaviour as influenced by the purification process. *Food Research International*, *42*(8), 1197–1202. https://doi.org/10.1016/j.foodres.2009.06.002

Ye, F., Tao, B., Liu, J., Zou, Y., & Zhao, G. (2016). Effect of micronization on the physicochemical properties of insoluble dietary fiber from citrus (Citrus junos Sieb. ex Tanaka) pomace. *Food Science and Technology International*, *22*(3), 246–255. https://doi.org/10.1177/1082013215593394

Yi, Y., Xu, W., Wang, H. X., Huang, F., & Wang, L. M. (2020). Natural polysaccharides experience physiochemical and functional changes during preparation: A review. *Carbohydrate Polymers*, *234*(68), 115896. https://doi.org/10.1016/j.carbpol.2020.115896

Yu, L. (2001). Amorphous pharmaceutical solids: Preparation, characterization and stabilization. *Advanced Drug Delivery Reviews*, *48*(1), 27–42. https://doi.org/10.1016/S0169-409X(01)00098-9

Yu, Y., Wang, Y., Liu, X., Liu, Y., Ji, L., Zhou, Y., & Sun, L. (2021). Comparison of analytical methods for determining methylesterification and acetylation of pectin.

Applied Sciences, *11*(10), 4461. https://doi.org/https://doi.org/10.3390/app11104461

Zafeiropoulos, N. E., Vickers, P. E., Baillie, C. A., & Watts, J. F. (2003). An experimental investigation of modified and unmodified flax fibres with XPS, ToF-SIMS and ATR-FTIR. *Journal of Materials Science*, *38*(19), 3903–3914. https://doi.org/10.1023/A:1026133826672

Zain, N. F. M. (2014). Preparation and Characterization of Cellulose and Nanocellulose From Pomelo (Citrus grandis) Albedo. *Journal of Nutrition & Food Sciences*, *5*(1), 1000334. https://doi.org/10.4172/2155-9600.1000334

Zhang, S., He, Z., Cheng, Y., Xu, F., Cheng, X., & Wu, P. (2021). Physicochemical characterization and emulsifying properties evaluation of RG-I enriched pectic polysaccharides from Cerasus humilis. *Carbohydrate Polymers*, *260*, 117824. https://doi.org/10.1016/j.carbpol.2021.117824

Zhang, X., Tschopp, M. A., Shi, S. Q., & Cao, J. (2012). Molecular dynamics simulations of the glass transition temperature of amorphous cellulose. *Applied Mechanics and Materials*, *214*, 7–11. https://doi.org/10.4028/www.scientific.net/AMM.214.7

Zhang, Y., Liao, J., & Qi, J. (2020a). Functional and structural properties of dietary fiber from citrus peel affected by the alkali combined with high-speed homogenization treatment. *LWT - Food Science and Technology*, *128*, 109397. https://doi.org/10.1016/j.lwt.2020.109397

Zhang, Y., Qi, J., Zeng, W., Huang, Y., & Yang, X. (2020b). Properties of dietary fiber from citrus obtained through alkaline hydrogen peroxide treatment and homogenization treatment. *Food Chemistry*, *311*, 125873. https://doi.org/10.1016/j.foodchem.2019.125873

Zhao, H., Chen, Z., Du, X., & Chen, L. (2019). Contribution of different state of adsorbed water to the sub-T g dynamics of cellulose. *Carbohydrate Polymers*, *210*, 322–331. https://doi.org/10.1016/j.carbpol.2019.01.087

Zhao, S., Ren, W., Gao, W., Tian, G., Zhao, C., Bao, Y., … Zheng, J. (2020). Effect of mesoscopic structure of citrus pectin on its emulsifying properties: Compactness is more important than size. *Journal of Colloid and Interface Science*, *570*, 80–88. https://doi.org/10.1016/j.jcis.2020.02.113

Zhao, Z., Crespi, V. H., Kubicki, J. D., Cosgrove, D. J., & Zhong, L. (2014). Molecular dynamics simulation study of xyloglucan adsorption on cellulose surfaces: Effects of surface hydrophobicity and side-chain variation. *Cellulose*, *21*(2), 1025–1039. https://doi.org/10.1007/s10570-013-0041-1

Zhu, C., Wang, S., Bai, Y., Zhang, S., Zhang, X., Wu, Q., & He, X. (2023). Effect of Citrus Fiber on the Gel Properties of Mutton Myofibrillar Protein. *Foods*, *12*(4), 1–10. https://doi.org/10.7506/spkx1002-6630-20211220-230

Zhu, J., Wang, H., Guo, F., Salmén, L., & Yu, Y. (2021). Cell wall polymer distribution in bamboo visualized with in situ imaging FTIR. *Carbohydrate Polymers*, *274*(15), 118653. https://doi.org/10.1016/j.carbpol.2021.118653

Zykwinska, A. W., Ralet, M. C. J., Garnier, C. D., & Thibault, J. F. J. (2005). Evidence for in vitro binding of pectin side chains to cellulose. *Plant Physiology*, *139*(1), 397–407. https://doi.org/10.1104/pp.105.065912

Annexes

Annex A

Published review article: Multiscale dynamics and molecular mobility in cellulose-rich materials

Carbohydrate Polymers 344 (2024) 122490

Contents lists available at ScienceDirect

Carbohydrate Polymers

journal homepage: www.elsevier.com/locate/carbpol

Review

Multiscale dynamics and molecular mobility in cellulose-rich materials

G.O. Coelho [a], I. Deleris [b], D. Champion [a], J. Wallecan [b], S. Debon [b], G. Roudaut [a,*]

[a] Université Bourgogne Franche-Comté, Institut Agro, Université Bourgogne, INRAE, PAM UMR A 02.102, F-21000 Dijon, France
[b] Cargill R&D Centre Europe, Havenstraat 84, 1800 Vilvoorde, Belgium

ARTICLE INFO

Keywords:
Cellulose
Molecular mobility
Dynamics
Glass transition
Multi-scale
Heterogeneity

ABSTRACT

Cellulose, an abundant biopolymer in nature as a structural component of plant cell walls, has a native semi-crystalline structure in which the arrangement of amorphous-crystalline domains governs its key properties such as mechanical and physico-chemical properties. The performance of the material in different situations is shaped by molecular mobility, which affects attributes such as mechanical properties, chemical reactivity, and water absorption. Nevertheless, it is difficult to investigate experimentally the structural and dynamic properties of cellulose-rich materials. This is especially the case for the glass transition, which impacts its quality and properties. This experimental challenge is notably evidenced by the considerable variability in data across the literature. The purpose of this study is to offer a comprehensive multi-scale exploration of dynamics within cellulose-rich materials, emphasizing literature data on cellulose glass transition and molecular relaxations, and providing insights into methods for characterizing their physical state and underscoring the impact of water-cellulose interactions on molecular mobility in these systems. The promising results obtained using multiple approaches bring out the importance of combining methods to achieve a more accurate and detailed understanding of the complex thermal transition in cellulose materials, particularly when considering the influence of water on their thermal dynamics and properties.

1. Introduction

Cellulose is a fascinating biopolymer considered as the most abundant natural biopolymer. Because of its extensive availability, and its broad range of properties, it is highly used in many segments of industry such as textiles, paper, construction materials, pharmaceutical, cosmetics, and chemical derivatives (Rongpipi et al., 2019). Besides, cellulose is also an abundant organic compound in agro-industrial food wastes, and many studies are conducted to valorise it in biotechnological applications such as ingredients, food packaging, tissue engineering and bioplastic (Gautam et al., 2022). Due to its wide application range, a better understanding of its characteristic structure-function relationships is key to guaranteeing its functionality and expanding its use.

The challenge is that in plant cell wall materials, cellulose is not present alone but is associated with other components such as hemicellulose, pectin, lignin, and structural proteins depending on the type of plant cell wall and plant species (Meychik et al., 2021). These arrangements provide the plant its mechanical strength but also its flexibility and extensibility required for growth (notably related to interactions with water) (Cosgrove, 1997).

At the heart of understanding the stability of these cellulose-rich materials lies the concept of molecular mobility, particularly correlated to cellulose-water interaction. Molecular mobility influences characteristics like water absorption, mechanical properties, and chemical reactivity, thereby shaping the material's performance in various contexts (Rolandelli et al., 2022; Roudaut et al., 2004; Vittadini et al., 2001).

The cellulose-water interaction and the cellulose molecular mobility has been extensively studied for over a century encompassing both primary and secondary plant cell wall (Chen et al., 2022; Cresswell et al., 2021; Etale et al., 2023; Hatakeyama & Hatakeyama, 2000; Hediger et al., 2002; Ibbett et al., 2014; Jarvis, 2023; Lindh et al., 2017; Nakamura et al., 1981; White et al., 2014; Wohlert et al., 2022). Given the complex structure of cellulose, cellulose-water systems have been studied by different methods. Recent advancements in molecular modelling and nuclear magnetic resonance (NMR) have significantly enhanced the comprehension of morphology of microfibrils, the distribution of crystalline domains within them, and the intrinsic structural role of water within cellulose fibril aggregates. Despite extensive research, the picture remains incomplete especially regarding the roles

* Corresponding author.
E-mail address: gaelle.roudaut@institut-agro.fr (G. Roudaut).

https://doi.org/10.1016/j.carbpol.2024.122490
Received 18 March 2024; Received in revised form 9 July 2024; Accepted 11 July 2024
Available online 14 July 2024

of other components in cellulose-rich materials (complex assemblies) and the impact of crystalline and amorphous fraction in water interaction (Grunin et al., 2020; Solhi et al., 2023).

Hence, the structure and dynamic properties of plant-based materials is challenging to explore through experimentation particularly if the focus is made on cellulose molecules within complex matrices. Indeed, the glass transition temperature of cellulose, which is an important characteristic related to the amorphous fraction of cellulose, has never been precisely measured (Mazeau & Heux, 2003). The fact that amorphous cellulose is associated with crystalline domains and that moisture content and distribution are heterogeneous, makes its characterization difficult (Al-Khalili et al., 2023; Mazeau, 2015).

Although there are >600 reviews involving cellulose over the last two decades, exploring cellulose applications, cellulose nanomaterials, bacterial cellulose, cellulose derivatives, and treatment and processing applied to it, none of them specifically gathers what is known about molecular mobility of cellulose-rich primary cell wall materials.

In this context, this review aims to provide a multi-scale overview of molecule dynamics in cellulose-rich materials, mainly focusing on literature data on cellulose molecules, their glass transition, and molecular relaxations. Information about methods to characterize its physical state and highlighting the role water-cellulose interactions on molecular mobility in these systems will be given.

2. Morphology of cellulose-rich materials

Cellulose exists in nature as microfibrils or elementary fibrils which have a length and widths in the order of micrometers and nanometers, respectively (Chen et al., 2022). Primary cell wall microfibrils are about 3 nm diameter as estimated for celery collenchyma (Thomas et al., 2013). Hydrogen bonds are responsible for creating fibril structures, and in addition to that, crystalline order is established by a combination of interactions (Van der Waals, ionic interactions, and hydrogen bonds) (Wohlert et al., 2022).

The cellulose chains within microfibrils can arrange themselves into various geometries, predominantly "rectangular" or "diamond" cross-sections, influenced by the number and spatial organization of the cellulose chains (Fig. 1). Although a 36-chain model is frequently discussed in the literature as a model of cellulose chain organization into microfibrils, there is growing evidence that microfibril may contain 18–24 chains with an inter-chain distance of around 0.3 nm. In the "rectangular" shape arrangement, cellulose chains are arranged in eight hydrogen-bonded sheets of three chains and the (200) and (010) crystal faces are exposed (Fig. 1a). In the a "diamond" shape arrangement, the (110) and (1−10) crystal faces are exposed (Fig. 1c). Rectangular configurations often result in planar alignments, whereas diamond arrangements provide a more compact and energetically favorable structure due to uniform chain spacing (Cosgrove, 2014; Fernandes et al., 2011; Thomas et al., 2013). Due to the extensive disorder observed in the primary cell wall, it is not certain that it has a cross section of constant shape (Thomas et al., 2013).

This organization of cellulose results in a semi-crystalline structure with varying degrees of crystallinity from 25 % to 80 % (Dassanayake et al., 2019; Ioelovich, 2021) depending on its botanical origin (Table 1). A semi crystalline structure is defined as comprising both a highly ordered fraction and a disordered amorphous domain with mobility between them and isotropic chain orientation (Molnár et al., 2021; Schäler, 2012; Termonia, 1995). The interphase is considered partially ordered and with restricted mobility compared to amorphous phase, it corresponds to crystal-amorphous transition layer named amorphous rigid fraction or paracrystalline domain (Walczak, 2012).

Crystalline cellulose exists in four distinct polymorphs, with natural cellulose occurring as cellulose Iα (triclinic) and Iβ (monoclinic), differing in hydrogen bonding patterns (Goldberg et al., 2015; Mazeau & Heux, 2003). Cellulose II and III are derived through treatments like regeneration or mercerization and liquid ammonia or organic amine treatment, respectively (Ciolacu et al., 2012; Goldberg et al., 2015; Jiang et al., 2011).

The organization of crystalline, paracrystalline, and amorphous fractions in cellulose microfibrils has been extensively studied, resulting in two primary models (Cosgrove, 2014; Fernandes et al., 2011; Thomas et al., 2013). One model, supported by NMR data, suggests that the core of each microfibril is predominantly crystalline, surrounded by a paracrystalline or amorphous shell. The second model, based on X-ray

Table 1
Crystallinity index of different plant fibers.

	Crystallinity Index (%)	Cellulose content (%)	Method	Reference
Corn stover	47	33	X-ray diffraction (Segal method)	Thygesen et al. (2005)
Norway spruce	47	49		
Hemp fibers	77	63		
Citrus Pomelo fiber	25	21	X-ray diffraction (Segal method)	Zain (2014)
Jute fiber	34	45–71	X-ray diffraction (Segal method)	Poletto et al. (2014)
Kenaf	35	31–72		
Ramie	35	69–91		
Sisal	57	65–67		
Citrus Fiber	33	40	X-ray diffraction (Segal method)	Zhang et al. (2020)
Pineapple crown fiber	62	17	X-ray diffraction (Segal method)	Pereira et al. (2021)
Pure cotton cellulose	70	100	X-ray diffraction (ratio of intensities of crystalline regions and the whole sample)	Ioelovich (2021)
Flax fiber	67	64–85	X-ray diffraction (peak deconvolution)	Simon et al. (2022)

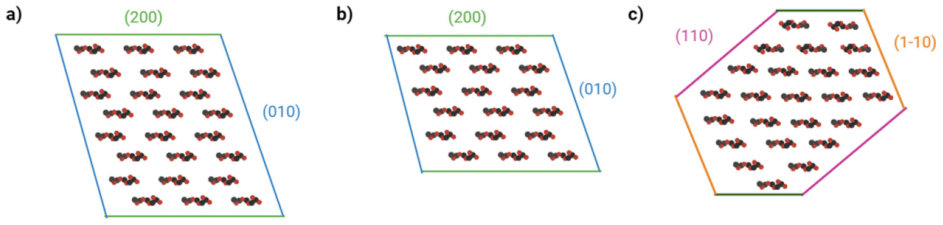

Fig. 1. Models for the cross section of cellulose fibrils (a) 24- chain rectangular model, (b) 18-chain rectangular model, (c) 24-chain diamond-shaped model. After Thomas et al. (2013).

diffraction data, proposes that the amorphous and paracrystalline domains on the microfibril surfaces are packed laterally similarly to the crystalline core, albeit with differences in conformation and hydrogen bonding. In this latter model, the disorder is spread throughout the structure and is not restricted to the surface.

These fractions have dramatically different characteristics (Mazeau & Heux, 2003), affecting water interaction, gas/ion permeation, biodegradation, molecular mobility and dynamics. Crystalline regions exhibit lower water sorption due to fewer accessible hydroxyl groups, while amorphous regions have higher sorption capacity (Hatakeyama & Hatakeyama, 2000; Simon et al., 2022; Voelker et al., 2020). The crystalline fraction organised in a tortuous pathway results in a controlled gas, ion and electron conduction while the amorphous phase allows the gas and ion permeation (Li, 2020; Wang et al., 2009). The crystallinity also impacts the biodegradability of the biopolymer: high crystallinity slows the enzymatic degradation of cellulose due to its compact structure (Ciolacu et al., 2008; Yazdi et al., 2021). Although amorphous cellulose may have a short-range molecular order similar to crystalline fractions (few angstroms) *i.e.* a single molecule has similar number of neighbour molecules with the same distance between them, they lack long-range order and have greater chain mobility and lower density (Liu et al., 2006; Mazeau & Heux, 2003).

The morphological properties and phase arrangements of cellulose microfibrils significantly impact the experimental methods and simulations used to study them. However, their physical forms may also be influenced by interaction among cell wall components such as xyloglucan and pectin in primary cell walls (Ding et al., 2012; Park & Cosgrove, 2015). Precise modelling of microfibrils requires a thorough understanding of their geometric configurations and the spatial distribution of different phases. In addition, this knowledge is crucial for predicting the behavior of cellulose under various environmental conditions and for optimizing its applications in material science, biophysics, and other related fields.

3. Molecular mobility in biopolymers

To progress in the understanding of the behavior of biosystems during processing and shelf life, investigation of transitions at the molecular and supramolecular scales is of importance (Al-Khalili et al., 2023; Paes et al., 2010; Rolandelli et al., 2022). This investigation scans different kinds of motion such as rotation of atoms groups and/or polymeric segments linked by covalent bonds, molecular displacement/deformation due to solvent migration, molecular diffusion (Brownian movements), and migration of solvent or solute molecules resulting from chemical potential gradient or electric field (Roudaut et al., 2004).

The properties of polymers may change gradually with temperature until achieving the critical temperature(s) at which an abrupt alteration of various characteristics is observed due to an associated molecular mobility increase. This phase transition is commonly known as glass transition or α-relaxation when related to mobility inducing the flow and/or a rubbery behavior. This transition is associated with the large-scale mobility of polymer chains.

In addition to the glass transition, polymers exhibit secondary relaxations, known as β and γ relaxations, occur at temperatures below the glass transition temperature and are associated with localized mobility within the polymer structure. β-relaxation involves the motion of segments of the polymer backbone, providing insight into the flexibility and interaction of these segments. On the other hand, γ-relaxation involves even more localized motions of atomic groups or side chains, reflecting the mesoscopic-level dynamics of the polymer (Ioelovich, 2016).

The phase transition can be measured by different ways such as calorimetric (differential scanning calorimetry (DSC)), mechanical (dynamic mechanical analysis (DMA)) or dielectric (dielectric relaxation spectroscopy (DRS)) spectroscopies, and even methods including measurements of volume expansion coefficient (Blanshard, 1995; Perdomo et al., 2009). These methods provide insight into dynamics at macro and mesoscopic scale.

3.1. Macroscale: glass transition temperature of cellulose rich material

The determination of the glass transition temperature (Tg) of cellulose-based systems with DSC is challenging for multiple reasons:

- the semi-crystalline nature of these materials makes it difficult to characterize the transitions due to the weak and short fraction of amorphous phase (Roig et al., 2011).
- the Tg of cellulose (Table 2) is close to its degradation temperature (above 200 °C) (Al-Khalili et al., 2023; Paes et al., 2010).
- this kind of material may have a complex glass transition, due to multi-domain phases, with a small change in heat capacity compared to the conventional polymers, especially in the dry state (Al-Khalili et al., 2023; Liu et al., 2009; Paes et al., 2010).

Moreover, for several plant cell wall extracts, cellulose is not pure cellulose and even if it is the main component, some residues of pectin, hemicellulose and non-polysaccharide compounds may impact the glass transition determination.

Consequently, the DSC analysis shows a wide range of data attributed to Tg of cellulose (Table 2).

Denham (2016) determined the Tg of cellulose-rich materials with varying degrees of crystallinity, including cotton fiber, viscose fiber, and microcrystalline cellulose (MCC). Cotton fiber possesses the highest crystalline index (CI) and exhibited the highest Tg among the materials studied. In addition, although viscose fiber (CI 65 %) has a crystallinity index similar to cellulose-rich material derived from defatted date pits (CI 63 %) studied by Al-Khalili et al. (2023), the latter demonstrated a lower Tg. This discrepancy can be attributed to the complex composition of the cellulose-rich material from defatted date pits, which also contains soluble fibers, hemicellulose and lignin. Some of these additional components (soluble fibers and hemicellulose) likely contribute to increase the molecular mobility within the sample, resulting in a reduced Tg. As previously mentioned, both the crystallinity and the complex composition of the sample play significant roles in determining the Tg value.

Goring (1963) determined a phase transition between 231 and 253 °C (Table 2) by an unusual method consisting in measuring the softening temperature related to the height change of a cellulose powder column. In this study, the cellulose powder was transferred to a glass capillary compressed under constant load and heated at constant rate. The change of height was associated with the collapse of the powder into a solid plug. The thermal treatment causes the material to become rubbery or leather-like due to the glass transition.

Besides, molecular modelling may also be an interesting approach to determine the organization of cellulose, of its hydrated structure as well as to determine its properties when experimental design failed to do it (Mazeau, 2015; Mazeau & Heux, 2003). Thus, applying molecular modelling, Mazeau and Heux (2003) used a computational method to model native cellulose, considering it as a bulk native Iα and Iβ crystal phases with 16 (32 cellobiose units) and 18 chains (36 cellobiose units), respectively, and a solid amorphous phase. From this model, they estimated the Tg of dry cellulose around 377 °C (Table 2). Chen et al. (2004) also produced models with one cellulose chain of 20 cellobiose repeat units to study the relaxation. The Tg observed in this model was around 227 °C, close to the experimental values reported in the literature (Back & Didriksson, 1969; Goring, 1963).

A Tg lower than in other modelling studies was found around 63 °C by Zhang et al. (2012), in exploring a model formed of multiple cellulose chains with two different chains lengths (10 and 20 monomers) with 20 glucose units, arranged parallel up and edge-to-edge. More recent studies (Mazeau, 2015) determined by molecular modelling the Tg of dry cellulose around 357 °C in a cellulose model similar to that used by Mazeau and Heux (2003), and this temperature decreased to 247 °C with

Table 2
Literature values for Tg or Tα for cellulosic materials with the respective methods used and their references.

	Tg (°C)	Crystallinity Index (%)	Presence of other components	Water content (% w/w)	Method		Reference
Cellulose	220	N.P.	No	~Dry	Experimental	DSC	Kargin et al. (1960)
Avicel	253	N.P.	N.P.				
Cellophane	244	N.P.	N.P.				
Bleached spruce sulphite pulp	231	N.P.	N.P.	~Dry	Experimental	DSC	Goring (1963)
Unbleached spruce kraft pulp	245	N.P.	N.P.				
Hollow filament rayon	237	N.P.	N.P.				
Cellulose	230	N.P.	No	~Dry	Experimental	DSC	Back and Didriksson (1969)
Microcrystalline cellulose (MCC)	−34	66	No	~15	Experimental	DSC	Szcześniak et al. (2008)
Cotton fiber	151	80	88–96 % of cellulose 4–12 % of waxes, pectins and other non-cellulosic compounds	~Dry	Experimental	DSC	Denham (2016)
Viscose fiber	145	65	No				
MCC	145	73	No				
Cotton cellulose	160–180	76	No	~4	Experimental	DSC	Nam et al. (2020)
Cellulose rich material (from defatted date-pits)	136	63	35 % of cellulose 25 % of hemicellulose 11 % of lignin	3	Experimental	DSC	Al-Khalili et al. (2023)
Hydroxypropyl methylcellulose (HPMC)	161	N.P.	No	~Dry	Experimental	DSC modulated	McPhillips et al. (1999)
MCC	160	N.P.	No	~Dry	Experimental	DSC modulated	Picker and Hoag (2002)
HPMC film	160–175	N.P.	No	~Dry	Experimental	DMA	Kararli et al. (1990)
Cellulose film	300	36	No	~Dry	Experimental	DSC | DMA	Kim et al. (2013)
Ball milled cellulose	117 205	30 N.P.	No No	0–19 ~Dry	Experimental Couchman–Karasz	DMA –	Paes et al. (2010)
Cellulose	−33	N.P.	No	~11	Theoretical -Kaelbe's approach	–	Salmen and Back (1977)
Cellulose	220	N.P.	N.P.	~Dry	Gordon-Taylor	–	Batzer and Kreibich (1981)
Cellulose rich material (from lemon peels)	37	N.P.	59 % of cellulose 18 % of hemicellulose 16 % of pectin 7 % of protein	Dry	Gordon-Taylor	–	Putri et al. (2024)
Cellulose	183	67	No	~Dry	Gordon-Taylor (ionic liquid)	–	Wu et al. (2015)
Cellulose	377	N.P.	No	~Dry	Molecular modelling	–	Mazeau and Heux (2003)
Amorphous cellulose	227	N.P.	No	~Dry	Molecular modelling	–	Chen et al. (2004)
Cellulose	63	N.P.	No	–	Molecular modelling	–	Zhang et al. (2012)
Cellulose	357 247	N.P. N.P.	No No	~Dry 5	Molecular modelling	–	Mazeau (2015)
Cellulose (cotton linters)	128	N.P.	No	~ 4.5	Experimental	TSC	Jafarpour et al. (2007)

N.P. means not provided in the article.

increasing water content at 5 % *w*/w, showing the plasticizing effect of water.

As observed even through modelling, the glass transition temperature of cellulose varies, as this depends on the cellulose structure/model used, which is not entirely clear until now. A way to approach the high amplitude mobility in cellulose rich materials, can be to use plasticizers in order to experimentally determine Tg in a temperature range that is non-destructive for the sample.

3.1.1. *Impact of plasticizers*

To overcome the difficulty to determine Tg_{DSC}, the impact of plasticizers has been used to reduce and shift Tg below the temperature of thermal decomposition (Ioelovich, 2016; Paes et al., 2010; Xiao et al., 2003).

Szcześniak et al. (2008) investigated the Tg of cellulose powder at different humidities by DSC, obtaining a very low value of Tg of 25 °C at 7 % moisture content (Table 2) (Fig. 2). Salmen and Back (1977) applied a theoretical approach (Kaelbe's approach) to demonstrate the plasticizing effect of water on cellulose. This model is based on the cohesive energy of components and the predicted Tg of cellulose at 11 % *w*/w of water was −33 °C.

Batzer and Kreibich (1981) investigated the Tg of cellulose from cotton fabric at various hydrations (5 to 60 % w/w water) and applied the Gordon-Taylor equation (Eq. (1)) to model the plasticizing effect of water. Extrapolating the curve and based on Kargin et al. (1960), Tg of dry cellulose was around 220 °C and a Tg around −113 °C for cellulose at 60 % w/w water content (Batzer & Kreibich, 1981), but this last calculated value did not take into account the water freezing in the sample, that should induce a cryoconcentration of dry matter.

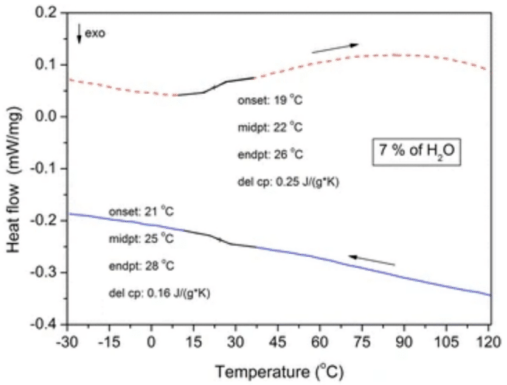

Fig. 2. DSC measurements of cellulose pellets with 7 % of water under argon atmosphere for heating (dashed line) and cooling runs (solid line). Reprinted with permission of Szcześniak et al. (2008). Copyright 2008, by Springer Nature.

$$Tg_m = X_s.Tg_s + K_s.X_w.Tg_w/X_s + K_s.X_w \quad (1)$$

where Tg_m, Tg_s, Tg_w are glass transition temperature (K) of mixture, anhydrous solids and water, respectively; x_s and x_w are the mass fraction of solids and water, respectively; and k_s is a constant proportional to the plasticizing effect of water.

Additionally, employing the Gordon Taylor equation in data obtained by Thermal Mechanical Compression (TMCT-DMA), Putri et al. (2024) identified the relaxation temperature of cellulose-rich material derived from lemon peels. The determined relaxation temperature was around 40 °C for anhydrous material, which was not measurable by DSC. Surprisingly, this temperature was significantly lower than expected for a cellulose-rich material characterized in low water content. It suggested the measurement of a completely different transition/relaxation phenomena generally observed in the literature. However, a clear plasticizing effect of water was observed on the curves obtained.

Moreover, ionic liquids are useful plasticizers for synthetic polymers (Choi et al., 2011; Scott et al., 2002) and can be used to dissolve cellulose-based materials (El Seoud et al., 2021; Heinze, 2016). Wu et al. (2015) estimated the Tg of dry cellulose at 183 °C using ionic liquid (1-Butyl-3-methylimidazolium chloride (BmimCl)) as a plasticizer and applying the Gordon-Taylor modelling. Varying the concentration between 30 and 70 % w/w, Tg decreased from 8.7 °C to −18.3 °C. This solvent also increased the heat capacity which made the transition clear.

Kim et al. (2013) determined the Tg of cellulose films, produced by casting a solution of microcrystalline cellulose (Avicel PH-101, CI ~92 %) dissolved in LiCl/DMAc, by DSC applying step can mode in which the sample is heated through small temperature increments (5 °C/min) and hold for a short interval, to be able to distinguish reversing heat flow (dependent on rate of change of temperature and heat capacity) and non-reversing heat flow (time and temperature dependent events). Through this method it is possible to detect the weak glass transition (reversing heat flow event) which can be hidden by non-reversing event (enthalpy relaxation, melting) in conventional DSC method (McPhillips et al., 1999; Picker & Hoag, 2002; Schick, 2009). The Tg is clearly observed in the reversing heat flow signal measured around 161 °C for hydroxypropyl methylcellulose (HPMC) (0.98 % w/w water content) (McPhillips et al., 1999). Similarly, Picker and Hoag (2002) found a strong transition at 160 °C for dried microcrystalline cellulose (MCC).

3.2. Mesoscopic scale: exploring the dynamics and behaviours of molecular arrangements

Another experimental alternative to overcome the difficult identification of the glass transition of semi-crystalline materials is to use DMA, because mechanical changes are more pronounced than heat capacity change (Fig. 3). Consequently, DMA can detect short-range motions (β, γ) before the main relaxation, and identify the onset of main chain motion associated with the glass transition (Paes et al., 2010; Patra et al., 2021).

DMA is a dynamic method which measures Tα (with a frequency dependence) while DSC measures Tg (with thermal scanning rate dependence) and even if they are both used to measure the glass transition, they use different solicitations and can result in slight temperature differences (Torres et al., 2019). However, at a frequency of 1 Hz in DMA, and 10 °C/min in DSC the results of both techniques may be comparable (Gracia-Fernández et al., 2010; Sakellariou et al., 1985).

DMA should always consider sample behavior at different solicitation frequencies, indeed a frequency effect on the relaxation temperature would ascertain the relaxational origin of an observed phenomenon. The used frequency range allowed the activation energy (Ea) calculation (Eq. (2)) and this value represents the cooperativity of movements in the material: the lower the Ea, the lower the cooperativity of the associated movement, and thus the more local will be the mobility with Ea values ranging around 50 or 300 kJ/mol for secondary and primary relaxations respectively. However, the studies considering the frequency effect on cellulose primary relaxation remain scarce.

$$ln\, f = -Ea/R.T + ln\, A \quad (2)$$

where f is the frequency (Hz), R is the gas constant (8.314 J/K.mol), T is the temperature (K), and A is a pre-exponential factor.

Kim et al. (2013) detected an α-relaxation at 300 °C (by the maximum temperature on the tan δ curve) for cellulose films whereas for hydroxypropyl methylcellulose (HPMC), the observed relaxation temperature was below 200 °C (Table 2) and enhanced with increasing molecular weight and/or crystallinity (Kararli et al., 1990). Also, with DMA, Paes et al. (2010) investigated the glass transition of ball-milled cellulose from eucalyptus and softwood in a lower temperature range (Fig. 3b). Indeed, in this study a water-dependent mechanical relaxation was observed between 30 and 100 °C, and another one only weakly water dependent around 117 °C which was associated with an α-relaxation of a rigid fraction less sensitive to water content. The multiple peaks observed in this study suggests the presence of at least 2 domains with different dynamics; this heterogeneity could be correlated to the structure of the cellulose with amorphous zones, and amorphous-crystalline interfaces that have different sensitivities to water. Indeed, dynamics simulations showed cellulose matrices may have at least 3 kinds of organisations: crystalline, amorphous and paracrystalline (interphase regions between crystalline and amorphous zones) differing by their dynamics and physical properties (Kulasinski et al., 2014). Among these properties, the affinity for water is expected to decrease from amorphous to paracrystalline suggesting the co-existence of water-rich and water-poor zones in the matrix.

Among cellulose plasticizers, trimethylphenyl ammonium hydroxide has been investigated at different concentrations using DMA (Kargin et al., 1960). The α-relaxation of cellulose with 10 % *w*/w of plasticizer was around 180 °C (by the maximum temperature on the tan δ curve) and reduced to 65 °C with 37 % of plasticizer. The Tα of cellulose without plasticizer was determined around 220 °C by extrapolating the solvent dependence of Tα to zero solvent concentration.

As previously observed for the Tg_{DSC} values, the Tα provided by literature spans over a wide range of temperature possibly as a result of a wide diversity of botanical origin, preparation and extraction processes and composition of the cellulose-based materials which are not always precisely given.

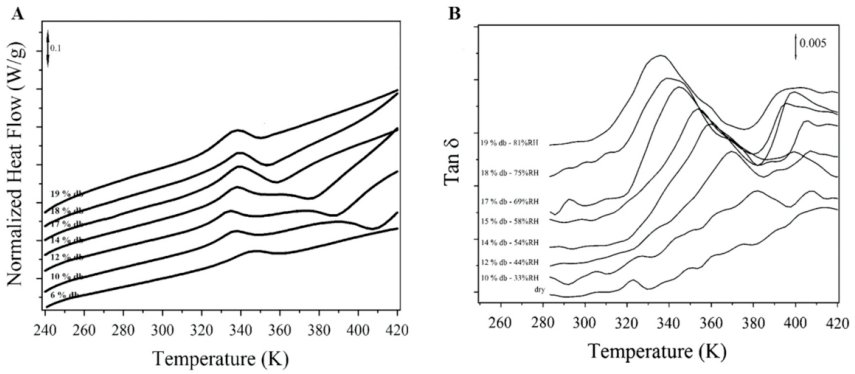

Fig. 3. DSC analysis for ball-milled cellulose (heating rate 10 °C/min) (A); tan delta as a function of temperature (K) from DMA analysis of ball-milled cellulose (frequency 10 Hz) (B). Reprinted with permission of Paes et al. (2010). Copyright 2010, by Springer Nature.

Dielectric spectroscopy (DRS) has been also used to study the relaxations of cellulose and its derivatives (Roig et al., 2011; Diogo & Moura-ramos, 2009; Einfeldt et al., 2001; Einfeldt & Kwasniewski, 2002; Jafarpour et al., 2007; Jafarpour et al., 2009; Zhao et al., 2019). It measures the rate of orientational dynamics distinguishing the molecular units of a polymeric system. The response of dielectric measurement is the sum of all dipolar moments of the system in their present orientation at one given temperature (Einfeldt & Kwasniewski, 2002). The primary relaxation (α-relaxation) which is usually studied by DMA, and related to the glass transition, could not be observed by DRS for cellulose at low moisture content (Einfeldt et al., 2004), only secondary relaxations were evidenced (Table 3).

Different varieties of cellulose (amorphous bead cellulose, Valonia cellulose, bacterial cellulose, regenerated cellulosic fiber: viscose, mocal and lyocell fiber) were investigated between 10 mHz to 1 MHz and in low temperature (−130 to 20 °C) range. In this frequency range, the predominant relaxation was a β-relaxation associated to local chain dynamics, and also β_{wet}-relaxation for a collective motion of water-cellulose mixed phase, both were characterized by activation energy below 100 kJ/mol as expected for secondary relaxations. The β_{wet}-relaxation disappears completely after drying ($T > 130$ °C). At −30 °C, β_{wet}-relaxation of cellulose at 1 % *w*/w of water content is observed at −1 Hz whereas β-relaxation presents a maximum around 5 Hz. In this study, no significant structural influence on the local chain dynamics for different cellulose sources was observed. The relaxation intensity decreased with increasing degree of crystallinity (amorphous bead cellulose>bacterial cellulose>valonia cellulose) as expected from a decreasing amorphous phase contributing to the relaxation (Einfeldt & Kwasniewski, 2002).

A complementary technique for the elucidation of some characteristics of molecular mobility for cellulose-rich materials is thermally stimulated currents (TSC). DRS and TSC are both dielectric techniques, whereas DRS has isothermal nature and covers a wide frequency range, TSC requires a temperature scan and a narrow frequency range. Moreover, TSC is able to resolve a global distributed peak into its individual relaxation modes and determine the temperature-dependent relaxation time (Diogo & Moura-ramos, 2009).

Contrary to DRS, TSC allows the determination of α-relaxation through the compensation phenomenon since it has been shown to characterize cooperative movements and thus to relate to the glass transition (Lacabanne et al., 1994). Cellulose showed a compensation temperature around 128 °C for hydrated sample and 138 °C for dry sample with Ea of 320 $kJ.mol^{-1}$ which corresponds to softening of the vitreous phase upon hydrogen bonds breaking. This result is comparable to the α-relaxation temperature determined by DMA for hydroxypropyl methylcellulose film and ball-milled cellulose shown in Table 2 (Jafarpour et al., 2007).

In agreement with DRS (Einfeldt & Kwasniewski, 2002), two relaxations at −130 °C and − 70 °C were attributed to γ- (side group reorientation) and β-relaxation (localized movements of the backbone) (Table 3), respectively (Jafarpour et al., 2007).

4. Dynamics of cellulose-rich products at molecular scale with time domain NMR

Nuclear magnetic resonance (NMR) relaxometry, also called time domain NMR (TD NMR), is a powerful technique for studying the dynamics and interactions of molecules in various materials, including plant materials up to pure cellulose. TD NMR, when applied to pure cellulose, provides valuable insights into its molecular dynamics, structure, and interactions, without the complexities introduced by other components of plant cell wall matrix when applied to complex plant-based systems (Garvey et al., 2019; Ibbett et al., 2014; Nyström et al., 1981; Suekuni et al., 2022; Topgaard & Söderman, 2002).

Proton spin-lattice relaxation (T_1) and spin-spin relaxation (T_2) are the main parameters of TD NMR to characterize proton relaxations (Song et al., 2021). T_1 relaxation corresponds to longitudinal relaxation, thermal relaxation and spin-lattice relaxation and is related to the molecular reorientation or rotational motions of molecule controlled by viscosity at the proton scale (the lattice). T_2 relaxation is related to the

Table 3
Literature values of secondary relaxations for cellulose measured by DMA, DRS and TSC methods, and references citing these data.

	Water content (%w/w)	T_γ (°C)	Ea_γ (kJ/mol)	T_β (°C)	Ea_β (kJ/mol)	Freq (Hz)	Method	Reference
Amorphous cellulose	0	−123	36	−43	85	0.1	DMA	Montès et al. (1997)
MCC	0	~ -120	35	–	–	0.1	DRS	Jafarpour et al. (2007)
Cellulose	3	~-120	45	−50	75	1	DRS	Roig et al. (2011)
MCC	0	−130	~ 32	−70	~ 90	0.1	TSC	Jafarpour et al. (2007)
Cellulose	0	−135	~35	−65	~85	1	TSC	Roig et al. (2011)

transverse energy exchange process between close nuclear spins to neighbouring other spins, inducing a decay of magnetization. Indeed, T_1 and T_2, reflect the timescales of energy dissipation by motions and the signal decay by magnetization transfer, respectively. In cellulose materials, these relaxation times can provide information about the molecular mobility and interactions within the material, and they have been mainly determined to describe the interactions with water molecules. In fact, the main part of the transverse relaxation mechanism (measured by T_2) is proton exchange taking place between water and hydroxyl groups. Additionally, these relaxations T_1 and T_2 may be affected by both the conformation and mobility changes of molecules in the cellulose-rich materials (Hills et al., 1991).

T_1 range reported in literature covers a width of time which depends on the hydration level of the cellulose-rich material: for low hydration levels (below 20 % *w*/w), only one T_1 value is extracted from the NMR signal; it tends to be dependent on water content. For water contents ranging from dry to 7 % *w*/w: the T_1 values decrease *i.e.* from 400 ms to 154 ms for cotton cellulose with an increase in water content (Grunin et al., 2017), then for higher water contents (up to 20 %), a reverse tendency can be observed with an increase of T_1 with water amount. Vittadini et al. (2001) studied the mobility of water in cellulose by solid-state ^{1}H and high-resolution ^{2}H NMR as a function of moisture content (0–19 % dry basis) and found T_1 values increasing from 8 to 43 ms for water content increasing from 6 to 18 % *w*/w. This "V" shape curves tendency of the T_1 as a function of water content was also observed upon material drying with a T_1 minimum for around 10 % w/w water amount slightly changing for different cellulose-based materials (Topgaard & Söderman, 2002). The values of T_1 may also widely vary with sample preparation, *i.e.* the intact plant cell wall showing the shortest ^{1}H T_1 (120 ms at 20 % w/w water content), whereas the extracted cell walls at the same water content, exhibited longer T_1's of 900–1400 ms, values closer to bulk water properties (White et al., 2014). However, above 20 % w/w water content, it was shown, for complex matrices, that three pools of T_1 could be identified and attributed to water: i) adsorbed on crystals structure, for the first one, with T_1 below 10 ms), ii) in para-crystalline zones (T_1 from 5 to 20 ms), and iii) in fully amorphous zones (from 20 to 200 ms) (Wiesman et al., 2018). These results suggest that the water distribution may be heterogeneous in a cellulose-based matrix according to the structural organization of molecules, even if at low water content, only one value of T_1 can be measured.

The proton NMR relaxation time T_2 provides information for the study of water in cellulose materials about different water environments and by inference about the internal structure of the cellulosic matrix. Water within cellulose morphologies leads to the appearance of a separate proton NMR signal, which relaxes slower than the signal from the cellulose polymer protons, but quicker than the bulk liquid, as water molecules are able to interact with available cellulose sites (Garvey et al., 2019). T_2 values can also be related to how tight water is bound to matrix hydroxyl groups: the shorter the T_2, the tighter the bonding, suggesting water molecules are trapped in the interstitial space between the fibrils and thus exhibit limited proton mobility. Zhao et al. (2019) showed that, for the cellulosic samples with moisture content of 4.5 % and 6.5 % w/w, only one proton population with T_2 below 1 ms can be observed, which reveals that all water is adsorbed. Increasing with water content, their T_2 is noticeably larger, suggesting a larger mobility compared to that of anhydrous cellulose. For the samples at 11 % and 28 % w/w moisture, in addition to a main peak observed at T_2 below 10 ms, a tiny peak can be observed around 40 ms for both samples and an additional peak around 1000 ms only for the sample at 28 % w/w. Thus, at high water content, three pools of water coexist in cellulose according to Zhao et al. (2019): water in tight interactions, directly bound with hydroxyl groups on cellulose (H-bonds), then water located not far from the cellulose chain, which is non-freezing water, and finally water which should be further away from cellulose molecules, thus able to freeze and that then can be considered as bulk water (Fig. 4). The detection of extra-population with different T_2 when water amount reached >10 % w/w may be in relation with the ability of the material to show two secondary relaxations (β- and β_{wet}-) as detected with DRS. A given pool of water can contribute in quite different ways to a specific relaxation, and it can also play a different role in a variety of relaxations. Bulk water has negligible contribution to secondary relaxations (β-, γ- relaxations), tightly bound water and non-freezing water are involved in the dynamics by acting as a part of the relaxing unit in β-relaxation and may play a role of plasticizer. However, these water-cellulose interactions and their contribution to relaxation cannot be applied to all kinds of cellulose, because they mainly depend on morphology and crystallinity

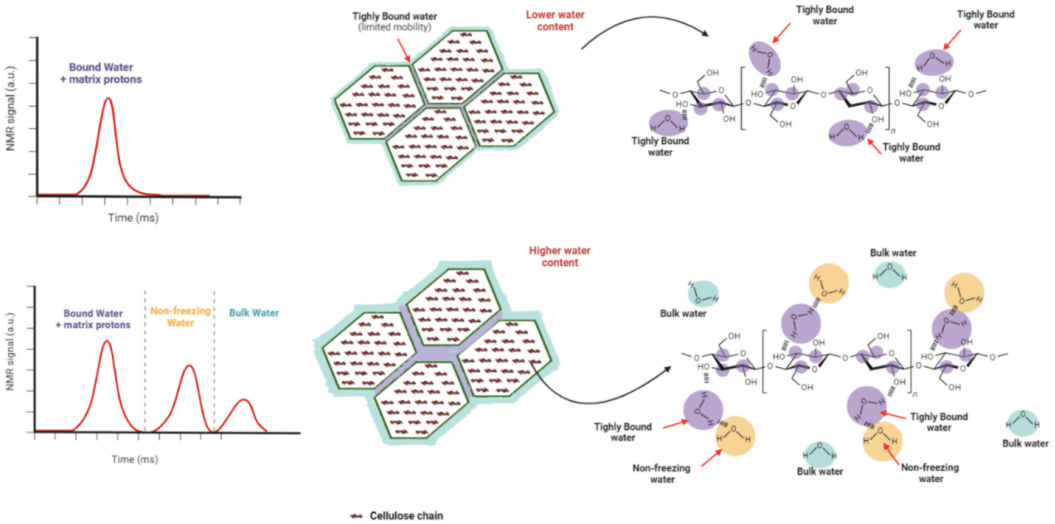

Fig. 4. Types of protons distributed in the matrix based on Chen et al. (2022); Falourd et al. (2022); Rahman et al. (2021); Zhao et al. (2019).

(Zhao et al., 2019).

T_2, spin-spin relaxations, were found to slightly increase from 0.1 to 0.15 ms as a function of moisture content from 5 to 11 % w/w in the cellulose matrix studied by solid-state H-NMR (Vittadini et al., 2001). However, the relaxation time exhibited a sharp increase (values multiplied by 7) for moisture content varying from 11 to 19 % w/w.

The determination of both T_1 and T_2 in cellulose-based materials gives a general view of the different range of mobility as function of water content: below around 5–10 % w/w water, we may consider the water as structural water, strongly associated with molecules with a low mobility, then between around 9–19 % w/w, the water may be heterogeneously distributed in association with different zones at the molecular level, playing in some zones the role of plasticizer and finally, above 20 % w/w, the water shows almost bulk water properties. In cellulose extract, is still difficult to attribute the mobile zone to a specific component (pectin, hemicellulose, cellulose…) but is probably more in relation to the physical state (vitreous/rubbery) of these components and to the amorphous/crystalline ratio; moreover the supra organization of plant cell wall can expose spaces where water in high amount (>20 % *w*/w), may be confined between microfibrils by capillary forces with some bulk water properties such as relatively high mobility.

5. Multi-scale real-time techniques for cellulose water dynamics

In addition to the methods previously mentioned in this review, a broad array of key analytical techniques from the literature has also significantly enhanced the understanding of water dynamics in cellulose materials (Fig. 5). The diverse range of analytical methods and protocols developed to investigate interactions between cellulose-rich materials and water reflects the complexity of these interactions and the need to examine them from different perspectives (Solhi et al., 2023).

Recent advances include the integration of Small-Angle X-ray Scattering (SAXS) and Wide-Angle X-ray Scattering (WAXS) with complementary techniques such as NMR, DMA, Fourier-Transform Infrared Spectroscopy (FTIR), Atomic Force Microscopy (AFM) and neutron scattering. Small-angle X-ray scattering (SAXS) and small-angle neutron scattering (SANS) are able to provide information on the structure and morphology of cellulose materials on a multiscale length (Li et al., 2021; Okugawa et al., 2021; Paajanen et al., 2022). Despite challenges in data interpretation, these methods provide the advantage of monitoring real-time changes: such as changes occurring upon hydration or drying. Moreover, integration of SAXS and WAXS with different methods facilitates a comprehensive understanding of cellulose-rich materials and water interaction spanning various scales (Solhi et al., 2023).

For instance, Li et al. (2021) utilized micro-focusing Grazing-Incidence Small-Angle X-ray Scattering (μGISAXS) along with Atomic Force Microscopy (AFM) to explore structural rearrangements and interphase development of cellulose materials during drying at nano- to microscale level, highlighting strong adhesion due to molecular interdiffusion and structural rearrangement at the interface. Similarly, Paajanen et al. (2022) combined X-ray scattering with molecular simulations to investigate structural changes in wood at different hierarchical levels, providing a comprehensive view of moisture's impact on microfibril packing, orientation, and crystal size, which enhances the interpretation of nanoscale interactions between water and plant cell walls.

Okugawa et al. (2021) integrated SAXS, WAXS, and DMA to demonstrate the impact of water on the semicrystalline structure of cellulose. They observed the tan δ peak of regenerated cellulose between 240 and 279 °C in the dry state. This peak was higher in the presence of water compared to organic solvents (ethanol, methanol, propanol, butanol, hexane, heptane, octane), indicating a greater partial loosening of the polymer structure and increased mobility of groups and small chain segments. SAXS experiments showed that the apparent crystal sizes (ACS) and the width of microfibrils increased from 3.4 nm (dry state) to 6.3 nm (water regain of 100 wt%), reflecting the influence of water on electron density between microfibrils and inter-microfibril regions. Their findings highlight how water affects the density in amorphous regions, crystallinity, and mechanical properties such as tan δ, underscoring its critical role in modulating cellulose properties.

These studies collectively highlight the efficacy of integrating multiple analytical techniques to achieve an understanding of water's impact on cellulose-rich material structure and dynamics in real-time at multiple scale (atomic to mesoscale). Furthermore, advanced simulation techniques coupled to experimental data have also been employed to model biomolecular systems, elucidate mechanisms, and explore the interactions within plant cell wall materials (Gurina et al., 2020; Lin & Wang, 2023; Singh & Li, 2019).

6. Conclusion

Adopting a multidisciplinary approach that combines various analytical techniques appears to be a promising strategy for investigating the dynamics in cellulose-based systems. By integrating multiple analytical methods on specific materials, researchers will deepen their understanding of the dynamics at multiple scales, taking into account materials structure/physical state, as well as water-matrix interactions. This approach can provide valuable insights into the dynamic behavior of cellulose-rich materials and pave the way for the development of tailored solutions with optimized performance and functionality.

While significant progress has been made in assessing molecular mobility in cellulose-rich primary cell wall material, there is still a need to explore the contributions of other components, such as pectin and hemicellulose, in cellulose-rich primary cell wall materials. Understanding the synergistic effects of these components and their interactions with cellulose should offer new perspectives on material behavior and properties. In addition, current techniques often struggle to address the structural and composition heterogeneity of cellulose-based materials, posing challenges in uniformly assessing molecular

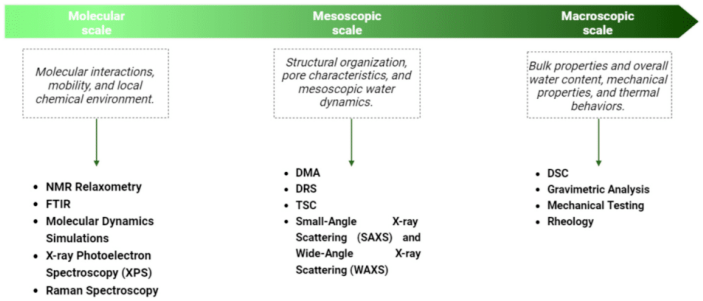

Fig. 5. Analytical techniques for molecular mobility and dynamics enabling characterization of cellulose-rich materials at different scales. After Solhi et al. (2023).

mobility and dynamics across complex materials. Common methods used for studying water dynamics and molecular mobility frequently lack the sensitivity needed to detect subtle changes at lower temperatures or minor compositional differences. Furthermore, investigating the role of ions, particularly in the context of water relationships remains crucial. There is also a need for more studies focusing on the one hand on real-time monitoring of changes in molecular mobility under varying conditions, such as temperature and humidity and on the other hand on the simultaneous analyses of surface and bulk properties to obtain a more comprehensive global picture.

Hence, the application of advanced techniques such as Dynamic Nuclear Polarization (DNP)-NMR, non-destructive methods like X-ray Computed Tomography (XCT), and the investigation of local mechanical properties through nanoindentation and micromechanical testing, presents intriguing avenues for future research. Additionally, leveraging machine learning to analyse data from multiple techniques and identify patterns and correlations not apparent through traditional analysis can further unravel the complexities of cellulose-rich materials. These approaches will collectively enhance our knowledge of the molecular dynamics and interactions within these materials.

CRediT authorship contribution statement

G.O. Coelho: Writing – review & editing, Writing – original draft, Visualization, Investigation, Data curation, Conceptualization. **I. Deleris:** Writing – review & editing, Visualization, Validation, Conceptualization. **D. Champion:** Writing – review & editing, Visualization, Validation, Supervision, Conceptualization. **J. Wallecan:** Writing – review & editing, Visualization, Validation, Funding acquisition. **S. Debon:** Writing – review & editing. **G. Roudaut:** Writing – review & editing, Visualization, Validation, Supervision, Project administration, Funding acquisition, Conceptualization.

Declaration of competing interest

The authors declare that they have no known competing financial interests or personal relationships that could have appeared to influence the work reported in this paper.

Data availability

No data was used for the research described in the article.

Acknowledgements

The authors are grateful for the financial support of Cargill.

References

Al-Khalili, M., Al-Habsi, N., Al-Khusaibi, M., & Rahman, M. S. (2023). Proton, thermal and mechanical relaxation characteristics of a complex biomaterial (de-fatted date-pits) as a function of temperature. *Journal of Thermal Analysis and Calorimetry, 148*(9), 3525–3534. https://doi.org/10.1007/s10973-023-11943-6

Back, E., & Didriksson, E. (1969). Four secondary and glass transition temperature of cellulose evaluated by sonic pulse technique. *Svensk Papperstidning, 72*(21), 687–694.

Batzer, H., & Kreibich, U. T. (1981). Influence of water on thermal transition in natural polymers and synthetic polyamides. *Polymer Bulletin, 5*, 585–590. https://doi.org/10.1007/BF00255296

Blanshard, J. M. (1995). The glass transition, its nature and significance in food processing. In S. T. Beckett (Ed.), *Physico-chemical aspects of food processing. Physico-Chemical Aspects of Food Processing*. https://doi.org/10.1007/978-1-4613-1227-7

Chen, P., Wohlert, J., Berglund, L., & Furó, I. (2022). Water as an intrinsic structural element in cellulose fibril aggregates. *Journal of Physical Chemistry Letters, 13*(24), 5424–5430. https://doi.org/10.1021/acs.jpclett.2c00781

Chen, W., Lickfield, G. C., & Yang, C. Q. (2004). Molecular modeling of cellulose in amorphous state. Part I: Model building and plastic deformation study. *Polymer, 45*(3), 1063–1071. https://doi.org/10.1016/j.polymer.2003.11.020

Choi, S. Y., Rodriguez, H., Mirjafari, A., Gilpin, D. F., McGrath, S., Malcolm, K. R., … McNally, T. (2011). Dual functional ionic liquids as plasticisers and antimicrobial agents for medical polymers. *Green Chemistry, 13*, 1527–1535. https://doi.org/10.1039/C1GC15132K

Ciolacu, D., Ciolacu, F., & Popa, V. I. (2008). Supramolecular structure - A key parameter for cellulose biodegradation. *Macromolecular Symposia. Macromolecular Symposia.*. https://doi.org/10.1002/masy.200851220

Ciolacu, D., Pitol-Filho, L., & Ciolacu, F. (2012). Studies concerning the accessibility of different allomorphic forms of cellulose. *Cellulose, 19*(1), 55–68. https://doi.org/10.1007/s10570-011-9620-1

Cosgrove, D. J. (1997). Assembly and enlargement of the primary cell wall in plants. *Annual Review of Cell and Developmental Biology, 13*, 171–201. https://doi.org/10.1146/annurev.cellbio.13.1.171

Cosgrove, D. J. (2014). Re-constructing our models of cellulose and primary cell wall assembly. *Current Opinion in Plant Biology, 22*, 122–131. https://doi.org/10.1016/j.pbi.2014.11.001

Cresswell, R., Dupree, R., Brown, S. P., Pereira, C. S., Skaf, M. S., Sorieul, M., … Hill, S. (2021). Importance of water in maintaining softwood secondary cell wall nanostructure. *Biomacromolecules, 22*(11), 4669–4680. https://doi.org/10.1021/acs.biomac.1c00937

Dassanayake, R. S., Acharya, S., & Abidi, N. (2019). *Biopolymer-based materials from polysaccharides: Properties, Processing, Characterization and Sorption Applications*. IntechOpen. https://doi.org/10.5772/intechopen.80898

Denham, C. (2016). *The glass transition of cotton*. Deakin University. doi:https://dro.deakin.edu.au/articles/thesis/The_glass_transition_of_cotton/21111037.

Ding, S. Y., Liu, Y. S., Zeng, Y., Himmel, M. E., Baker, J. O., & Bayer, E. A. (2012). How does plant cell wall nanoscale architecture correlate with enzymatic digestibility? *Science, 338*(6110), 1055–1060. https://doi.org/10.1126/science.1227491

Diogo, H. P., & Moura-ramos, J. J. (2009). Secondary molecular mobility in amorphous ethyl cellulose : Aging effects and degree of co-operativity. *Journal of Polymer Science Part B: Polymer Physics, 47*(8), 820–829. https://doi.org/10.1002/polb.21688

Einfeldt, J., & Kwasniewski, A. (2002). Characterization of different types of cellulose by dielectric spectroscopy. *Cellulose, 9*(3–4), 225–238. https://doi.org/10.1023/A:1021184620045

Einfeldt, J., Meißner, D., & Kwasniewski, A. (2001). Polymer dynamics of cellulose and other polysaccharides in solid state-secondary dielectric relaxation processes. *Progress in Polymer Science, 26*(9), 1419–1472. doi:S0079-6700(01)00020-X.

Einfeldt, J., Meißner, D., & Kwasniewski, A. (2004). Molecular interpretation of the main relaxations found in dielectric spectra of cellulose - experimental arguments. *Cellulose, 11*(2), 137–150. https://doi.org/10.1023/B:CELL.0000025404.61412.d6

El Seoud, O. A., Bioni, T. A., & Dignani, M. T. (2021). Understanding cellulose dissolution in ionic liquid-dimethyl sulfoxide binary mixtures: Quantification of the relative importance of hydrogen bonding and hydrophobic interactions. *Journal of Molecular Liquids, 322*(114848). https://doi.org/10.1016/j.molliq.2020.114848

Etale, A., Onyianta, A. J., Turner, S. R., & Eichhorn, S. J. (2023). Cellulose: A review of water interactions, applications in composites, and water treatment. *Chemical Reviews, 123*(5), 2016–2048. https://doi.org/10.1021/acs.chemrev.2c00477

Falourd, X., Lahaye, M., & Rondeau-Mouro, C. (2022). Assessment of cellulose interactions with water by ssNMR: 1H->13C transfer kinetics revisited. *Carbohydrate Polymers, 298*(July), Article 120104. https://doi.org/10.1016/j.carbpol.2022.120104

Fernandes, A. N., Thomas, L. H., Altaner, C. M., Callow, P., Forsyth, V. T., Apperley, D. C., … Jarvis, M. C. (2011). Nanostructure of cellulose microfibrils in spruce wood. *Proceedings of the National Academy of Sciences of the United States of America, 108*(47). https://doi.org/10.1073/pnas.1108942108

Garvey, C. J., Simon, G. P., Whittaker, A. K., & Parker, I. H. (2019). Moisture-activated dynamics on crystallite surfaces in cellulose. *Colloid and Polymer Science, 297*(4), 521–527. https://doi.org/10.1007/s00396-018-04464-4

Gautam, K., Vishvakarma, R., Sharma, P., Singh, A., Kumar Gaur, V., Varjani, S., & Kumar Srivastava, J. (2022). Production of biopolymers from food waste: Constrains and perspectives. *Bioresource Technology, 361*(127650). https://doi.org/10.1016/j.biortech.2022.127650

Goldberg, R. N., Schliesser, J., Mittal, A., Decker, S. R., Santos, A. F. L. O. M., Freitas, V. L. S., … Johnson, D. K. (2015). A thermodynamic investigation of the cellulose allomorphs: Cellulose(am), cellulose Iβ(cr), cellulose II(cr), and cellulose III (cr). *Journal of Chemical Thermodynamics, 81*, 184–226. https://doi.org/10.1016/j.jct.2014.09.006

Goring, D. A. I. (1963). *Thermal Softening of Lignin, Hemicellulose and Cellulose. Pulp and Paper in Canada*.

Gracia-Fernández, C. A., Gómez-Barreiro, S., López-Beceiro, J., Tarrío Saavedra, J., Naya, S., & Artiaga, R. (2010). Comparative study of the dynamic glass transition temperature by DMA and TMDSC. *Polymer Testing, 29*(8), 1002–1006. https://doi.org/10.1016/j.polymertesting.2010.09.005

Grunin, L. Y., Grunin, Y. B., Nikolskaya, E. A., Sheveleva, N. N., & Nikolaev, I. A. (2017). An NMR relaxation and spin diffusion study of cellulose structure during water adsorption. *Biophysics (Russian Federation), 62*(2), 198–206. https://doi.org/10.1134/S0006350917020087

Grunin, Y. B., Grunin, L. Y., Schiraya, V. Y., Ivanova, M. S., & Masas, D. S. (2020). Cellulose–water system's state analysis by proton nuclear magnetic resonance and sorption measurements. *Bioresources and Bioprocessing, 7*(1). https://doi.org/10.1186/s40643-020-00332-8

Gurina, D., Surov, O., Voronova, M., & Zakharov, A. (2020). Molecular dynamics simulation of polyacrylamide adsorption on cellulose nanocrystals. *Nanomaterials, 10*(7), 1–15. https://doi.org/10.3390/nano10071256

Hatakeyama, H., & Hatakeyama, T. (2000). Interaction between cellulosic polysaccharides and water. *Hydrocolloids, 261–270*. https://doi.org/10.1016/b978-044450178-3/50032-9

Hediger, S., Lesage, A., & Emsley, L. (2002). A new NMR method for the study of local mobility in solids and application to hydration of biopolymers in plant cell walls. *Macromolecules, 35*(13), 5078–5084. https://doi.org/10.1021/ma020065h

Heinze, T. (2016). Cellulose: Structure and properties. In O. J. Rojas (Ed.), *Cellulose chemistry and properties: Fibers, nanocelluloses and advanced materials* (pp. 1–52). Cham: Springer International Publishing. https://doi.org/10.1007/12_2015_319.

Hills, B. P., Cano, C., & Belton, P. S. (1991). Proton NMR relaxation studies of aqueous polysaccharide systems. *Macromolecules, 24*(10), 2944–2950. https://doi.org/10.1021/ma00010a047

Ibbett, R., Wortmann, F., Varga, K., & Schuster, K. C. (2014). A morphological interpretation of water chemical exchange and mobility in cellulose materials derived from proton NMR T2 relaxation. *Cellulose, 21*(1), 139–152. https://doi.org/10.1007/s10570-013-0106-1

Ioelovich, M. (2016). Isophase transitions of cellulose – A short review. *Athens Journal of Sciences, 3*(4), 309–322. https://doi.org/10.30958/ajs.3-4-4

Ioelovich, M. (2021). Adjustment of hydrophobic properties of cellulose materials. *Polymers, 13*(8). https://doi.org/10.3390/polym13081241

Jafarpour, G., Dantras, E., Boudet, A., & Lacabanne, C. (2007). Study of dielectric relaxations in cellulose by combined DDS and TSC. *Journal of Non-Crystalline Solids, 353*(44–46), 4108–4115. https://doi.org/10.1016/j.jnoncrysol.2007.06.026

Jafarpour, G., Roig, F., Dantras, E., Boudet, A, & Lacabanne, C. (2009). Influence of water on localized and delocalized molecular mobility of cellulose. *Journal of Non-Crystalline Solids, 355*(34–36), 1669–1672. https://doi.org/10.1016/j.jnoncrysol.2009.06.026

Jarvis, M. C. (2023). Hydrogen bonding and other non-covalent interactions at the surfaces of cellulose microfibrils. *Cellulose, 30*(2), 667–687. https://doi.org/10.1007/s10570-022-04954-3

Jiang, W., Sun, L., Hao, A., & Chen, J. (2011). Regenerated cellulose fibers from waste bagasse using ionic liquid. *Textile Research Journal, 81*(18), 1949–1958. https://doi.org/10.1177/0040517511414974

Kararli, T. T., Hurlbut, J. B., & Needham, T. E. (1990). Glass–rubber transitions of cellulosic polymers by dynamic mechanical analysis. *Journal of Pharmaceutical Sciences, 79*(9), 845–848. https://doi.org/10.1002/jps.2600790922

Kargin, V. A., Kozlov, P. V., & Nai-chan, W. (1960). Classification temperature of cellulose. *Doklady Akademii Nauk SSSR, 130*(2), 356–358. doi:http://mi.mathnet.ru/dan39549.

Kim, J. W., Park, S., Harper, D. P., & Rials, T. G. (2013). Structure and thermomechanical properties of stretched cellulose films. *Journal of Applied Polymer Science, 128*(1), 181–187. https://doi.org/10.1002/app.38149

Kulasinski, K., Keten, S., Churakov, S. V., Derome, D., & Carmeliet, J. (2014). A comparative molecular dynamics study of crystalline, paracrystalline and amorphous states of cellulose. *Cellulose, 21*(3), 1103–1116. https://doi.org/10.1007/s10570-014-0213-7

Lacabanne, C., Lamure, A., Teyssedre, G., Bernes, A., & Mourgues, M. (1994). Study of cooperative relaxation modes in complex systems by thermally stimulated current spectroscopy. *Journal of Non-Crystalline Solids, 172–174*(Part 2), 884–890. https://doi.org/10.1016/0022-3093(94)90593-2

Li, C. Y. (2020). The rise of semicrystalline polymers and why are they still interesting. *Polymer, 211*(October), Article 123150. https://doi.org/10.1016/j.polymer.2020.123150

Li, H., Roth, S. V., Freychet, G., Zhernenkov, M., Asta, N., Wågberg, L., & Pettersson, T. (2021). Structure development of the interphase between drying cellulose materials revealed by in situ grazing-incidence small-angle X-ray scattering. *Biomacromolecules, 22*(10), 4274–4283. https://doi.org/10.1021/acs.biomac.1c00845

Lin, K., & Wang, Z. (2023). Multiscale mechanics and molecular dynamics simulations of the durability of fiber-reinforced polymer composites. *Communications Materials, 4*(1), 1–16. https://doi.org/10.1038/s43246-023-00391-2

Lindh, E. L., Terenzi, C., Salmén, L., & Furó, I. (2017). Water in cellulose: Evidence and identification of immobile and mobile adsorbed phases by 2H MAS NMR. *Physical Chemistry Chemical Physics, 19*(6), 4360–4369. https://doi.org/10.1039/c6cp08219j

Liu, P., Yu, L., Liu, H., Chen, L., & Li, L. (2009). Glass transition temperature of starch studied by a high-speed DSC. *Carbohydrate Polymers, 77*(2), 250–253. https://doi.org/10.1016/j.carbpol.2008.12.027

Liu, Y., Bhandari, B., & Zhou, W. (2006). Glass transition and enthalpy relaxation of amorphous food saccharides: A review. *Journal of Agricultural and Food Chemistry, 54*(16), 5701–5717. https://doi.org/10.1021/jf060188r

Mazeau, K. (2015). The hygroscopic power of amorphous cellulose: A modeling study. *Carbohydrate Polymers, 117*, 585–591. https://doi.org/10.1016/j.carbpol.2014.09.095

Mazeau, K., & Heux, L. (2003). Molecular dynamics simulations of bulk native crystalline and amorphous structures of cellulose. *Journal of Physical Chemistry B, 107*(10), 2394–2403. https://doi.org/10.1021/jp0219395

McPhillips, H., Craig, D. Q. M., Royall, P. G., & Hill, V. L. (1999). Characterisation of the glass transition of HPMC using modulated temperature differential scanning calorimetry. *International Journal of Pharmaceutics, 180*(1), 83–90. https://doi.org/10.1016/S0378-5173(98)00407-4

Meychik, N., Nikolaeva, Y., & Kushunina, M. (2021). The significance of ion-exchange properties of plant root cell walls for nutrient and water uptake by plants. *Plant Physiology and Biochemistry, 166*, 140–147. https://doi.org/10.1016/j.plaphy.2021.05.048

Molnár, J., Zuba, Z., Sepsi, Ujhelyi, F., Erdei, G., Lenk, S., & Menyhárd, A. (2021). Structural investigation of semicrystalline polymers. *Polymer Testing, 95*, Article 107098. https://doi.org/10.1016/j.polymertesting.2021.107098

Montès, H., Mazeau, K., & Cavaillé, J. Y. (1997). Secondary mechanical relaxations in amorphous cellulose. *Macromolecules, 30*(22), 6977–6984. https://doi.org/10.1021/ma9611329

Nakamura, K., Hatakeyama, T., & Hatakeyama, H. (1981). *Studies on bound water of cellulose by differential scanning calorimetry, 607–613*.

Nam, S., Hillyer, M. B., & Condon, B. D. (2020). Method for identifying the triple transition (glass transition-dehydration-crystallization) of amorphous cellulose in cotton. *Carbohydrate Polymers, 228*, Article 115374. https://doi.org/10.1016/j.carbpol.2019.115374

Nyström, B., Moseley, M. E., Brown, W., & Roots, J. (1981). Molecular motion of small molecules in cellulose gels studied by NMR. *Journal of Applied Polymer Science, 26*(10), 3385–3393. https://doi.org/10.1002/app.1981.070261018

Okugawa, A., Yuguchi, Y., & Yamane, C. (2021). Relaxation phenomenon and swelling behavior of regenerated cellulose fibers affected by organic solvents. *Carbohydrate Polymers, 259*, Article 117656. https://doi.org/10.1016/j.carbpol.2021.117656

Paajanen, A., Zitting, A., Rautkari, L., Ketoja, J. A., & Penttilä, P. A. (2022). Nanoscale mechanism of moisture-induced swelling in wood microfibril bundles. *Nano Letters, 22*(13), 5143–5150. https://doi.org/10.1021/acs.nanolett.2c00822

Paes, S. S., Sun, S., MacNaughtan, W., Ibbett, R., Ganster, J., Foster, T. J., & Mitchell, J. R. (2010). The glass transition and crystallization of ball milled cellulose. *Cellulose, 17*(4), 693–709. https://doi.org/10.1007/s10570-010-9425-7

Park, Y. B., & Cosgrove, D. J. (2015). Xyloglucan and its interactions with other components of the growing cell wall. *Plant and Cell Physiology, 56*(2), 180–194. https://doi.org/10.1093/pcp/pcu204

Patra, S., Ajayan, P. M., & Narayanan, T. N. (2021). Dynamic mechanical analysis in materials science: The Novice's tale. *Oxford Open Materials Science, 1*(1), 1–12. https://doi.org/10.1093/oxfmat/itaa001

Perdomo, J., Cova, A., Sandoval, A. J., García, L., Laredo, E., & Müller, A. J. (2009). Glass transition temperatures and water sorption isotherms of cassava starch. *Carbohydrate Polymers, 76*(2), 305–313. https://doi.org/10.1016/j.carbpol.2008.10.023

Pereira, P. H. F., Ornaghi, H. L., Arantes, V., & Cioffi, M. O. H. (2021). Effect of chemical treatment of pineapple crown fiber in the production, chemical composition, crystalline structure, thermal stability and thermal degradation kinetic properties of cellulosic materials. *Carbohydrate Research, 499*, Article 108227. https://doi.org/10.1016/j.carres.2020.108227

Picker, K. M., & Hoag, S. W. (2002). Characterization of the thermal properties of microcrystalline cellulose by modulated temperature differential scanning calorimetry. *Journal of Pharmaceutical Sciences, 91*(2), 342–349. https://doi.org/10.1002/jps.10018

Poletto, M., Ornaghi Júnior, H. L., & Zattera, A. J. (2014). Native cellulose: Structure, characterization and thermal properties. *Materials, 7*(9), 6105–6119. https://doi.org/10.3390/ma7096105

Putri, N. I., Van Audenhove, J., Kyomugasho, C., Van Loey, A., & Hendrickx, M. (2024). Relaxation temperature and storage stability of the functionalized cell wall material residue from lemon peel. *Food Hydrocolloids, 150*, Article 109711. https://doi.org/10.1016/j.foodhyd.2023.109711

Rahman, M. S., Suresh, S., & Al-Habsi, N. (2021). Proton relaxation in freeze-dried broccoli as measured by low-frequency nuclear magnetic resonance (LF-NMR) and its relationship with the thermal glass transition. *Journal of Thermal Analysis and Calorimetry, 143*(4), 3147–3159. https://doi.org/10.1007/s10973-020-09401-8

Roig, F., Dantras, E., Dandurand, J., & Lacabanne, C. (2011). Influence of hydrogen bonds on glass transition and dielectric relaxations of cellulose. *Journal of Physics D: Applied Physics, 44*(4). https://doi.org/10.1088/0022-3727/44/4/045403

Rolandelli, G., Farroni, A. E., & Buera, M.d. P. (2022). Analysis of molecular mobility in corn and quinoa flours through 1H NMR and its relationship with water distribution, glass transition and enthalpy relaxation. *Food Chemistry, 373*, Article 131422. https://doi.org/10.1016/j.foodchem.2021.131422

Rongpipi, S., Ye, D., Gomez, E. D., & Gomez, E. W. (2019). Progress and opportunities in the characterization of cellulose – An important regulator of cell wall growth and mechanics. *Frontiers in Plant Science, 9*. https://doi.org/10.3389/fpls.2018.01894

Roudaut, G., Simatos, D., Champion, D., Contreras-Lopez, E., & Le Meste, M. (2004). Molecular mobility around the glass transition temperature: A mini review. *Innovative Food Science and Emerging Technologies, 5*(2), 127–134. https://doi.org/10.1016/j.ifset.2003.12.003

Sakellariou, P., Rowe, R. C., & White, E. F. T. (1985). The thermomechanical properties and glass transition temperatures of some cellulose derivatives used in film coating. *International Journal of Pharmaceutics, 27*(2), 267–277. https://doi.org/10.1016/0378-5173(85)90075-4

Salmen, N. L., & Back, E. L. (1977). The influence of water on the glass transition temperature of cellulose. In *Fibre-Water Interactions in Paper-Making, Trans. of the VIth Fund. Res. Symp. Oxford* (pp. 683–690). https://doi.org/10.1063/1.3633242

Schäler, K. (2012). *Low-field Nmr studies of structure and dynamics in semicrystalline polymers*. Martin Luther University Halle-Wittenberg. Retrieved from http://d-nb.info/1033306622/34.

Schick, C. (2009). Differential scanning calorimetry (DSC) of semicrystalline polymers. *Analytical and Bioanalytical Chemistry, 395*, 1589–1611. https://doi.org/10.1007/s00216-009-3169-y

Scott, M. P., Brazel, C. S., Benton, M. G., Mays, J. W., Holbrey, J. D., & Rogers, R. D. (2002). Application of ionic liquids as plasticizers for poly(methyl methacrylate). *Chemical Communications, 2*(13), 1370–1371. https://doi.org/10.1039/b204316p

Simon, M., Fulchiron, R., & Gouanvé, F. (2022). Water sorption and mechanical properties of cellulosic derivative fibers. *Polymers, 14*, 2836. https://doi.org/10.3390/polym14142836

Singh, N., & Li, W. (2019). Recent advances in coarse-grained models for biomolecules and their applications. *International Journal of Molecular Sciences, 20*(15). https://doi.org/10.3390/ijms20153774

Solhi, L., Guccini, V., Heise, K., Solala, I., Niinivaara, E., Xu, W., … Kontturi, E. (2023). Understanding Nanocellulose-water interactions: Turning a detriment into an asset. *Chemical Reviews, 123*(5), 1925–2015. https://doi.org/10.1021/acs.chemrev.2c00611

Song, P., Wang, Z., Song, P., Yue, X., Bai, Y., & Feng, L. L. (2021). Evaluating the effect of aging process on the physicochemical characteristics of rice seeds by low field nuclear magnetic resonance and its imaging technique. *Journal of Cereal Science, 99*, Article 103190. https://doi.org/10.1016/j.jcs.2021.103190

Suekuni, M. T., D'Souza, N., & Allgeier, A. M. (2022). NMR Relaxometry studies on the drying kinetics of cellulose nanofibers. *Industrial and Engineering Chemistry Research, 61*(16), 5475–5483. https://doi.org/10.1021/acs.iecr.1c04878

Szcześniak, L., Rachocki, A., & Tritt-Goc, J. (2008). Glass transition temperature and thermal decomposition of cellulose powder. *Cellulose, 15*(3), 445–451. https://doi.org/10.1007/s10570-007-9192-2

Termonia, Y. (1995). Chain conformations at Semicrystalline interphases. *Macromolecules, 28*(23), 7667–7670. https://doi.org/10.1021/ma00127a012

Thomas, L. H., Trevor Forsyth, V., Šturcová, A., Kennedy, C. J., May, R. P., Altaner, C. M., … Jarvis, M. C. (2013). Structure of cellulose microfibrils in primary cell walls from collenchyma. *Plant Physiology, 161*(1), 465–476. https://doi.org/10.1104/pp.112.206359

Thygesen, A., Oddershede, J., Lilholt, H., Thomsen, A. B., & Ståhl, K. (2005). On the determination of crystallinity and cellulose content in plant fibres. *Cellulose, 12*(6), 563–576. https://doi.org/10.1007/s10570-005-9001-8

Topgaard, D., & Söderman, O. (2002). Changes of cellulose fiber wall structure during drying investigated using NMR self-diffusion and relaxation experiments. *Cellulose, 9*(2), 139–147. https://doi.org/10.1023/A:1020158524621

Torres, F. G., Mayorga, J. P., Vilca, C., Arroyo, J., Castro, P., & Rodriguez, L. (2019). Preparation and characterization of a novel starch–chestnut husk biocomposite. *SN Applied Sciences, 1*(10), 1–7. https://doi.org/10.1007/s42452-019-1204-y

Vittadini, E., Dickinson, L. C., & Chinachoti, P. (2001). 1H and 2H NMR mobility in cellulose. *Carbohydrate Polymers, 46*(1), 49–57. https://doi.org/10.1016/S0144-8617(00)00282-4

Voelker, A. L., Sommer, A. A., & Mauer, L. J. (2020). Moisture sorption behaviors, water activity-temperature relationships, and physical stability traits of spices, herbs, and seasoning blends containing crystalline and amorphous ingredients. *Food Research International, 136*, Article 109608. https://doi.org/10.1016/j.foodres.2020.109608

Walczak, M. (2012). Role and properties of the confined amorphous phase of polymers. Ecole nationale supérieure d'arts et métiers (ENSAM). Retrieved from https://pastel.archives-ouvertes.fr/pastel-00839174.

Wang, H., Keum, J. K., Hiltner, A., Baer, E., Freeman, B., Rozanski, A., & Galeski, A. (2009). Confined crystallization of polyethylene oxide in nanolayer assemblies. *Science, 323*(5915), 757–760. https://doi.org/10.1126/science.1164601

White, P. B., Wang, T., Park, Y. B., Cosgrove, D. J., & Hong, M. (2014). Water-polysaccharide interactions in the primary cell wall of arabidopsis thaliana from polarization transfer solid-state NMR. *Journal of the American Chemical Society, 136*(29), 10399–10409. https://doi.org/10.1021/ja504108h

Wiesman, Z., Linder, C., Resende, M. T., Ayalon, N., Levi, O., Bernardinelli, O. D., … Jackman, R. (2018). 2D and 3D Spectrum graphics of the chemical-morphological domains of complex biomass by low field proton NMR energy relaxation signal analysis. *Energy and Fuels, 32*(4), 5090–5102. https://doi.org/10.1021/acs.energyfuels.7b03339

Wohlert, M., Benselfelt, T., Wågberg, L., Furó, I., Berglund, L. A., & Wohlert, J. (2022). Cellulose and the role of hydrogen bonds: Not in charge of everything. *Cellulose, 29*(1), 1–23. https://doi.org/10.1007/s10570-021-04325-4

Wu, J., Bai, J., Xue, Z., Liao, Y., Zhou, X., & Xie, X. (2015). Insight into glass transition of cellulose based on direct thermal processing after plasticization by ionic liquid. *Cellulose, 22*(1), 89–99. https://doi.org/10.1007/s10570-014-0502-1

Xiao, C., Zhang, Z., Zhang, J., Lu, Y., & Zhang, L. (2003). Properties of regenerated cellulose films plasticized with α-monoglycerides. *Journal of Applied Polymer Science, 89*(13), 3500–3505. https://doi.org/10.1002/app.12509

Yazdi, M. K., Seidi, F., Jin, Y., Zarrintaj, P., Xiao, H., Esmaeili, A., … Saeb, M. R. (2021). Crystallization of polysaccharides. *Polysaccharides, 283–300*. https://doi.org/10.1002/9781119711414.ch13

Zain, N. F. M. (2014). Preparation and characterization of cellulose and nanocellulose from pomelo (Citrus grandis) albedo. *Journal of Nutrition & Food Sciences, 5*(1), 1000334. https://doi.org/10.4172/2155-9600.1000334

Zhang, X., Tschopp, M. A., Shi, S. Q., & Cao, J. (2012). Molecular dynamics simulations of the glass transition temperature of amorphous cellulose. *Applied Mechanics and Materials, 214*, 7–11. https://doi.org/10.4028/www.scientific.net/AMM.214.7

Zhang, Y., Qi, J., Zeng, W., Huang, Y., & Yang, X. (2020). Properties of dietary fiber from citrus obtained through alkaline hydrogen peroxide treatment and homogenization treatment. *Food Chemistry, 311*, Article 125873. https://doi.org/10.1016/j.foodchem.2019.125873

Zhao, H., Chen, Z., Du, X., & Chen, L. (2019). Contribution of different state of adsorbed water to the sub-T g dynamics of cellulose. *Carbohydrate Polymers, 210*, 322–331. https://doi.org/10.1016/j.carbpol.2019.01.087

Annex B

Published research article: Impact of processing and storage on citrus fiber functionality: Insights from spectroscopic techniques

International Journal of Biological Macromolecules 282 (2024) 137281

Contents lists available at ScienceDirect

International Journal of Biological Macromolecules

journal homepage: www.elsevier.com/locate/ijbiomac

Impact of processing and storage on citrus fiber functionality: Insights from spectroscopic techniques

G.O. Coelho [a], D. Champion [a], O. Heintz [b], A. Krystianiak [b], S. Debon [c], I. Deleris [c], J. Wallecan [c], G. Roudaut [a,*]

[a] Université Bourgogne Franche-Comté, Institut Agro, Université Bourgogne, INRAE, PAM UMR A 02.102, F-21000 Dijon, France
[b] Laboratoire Interdisciplinaire Carnot de Bourgogne (LICB), UMR CNRS 6303, Université de Bourgogne Franche-Comté, 9 avenue Alain Savary, 21078 Dijon CEDEX, France
[c] Cargill R&D Centre Europe, Havenstraat 84, 1800 Vilvoorde, Belgium

ARTICLE INFO

Keywords:
Citrus fiber
Functional properties
Spectroscopy
Structure
Chemical composition
Surface composition
Process impact
Storage effect

ABSTRACT

To deliver their functionality when used in applications, citrus fibers need to be rehydrated. Factors such as chemical composition, structural organization as well as chemical surface composition are known to influence this functionality. Processing and storage conditions can affect these parameters, making it challenging to maintain stable functionality. This study used Fourier-transform infrared spectroscopy (FTIR) and X-ray photoelectron spectroscopy (XPS) to evaluate the effects of preparation and storage on citrus fibers. Samples dried at different scales and stored for 360 days under room and accelerated conditions were assessed for water holding capacity (WHC), water swelling capacity (WSC), and gel rigidity (G′). The results showed a decline in WHC, WSC, and G′ over time, confirming that aging negatively impacts moisture retention, particularly under higher water content or temperature. Drying scale had no effect on chemical composition or structure, but changes in the elemental surface composition of carbon and oxygen were noted. While prolonged storage altered the polysaccharides' chemical composition and structure, leading to functionality loss, XPS analysis revealed no changes in surface composition. Loss of functionality cannot be explained by chemical surface composition modifications.

1. Introduction

Citrus (i.e. orange, lemon, pomelo) are the most important crops in the world, with an annual production of around 104 million tons [1]. An important part of this production is processed in juice and jams [2]. However, this enormous range of applications results in a huge quantity of by-products, including peels, seeds and pomace, corresponding to 40–60 % of total fruit mass [3,4]. For this reason, many researchers are looking to maximize the utilization of citrus waste by finding valorization routes.

Citrus by-products can be a potential source of pectin and essential oils [4]. The peels by-product originating from pectin extraction, known as citrus fiber, has an interesting composition (80 % carbohydrate, 8 % of protein and small quantity of ash and lipids) [5]. This composition and the structural organization of citrus fiber give this system interesting functionalities, such as rheological properties, high-water holding capacity (WHC), water swelling capacity (WSC) as well as oil-holding capacity (OHC) [6–8]. It can be used as a gelling/thickening agent and be applied to dairy products, desserts, soft drinks, frozen foods, meat and pharmaceutical products [9]. Chemical and mechanical pretreatments applied to fibers such as bleaching, milling, and high-pressure homogenization are known to potentialize their functionalities [6–10] for many applications [9].

One of the major challenges in the industry is the functionality preservation during drying and storage [11]. The effect of drying on the rehydration behavior of powders has been widely studied and some mechanisms have been proposed to explain the alterations, such as the pressure unbalance between the inner of the material and external pressure; microscales structural modifications; and molecular bonding changes. These modifications enhance molecular contact, induce irreversible agglomeration, and thereby render functional recovery partially or completely impossible during the reconstitution process [12,13].

While the effects of drying have been studied, there is a lack of understanding of the impact of storage on the functional properties of

* Corresponding author.
E-mail address: gaelle.roudaut@institut-agro.fr (G. Roudaut).

https://doi.org/10.1016/j.ijbiomac.2024.137281
Received 28 June 2024; Received in revised form 17 October 2024; Accepted 4 November 2024
Available online 5 November 2024
0141-8130/

powders. Most published reports focused on the negative impact of aging on the solubility and hydration properties of dairy products [14–18]. For plant-based products, studies typically explore how drying or aging affects antioxidant compounds and functional properties, only suggesting potential physical changes [9–15]. However, the relationship between functional properties and factors such as chemical composition (e.g., monosaccharide sequence, glycosidic linkages) and surface characteristics (e.g., charge density, hydrophilic/hydrophobic balance) remains unexplored [26].

Storage has been shown to alter the degree of esterification of pectin, significantly affecting its emulsification and gelling properties, thus impacting its utilization in various products [27–30]. Chemical changes may also impact hydration properties by influencing the orientation and rearrangement of water molecules within functional groups [31,32]. As reported by Popescu et al. [33], polymeric materials age from the surface; sensitive methods of investigation of surface modifications are then necessary for an accurate representation of the early stages of deterioration.

Moreover, monitoring the complexity of aging materials appears crucial: Gaiani et al. [14] observed lipid migration to the surface in phosphocaseinate powder upon storage (60 days) which deteriorated the wetting properties of this powder.

Fourier transform infrared spectroscopy (FTIR) is a valuable tool for analyzing changes promoted by chemical reactions during drying and storage e.g. oxidation, depolymerization, decarboxylation and de-esterification [23,34,35]. This technique has also been applied to monitor the aging of cellulose particularly considering changes in the carbonyl region [36,37]. X-ray photoelectron spectroscopy (XPS) is a well-established technique for determining surface composition, which has been applied to various materials, including biological powders (e.g., dairy products), plant-based products (e.g., wood, agricultural products), and more [33,38–40]. XPS has been used to correlate surface deterioration with chemical reactions occurring on the surface during storage [33].

As noted, mechanistic studies on the loss of functional properties due to the drying and storage are scarce, especially for citrus cell wall-based materials [41,42]. Unlike previous studies, this study aims to fill this gap by employing advanced spectroscopic techniques (XPS and FTIR) to investigate the changes in citrus fiber's functional properties during processing and storage. For this purpose, citrus fiber dried at different scales were compared, and the impact of storage time and condition investigated by storing citrus fiber samples in ambient and accelerated conditions prior to their characterization. By examining the relationship between surface composition, chemical structure, and functional properties, we aim to provide new insights that could contribute significant information for shelf-life studies.

2. Experimental

2.1. Sample preparation and storage

Citrus fiber sample (CF) was prepared and provided by Cargill (Baupte, France). CF was extracted with isopropanol/water mixture using high pressure, then dried at pilot-scale, using a fluid-bed drier (Glatt GVW 32/WSG200, Germany) for 7 h with a maximum inlet temperature of 110 °C until product maximum temperature reached 50 °C. Its final dry matter content was 92 % and its bulk density 0.41 g/cm^3.

The resulting material is composed of cellulose, hemicellulose, pectin, protein, and ash, in a mass proportion of 53.0 ± 7.4 %, 20.0 ± 8.8 %, 17.0 ± 2.4 %, 6.3 ± 0.3 % and 3.7 ± 0.2 % g/100 g dry basis, respectively (data provided by the supplier). The coefficients of variability of the batches and campaigns are 14 % cellulose, 44 % hemicellulose, 14 % pectin, 7 % protein and 6 % ash.

To study the storage time effect, CF was stored for 360 days under two different controlled conditions of storage: in "accelerated" conditions (40 °C and 75 % relative humidity (RH)) (CF_A) and in room conditions (20 °C and 30 % RH) (CF_R). Extensive characterization was done every 45 days to evaluate the effect of storage on its properties (Fig. 1).

A second set of citrus fiber, CFV, corresponds to spent peels processed similarly to CF, but stored in 40–45 % isopropanol/water until final drying. Aliquots were dried every 45 days over 360 days at lab-scale, using a Mini Glatt fluid-bed drier (Glatt, Germany) for 40–45 min, with an inlet temperature of 50 °C until sample temperature reached 40 °C. Its characteristics were determined in parallel with that of sample CF. All samples were in a powder form, milled and sieved with 50 μm size sieve (Fig. 1). Its final dry matter content was 96 % and its bulk density 0.29 g/cm^3.

2.2. Physicochemical properties

2.2.1. Water holding capacity (WHC)

The citrus fiber was used as received (packaged material at around 7 % water content). It was suspended at 1 % *w*/w in a buffer solution containing 0.1 M potassium dihydrogen phosphate (pH 6.9), under constant magnetic stirring for 30 min at 700 rpm. Subsequently, the suspension was transferred to a centrifuge tube and centrifuged at 3000*g* for 10 min at 25 °C. The WHC was obtained using Eq. (1) [8,43].

$$WHC = \frac{(m_2 - m_1)}{m_0} \quad (1)$$

where m_0 is the dried sample weight, m_1 is the weight of the centrifuge tube with sample prior to hydration, and m_2 is the weight of centrifuge tube with hydrated fiber. In this calculation, $m_2 - m_1$ reflects the total mass gain due to the absorption of the buffer solution by the citrus fiber. Since the whole hydration occurs in the buffer, this value represents the total amount of solution absorbed by the sample.

2.2.2. Water swelling capacity (WSC)

Citrus fibers powders were dispersed in a buffer containing 0.1 M potassium dihydrogen phosphate (pH 6.9) at a concentration of 0.2 % *w*/w and magnetically stirred for 30 min at 700 rpm. Afterward, the dispersions were transferred into a 100 mL measuring cylinder. The bed volume was measured after 24 h and divided by the dried powder dry initially introduced into the test tube [44].

2.2.3. Storage modulus measurement

Rheological properties of samples were measured using MCR 302 (Anton Paar, Graz, Austria) rheometer with a concentric cylinder (CC17) device (conical bottom of 16.667 mm diameter and cup of 18.088 mm diameter). For the measurement, 2 % *w*/w citrus fiber dispersions were prepared in a buffer containing 0.1 M potassium dihydrogen phosphate (pH 6.9), under magnetic stirring for 30 min at 700 rpm. The suspension was homogenized using an IKA Ultra-Turrax T25 Homogenizer (IKA, Staufen, Germany) for 10 min at 9500 rpm. Samples were pre-sheared for 30 s to ensure temperature equilibration and avoid possible effects of sample manipulation and loading history. The linear viscoelastic region (LVR) of the samples, tested beforehand, was identified at a constant angular frequency of 6.28 rad/s (1 Hz) and a strain sweep from 0.01 to 1000 % strain. A similar procedure was carried out to investigate the dependency of the storage and loss moduli (G' and G'' respectively) on the angular frequency, keeping the strain amplitude of 1 % and varying the angular frequency between 628 and 0.628 rad/s (from 100 to 0.1 Hz). The viscoelastic characteristics of CF suspensions were obtained based on G' at 6.28 rad/s and 1 % strain. All measurements were performed in triplicate and mean values are reported with standard deviation.

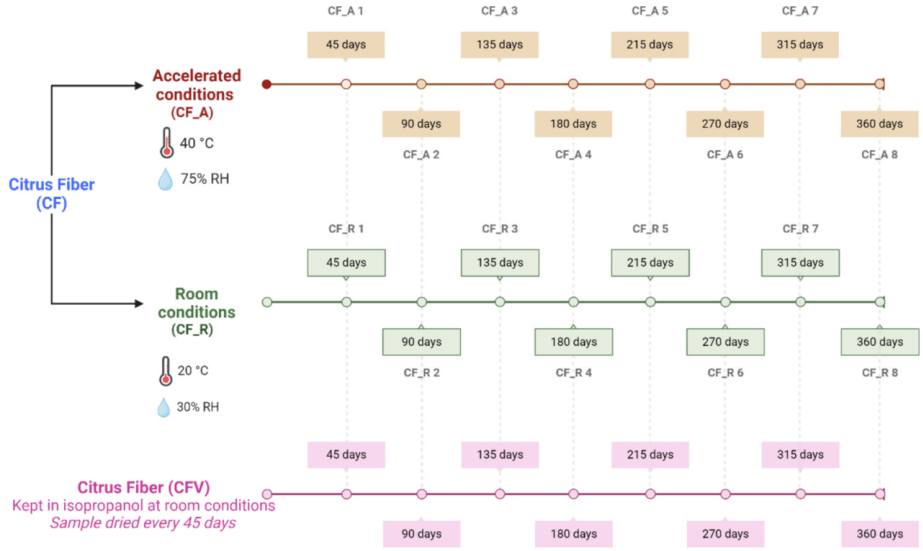

Fig. 1. Citrus fiber samples preparation and storage.

2.3. Chemical characterization of citrus fibers

Spectral acquisition was performed in Perkin Elmer Spectrum 65 FTIR spectrometer equipped with Spectrum 10 Software version 10.6.2.1159 (Perkin Elmer, Massachusetts, US) and attenuated total reflection (ATR) cell with single reflectance germanium crystal. The spectral resolution was fixed to 4 cm^{-1}, the number of scans to 16 and the selected spectral range between 4000 and 650 cm^{-1}, with a background spectrum recorded initially. The samples used were in dried powder form (equilibrated during at least 7 days at 0 % RH over phosphorus pentoxide (P_2O_5)). To assess repeatability, all samples were analyzed in triplicate, and the standard deviation along with the Margin of Error (MoE) was calculated to evaluate the variability between the replicates, with a focus on the regions exhibiting the greatest bands (3700–3000 cm^{-1}, 1500–1750 cm^{-1}, and 930–1196 cm^{-1}). Baseline corrections were done using the Spectrum 10 Spectroscopy software (PerkinElmer, US).

2.4. Powder surface composition characterization by X-ray photoelectron spectroscopy

The elemental surface composition of citrus fiber samples was measured by X-ray Photoelectron Spectroscopy (XPS). Spectra were obtained using an XPS-Auger PHI 5000 VersaProbe (Physical Electronics, Minnesota, US) equipped with a mono-chromatic Al Kα X-ray source ($h\nu = 1486.6$ eV) operated at 50 W (15 kV, 3.3 mA). Measurements were performed in ultra-high vacuum ($10^{-7}/10^{-8}$ Pa). The analytical area of analysis is a disc of 200 μm of diameter and the analytical information depth between 3 and 4 nm. The spectra were collected at a take-off angle of 45°. The repeatability of X-ray photoelectron measurements for citrus fiber samples was assessed with varying numbers of scans to define optimal analysis conditions (general spectra were obtained by 2 scans whereas high resolution analysis for carbon (C 1s) and oxygen (O 1s) were obtained by 4 scans), accounting for potential surface degradation due to prolonged high vacuum exposure. To evaluate the variability between the replicates, the standard deviation along with the MoE were calculated.

Before analysis, samples were stored at 0 % RH for 7 days, in a desiccator with phosphorus pentoxide (P_2O_5) to remove the water. Afterward, the samples were outgassed under vacuum for 24 h and pressed into indium foil.

XPS spectra were treated using the CasaXPS version 2.3.24 software. The C 1s peak at 285 eV was used to calibrate the binding energy scale. The main elements (C, O, N, Na) detected on the sample's surface were identified by means of their respective binding energy, and the result was given in atomic percentage (% At.). Besides, the carbon and oxygen peaks were decomposed into their main chemical bonds (C-C/C-H, C—O, C═O, O-C-O, O-C═O).

2.5. Statistical analysis

To verify the statistical significance of all parameters the values of means ($n = 3$) ± SD were calculated. Analysis of variance was conducted for each variable measured to investigate the effect of storage time and conditions. One-way ANOVA and Tukey's test were performed using Origin 2023 software (OriginLab, US). The level of statistical significance was $p < 0.05$. To evaluate the interaction effects between the functional properties (WHC, WSC and storage modulus) and to identify chemical changes during storage time in citrus fiber, principal component analysis (PCA) was applied. Orange Data Mining Software version 3.33.0 (University of Ljubljana, SI) was used to perform PCA analysis. Each spectrum was preprocessed, normalized (standard normal variate (SNV)) and transformed from transmittance to absorbance.

3. Results and discussion

3.1. Physicochemical characterization of citrus fiber

Table 1 shows the WHC and storage modulus of citrus fibers CF and CFV. The WHC of samples CF and CFV at time 0 were 17.6 ± 0.5 g of water/g of dry sample and 17.4 ± 0.4 g of water/g of dry sample, respectively, and were not significantly different. Similar values were

Table 1
Functional properties of samples CF and CFV at time 0.

Samples	WHC (g/g of sample)	WSC (mL/g of sample)	G′ (Pa)
CF	$17.6^{a} \pm 0.5$	$63.0^{a} \pm 6.4$	$424^{a} \pm 3$
CFV	$17.4^{a} \pm 0.4$	$52.8^{a} \pm 5.9$	$430^{a} \pm 36$

Data were expressed by means ($n = 3$) ± standard deviation. Values followed by different letters in the same column are significantly different ($p < 0.05$).

found in the literature for so called citrus fibers between 14.97 and 15.75 g/g for citrus fiber from orange homogenized under pressure (30 MPa) [8]; 18.26 and 21.32 g/g to citrus fiber from citrus peels submitted to homogenization and alkaline treatment, respectively [10]; 22 g/g for untreated citrus fiber from Fiberstar company [45].

The WSC of CF and CFV (Table 1) at time 0 were higher than those observed in the literature which varied from 15 to 36 mL/g. It could be explained by the different structure (surface, porosity) and chemical composition, known to impact the water swelling capacity [46]. Additionally, the measurement protocols are not always the same, notably the sample concentration.

The G′ at time 0 (freshly dried sample) was equal to 424 ± 3 Pa for CF and 430 ± 36 Pa for CFV (Table 1). No significant difference was observed between CF and CFV samples on WHC, WSC and G′ values, indicating that drying at different scales did not impact sample functionality.

3.1.1. Survey of stability of citrus fiber in long term storage

Fig. 2 shows the variation of functional properties of citrus fiber upon storage in both accelerated and room conditions.

Fig. 2a illustrates the variation of WHC values for samples CF_R and CF_A. The sample stored in room conditions (CF_R) only showed significant difference with the value at time 0 after 135 and 270 days of storage in room conditions which indicates a minimal effect of time on WHC. For samples stored under accelerated conditions significantly lower values were observed between WHC at time 0 and 45, 135, 270, 315, and 360 days.

When CF was stored in room conditions (CF_R), the WSC decreased from 63 to 28 mL/g of sample (Fig. 2b). When the sample was stored in accelerated conditions, WSC decreased from 63 to 23 mL/g of sample during the first 135 days of storage. Then, WSC continued to decrease but to a lesser extent. For this functional parameter, keeping the citrus fiber at both milder temperature and humidity conditions helped slow down the evolution observed in the samples during storage.

The storage modulus (G′) of CF_A decreased from 424 Pa to 109 Pa, between 180 and 360 days-period (Fig. 2c). It is especially marked after 180 days. Stored in room conditions, the sample's storage modulus remained almost constant until 180 days of storage and also showed a significant decrease (40 %) although to a lesser extent than in

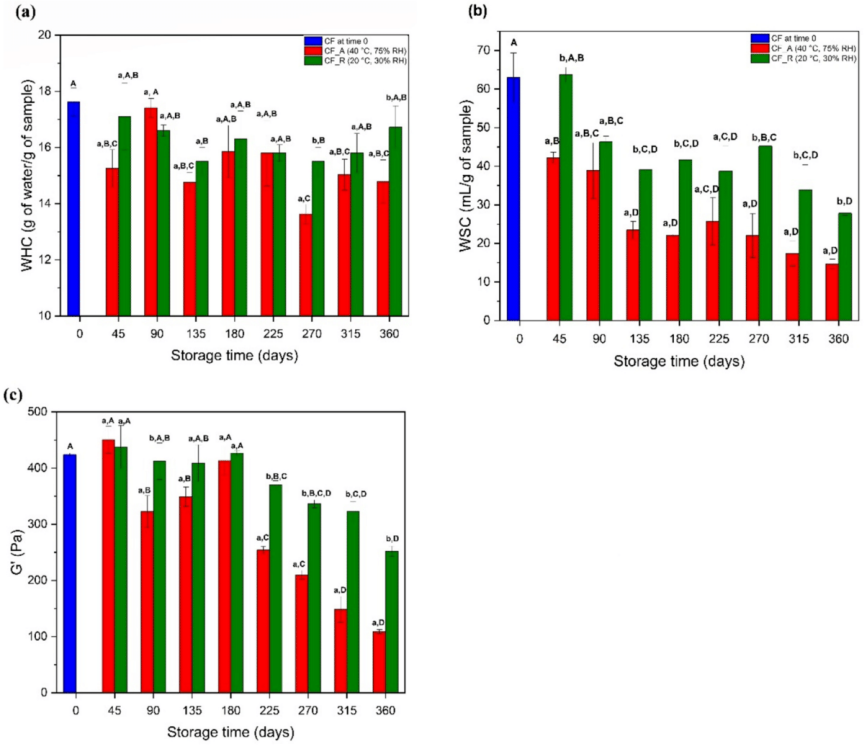

Fig. 2. Evolution of WHC (a); WSC (b); and storage modulus (G′) (c) for citrus fiber after being storage in accelerated aging conditions (CF_A) (40 °C, 75%RH), or room conditions (CF_R) (20 °C, 30 % RH). *Data were expressed by means ($n = 3$) ± standard deviation. Values followed by capital letters are significantly different from other storage time (each storage condition was compared separately) ($p < 0.05$). Different lower-case letters denote significant differences between storage conditions for each storage time ($p < 0.05$).*

accelerated conditions (74 %). This result was in agreement with the variation of the WSC after storage in the different conditions (Fig. 2b).

PCA analysis was performed on the 3 functional properties (WHC, WSC and storage modulus) to further evaluate their interactions effect (Fig. 3) and possibly highlight the time effect.

The first principal component (PC1) has a higher significance, explaining 72.6 % of the total variance whereas the second principal component (PC2) explained 18.4 % of the total variance.

PC1 generally separated the samples according to storage time whereas PC2 did not. The CF at time 0 and the samples aged up to 90 days of storage in accelerated aging conditions (CF_A 1 and CF_A 2) were distributed on the positive side of PC1. The samples stored between 90 and 225 days (CF_A 3, CF_A 4, CF_A 5) showed scores close to the crossing of axes, indicating fewer variance in functional properties, whereas those stored for >225 days (CF_A 6, CF_A 7 and CF_A 8), stayed in the negative side of PC1.

PC1 was most positively influenced by WSC, meaning that changes in the water swelling capacity had the greatest impact on the separation of samples along this component. PC2, on the other hand, was positively influenced by G′ and negatively by WHC, indicating an inverse relationship between WHC and G′ in explaining the variance along PC2.

To further reveal the relationship among different functional properties, the angle of the loading plots of PC1 versus PC2 were produced. Pair-wise parameters with small angles had positive correlation among them: suggesting WSC was positively related to G′ and to WHC (small angles). On the other hand, WHC and storage modulus do not seem to be related (as revealed by a 90°-angle).

Although there are some studies on the stability of fibers containing foods during processing and storage [47–51], no clear explanation exists for the loss of citrus fibers' functional properties during storage. Several researchers discussed the hornification as a cause of decrease in water absorption for cellulosic matrices [12,52–54]. The decrease of hydration capacity with increasing storage time may be related to the decreased capacity of fibers to expand, possibly due to a reallocation of internal hydrogen bonds [55].

A better knowledge of storage effects on the chemical properties of citrus fiber remains needed to explain the reduction of functional properties as well as the combined effect of temperature and humidity.

3.2. Chemical characterization of citrus fiber

3.2.1. Effect of sample preparation in a chemical composition of citrus fiber

Fig. 4 compares the FTIR spectra of non-aged sample dried either at pilot scale (CF) or at lab-scale (CFV).

Full information of all the vibrational modes present in the spectra is shown in Table 2. The two samples showed a very similar spectra with slight intensity differences between some bands in the region 1800–1200 cm^{-1}. The region between 1200 and 850 cm^{-1}, known as fingerprint region, is ascribed to the polysaccharides, and is very complex. Then, it is almost impossible to differentiate and associate specifically these bands to cellulose, hemicellulose and pectin separately [56].

The variability between replicates for both samples was minimal, with a low standard deviation and an average coefficient of variation (CV) of 7.6 %. Additionally, the relative MoE was below 10 % with a 99 % confidence level, indicating that the results are reliable. Furthermore, no significant difference was observed between CF and CFV, suggesting that the drying scale had no impact on the chemical composition, molecular structure, or chemical bonds of the citrus fibers.

3.2.2. Effect of long-term storage on the chemical structure of citrus fiber

The FTIR spectra for citrus fiber stored in different conditions for different storage times are presented in the *supplementary material* (Fig. S-1). Most of the differences between samples stored in accelerated conditions (Fig. S-1a), were observed in three regions in which band intensity oscillated with time: in the broad band between 3000 and 3750 cm^{-1} is associated with -OH stretching of cellulose and hemicellulose; in the band around 3000 and 2850 cm^{-1} corresponding to CH and CH_2 stretching of cellulose and hemicellulose; and in the band around 1030 cm^{-1} related to C—O deformation at C6 in cellulose [57,60].

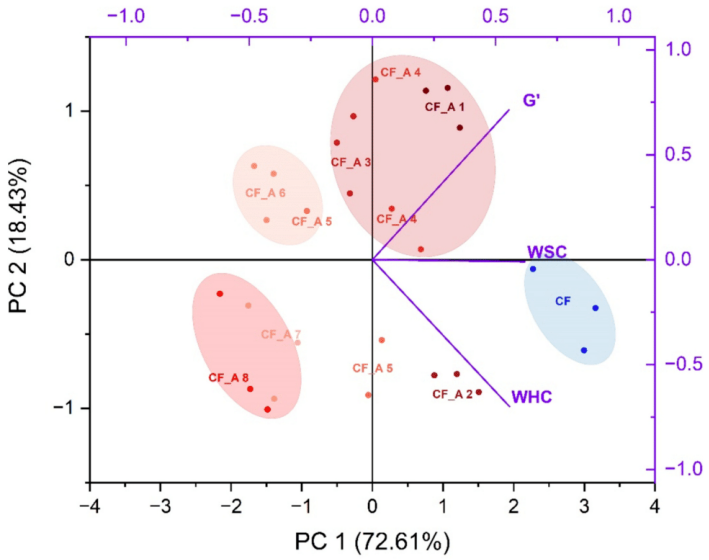

Fig. 3. Principal component analysis (PCA) describing the variations in physicochemical properties of CF: simplified loading and score plot for G′, WHC, WSC values for samples stored for different time in accelerated aging conditions (CF_A) (40 °C, 75 % RH) ($n = 3$).

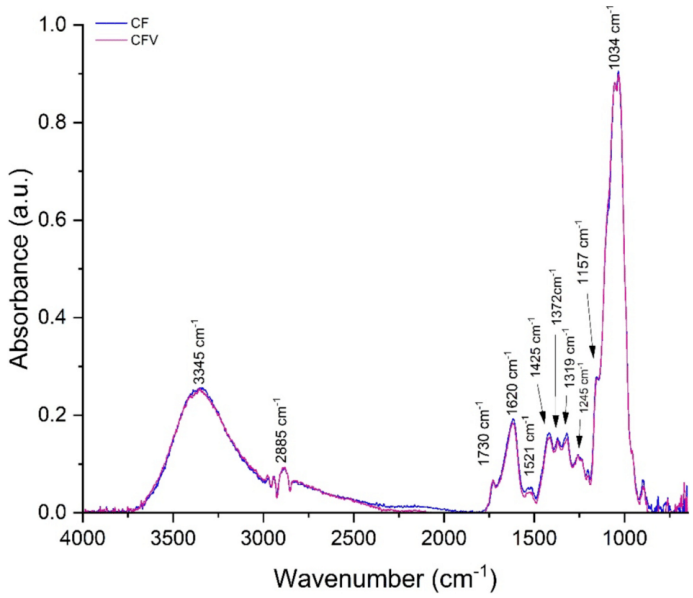

Fig. 4. FTIR spectra of dry citrus fibers dried in two different conditions: CF and CFV.

Table 2
Assignment of the main absorption bands in FTIR spectra of citrus fibers. FTIR data were assigned according to Célino et al. [57]; Liu et al. [58]; Szymanska-Chargot & Zdunek [59].

Wavelength (cm^{-1})	assignment
3345	Hydrogen bonded of OH stretching in cellulose and/or hemicellulose
2285	Stretching of C—H bonds from methyl and methylene groups of polysaccharides
1730	C=O stretching acetyl or carboxylic acid of galacturonic acid in pectin
1620	COO- antisymmetric stretching ions from polygalacturonic acid (pectin ester group)
1521	Amid II N—H deformation from protein
1425	Carboxylic acid of pectin and COO− vibration
1372	CH bending of cellulose (amorphous)
1319	CH_2 bending of cellulose (crystalline)
1245	C–O stretching (pectin)
1157	Anti-symmetrical deformation of the C-O-C band (cellulose or hemicellulose)
1034	C–O stretching, C—C stretching (cellulose or hemicellulose)

In addition, a slight increase in the intensity of the band around 1318 cm^{-1} from 180 days of storage was observed, could suggest an increase in crystallinity, however this is not supported by a clear reduction of the band around 1337 cm^{-1} which could confirm a conversion from amorphous to crystalline cellulose [61]. The band around 898 cm^{-1} varied after 225 days of storage in accelerated conditions, it may represent a rearrangement of cellulose fraction in CF.

When storage conditions were compared (Fig. S-1b), the overall FTIR spectra appeared similar, suggesting no impact of humidity and/or temperature on chemical bonds.

Despite all possible modifications described in the literature, identifying changes in the spectrum represented in Fig. S-1a was challenging due to the large number of samples. PCA analysis was applied for unique storage condition (accelerated conditions) and for different storage times to better investigate the effect of time.

3.2.2.1. Exploratory data analysis of samples stored in accelerated aging conditions. As reported by Szymanska-Chargot & Zdunek [59], the region between 1200 and 850 cm^{-1} is characteristic of stretching vibration of C—O, C—C, CH_2 of ring structures, and is the one to favor to study carbohydrates. In this region, there is almost no influence of proteins and water absorption. Another interesting region is between 1800 and 1200 cm^{-1} [62,63] which can be related to carbonyl esters, and carboxylates from pectin. The PCA analysis was therefore carried out for these two spectra ranges 1800–1200 cm^{-1} and 1200–850 cm^{-1}, to try and reveal differences between samples with storage time at 40 °C and 75 % RH.

Fig. 5 presents the scores scatter plot PC1 (61.8 %) × PC2 (21.8 %) for data in the 1800 to 1200 cm^{-1} region and demonstrates the differences between samples. The major variability is observed in PC1 which separated the samples for the shortest storage time (CF, CF_A 1, CF_A 2 and CF_A 3) on positive side from the samples stored for long time (CF_A 4, CF_A 5, CF_A 6, CF_A 7) on the negative side, while CF_A 8 appeared in the middle. PC2 seems to distinguish samples as a function of storage time, with the exception of CF_A 2 and CF_A 8 samples.

Variable loadings for PC1 and PC2 are presented in Fig. 5b. Positive loadings for PC1 cover the wavenumbers characteristic of pectin (1741, 1394, 1228 cm^{-1}) and one for cellulose and/or hemicellulose (1295 cm^{-1}). Negative loadings for PC1 are limited to the region around 1648 cm^{-1} which may be associated with tautomer carbonyl group/enolic (ketone/aldehyde) or amide I. It suggested changes over storage, mainly in the content and/or structure of pectin or proteins. On the other hand, PC2 positive loadings pattern is characteristic of COO^- antisymmetric stretching polygalacturonic acid (1616 cm^{-1}) and water (1640 cm^{-1}) while the wavenumbers which negatively influenced PC2 scores are correlated to cellulose or xylose-containing hemicellulose (1467 cm^{-1}) and to esterified carboxyl groups of pectin (1745 cm^{-1}) [58,59,64].

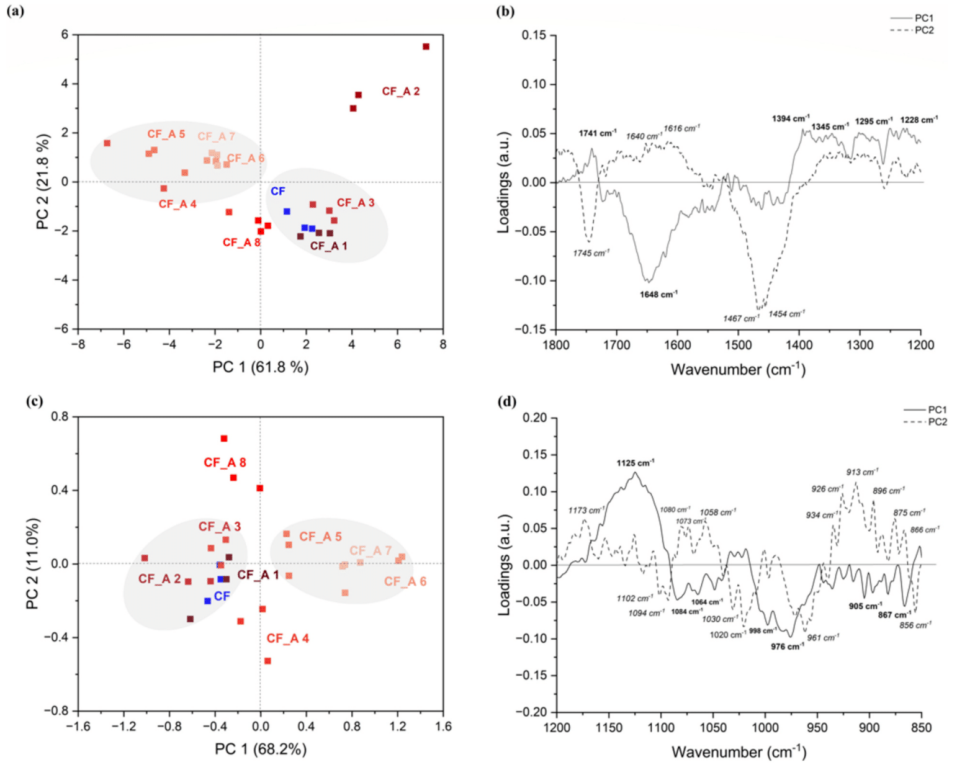

Fig. 5. PCA scores scatter plot (a) and loadings plot (PC1 and PC2) (b) of citrus fiber FTIR spectra in the 1800–1200 cm^{-1} region, PCA scores scatter plot (c) and loadings plot (PC1 and PC2) (d) of citrus fiber FTIR spectra in the 1200–850 cm^{-1} region in different storage times.

Combining the information loadings pattern of PC1 and PC2 suggested that some pectin de-esterification happened during the storage of citrus fiber or alteration in protein structure after 135 days of storage.

Considering the region 1200–850 cm^{-1} (Fig. 5c), the scores scatter plots PC1 (68.2 %) x PC2 (11.0 %) showed a spreading of the data along the PC1 axis. PC2 axis seems to separate mainly CF_A 4 and CF_A 8.

PC1 loadings have negative values around 1084 and 976 cm^{-1} characteristic of pectin (C—O and C—C stretching and CO bending) and 1064, 998, 905 and 867 cm^{-1} characteristic of hemicellulose and cellulose (Fig. 5d) whereas the loadings were only positive for PC1 at 1125 cm^{-1} characteristic of C—O and C—C stretching of cellulose or hemicellulose. Thus, PC1 suggested that after 135 days, the impact of storage became more pronounced, and the samples are mainly differentiated through pectin and cellulose and/or hemicellulose contribution. In the initial period of storage (before 135 days), the samples were separated by the bands associated with pectin. However, after 135 days, the bands are correlated to cellulose and/or hemicellulose became more prominent in their differentiation.

PC2 loadings showed negative and positive values (Fig. 5d). The wavenumbers which positively influenced the scores are around 1173, 1080, 1073, 1058, 934, 926,896, 875, 866 cm^{-1}, corresponding to cellulose and hemicellulose and only 913 cm^{-1} related to pectin. The negative influence is in the wavenumbers 1102, 1094, 1020, 961 and 856 cm^{-1} mainly associated with pectin (C—O and C—C stretching, CO bending and ring vibration) and 1030 cm^{-1} correlated to cellulose [58,59,64]. Comparing CF_A 4 and CF_A 8, PC2 indicated that CF_A 8 was separated by the bands primarily associated with cellulose and hemicellulose, whereas CF_A 4 was differentiated by bands correlated to both cellulose and pectin.

Although the group separation in the region 1200–850 cm^{-1} is less clear, the PCA analysis underscored a distinct transformation in the chemical structure of citrus fiber over the storage period, with an initial dominance of pectin and/or protein influence transitioning to a greater contribution from cellulose and hemicellulose as storage time increased. This finding suggests that prolonged storage under accelerated conditions significantly affects the composition and structural integrity of citrus fiber.

3.3. *Chemical surface composition of citrus fibers studied with XPS*

3.3.1. *The impact of sample preparation on surface composition of citrus fibers*

In citrus fiber, the two most common chemical elements detected were carbon (70 %) at 284.9 eV and oxygen (30 %) at 532.9 eV (Table 3). Sodium (0.2 %) and nitrogen (0.6 %) only represented traces. Quantitative analysis of the repeatability of XPS measurements showed a standard deviation of 0.6 % for carbon and oxygen, and <0.05 % for sodium and nitrogen. Moreover, the relative MoE (99 % confidence level) was evaluated to be below 10 %, indicating the reliability of the measurements.

Table 3
Quantitative analysis of surface composition of citrus fibers prepared in two different ways: immediately dried (CF) and kept in IPA for 45 days before drying (CFV) then dried at different scales.

Sample	C (%)	O (%)	N (%)	Na (%)	O/C
CF	68.7 ± 0.7^{a}	30.3 ± 0.6^{a}	0.6 ± 0.1^{a}	0.3 ± 0.1^{a}	0.4 ± 0.0^{a}
CFV	62.4 ± 0.4^{b}	36.5 ± 0.4^{b}	0.7 ± 0.1^{a}	0.3 ± 0.2^{a}	0.6 ± 0.0^{b}

Data were expressed by means ($n = 9$) $\pm$ standard deviation. Values followed by different letters in the same column are significantly different ($p < 0.05$).

The carbon and oxygen values observed for sample CF at time 0 were similar to the results obtained on fruits powders by Gaudel et al. [65] or grewia polysaccharide gum [40]. Considering an average conversion factor of 6 for vegetable proteins [66], the percentage of proteins on the surface would not reach 4 %, which is less than the total protein amount of 6.3 %. This observation suggests that the proteins present in the citrus fiber samples studied are under-represented on the surface of the fiber particles and therefore are more present in the core of these particles. This can be due to strong interactions of these proteins with other components located in the core or due to the migration of some components to the core during the drying. The origin of sodium atoms may be from the pretreatment of citrus fiber, such as bleaching i.e. use of hydrogen peroxide and sodium bisulfite.

The greatest difference between samples CF and CFV was in carbon and oxygen content (Table 3). Sample CFV showed a lower carbon content and a higher oxygen content, with a difference of ~6 %.

The ratio O/C obtained for samples CF and CFV were 0.4 and 0.6, respectively (Table 3). These values were lower than the theoretical O/C value for cellulose (0.83), which suggested that their surfaces do not contain pure cellulose in agreement with the composition of the samples (Fig. 6). This value was similar to the value measured by Fras et al. [67] for pre-purified cotton specimens. Several studies attributed this low ratio to the presence of lignin and/or waxes [68]. However, citrus fiber does not contain lignin and the O/C ratio inferior of 0.83 may be due to a residual content of wax [69] and matrix complexity composition (cellulose, pectin, hemicellulose and low content of protein and ash).

Several researches investigated the effect of the drying process on the characteristics and functional properties of carbohydrate powders [40,70–72]. Nep & Conway [40] who studied the effect of drying method on the surface composition of grewia gum polysaccharide, only observed lower O/C ratio for air-dried sample compared to freeze-dried ones. According to Kim et al. [15], the water diffusion towards the surface is accompanied upon drying by an opposite diffusion of components towards the center. The surface composition depends on the size of molecules, *i.e.* larger molecules diffusing slower than smaller molecules; on the drying rates and temperatures: i.e. lower rates and slow temperature providing the components more time to migrate. Besides, the longer exposition to high temperature may promote degradation, reducing the O/C ratio [73].

Samples CF and CFV were dried at different process scales, sample CF

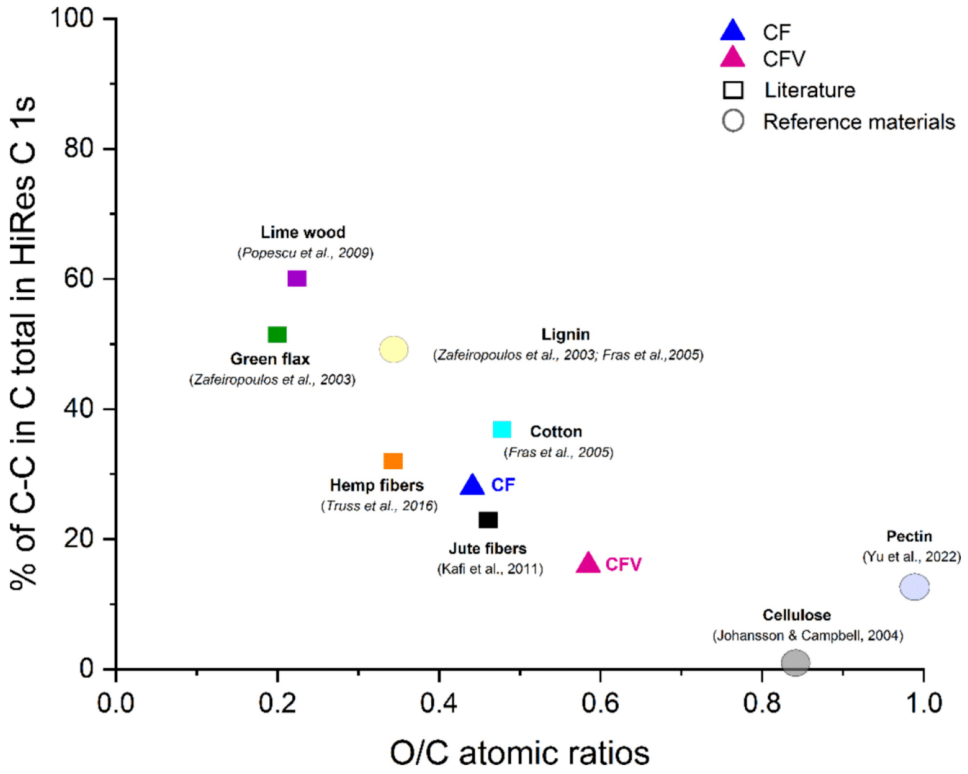

Fig. 6. Calculated O/C ratios and relative amounts of C—C bonded carbon in samples CF (immediately dried) and CFV (kept in IPA for 45 days and dried in different scale), calculated from XPS data compared with reference materials (cellulose, pectin and lignin and various literature values).

experienced longer drying time (7 h) and a higher temperature (sample temperature 50 °C) compared to sample CFV (45 min maximum, sample temperature of 40 °C). This could have led to more time for component migration to the surface, resulting in a different surface composition. In addition, the components on the surface of sample CF may be degraded by the longer exposure to 50 °C during drying, possibly reducing the ratio O/C.

Fig. 7 represents the area of the peaks from deconvolution of C1s and O1s high resolution scans. The C1s spectra was decomposed into 4 components (Fig. 7a). The carbon atoms bonded with one oxygen atom (C—O) (C2) appeared to be the most abundant for both CF and CFV, representing between 40 and 50 % of the total area of C. It most likely corresponds to the presence of polysaccharides on the surface (Truss et al., 2016). C1 can be associated with carbon atoms bonded with other carbon or hydrogen (C1) (C-C/C-H) while C3 could be correlated to carbon bonded with two oxygen atoms (C=O/O-C-O). CF had more carbon bonded to another carbon or hydrogen (C-C/C-H) than carbon double bonded to oxygen (C=O) or carbon bonded to two different atoms of oxygen (O-C-O), whereas sample CFV showed a higher quantity of carbon bonded to one or two oxygen atoms (C=O/O-C-O). These results agree with the elementary composition, since sample CFV had a higher quantity of oxygen than sample CF. It may correspond to by-products with lower oxygen content produced in CF (more intense drying) from the dehydration and/or degradation of biopolymers [73]. In addition, the lowest value of C4 (O-C=O) observed for both samples may indicate a low quantity of acid or ester on the citrus fiber surface [74]. However, the core of the fibers is likely to contain a significant presence of esters and acids, particularly due to the high pectin content.

Fig. 7b illustrates the high resolution of O 1 s, showing no significant difference between samples CF and CFV regarding carbon-oxygen bonds on the surface, mainly containing C═O bonds.

Another parameter widely used to characterize the surface is the ratio between C-C/C-H and other C bonds. These proportions provide information about the surface hydrophilicity/hydrophobicity. Both samples showed a ratio between 0 and 1 (CF ratio 0.40 ± 0.03 and CFV ratio 0.21 ± 0.02), corresponding to a hydrophilic character. Most of the polysaccharides are hydrophilic which explains the hydrophilic character of the citrus surface [75]. As observed before, CFV has more carbon bonded to oxygen, in agreement with a more hydrophilic surface than CF.

These results showed that the drying mode of citrus fiber can affect the surface composition: the drying process could degrade some compounds on the surface depending on the time and temperature. Then, controlling the sample preparation can be essential to obtain a more hydrophilic surface, to directly control the properties and applications of the product.

3.3.2. *The impact of storage time in surface composition of citrus fibers*

XPS analysis was performed on sample CF after different storage times in different conditions of storage to evaluate the impact of time on the surface composition as well as the impact of temperature and/or humidity.

The data of the surface atomic concentration of chemical elements (Supplementary material - Table S-1) showed there was no impact of storage time nor conditions on the surface composition of studied powders. Nonetheless, the effect of prior hydration and/or storage may have been masked by the sample's drying (desiccation over P_2O_5 before analysis). Additionally, XPS analysis only considers the sample's surface (the top few nanometers), and the functional property changes could be driven by deeper, bulk changes in the internal structure of the fibers rather than surface alterations.

Using the total area of the carbon and oxygen peaks, the ratio O/C was determined (Table 4): it varied between 0.41 and 0.46 for CF_A and CF_R respectively, with no clear effect of storage time. A slight variation with time was observed, but no trend versus time on C and O contents. If hydrolysis and/or oxidation had occurred during storage, this ratio would have risen [33].

Additional to the O/C ratio, the N/C was also calculated. The values hovered around 0.01, with no notable variation detected across storage conditions throughout the storage period. It discarded the possibility of changes in surface protein structure upon storage [76].

Table 4
Relative amounts of differently bound carbon and oxygen determined from high-resolution carbon C 1s and oxygen O 1s.

Days of storage	O/C	Area (%)					
		C1 (C-C/C-H)	C2 (C—O)	C3 (C=O/O-C-O)	C4 (O-C=O)	O1 (O-C=O)	O2 (C—O)
CF_A							
90	0.41	35.2	43.1	16.4	5.2	95.5	4.5
180	0.44	18.9	42.7	29.5	8.9	59.4	40.6
270	0.45	25.5	44.2	23.2	7.1	80.3	19.7
360	0.44	30.4	43.4	19.9	6.3	88.6	11.4
CF_R							
90	0.43	26.9	44.7	22.0	6.4	77.7	22.3
180	0.46	22.4	44.0	26.2	7.4	69.3	30.7
270	0.45	27.2	41.3	24.5	7.0	89	11.0
360	0.44	28.6	43.3	21.6	6.5	89.3	10.7

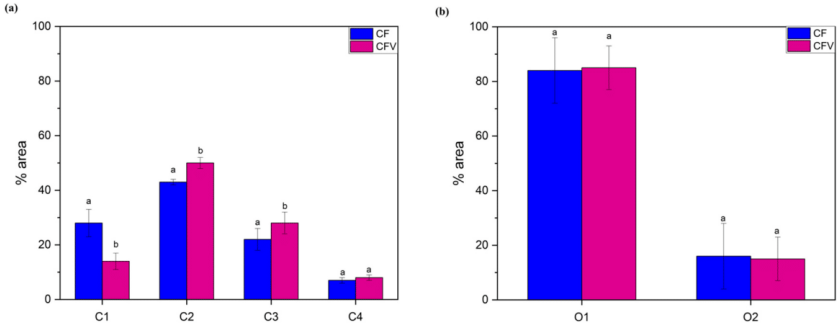

Fig. 7. Comparison of the % area of high-resolution scans of XPS spectra of C 1s and O 1s peaks for CF and CFV from different drying conditions: 4 components from C 1s peak deconvolution (a), and 2 components from O 1s peak deconvolution. Error bars represent standard deviation of the mean ($n = 9$). Means followed by the same letter in each bar group are not significantly different ($p < 0.05$).

As described before, the C 1s spectra was decomposed into 4 bonding states (Table 4). The initial relative amounts of different components were 33 % of C1, 43 % C2, 19 % of C3 and 5 % C4. CF_A and CF_R showed no significant difference for any C 1s. Then, as with the other determined parameters, no effect of temperature or humidity was observed on surface composition upon storage. CF had an initial composition of 91 % of O1 and 9 % of O2 (Table 4). The oxygen components oscillated during the storage more than carbon components, with a standard deviation of 10 %. Although this variation was considerable, the same behavior was equally noted for CF_A and CF_R, suggesting no influence of the storage time and conditions on surface composition in oxygen.

This lack of correlation between surface analysis and the observed functional changes in this study suggests that deeper chemical (no surface effect) or physical changes such as molecular mobility, reorganization of polysaccharide structures, or modification in the degree of esterification are taking place within the fiber matrix, influencing its capacity to interact with water.

4. Conclusions

Although important functionalities of citrus fibers (WSC and G′) were significantly affected by storage time and conditions (especially at 40 °C and 75 % RH), citrus fibers did not exhibit chemical changes that XPS could detect. Conversely, PCA analysis of FTIR data suggests that chemical changes over time may occur in pectin and/or protein rather than in cellulose and/or hemicellulose. These internal structural modifications likely contribute to the observed reduction in functional properties. In contrast, drying at different scales did not affect the functionality of citrus fibers. However, XPS analysis revealed significant differences in surface composition, particularly in the carbon and oxygen content, for samples dried using different scales. Extended drying times and higher temperatures may lead to the migration of components from the inner matrix to the surface or promote the degradation of surface components. While these surface changes do not immediately impact functionality, they could influence long-term stability and interactions with water.

The findings suggest that the functionality of citrus fibers is more closely related with their overall chemical composition and internal structure (e.g., changes in the degree of methyl esterification, cross-linking, or reorganization) rather than with surface composition. Food powders are generally considered stable compared to other high-water-content food products, posing challenges in studying stability in dry systems. The combined use of FTIR and XPS provides valuable insights into shelf-life studies.

Nevertheless, further investigation is necessary to fully understand the chemical profile changes of citrus fibers over time and to draw definitive conclusions about how these chemical transformations impact their functionality. To enhance the generalizability of these findings, future studies should consider analyzing citrus fiber samples from various sources and processing methods. This would provide a more comprehensive understanding of the factors influencing their functional properties. Moreover, in addition to chemical properties, the stability of citrus fibers could be further understood by an investigation of either their physical properties such as physical state or their molecular mobility.

CRediT authorship contribution statement

G.O. Coelho: Writing – original draft, Visualization, Methodology, Investigation, Formal analysis, Conceptualization. **D. Champion:** Writing – review & editing, Visualization, Supervision, Methodology, Conceptualization. **O. Heintz:** Writing – review & editing, Investigation, Formal analysis. **A. Krystianiak:** Validation, Investigation. **S. Debon:** Writing – review & editing. **I. Deleris:** Writing – review & editing, Visualization, Supervision. **J. Wallecan:** Writing – review & editing, Visualization, Project administration, Funding acquisition. **G. Roudaut:** Writing – review & editing, Visualization, Supervision, Methodology, Funding acquisition, Conceptualization.

Declaration of competing interest

The authors declare that they have no known competing financial interests or personal relationships that could have appeared to influence the work reported in this paper.

Acknowledgements

The authors are grateful for the financial support of Cargill R&D Centre Europe B.V., Vilvoorde, Belgium.

Appendix A. Supplementary data

Supplementary data to this article can be found online at https://doi.org/10.1016/j.ijbiomac.2024.137281.

Data availability

Data will be made available on request.

References

[1] USDA, Citrus: World Markets and Trade, United States, 2024, pp. 1–15.
[2] M.A. Andrade, C.H. Barbosa, M.A. Shah, N. Ahmad, F. Vilarinho, K. Khwaldia, A. S. Silva, F. Ramos, Citrus by-products: valuable source of bioactive compounds for food applications, Antioxidants 12 (2023) 1–20, https://doi.org/10.3390/antiox12010038.
[3] Z. Jiang, M. Zhang, Y. Huang, C. Ma, S. Mu, H. Li, X. Liu, Y. Ma, Y. Liu, J. Hou, Comparison and characterization of the structure and physicochemical properties of three citrus fibers: effect of ball milling treatment, Foods 11 (2022), https://doi.org/10.3390/foods11172665.
[4] A. Bejar, N. Mihoubi, N. Kechaou, Moisture sorption isotherms - experimental and mathematical investigations of orange (Citrus sinensis) peel and leaves, Food Chem. 132 (2012) 1728–1735, https://doi.org/10.1016/j.foodchem.2011.06.059.
[5] B. Lundberg, X. Pan, A. White, H. Chau, A. Hotchkiss, Rheology and composition of citrus fiber, J. Food Eng. 125 (2014) 97–104, https://doi.org/10.1016/j.jfoodeng.2013.10.021.
[6] D. Panwar, P.S. Panesar, H.K. Chopra, Evaluation of nutritional profile, phytochemical potential, functional properties and anti-nutritional studies of Citrus limetta peels, J. Food Sci. Technol. 60 (2023) 2160–2170, https://doi.org/10.1007/s13197-023-05743-x.
[7] S. Schalow, M. Baloufaud, T. Cottancin, J. Fischer, S. Drusch, Orange pulp and peel fibres: pectin-rich by-products from citrus processing for water binding and gelling in foods, Eur. Food Res. Technol. 244 (2018) 235–244, https://doi.org/10.1007/s00217-017-2950-y.
[8] Y. Zhang, J. Qi, W. Zeng, Y. Huang, X. Yang, Properties of dietary fiber from citrus obtained through alkaline hydrogen peroxide treatment and homogenization treatment, Food Chem. 311 (2020) 125873, https://doi.org/10.1016/j.foodchem.2019.125873.
[9] Y. Zhang, J. Liao, J. Qi, Functional and structural properties of dietary fiber from citrus peel affected by the alkali combined with high-speed homogenization treatment, LWT Food Sci. Technol. 128 (2020) 109397, https://doi.org/10.1016/j.lwt.2020.109397.
[10] J. yi Huang, J. song Liao, J. ru Qi, W. xin Jiang, X. quan Yang, Structural and physicochemical properties of pectin-rich dietary fiber prepared from citrus peel, Food Hydrocoll. 110 (2021) 106140, https://doi.org/10.1016/j.foodhyd.2020.106140.
[11] G. Agoda-Tandjawa, J. Mazoyer, J. Wallecan, V. Langendorff, Effects of sucrose addition on the rheological properties of citrus peel fiber suspensions before and after drying, Food Hydrocoll. 101 (2020) 105473, https://doi.org/10.1016/j.foodhyd.2019.105473.
[12] I. Déléris, J. Wallecan, Relationship between processing history and functionality recovery after rehydration of dried cellulose-based suspensions: a critical review, Adv. Colloid Interf. Sci. 246 (2017) 1–12, https://doi.org/10.1016/j.cis.2017.06.013.
[13] W. Mo, B. Li, X.S. Chai, Impact of fiber initial water content on the water retention capacity of poplar APMP fibers during the thermal drying, Wood Sci. Technol. 54 (2020) 227–235, https://doi.org/10.1007/s00226-019-01148-2.
[14] C. Gaiani, J. Scher, J.J. Ehrhardt, M. Linder, P. Schuck, S. Desobry, S. Banon, Relationships between dairy powder surface composition and wetting properties during storage: importance of residual lipids, J. Agric. Food Chem. 55 (2007) 6561–6567, https://doi.org/10.1021/jf070364b.
[15] E.H.J. Kim, X.D. Chen, D. Pearce, Surface composition of industrial spray-dried milk powders. 2. Effects of spray drying conditions on the surface composition,

J. Food Eng. 94 (2009) 169–181, https://doi.org/10.1016/j.jfoodeng.2008.10.020.
[16] E.H.J. Kim, X.D. Chen, D. Pearce, Surface composition of industrial spray-dried milk powders. 3. Changes in the surface composition during long-term storage, J. Food Eng. 94 (2009) 182–191, https://doi.org/10.1016/j.jfoodeng.2008.12.001.
[17] A.K.M. Masum, J. Chandrapala, T. Huppertz, B. Adhikari, B. Zisu, Influence of drying temperatures and storage parameters on the physicochemical properties of spray-dried infant milk formula powders, Int. Dairy J. 105 (2020) 104696, https://doi.org/10.1016/j.idairyj.2020.104696.
[18] A.K.M. Masum, J. Chandrapala, T. Huppertz, B. Adhikari, B. Zisu, Effect of storage conditions on the physicochemical properties of infant milk formula powders containing different lactose-to-maltodextrin ratios, Food Chem. 319 (2020) 126591, https://doi.org/10.1016/j.foodchem.2020.126591.
[23] S. Suri, A. Singh, P.K. Nema, S. Malakar, V.K. Arora, Sweet lime (Citrus limetta) peel waste drying approaches and effect on quality attributes, phytochemical and functional properties, Food Biosci. 48 (2022) 101789, https://doi.org/10.1016/j.fbio.2022.101789.
[26] D. Dehnad, S.M. Jafari, M. Afrasiabi, Influence of drying on functional properties of food biopolymers: from traditional to novel dehydration techniques, Trends Food Sci. Technol. 57 (2016) 116–131, https://doi.org/10.1016/j.tifs.2016.09.002.
[27] G. Agoda-Tandjawa, S. Durand, C. Gaillard, C. Garnier, J.L. Doublier, Properties of cellulose/pectins composites: implication for structural and mechanical properties of cell wall, Carbohydr. Polym. 90 (2012) 1081–1091, https://doi.org/10.1016/j.carbpol.2012.06.047.
[28] A.K. Chatjigakis, C. Pappas, N. Proxenia, O. Kalantzi, P. Rodis, M. Polissiou, FT-IR spectroscopic determination of the degree of esterification of cell wall pectins from stored peaches and correlation to textural changes, Carbohydr. Polym. 37 (1998) 395–408, https://doi.org/10.1016/S0144-8617(98)00057-5.
[29] R. Ciriminna, A. Fidalgo, R. Delisi, A. Tamburino, D. Carnaroglio, G. Cravotto, L. M. Ilharco, M. Pagliaro, Controlling the degree of esterification of citrus pectin for demanding applications by selection of the source, ACS Omega 2 (2017) 7991–7995, https://doi.org/10.1021/acsomega.7b01109.
[30] J.N. Humerez-Flores, S.H.E. Verkempinck, A.M. Van Loey, P. Moldenaers, M. E. Hendrickx, Targeted modifications of citrus pectin to improve interfacial properties and the impact on emulsion stability, Food Hydrocoll. 132 (2022) 107841, https://doi.org/10.1016/j.foodhyd.2022.107841.
[31] R. Barbucci, A. Magnani, M. Consumi, Swelling behavior of carboxymethylcellulose hydrogels in relation to cross-linking, pH, and charge density, Macromolecules 33 (2000) 7475–7480, https://doi.org/10.1021/ma0007029.
[32] M. Di Gioacchino, F. Bruni, S. Imberti, M.A. Ricci, Hydration of carboxyl groups: a route toward molecular recognition? J. Phys. Chem. B 124 (2020) 4358–4364, https://doi.org/10.1021/acs.jpcb.0c03609.
[33] C.M. Popescu, C.M. Tibirna, C. Vasile, XPS characterization of naturally aged wood, Appl. Surf. Sci. 256 (2009) 1355–1360, https://doi.org/10.1016/j.apsusc.2009.08.087.
[34] U. Einhorn-Stoll, H. Kastner, A. Fatouros, A. Krähmer, L.W. Kroh, S. Drusch, Thermal degradation of citrus pectin in low-moisture environment – investigation of backbone depolymerisation, Food Hydrocoll. 107 (2020) 105937, https://doi.org/10.1016/j.foodhyd.2020.105937.
[35] J. Łojewska, A. Lubańska, P. Miśkowiec, T. Łojewski, L.M. Proniewicz, FTIR in situ transmission studies on the kinetics of paper degradation via hydrolytic and oxidative reaction paths, Appl. Phys. A Mater. Sci. Process. 83 (2006) 597–603, https://doi.org/10.1007/s00339-006-3529-9.
[36] M. Ali, A.M. Emsley, H. Herman, R.J. Heywood, Spectroscopic studies of the ageing of cellulosic paper, Polymer (Guildf). 42 (2001) 2893–2900, https://doi.org/10.1016/S0032-3861(00)00691-1.
[37] J. Łojewska, P. Miśkowiec, T. Łojewski, L.M. Proniewicz, Cellulose oxidative and hydrolytic degradation: in situ FTIR approach, Polym. Degrad. Stab. 88 (2005) 512–520, https://doi.org/10.1016/j.polymdegradstab. 2004.12.012.
[38] M.A. Nawaz, C. Gaiani, S. Fukai, B. Bhandari, X-ray photoelectron spectroscopic analysis of rice kernels and flours: measurement of surface chemical composition, Food Chem. 212 (2016) 349–357, https://doi.org/10.1016/j.foodchem.2016.05.188.
[39] K.N. Fyfe, O. Kravchuk, T. Le, H.C. Deeth, A.V. Nguyen, B. Bhandari, Storage induced changes to high protein powders: influence on surface properties and solubility, J. Sci. Food Agric. 91 (2011) 2566–2575, https://doi.org/10.1002/jsfa.4461.
[40] E.I. Nep, B.R. Conway, Physicochemical characterization of grewia polysaccharide gum: effect of drying method, Carbohydr. Polym. 84 (2011) 446–453, https://doi.org/10.1016/j.carbpol.2010.12.005.
[41] J. Fernández-López, E. Sendra-Nadal, C. Navarro, E. Sayas, M. Viuda-Martos, J.A. P. Alvarez, Storage stability of a high dietary fibre powder from orange by-products, Int. J. Food Sci. Technol. 44 (2009) 748–756, https://doi.org/10.1111/j.1365-2621.2008.01892.x.
[42] N.I. Putri, J. Van Audenhove, C. Kyomugasho, A. Van Loey, M. Hendrickx, Relaxation temperature and storage stability of the functionalized cell wall material residue from lemon peel, Food Hydrocoll. 150 (2024) 109711, https://doi.org/10.1016/j.foodhyd.2023.109711.
[43] J. Wallecan, C. McCrae, S.J.J. Debon, J. Dong, J. Mazoyer, Emulsifying and stabilizing properties of functionalized orange pulp fibers, Food Hydrocoll. 47 (2015) 115–123, https://doi.org/10.1016/j.foodhyd.2015.01.009.
[44] K.L.D.D. Willemsen, A. Panozzo, K. Moelants, J. Wallecan, M. Hendrickx, Towards improved understanding of the viscoelastic properties of functionalized lemon peel fibers in suspension based on microstructure, hydration value and swelling volume, J. Food Eng. 278 (2020) 109950, https://doi.org/10.1016/j.jfoodeng.2020.109950.
[45] D. Su, X. Zhu, Y. Wang, D. Li, L. Wang, Effect of high-pressure homogenization on rheological properties of citrus fiber, LWT Food Sci. Technol. 127 (2020) 109366, https://doi.org/10.1016/j.lwt.2020.109366.
[46] M. Spinei, M. Oroian, Structural, functional and physicochemical properties of pectin from grape pomace as affected by different extraction techniques, Int. J. Biol. Macromol. 224 (2023) 739–753, https://doi.org/10.1016/j.ijbiomac.2022.10.162.
[47] N. Harnkarnsujarit, S. Charoenrein, Effect of water activity on sugar crystallization and β-carotene stability of freeze-dried mango powder, J. Food Eng. 105 (2011) 592–598, https://doi.org/10.1016/j.jfoodeng.2011.03.026.
[48] C. Kyomugasho, P.G. Kamau, S. Aravindakshan, M.E. Hendrickx, Evaluation of storage stability of low moisture whole common beans and their fractions through the use of state diagrams, Food Res. Int. 140 (2021) 109794, https://doi.org/10.1016/j.foodres.2020.109794.
[49] Y. Liu, B. Bhandari, W. Zhou, Glass transition and enthalpy relaxation of amorphous food saccharides: a review, J. Agric. Food Chem. 54 (2006) 5701–5717, https://doi.org/10.1021/jf060188r.
[50] E. Ostrowska-Ligęza, E. Jakubczyk, A. Górska, M. Wirkowska, J. Bryś, The use of moisture sorption isotherms and glass transition temperature to assess the stability of powdered baby formulas, J. Therm. Anal. Calorim. 118 (2014) 911–918, https://doi.org/10.1007/s10973-014-3846-8.
[51] Y.H. Roos, Water activity and physical state effects on amorphous food stability, J. Food Process. Preserv. 16 (1993) 433–447, https://doi.org/10.1111/j.1745-4549.1993.tb00221.x.
[52] V.A. Lovikka, L. Rautkari, T.C. Maloney, Changes in the hygroscopic behavior of cellulose due to variations in relative humidity, Cellulose 25 (2018) 87–104, https://doi.org/10.1007/s10570-017-1570-9.
[53] W. Mo, K. Chen, X. Yang, F. Kong, J. Liu, B. Li, Elucidating the hornification mechanism of cellulosic fibers during the process of thermal drying, Carbohydr. Polym. 289 (2022) 1–7, https://doi.org/10.1016/j.carbpol.2022.119434.
[54] Š. Šutý, K. Petriláková, S. Katuščák, S. Kirschnerová, M. Jablonský, K. Vizarová, M. Vrška, Change in the capability of cellulose fibres to retain water during thermally accelerated ageing of paper, Cellul. Chem. Technol. 46 (2012) 631–635.
[55] K.L. Kato, R.E. Cameron, A review of the relationship between thermally-accelerated ageing of paper and hornification, Cellulose 6 (1999) 23–40, https://doi.org/10.1023/A:1009292120151.
[56] M. Makarem, H. Kim, P. Emami, J. Melendez, A. Steinbach, T. Lipkie, I. Deleris, C. Desmet, J. Wallecan, S.H. Kim, Impact of drying on meso-and nanoscale structures of citrus fiber: a study by SFG, ATR-IR, XRD, and DLS, Ind. Eng. Chem. Res. 59 (2020) 2718–2724, https://doi.org/10.1021/acs.iecr.9b06194.
[57] A. Célino, O. Gonçalves, F. Jacquemin, S. Fréour, Qualitative and quantitative assessment of water sorption in natural fibres using ATR-FTIR spectroscopy, Carbohydr. Polym. 101 (2014) 163–170, https://doi.org/10.1016/j.carbpol.2013.09.023.
[58] X. Liu, C.M.G.C. Renard, S. Bureau, C. Le Bourvellec, Revisiting the contribution of ATR-FTIR spectroscopy to characterize plant cell wall polysaccharides, Carbohydr. Polym. 262 (2021) 117935, https://doi.org/10.1016/j.carbpol.2021.117935.
[59] M. Szymanska-Chargot, A. Zdunek, Use of FT-IR spectra and PCA to the bulk characterization of cell wall residues of fruits and vegetables along a fraction process, Food Biophys. 8 (2013) 29–42, https://doi.org/10.1007/s11483-012-9279-7.
[60] Z. Chen, T.Q. Hu, H.F. Jang, E. Grant, Modification of xylan in alkaline treated bleached hardwood kraft pulps as classified by attenuated total-internal-reflection (ATR) FTIR spectroscopy, Carbohydr. Polym. 127 (2015) 418–426, https://doi.org/10.1016/j.carbpol.2015.03.084.
[61] A. Boukir, S. Fellak, P. Doumenq, Structural characterization of Argania spinosa Moroccan wooden artifacts during natural degradation progress using infrared spectroscopy (ATR-FTIR) and X-Ray diffraction (XRD), Heliyon 5 (2019) e02477, https://doi.org/10.1016/j.heliyon.2019.e02477.
[62] D. Ferreira, A. Barros, M.A. Coimbra, I. Delgadillo, Use of FT-IR spectroscopy to follow the effect of processing in cell wall polysaccharide extracts of a sun-dried pear, Carbohydr. Polym. 45 (2001) 175–182, https://doi.org/10.1016/S0144-8617(00)00320-9.
[63] R. Hori, J. Sugiyama, A combined FT-IR microscopy and principal component analysis on softwood cell walls, Carbohydr. Polym. 52 (2003) 449–453, https://doi.org/10.1016/S0144-8617(03)00013-4.
[64] M. Szymanska-Chargot, M. Chylinska, B. Kruk, A. Zdunek, Combining FT-IR spectroscopy and multivariate analysis for qualitative and quantitative analysis of the cell wall composition changes during apples development, Carbohydr. Polym. 115 (2015) 93–103, https://doi.org/10.1016/j.carbpol.2014.08.039.
[65] N. Gaudel, C. Gaiani, Y.M. Harshe, J. Kammerhofer, M. Pouzot, S. Desobry, J. Burgain, Reconstitution of fruit powders: a process–structure–function approach, J. Food Eng. 315 (2022) 110800, https://doi.org/10.1016/j.jfoodeng.2021.110800.
[66] F.W. Sosulski, G.I. Imafidon, Amino acid composition and nitrogen-to-protein conversion factors for animal and plant foods, J. Agric. Food Chem. 38 (1990) 1351–1356, https://doi.org/10.1021/jf00096a011.
[67] L. Fras, L.S. Johansson, P. Stenius, J. Laine, K. Stana-Kleinschek, V. Ribitsch, Analysis of the oxidation of cellulose fibres by titration and XPS, Colloids Surfaces A Physicochem. Eng. Asp. 260 (2005) 101–108, https://doi.org/10.1016/j.colsurfa.2005.01.035.
[68] N.E. Zafeiropoulos, P.E. Vickers, C.A. Baillie, J.F. Watts, An experimental investigation of modified and unmodified flax fibres with XPS, ToF-SIMS and ATR-

FTIR, J. Mater. Sci. 38 (2003) 3903–3914, https://doi.org/10.1023/A:1026133826672.
[69] A.G. Cruz, A.I. Mtz-Enríquez, L. Díaz-Jiménez, R. Ramos-González, J.A.A. Valdés, M.E.C. Flores, J.L.H. Martínez, A. Ilyina, Production of fatty acid methyl esters and bioactive compounds from citrus wax, Waste Manag. 102 (2020) 48–55, https://doi.org/10.1016/j.wasman.2019.10.021.
[70] O.A. Caparino, J. Tang, C.I. Nindo, S.S. Sablani, J.R. Powers, J.K. Fellman, Effect of drying methods on the physical properties and microstructures of mango (Philippine "Carabao" var.) powder, J. Food Eng. 111 (2012) 135–148, https://doi.org/10.1016/j.jfoodeng.2012.01.010.
[71] H. Mirhosseini, B.T. Amid, Effect of different drying techniques on flowability characteristics and chemical properties of natural carbohydrate-protein gum from durian fruit seed, Chem. Cent. J. 7 (2013) 1–14, https://doi.org/10.1186/1752-153X-7-1.
[72] P. Mishra, V. Srivastava, D. Verma, O.P. Chauhan, G.K. Rai, Physico-chemical properties of Chakiya variety of Amla (Emblica officinalis) and effect of different dehydration methods on quality of powder, African, J. Food Sci. 3 (2009) 303–306. http://www.academicjournals.org/ajfs.
[73] N.G. Inari, M. Petrissans, J. Lambert, J.J. Ehrhardt, P. Férardin, XPS characterization of wood chemical composition after heat-treatment, Surf. Interface Anal. 38 (2006) 1336–1342, https://doi.org/10.1002/sia.2455.
[74] R.W. Truss, B. Wood, R. Rasch, Quantitative surface analysis of hemp fibers using XPS, conventional and low voltage in-lens SEM, J. Appl. Polym. Sci. 133 (2016) 1–9, https://doi.org/10.1002/app.43023.
[75] Q. Tang, G. Huang, Improving method, properties and application of polysaccharide as emulsifier, Food Chem. 376 (2022) 131937, https://doi.org/10.1016/j.foodchem.2021.131937.
[76] M.C. Wehrli, T. Kratky, M. Schopf, K.A. Scherf, T. Becker, M. Jekle, Thermally induced gluten modification observed with rheology and spectroscopies, Int. J. Biol. Macromol. 173 (2021) 26–33, https://doi.org/10.1016/j.ijbiomac.2021.01.008.